# Modelling the atmospheric influence of coral reef-derived dimethyl sulfide

Sonya Louise Fiddes, MSc

ORCID: 0000-0002-2752-0845

Submitted in fulfilment of the requirements
for the degree of Doctor of Philosophy

February 2020

School of Earth Science

The University of Melbourne

# Abstract

Dimethyl sulfide (DMS) is a naturally occurring aerosol precursor gas which plays an important role in the global sulfur budget, aerosol formation and climate. While DMS is produced predominantly by phytoplankton, recent observational literature has suggested that corals and their symbionts produce a significant amount of DMS, which is currently unaccounted for in modelling studies. It has further been hypothesised that the coral reef source of DMS may modulate the climate. In this thesis, two atmospheric models coupled to online chemistry and aerosol schemes were used for the first time to explore the influence of coral reef-derived DMS on atmospheric composition and meteorology across temporal and spatial scales.

A simple non-varying representation of coral reef-derived DMS was developed and added to a common DMS surface water climatology. By comparing the differences between simulations with and without coral reef-derived DMS, the role of coral reef-derived DMS was quantified.

The Australian Community Climate Earth System Simulator coupled to the United Kingdom Chemistry and Aerosol model (ACCESS-UKCA) was used to quantify the influence of coral reefs at the global scale. ACCESS-UKCA was evaluated against satellite observations and other global climate models and the sensitivity of aerosol, clouds and radiation to large scale perturbations of DMS was tested. ACCESS-UKCA was found to have similar biases and DMS sensitivity compared to other models and it was estimated that marine DMS contributes 0.45 K cooling to the present climate. The influence of coral reef-derived DMS on global to regional scale climate was then investigated. In the Maritime Continent-Australian region,

where the highest density of coral reefs exist, a small decrease in nucleation and Aitken mode aerosol was found when coral reefs were removed from the system. However, these small responses were found to have no robust effect on global or regional climate.

The Weather Research Forecast model coupled to the CBMZ-MOSAIC (Carbon Bond Mechanism Z - Model for Simulating Aerosol Interactions and Chemistry) chemistry-aerosol scheme (WRF-Chem) was then used to study the same question at higher spatial and temporal scales. WRF-Chem was run to coincide with an October 2016 field campaign over the Great Barrier Reef, Australia, against which the model was evaluated. After halving the DMS surface water climatology, the model performed well for DMS and sulfur processes, though aerosol number was overestimated. The inclusion of coral reef-derived DMS resulted in no compositional change in sulfate aerosol mass or total aerosol number. No direct or indirect aerosol effects were detected.

Throughout this work, the complexities of the aerosol-climate system have been emphasised and the limitations of current modelling capabilities highlighted. In conclusion, while total marine DMS was found to have an important climatic influence, this thesis has found no robust link between coral reef-derived DMS and climate or weather. Thus, these results do not support hypotheses around the ability of coral reefs to modulate global or regional climate.

# Declaration

This is to certify that:

i. this thesis comprises only my original work towards the PhD except where indicated in the preface;

ii. due acknowledgement has been made in the text to all other material used; and

iii. this thesis is fewer than the maximum word limit in length, exclusive of tables, maps, bibliographies and appendices

Signed .....

Dated .....

# Preface

A significant proportion of the results presented in Chapters 4 and 5, in addition to the relevant background and methods in Chapters 2 and 3, have been published in the following journal paper. My co-authors contributed to direction of the project, to less than 10 % of the written text and to the revisions of the manuscript.

Fiddes, S. L., Woodhouse, M. T., Nicholls, Z., Lane, T. P., & Schofield, R. (2018). Cloud, precipitation and radiation responses to large perturbations in global dimethyl sulfide. Atmospheric Chemistry and Physics, 18(14), 1017710198. http://doi.org/10.5194/acp-18-10177-2018

Chapter 6 and the relevant background and methods in Chapters 2 and 3 are in preparation for publication with the tentative citation listed below. My co-authors have contributed to direction of the project and to revisions of the manuscript.

Fiddes, S. L., Woodhouse, M. T., Lane, T. P., & Schofield, R. (2020). Quantification of the influence of coral reef-derived dimethyl sulfide on atmospheric composition and climate with the global coupled climate-chemistry model ACCESS-UKCA. *In preparation for Atmospheric Chemistry and Physics*

Chapter 7, and the relevant background and methods in Chapters 2 and 3, are in preparation for publication with the tentative citation listed below. SU, TL, MW and RS contributed to the direction and development of the project, while

the remaining co-authors provided the observational data and less than 10 % of the written text in relation to the observational methods.

Fiddes, S. L., Woodhouse, M. T., Utembe, S., Ristovski, Z., Cravigan, L., Alroe, J., Miljevic, B., Ryan, R., Omori, Y., Tanimoto, H., Swan, H., Lawson, S., Dunne, E., Keywood, M., Williams, A., Chambers, S., Chen, Z., Protat, A., Alexander, S., Lane, T., & Schofield, R. (2020). Evaluation of dimethyl sulfide, aerosol and meteorological fields in WRF-Chem over the Great Barrier Reef. *In preparation for Atmospheric Chemistry and Physics*

Chapter 8, and the relevant background and methods in Chapters 2 and 3, are in preparation for publication with the tentative citation listed below. My co-authors have contributed to the direction of the project and to revisions of the manuscript.

Fiddes, S. L., Utembe, S., Woodhouse, M. T., Lane, T. P., & Schofield, R. (2020). Assessing the importance of coral reef-derived dimethyl sulfide for atmospheric composition and meteorology over the Great Barrier Reef in WRF-Chem. *In preparation for Atmospheric Chemistry and Physics Letters*

This work was supported through funding from the Australian Research Council's Centre of Excellence for Climate System Science (CE110001028) and an Australian Government Research Training Program Scholarship.

# Acknowledgments

Along this PhD journey I have been honoured to have had the help and support of some brilliant, caring and inspiring people and organisations, without which, this PhD may have turned out quite differently.

To my primary supervisor, Robyn Schofield, thank you for being not only my supervisor but also my friend, mentor and advocate. The fact that our meetings more often than not turned into conversations about our daily goings-on made me feel I was trusted and amongst peers, giving me the confidence to achieve. To my co-supervisor Todd Lane, thank you for your careful guidance and patience in this journey. I greatly appreciate the help you have given me, especially when I was feeling frustrated and overwhelmed. Last, but by no means least, to my co-supervisor Matt Woodhouse, I cannot thank you enough for all the help, advice, pep-talks and coffee you have given me over the last three and a half years. I greatly value our friendship and your unwavering confidence in my work and myself. I couldn't have achieved what I have without your help.

I have also had incredible help and support from many outside of my supervisory team, for which I am eternally grateful. In particular, I'd like to thank Peter Rayner, a member of my panel, but more importantly, a nonjudgmental, honest and kind person. Our Monday group meetings always left me feeling hopeful and with the knowledge that I wasn't alone. To Steve Utembe, with out your help, learning WRF-Chem would have been an insurmountable challenge. I cannot thank you enough for spending hours on end explaining and debugging WRF-Chem with me. Similarly, I'd like to extend my thanks Scott Wales from the CMS team who helped

me over many days and weeks with getting ACCESS-UKCA up and running. To Anita Talberg, your leadership at the Climate and Energy College and your loyal friendship has been of great value. Thank you for being someone I could always turn to in need. In addition, thanks to Malte Meinshausen for fostering such a motivated, friendly and hugely intellectual culture at the Climate and Energy College.

I would like to express my sincere gratitude to the people of the Climate and Energy College themselves. Being a part of this community has broadened my horizons and motivated me to be the best I could amongst such inspirational peers. In a similar vein, I'd like to thank the atmospheric composition group in the School of Earth Science. Our regular Monday meetings made the challenges of a PhD feel less lonely. I would also like to thank the Australian Research Council's Centres of Excellence for Climate System Science and Climate Extremes. These two centres have given me so many opportunities over the last three and a half years, providing training, networking, travel and financial support. In addition, I'd like to acknowledge that without help and support from the National Computational Infrastructure, and the q90 project, this PhD would not have been possible.

Throughout this PhD I have been fortunate enough to participate in some amazing field work, from the Great Barrier Reef to Antarctica. I've met some incredible people along the way, who have taught me so much about atmospheric processes and how to observe them; I think an essential experience for any modeller to gain! In particular, I'd like to thank everyone involved in the Reef to Rainforest campaign circumnavigating the Great Barrier Reef on board the RV Investigator and at AIRBOX in Mission Beach, the CAMPCANN campaign on board the RSV Aurora Australis to Casey Station and the Garden Island campaign in Western Australia, with AIRBOX again.

This PhD has been an intense experience, filled with emotions across the spectrum. I am so grateful to have made such amazing friends with whom to share these emotions and navigate this journey. In particular, I'd like to thank my fellow 'Climate Ladies', Mandy, Tash, Lisa, Caro and Kate, your friendship has meant the world to me. Knowing I could always count on you to laugh or cry with has made

this time so special. To Zeb, Dylan, Alister, Alex and Rob too, you guys have made this journey a joy, I have so much gratitude for the light hearted fun and the serious debates we have had over this time.

I wish to express my heartfelt thanks to my family. Thank you Mum and Dad for your lifelong confidence and encouragement that enabled me to achieve this PhD and for your support when it seemed impossible. To my sister Rachel, thank you for your understanding and for a welcoming home when I needed a break. To Alisa, Chris, Nyree and your families, your kind words throughout this journey have been much appreciated.

Finally, I'd like to give my utmost thanks to my partner Aaron. Knowing I had you and Mr Bills to come home to each night made hard moments easier. Thank you for being an unfaltering pillar in my life. Your belief in me, your support and your love have made this achievement possible.

# Contents

**Abstract** **i**

**List of Tables** **xi**

**List of Figures** **xiii**

**1 Introduction** **1**

1.1 Context and Motivation . . . . . 1

1.2 Research objectives . . . . . 3

1.3 Contributions to the state of knowledge . . . . . 5

1.4 Structure of thesis . . . . . 5

**2 Background** **9**

2.1 Aerosol and the climate system . . . . . 9

2.1.1 Aerosol radiative effects . . . . . 10

2.1.2 Aerosol sources, formation and growth . . . . . 11

2.1.3 Aerosol uncertainty . . . . . 14

2.2 Dimethyl sulfide . . . . . 17

2.2.1 DMS production . . . . . 18

2.2.2 DMS in the ocean surface water . . . . . 19

2.2.3 DMS ocean-atmosphere flux . . . . . 22

2.2.4 DMS in the atmosphere . . . . . 26

2.2.5 The Charlson, Lovelock, Andreae and Warren (CLAW) hypothesis . . . 26
2.2.6 Evidence of the influence of DMS on the climate system . . . 29
2.2.7 Global DMS-climate modelling . . . 31
2.2.8 Regional DMS-climate modelling . . . 33
2.3 Coral reefs and DMS . . . 35
2.3.1 Coral reefs . . . 35
2.3.2 Coral reef-derived DMS observations . . . 37
2.3.3 Applying the CLAW hypothesis to coral reefs . . . 40
2.3.4 The Reef to Rainforest Field Campaign . . . 42
2.4 Summary . . . 44

**3 Methods and data 46**

3.1 ACCESS-UKCA . . . 47
3.1.1 Model setup . . . 47
3.1.2 ACCESS . . . 48
3.1.3 UKCA . . . 49
3.1.4 DMS climatologies and perturbations . . . 55
3.1.5 Experiment setup . . . 59
3.1.6 Evaluation . . . 63
3.1.7 Global energy balance model . . . 63
3.2 WRF-Chem . . . 65
3.2.1 Chemistry and aerosol options . . . 67
3.2.2 Meteorology and physics options . . . 74
3.2.3 DMS climatologies . . . 77
3.2.4 Experiment setup . . . 81
3.2.5 Evaluation . . . 82
3.3 Statistical methods . . . 90

3.4 Summary . . . . . 92

**4 ACCESS-UKCA Model Evaluation 93**

4.1 Cloud evaluation . . . . . 94

4.2 Radiation evaluation . . . . . 96

4.3 Precipitation evaluation . . . . . 100

4.4 Discussion . . . . . 101

**5 Sensitivity of the current climate to large perturbations in global marine DMS 103**

5.1 Removal of global marine DMS . . . . . 104

5.1.1 Chemistry response . . . . . 104

5.1.2 Aerosol response . . . . . 107

5.1.3 Cloud, radiation and precipitation response . . . . . 110

5.2 Increasing DMS to the zonal maximum . . . . . 113

5.3 Determining the temperature response to changes in radiative forcing 115

5.4 Discussion . . . . . 116

**6 The atmospheric influence of coral reef-derived DMS globally 121**

6.1 Impacts of coral reef-derived DMS over the MC-Aus region . . . . . 123

6.1.1 DMS and sulfur dioxide . . . . . 123

6.1.2 Aerosol . . . . . 128

6.1.3 Direct aerosol radiative effects . . . . . 132

6.1.4 Indirect aerosol radiative effects in the large-scale cloud and precipitation scheme . . . . . 139

6.2 Implications for Queensland, Australia . . . . . 140

6.3 Discussion . . . . . 142

**7 WRF-Chem model evaluation and atmospheric sensitivity to large perturbations in DMS 147**

7.1 Meteorology . . . . . 148
7.2 DMS and sulfate aerosol . . . . . 155
7.3 Total aerosol . . . . . 158
7.4 Cloud height and albedo . . . . . 161
7.5 Discussion . . . . . 163

**8 The atmospheric influence of DMS derived from the Great Barrier Reef 168**

8.1 Differences in DMS, sulfate aerosol mass and the aerosol burden . . . 169
8.2 Direct and indirect aerosol effects . . . . . 174
8.3 Discussion . . . . . 175

**9 Conclusions 179**

**Definition of acronyms 188**

**Appendices 193**

**A ACCESS-UKCA DMS climatologies 193**

**B WRF-CHEM namelists 196**

**C Additional plots for ACCESS-UKCA 199**

**D Additional plots for WRF-CHEM 202**

**Bibliography 208**

# List of Tables


2.1 Annual total $\text{flux}_{\text{DMS}}$ reported by literature . . . . . 24

2.2 Coral DMS field measurements . . . . . 38

2.3 Coral DMS laboratory measurements . . . . . 41

3.1 ACCESS-UKCA aerosol modal size distributions . . . . . 50

3.2 DMS oxidation pathways in ACCESS-UKCA . . . . . 52

3.3 $\text{DMS}_{\text{w}}$ climatologies for ACCESS-UKCA . . . . . 56

3.4 DMS oxidation pathways in WRF-Chem . . . . . 71

3.4 DMS oxidation pathways in WRF-Chem cont. . . . . 72

3.5 WRF-Chem aerosol bin size distributions . . . . . 72

3.6 $\text{DMS}_{\text{w}}$ climatologies for WRF-Chem . . . . . 79

3.7 Summary of WRF-Chem simulations . . . . . 81

3.8 Observations for WRF-Chem evaluation . . . . . 83

3.9 Observations forWRF-Chem evaluation cont. . . . . 84

5.1 CCN sensitivity to $\text{flux}_{\text{DMS}}$ . . . . . 110

5.2 Global mean changes in radiation . . . . . 115

5.3 Temperature response to changes in $\text{flux}_{\text{DMS}}$ . . . . . 116

6.1 Seasonal changes in ACCESS-UKCA over the MC-Aus region . . . . 125

6.1 Seasonal changes in ACCESS-UKCA over the MC-Aus region cont. . 126

B.1 WRF-Chem chemistry namelist . . . . . 197

B.2 WRF-Chem physics namelist . . . . . 198

# List of Figures


1.1 Thesis overview . . . . . 6

2.1 Aerosol radiation effects . . . . . 11
2.2 Schematic of aqueous phase oxidation and cloud processing . . . . . 12
2.3 Aerosol modes and sizes . . . . . 14
2.4 The sulfur cycle . . . . . 15
2.5 Radiative forcing . . . . . 16
2.6 $DMS_w$ global observations . . . . . 20
2.7 The L11 climatology . . . . . 21
2.8 DMS oxidation pathways . . . . . 27
2.9 CLAW . . . . . 28
2.10 Global coral reefs . . . . . 36
2.11 The R2R campaign . . . . . 43

3.1 The L11MX January and July climatology . . . . . 57
3.2 Coral reef areal fraction of the ACCESS-UKCA grid . . . . . 58
3.3 The L11C50 January and July climatology . . . . . 59
3.4 Annual average $flux_{DMS}$ . . . . . 60
3.5 ACCESS-UKCA area average locations . . . . . 61
3.6 The WRF-Chem domains . . . . . 67
3.7 WRF-Chem aerosol bins . . . . . 73
3.8 The regridded L11 and L11S climatologies . . . . . 78
3.9 Example coral reef grid point $flux_{DMS}$ timeseries . . . . . 80
3.10 The L11SCH and L11SCVH climatologies . . . . . 80

4.1 ACCESS-UKCA cloud evaluation . . . . . 95
4.2 ACCESS-UKCA annual cycle evaluation . . . . . 97
4.3 ACCESS-UKCA radiation evaluation . . . . . 98
4.4 ACCESS-UKCA precipitation evaluation . . . . . 100

5.1 ACCESS-UKCA chemical sensitivity to large $DMS_w$ perturbations . . 105
5.2 Vertical profiles of ACCESS-UKCA chemical and aerosol sensitivity to large $DMS_w$ perturbations . . . . . 106
5.3 ACCESS-UKCA aerosol sensitivity to large $DMS_w$ perturbations . . . 108
5.4 ACCESS-UKCA cloud and radiation sensitivity to large $DMS_w$ perturbations . . . . . 111
5.5 ACCESS-UKCA water vapour and precipitation sensitivity to large $DMS_w$ perturbations . . . . . 112

6.1 ACCESS-UKCA $DMS_a$ in response to coral reefs . . . . . 124
6.2 ACCESS-UKCA $SO_2$ in response to coral reefs . . . . . 127
6.3 ACCESS-UKCA $N_3$ in response to coral reefs . . . . . 129
6.4 ACCESS-UKCA aerosol size distributions in response to coral reefs . 131
6.5 ACCESS-UKCA CCN in response to coral reefs . . . . . 133
6.6 ACCESS-UKCA direct effects in response to coral reefs . . . . . 134
6.7 ACCESS-UKCA vertical profiles of w, water vapour and v in response to coral reefs . . . . . 137
6.8 ACCESS-UKCA indirect effects in response to coral reefs . . . . . 139

7.1 WRF-Chem meteorology evaluation against the RVI . . . . . 149
7.2 WRF-Chem meteorology annual cycle evaluation against the RVI . . 150
7.3 WRF-Chem meteorology evaluation against AIRBOX . . . . . 152
7.4 WRF-Chem meteorology annual cycle evaluation against AIRBOX . . 153
7.5 WRF-Chem DMS and $SO_4$ evaluation against the RVI . . . . . 156
7.6 WRF-Chem DMS and $SO_4$ evaluation against AIRBOX . . . . . 157

7.7 WRF-Chem total aerosol evaluation against the RVI . . . . . 159
7.8 WRF-Chem total aerosol evaluation against AIRBOX . . . . . 159
7.9 WRF-Chem cloud evaluation along the RVI track . . . . . 162
7.10 WRF-Chem cloud evaluation at AIRBOX . . . . . 162

8.1 Timeseries and distributions of $DMS_a$, $SO_4$ and $N_{10}$ over a representative coral reef grid box in WRF-Chem . . . . . 170
8.2 Average $DMS_a$ for WRF-Chem at D02 . . . . . 171
8.3 Average $SO_4$ for WRF-Chem at D02 . . . . . 172
8.4 Average $N_{10}$ for WRF-Chem at D02 . . . . . 173
8.5 Average $SW{\downarrow}_{Surf,CS}$ for WRF-Chem at D02 . . . . . 174
8.6 Average liquid water path for WRF-Chem at D02 . . . . . 175
8.7 Average total rainfall for WRF-Chem at D02 . . . . . 176

A.1 The L11MX monthly climatology . . . . . 194
A.2 The L11C50 monthly climatology . . . . . 195

C.1 ACCESS-UKCA surface wind speed in response to coral reefs . . . . 200
C.2 ACCESS-UKCA large-scale rainfall in response to coral reefs . . . . . 201
C.3 ACCESS-UKCA $SW{\downarrow}_{Surf}$ in response to coral reefs . . . . . 201

D.1 WRF-Chem aerosol species evaluation against the RVI . . . . . 203
D.2 WRF-Chem aerosol species evaluation against AIRBOX . . . . . 204
D.3 Spatial timeseries average of $DMS_a$ for WRF-Chem at D03 . . . . . 205
D.4 Spatial timeseries average of $SO_4$ aerosol mass for WRF-Chem at D03 206
D.5 Spatial timeseries average of $CCN_{70}$ for WRF-Chem at D02 . . . . . 206
D.6 Spatial timeseries average of CDN for WRF-Chem at D02 . . . . . 207
D.7 Spatial timeseries average of total cloud fraction for WRF-Chem at D02 . . . . . 207

# Chapter 1

# Introduction

## 1.1 Context and Motivation

Current understanding of the Earth's climate and weather is underpinned by the concept of the radiation budget; the balance of energy entering and leaving the Earth's atmosphere. Aerosol, i.e. small liquid or solid particles suspended in the atmosphere, play an important role in maintaining this energy balance and represent one of the largest areas of uncertainty in atmospheric modelling.

Broadly, aerosol are considered to impact the radiation budget in two ways, with important consequences for climate. Direct aerosol effects absorb or scatter shortwave radiation while indirect aerosol effects can alter cloud characteristics including radiative properties, cloud lifetime, vertical extent and precipitation. While in theory the physical mechanisms behind aerosol effects are understood, the scale and variability of these make the modelling of such mechanisms highly uncertain.

This thesis focuses on one particular natural aerosol precursor: dimethyl sulfide or DMS. DMS is known to be produced by marine biota, including phytoplankton, algae and coral reefs, and is at the heart of the CLAW hypothesis (CLAW standing

for the authors surnames Charlson, Lovelock, Andreae and Warren, Charlson et al., 1987). The CLAW hypothesis proposes that marine biota can regulate their environment via the production of DMS and the subsequent impacts of sulfate aerosol on radiation and clouds. Although recent literature has found this hypothesis implausible, the importance of marine DMS for climate is widely acknowledged.

Correspondingly, concern as to what the effects of increasing atmospheric temperatures and ocean acidification may be for the production of DMS, and the ensuing feedbacks on climate, is becoming more prevalent within the literature. Alarmingly, coral reefs are expected to be one of the first major ecosystems to face near total collapse if further anthropogenic climate change is not avoided.

Limited observational studies have suggested that coral reef-derived aerosol may have some influence on local weather and climate and, by extension, imply that the loss of coral reefs may have further climatic effects. However, such studies struggle to isolate the influence of a single aerosol source and often rely on linear statistics which do not take into account the complex processes involved in aerosol-climate interaction.

Until now, no modelling study has included coral reef-derived DMS in surface water concentration inventories. Thus, no modelling study has considered the influence of coral reef-derived DMS on climate and weather or the implications of coral reef extinction for climate.

This thesis is subsequently motivated by two main themes:

- The importance of coral reefs for climate is currently unknown and at risk
- Analysis of aerosol-climate interactions, regardless of the aerosol source, is highly complex and uncertain. Modelling studies can help improve our understanding of this system

## 1.2 Research objectives

The overarching aim of this thesis is to **quantify the influence of coral reef-derived DMS on the atmosphere, in terms of composition and meteorology, over different temporal and spatial scales**. This aim is achieved using two different atmospheric-chemistry models run at global and regional scales: the Australian Community Climate and Earth System Simulator coupled to the United Kingdom Chemistry and Aerosol model (ACCESS-UKCA) and the Weather Research Forecast - Chemistry model (WRF-Chem) respectively. The key objectives of this thesis are outlined below:

**I Review the literature and describe the tools (Ch2 and Ch3)**

i Consolidate current understanding of the DMS-climate cycle at multiple scales

ii Contextualise current DMS-climate modelling with that of aerosol and cloud process uncertainty

iii Summarise current knowledge of the coral reef contribution to the DMS-climate system in order to apply this knowledge to modelling studies

iv Describe the two models and their limitations

**II Evaluate two atmospheric-chemistry models (Ch4 and Ch7)**

i Evaluate the ACCESS-UKCA climate-chemistry model against satellite observations and in the context of other climate models

ii Evaluate the WRF-Chem weather-chemistry model against field and satellite observations

**III Quantify the large-scale sensitivity of DMS within the current climate (Ch5 and Ch7)**

i Comprehensive quantification of the climatic impacts of global DMS beyond the radiative response (i.e. including composition, cloud and precipitation response) and assessment of the sensitivity of ACCESS-UKCA to large changes in DMS

ii Quantification of the impacts of DMS at high time and space resolution for the first time, including assessment of the sensitivity of WRF-Chem to large changes in DMS

**IV Quantify the DMS contribution by coral reefs (Ch3)**

i Using observations from the literature, create a gridded estimate of coral reef-derived DMS to include into a common DMS climatology at both global and regional scales

**V Determine the impact of coral reefs on global composition and climate (Ch6)**

i Assess if the coral reef source of DMS can impact the climate, both compositionally and meteorologically, and at what scale

ii Quantify what the impact on climate may be if mass coral extinction occurred in the current climate

**VI Determine the impact of the Great Barrier Reef on local atmospheric composition and weather (Ch8)**

i Determine if coral reef-derived DMS interacts with local atmospheric composition and meteorology

ii Contextualise these results within current literature and field observations

## 1.3 Contributions to the state of knowledge

By addressing the aims and objectives outlined above, this thesis aims to contribute to DMS, aerosol and atmospheric modelling literature as outlined below:

- The first global estimate of coral reef-derived DMS has been created in this thesis in order to understand the importance of coral reefs for the atmosphere.
- Current coral reef-derived DMS literature is entirely based on observational studies which are unable to capture the full complexity of this system. This thesis is the first atmospheric modelling study to consider the impact of coral reef-derived DMS.
- The original CLAW hypothesis considered a bioregulatory feedback system that occurs over short time scales (days-weeks). No atmospheric modelling study has attempted to quantify the DMS-climate system at this scale. This thesis presents the first regional-local scale study exploring the DMS-climate system and the potential for a bioregulatory feedback.

## 1.4 Structure of thesis

In order to address the research questions and objectives outlined above, the structure of this thesis is outlined below and Figure 1.1 provides a visual overview of the conceptual structure.

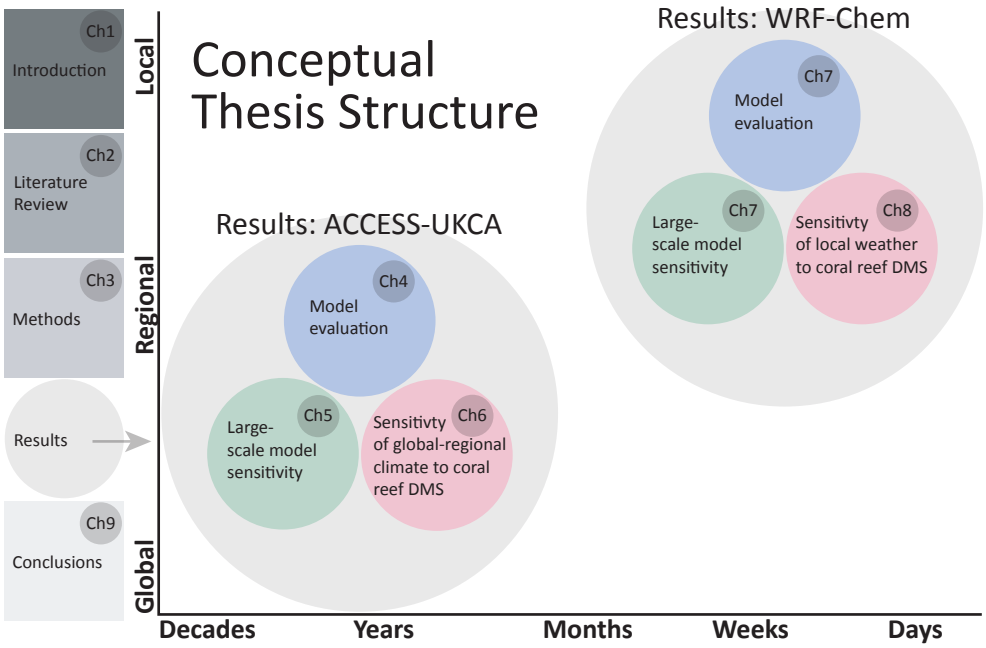


Figure 1.1: The conceptual structure of this thesis showing how the result Chapters aim to address the same objectives over different temporal and spatial scales

### Chapter 2

Chapter 2 presents and reviews the literature relevant to this thesis. It includes an introduction to aerosol-climate processes and uncertainties, the DMS-climate system, a review of global and regional modelling of the DMS-climate system and the current understanding of the contribution and influence of coral reef-derived DMS.

### Chapter 3

Chapter 3 describes the two atmospheric-chemistry models used to quantify the overall aim of this thesis at different temporal and spatial scales. Here, the underlying structure and capabilities of the models are described as well as the relevant input files required for each model, how the experiments for the subsequent chapters are set up and how the model evaluations are performed. Additionally, this Chapter outlines the statistical methods employed in the analysis of the modelling results.

**Chapter 4**

The model evaluation of ACCESS-UKCA is provided in Chapter 4. This evaluation is performed based on satellite observations of cloud, radiation and precipitation fields and puts the biases found in ACCESS-UKCA into context with other GCMs.

**Chapter 5**

Chapter 5 examines the sensitivity of the ACCESS-UKCA model to large-perturbations of global DMS from all marine sources. This Chapter provides an initial understanding of how changes to marine DMS manifests within the climate system of ACCESS-UKCA and to determine what the sensitivity of the ACCESS-UKCA model is to DMS compared to other studies.

**Chapter 6**

In Chapter 6, the importance of coral reef-derived DMS on global and regional atmospheric composition and climate is assessed for the first time. The ACCESS-UKCA climate-chemistry model is run both as a free running ensemble and nudged to reanalysis meteorology in order to help identify direct and indirect aerosol effects.

**Chapter 7**

WRF-Chem is evaluated in Chapter 7 against observations from a recent field campaign over the Great Barrier Reef. In addition, the sensitivity of atmospheric fields in WRF-Chem to a halving of DMS is examined.

**Chapter 8**

In Chapter 8, the influence of coral reef-derived DMS is studied at high temporal and spatial resolutions over the Great Barrier Reef, Queensland, Australia. WRF-Chem is run over three nested domains to ensure the effects of cloud parameterising and cloud resolving scales are represented.

**Chapter 9**

Finally, Chapter 9 summarises the findings of this thesis and relates the results back to the overarching objectives identified above.

# Chapter 2

# Background

This Chapter discusses aspects of the DMS-climate system such as aerosol formation, aerosol-climate interaction, DMS production, chemical life cycle and the uncertainties surrounding these processes. Section 2.1 reviews how aerosol form, grow and interact with the climate system and highlights why aerosol are a considerable source of uncertainty for climate. Section 2.2 considers the role of DMS as a major source of atmospheric sulfur and natural aerosol, as well as how DMS is observed and parameterised. Section 2.2 also discusses how DMS interacts with the climate and presents modelling studies that have aimed to quantify this impact. Finally, Section 2.3 introduces coral reefs as a source of DMS and provides the motivation for the inclusion of coral reef-derived DMS in climate modelling.

## 2.1 Aerosol and the climate system

In this Section, the radiative effects of aerosol are introduced first to establish the importance of aerosol in the climate system (Section 2.1.1). Sources, formation and growth of aerosol are then introduced and key characteristics of certain aerosol are highlighted (Section 2.1.2), in particular sulfate aerosol. Finally, the uncertainties

surrounding aerosol in the climate system are discussed in the context of global climate modelling (Section 2.1.3).

### 2.1.1 Aerosol radiative effects

Aerosol influence the Earth's radiation budget in a number of different ways depending on atmospheric conditions and the composition of the aerosol. These effects are typically split into the 'direct' and 'indirect' effects and are summarised in Figure 2.1. The direct effect occurs when aerosol, such as sulfate aerosol, physically scatters incident solar radiation via Rayleigh or Mie scattering. Scattering of light by particles attenuates incoming solar radiation reaching the surface and hence has a cooling effect (McCormick and Ludwig, 1967). Semi-direct effects also occur when aerosol such as black carbon absorb incoming solar radiation causing a local atmospheric warming effect (Ackerman et al., 2004).

Indirect aerosol effects occur when aerosol interact with cloud processes, subsequently changing cloud properties and energy fluxes throughout the atmosphere. For example, increased aerosol number concentration can in turn increase the cloud condensation nuclei (CCN) and cloud droplet number (CDN) concentration. Increased CDN, with constant liquid water content (LWC), results in smaller cloud droplets, which can influence cloud characteristics such as reflectivity (whiter, higher clouds, Twomey, 1974; Pincus and Baker, 1994) and cloud lifetime (Albrecht, 1989). Increases in cloud albedo and lifetime can cause more solar radiation to be reflected off the cloud tops, also resulting in a cooling effect at the surface. In addition, with increased CDN concentration, greater surface area is available within the cloud onto which water can condense. This can cause drizzle suppression and increases in the LWC of the cloud (Warner, 1968), impacting the hydrological cycle.

As such, direct and indirect effects have a substantial effect on the Earth's

atmosphere through radiation, cloud and precipitation. Importantly, there effects are also dependent on the aerosol composition, where some species are better at scattering or absorbing radiation than others, or are more able to act as nuclei (liquid or ice) than others. For example, a sulfate aerosol is able to scatter light, while black carbon tends to absorb light. An aerosol that made is up of black carbon with a sulfate coating will be less able to absorb or scatter light, demonstrating the importance of aerosol composition understanding.

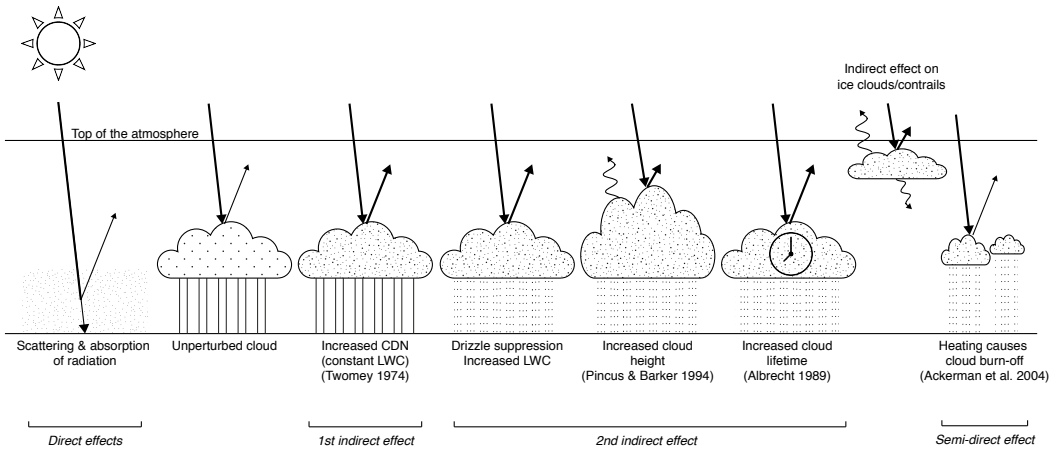


Figure 2.1: Schematic diagram showing the various mechanisms by which aerosol can influence the radiation budget and cloud properties. Straight lines represent the incident and reflected shortwave radiation, and wavy lines represent longwave radiation. The vertical grey dashes represent rainfall. Figure adapted from the 2007 IPCC report (Forster et al., 2007)

### 2.1.2 Aerosol sources, formation and growth

In the atmosphere, primary aerosol are directly emitted from their environment, such as sea salt or dust. Secondary aerosol are formed from precursor gases which then nucleate, for example $H_2SO_4$. Aerosol growth occurs via heterogeneous nucleation, i.e. by condensation onto a pre-existing particle. Alternatively, in sufficiently high atmospheric supersaturation and in the absence of pre-existing surfaces, homogeneous nucleation can occur to form new particles. In the free troposphere, cooler

temperatures, higher supersaturation, and fewer pre-existing particles can provide ideal conditions for aerosol precursor gases to undergo homogeneous nucleation.

In-cloud aqueous-phase oxidation of $SO_2$ is an additional mechanism of aerosol growth, the processes known as cloud processing (shown in Figure 2.2). Once entrained into a cloud, $SO_2$ is dissolved into existing cloud droplets, where it is subsequently oxidised primarily by $O_3$ or $H_2O_2$. This cloud droplet can later be detrained from the cloud and evaporate (alternatively it can be precipitated out). Importantly, coalescence of droplets within the cloud can increase the size of particles while reducing the number, which can have important implications for aerosol characteristics if the cloud evaporates or these droplets are detrained (Feingold et al., 1996).

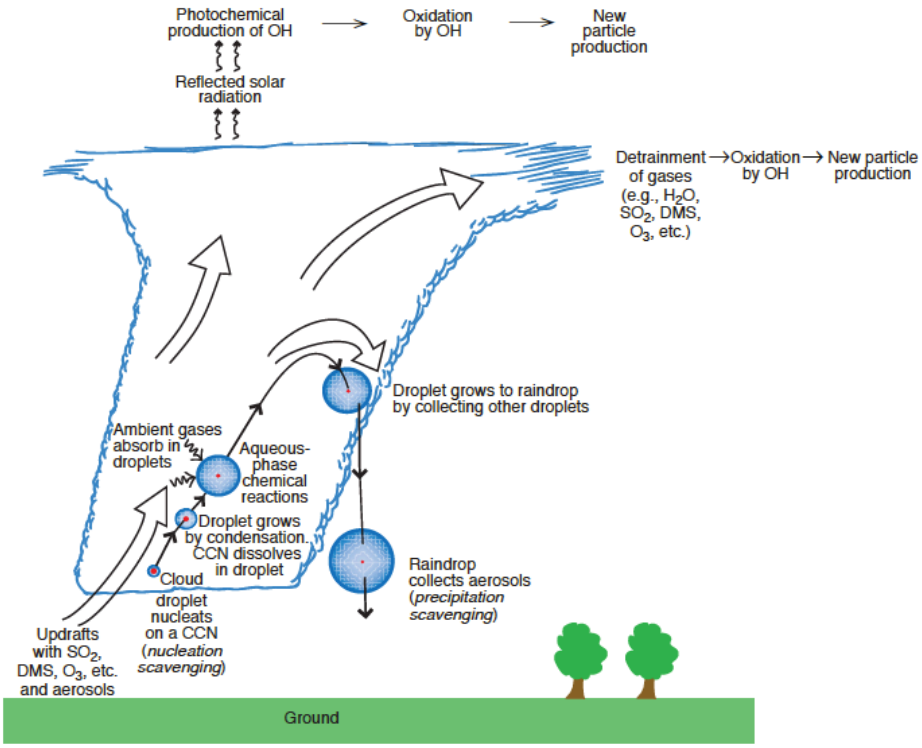


Figure 2.2: Schematic of cloud and precipitation processes that affect the distribution and nature of chemicals in the atmosphere and the chemical compositions of cloud water and precipitation. The broad arrows indicate airflow. Figure from Wallace and Hobbs (2006)

The composition and size of aerosol are important to consider for both optical

properties and cloud-interactions in climate modelling. For example, aerosol activation into cloud droplets depends not only on aerosol concentration, but on its size (foremost) and composition. Primary aerosol can enter the atmosphere at a range of sizes, from tens of nanometers to larger particles of several micrometers. Precursor gases can either grow pre-existing particles at any size (via condensational growth), or, if homogeneous nucleation occurs, will form aerosol of approximately 1-3 nm in size. The size characteristics and typical concentrations of aerosol in the atmosphere occur over four distinct size ranges, known as aerosol modes. From smallest to largest, these modes are called nucleation, Aitken, accumulation and coarse modes. Particle growth (via condensation, coagulation or cloud processes) occurs between these modes. Figure 2.3 provides some approximate size ranges of a number of primary and secondary aerosol and the four aerosol modes.

**Sulfur as a precursor gas**

Sulfate aerosol are produced from sulfur precursor gases, such as $SO_2$ and DMS, and are a key component of the atmospheric aerosol budget. Sulfates make up 22-45% of the aerosol mass fraction over continents and up to 75% over the poles and are dominant at the submicrometre particle size range (Wallace and Hobbs, 2006). Figure 2.4 shows the tropospheric sulfur cycle with estimates of annual emissions (Sheng et al., 2015). Second to volcanic activity, DMS makes up approximately 18-40% of global sulfur emissions (Flato et al., 2013), with DMS flux ($\text{flux}_{\text{DMS}}$) estimates that range from 9-35 $\text{Tg year}^{-1}$ of sulfur (Belviso et al., 2004a; Elliott, 2009; Woodhouse et al., 2010; Tesdal et al., 2016b; Sheng et al., 2015; Flato et al., 2013). These large $\text{flux}_{\text{DMS}}$ ranges present a considerable problem for the quantification of aerosol effects. This problem will be discussed in Section 2.1.3, while uncertainties in DMS will be discussed in further detail in Section 2.2.

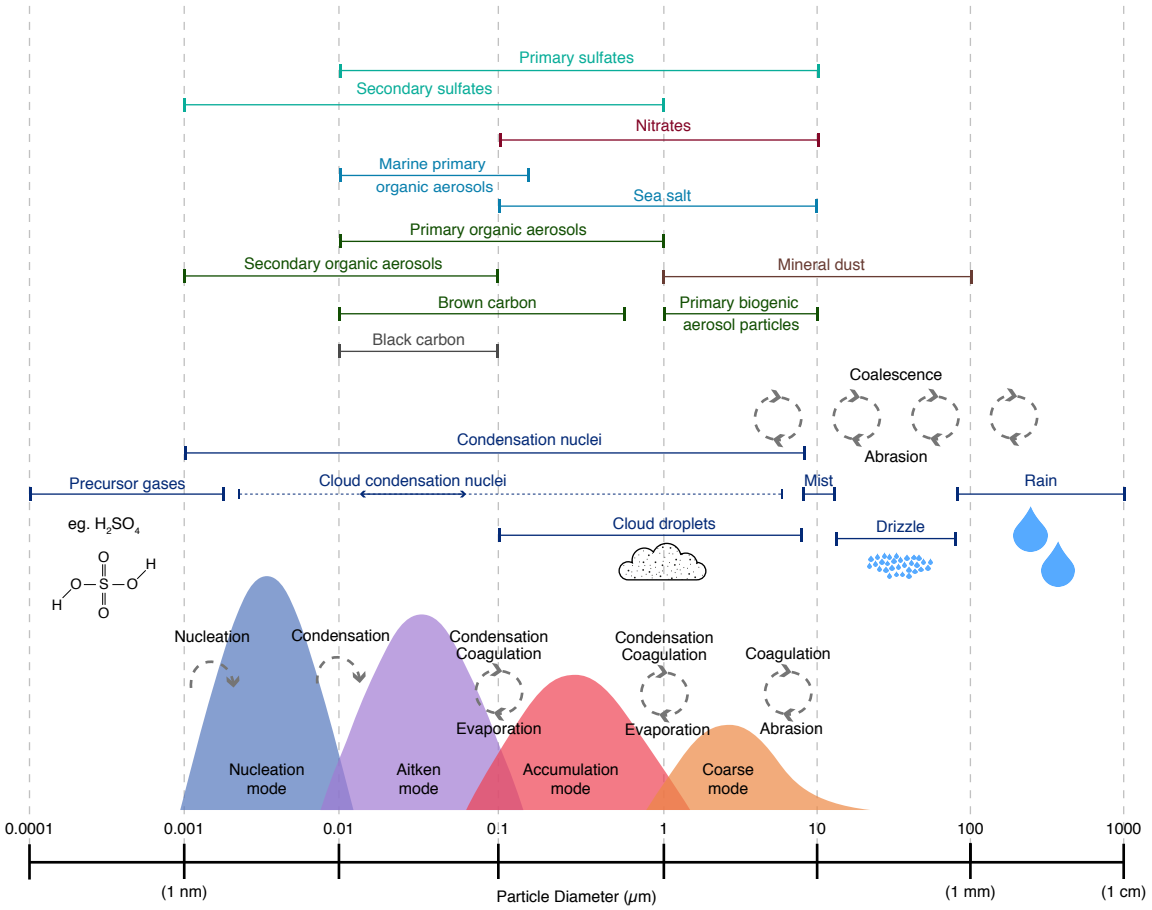


Figure 2.3: Schematic diagram showing the four modes of aerosol size concentration and their growth pathways; the relationship these size distributions have with cloud processes; and examples of approximate size distributions of common aerosol. Figure adapted from Deutscher Wetterdienst (2016) and further data obtained from the IPCC 2013 report (Boucher et al., 2013)

### 2.1.3 Aerosol uncertainty

Aerosol play an important role in the global radiation budget, via the direct and indirect effects described in Section 2.1.1. Total aerosol effective radiative forcing (ERF) was estimated to be -0.9 (-1.9 to -0.1) $\mathrm{W\,m^{-2}}$ by the 2013 IPCC report (Myhre et al., 2013b), substantially offsetting the well mixed greenhouse gases radiative forcing of 2.8 (2.26 to 3.40) $\mathrm{W\,m^{-2}}$ (Myhre et al., 2013b). While the direct aerosol effect can be approximately linearly related to aerosol mass concentration (Myhre et al., 2013a), aerosol-cloud processes, or the secondary aerosol indirect ef-

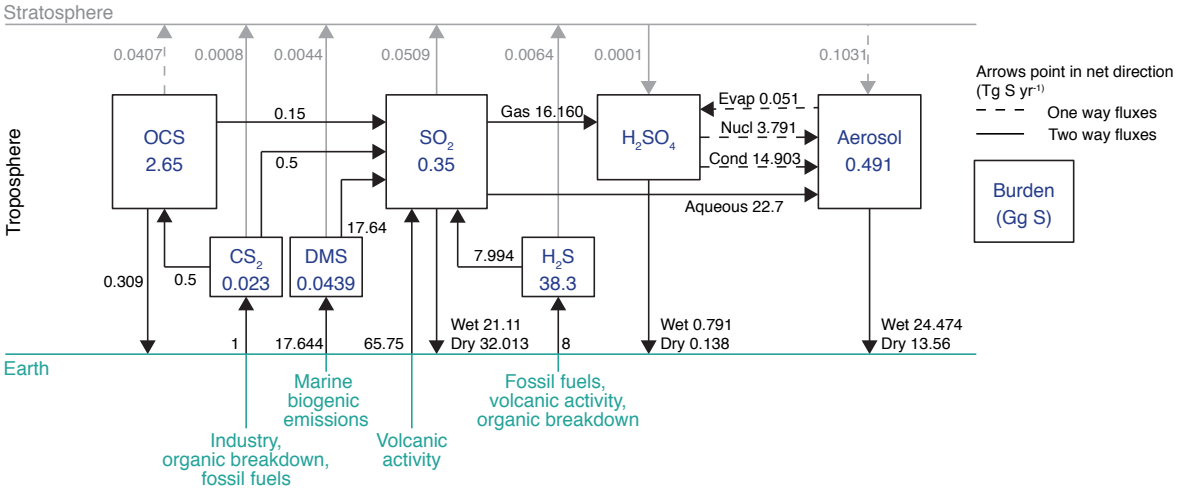


Figure 2.4: Global tropospheric sulfur budget. Solid arrows: net fluxes of surface emissions, cross-tropopause transport, wet/dry deposition, or chemical and microphysical transformations in $\mathrm{Tg\,S\,yr^{-1}}$. Arrows point to net direction. Dashed arrows: one-way fluxes. Boxes: burdens of gases and $H_2SO_4$ aerosol in Gg S. Figure adapted from Sheng et al. (2015)

fects, are highly complex and have larger uncertainties. This is demonstrated by the approximately 20% larger range of ERF values given to the aerosol-cloud interaction (-0.45 (-1.2 to 0.0) $\mathrm{W\,m^{-2}}$) compared to aerosol-radiation interaction (-0.45 (-0.95 to +0.05) $\mathrm{W\,m^{-2}}$) (see Figure 2.5) (Myhre et al., 2013b).

Figure 2.5 shows that the aerosol ERFs are currently the largest source of uncertainty in the overall radiation budget (Myhre et al., 2013b; Carslaw et al., 2013). Natural aerosol sources account for the largest portion of this uncertainty, contributing up to 45% of the variance of aerosol forcing, compared to 34% from anthropogenic aerosol emissions (Carslaw et al., 2013). Flato et al. (2013) highlight the sulfur cycle, including the sources, chemical processing, transport and removal, as major contributors to this uncertainty. These uncertainties due to aerosol emission affect not only the radiation budget, but also chemical and meteorological parameters such as ozone concentration and photolysis (Kushta et al., 2014), cloud formation, albedo, temperature and precipitation (Rosenfeld et al., 2014; Rotstayn et al., 2015;

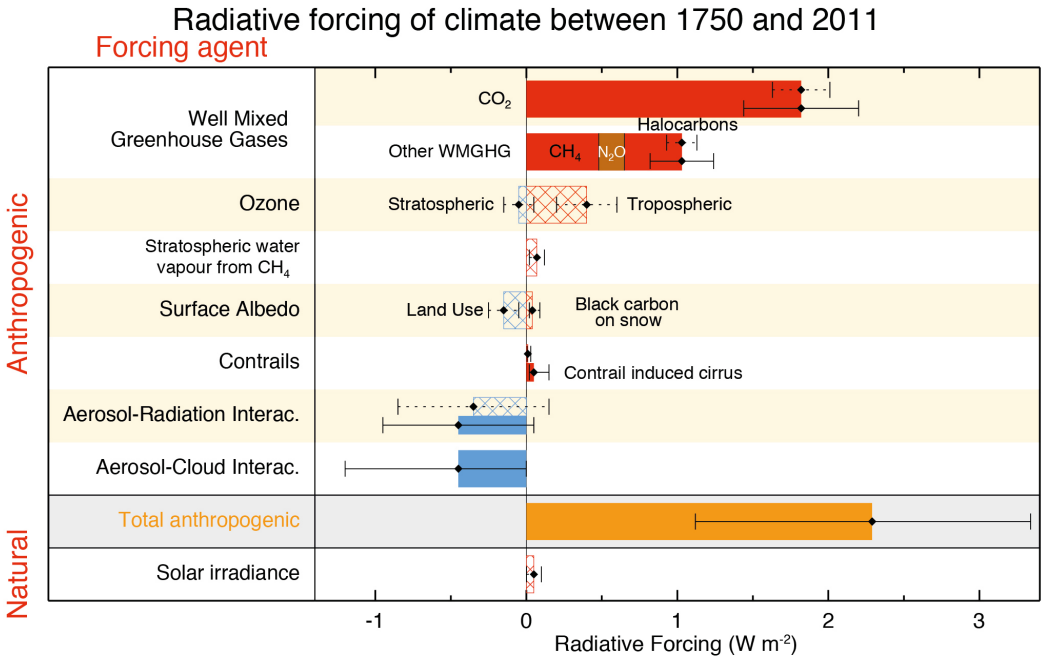


Figure 2.5: Bar chart for radiative forcing (hatched) and effective radiative forcing (solid) for the period 1750-2011. Uncertainties (5 to 95% confidence range) are given for radiative forcing (dotted lines) and effective radiative forcing (solid lines). Figure adapted from the 2013 IPCC report (Myhre et al., 2013b)

Seinfeld et al., 2016).

Whilst aerosol present a challenge for global climate modelling, the broader climate system must also be taken into account. Current climate models have considerable difficulty in simulating clouds and their characteristics, including height, structure, phase (liquid, ice or mixed), etc (Bony and Dufresne, 2005; Cesana and Chepfer, 2012; Nam et al., 2012; Klein et al., 2013; Bodas-Salcedo et al., 2014; Matus and L'Ecuyer, 2017). Large low level cloud biases are found in regions of low level stratiform cloud decks in eastern ocean basins and the Southern Ocean, as well as in convective cloud in tropical regions (and elsewhere) (Cesana and Chepfer, 2012; Nam et al., 2012; Klein et al., 2013). Clouds play a crucial role in regulating the global energy balance via cloud albedo and energy/water transport. The current problems in simulating important cloud characteristics has been found to have large implications for the global radiation budget and cloud feedbacks (Bony

and Dufresne, 2005; Bony et al., 2006; Leon et al., 2009). Many of the processes, including aerosol indirect effects, linking aerosol to cloud and subsequently the radiation budget are only just beginning to be included specifically in global climate models, placing additional difficulty on understanding these complex processes. In this thesis, the modelling limitations surrounding both aerosol and cloud processes are considered.

## 2.2 Dimethyl sulfide

DMS ($(CH_3)_2S$) is an important precursor gas for aerosol formation, coming second only to volcanic activity as a source of natural sulfur (see Figure 2.4). DMS is produced predominantly by marine organisms such as algae, phytoplankton and corals, which are vulnerable to large-scale changes in the climate (discussed in Section 2.2.1). Large uncertainty surrounds not only the amount of DMS released into the ocean (Section 2.2.2) and subsequently the atmosphere each year (Sections 2.2.3 and 2.2.4), but also how DMS influences the current climate. The role of DMS within the climate system has been a source of debate among scientists since the 1980s, specifically around the feedback system proposed by Charlson et al. (1987) (Section 2.2.5). Regardless of this debate, DMS has been identified as an important precursor for natural aerosol with a long-term influence on climate (Section 2.2.6). Numerous global modelling studies have aimed to quantify the large-scale impact of DMS, in particular in a changing climate (Section 2.2.7), however limited modelling research on DMS-climate interaction has been completed at a regional scale (Section 2.2.8).

### 2.2.1 DMS production

DMS is a product of the enzymatic cleavage of dimethyl sulfoniopropionate (DMSP) by catalytic enzymes (DMSP lyases), which are also produced by phytoplankton and bacteria (Stefels et al., 2007; Alcolombri et al., 2015; Curson et al., 2011). DMSP (an osmolyte that helps maintain osmotic pressure Vairavamurthy et al., 1985) is produced by marine organisms via numerous biological and chemical processes at the cellular level (Galí et al., 2018). DMSP production is influenced by light, salinity, temperature and nutrients, as well as being species specific and dependent on overall species health (Simó, 2004; Stefels et al., 2007). Whilst these influences are occurring at the cellular level, they have important implications in understanding and constraining global levels of DMS production.

Changes in the global environment via anthropogenic climate change and natural climate variability have important impacts on the production of DMSP and DMS. Whilst surface warming of the oceans will impact habitable areas, food availability and stratification of the ocean (to name a few), the effect of anthropogenic ocean acidification has received the most attention in the literature with regards to DMS production. Dutkiewicz et al. (2015) show that with increased atmospheric partial pressure of $CO_2$, many species of phytoplankton face extinction, whilst others may migrate and thrive. These varied responses make it difficult to quantify the magnitude and even sign of how DMS production will change with ocean acidification. Elevated $CO_2$ experiments have found that under doubled atmospheric $CO_2$, some phytoplankton produce 24% and 57% less DMSP and DMS respectively (Hopkins et al., 2010). However, more recently Hopkins et al. (2018) report that polar planktonic communities show resilience to ocean acidification. More research, considering different species of plankton and other major DMS producers, is necessary to determine the true impact of anthropogenic climate change on DMS production.

### 2.2.2 DMS in the ocean surface water

The number of surface water DMS ($DMS_w$) observations have increased substantially over the last three decades. However, significant gaps remain both spatially and temporally, which are indicated by the $DMS_w$ observations first described by Kettle et al. (1999) and later updated by Lana et al. (2011), shown in Figure 2.6 where the colours represent the month of observation while the size represents the magnitude. Both temporal and spatial sampling biases exist within this data set, with approximately half the observations collected in late spring through to summer, and more than two-thirds of the data collected in the Northern Hemisphere.

The $DMS_w$ database indicates that high latitude regions have the highest $DMS_w$ concentrations during the respective summer months in regions where high primary productivity exists. In these regions, $DMS_w$ can be of greater than 25 nM and up to as much as 420 nM. Similarly, regions of oceanic upwelling, also associated with increased biological activity, have high $DMS_w$ concentrations. The mean $DMS_w$ concentration, according to the observations making up Figure 2.6 is 4.3 nM with a median of 2.1 nM and a standard deviation of 11.2 nM.

Kettle et al. (1999); Kettle and Andreae (2000) and later updated by Lana et al. (2011), used these observations to derive a gridded global $DMS_w$ climatology, shown in Figure 2.7, via a piecewise cubic Hermite interpolation technique over fifty four well defined biogeographic ocean provinces. It is worth noting that with a three-fold increase in the number of observations used for the Lana et al. (2011) climatology (47,000), compared to the earlier Kettle et al. (1999) climatology (15,000), the estimated global DMS flux ($flux_{DMS}$) increased by approximately 17%.

In the years since the Lana et al. (2011) climatology was produced, many new observations of $DMS_w$ have been made available across the globe. For example, larger concentrations and/or fluxes of DMS than what is currently considered have

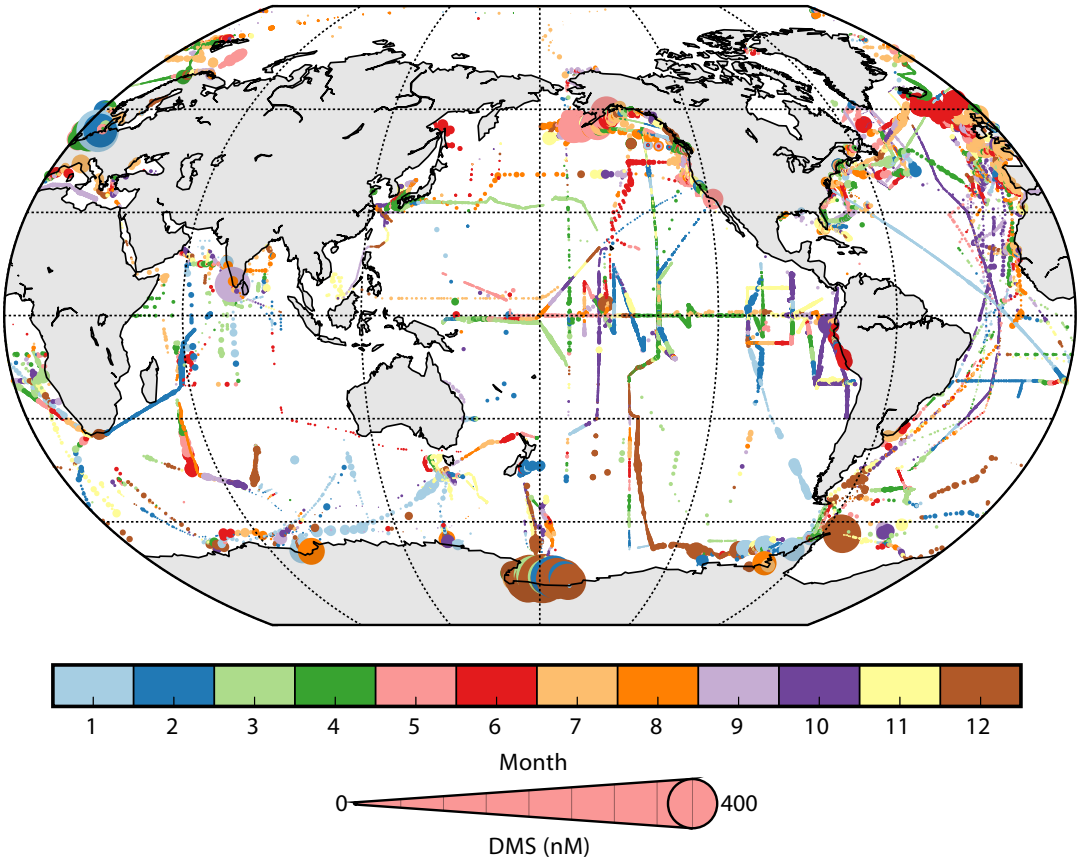


Figure 2.6: The $DMS_w$ observations first collated by Kettle et al. (1999) and updated by Lana et al. (2011) used to develop the $DMS_w$ gridded climatology (L11). The observations are coloured by month of measurement and sized by magnitude

been found at the poles, especially around sea ice and polynyas in both hemispheres (Nomura et al., 2011; Jarnikova and Tortell, 2016; Mungall et al., 2016; Kim et al., 2017; Gabric et al., 2018). Similarly, high measurements of $DMS_w$ have been made over tropical coral reefs in recent years (Broadbent et al., 2002; Broadbent and Jones, 2004; Jones and Trevena, 2005; Jones et al., 2007, 2018; Deschaseaux et al., 2019), which are corroborated by laboratory studies, suggesting that corals and their symbionts produce large amounts of $DMS_w$ (Deschaseaux et al., 2012; Raina et al., 2013; Hopkins et al., 2016). These studies will be discussed in further detail in Section 2.3. These more recent observations suggest it is possible that the current Lana et al. (2011) $DMS_w$ climatology is underestimating the true $DMS_w$ field.

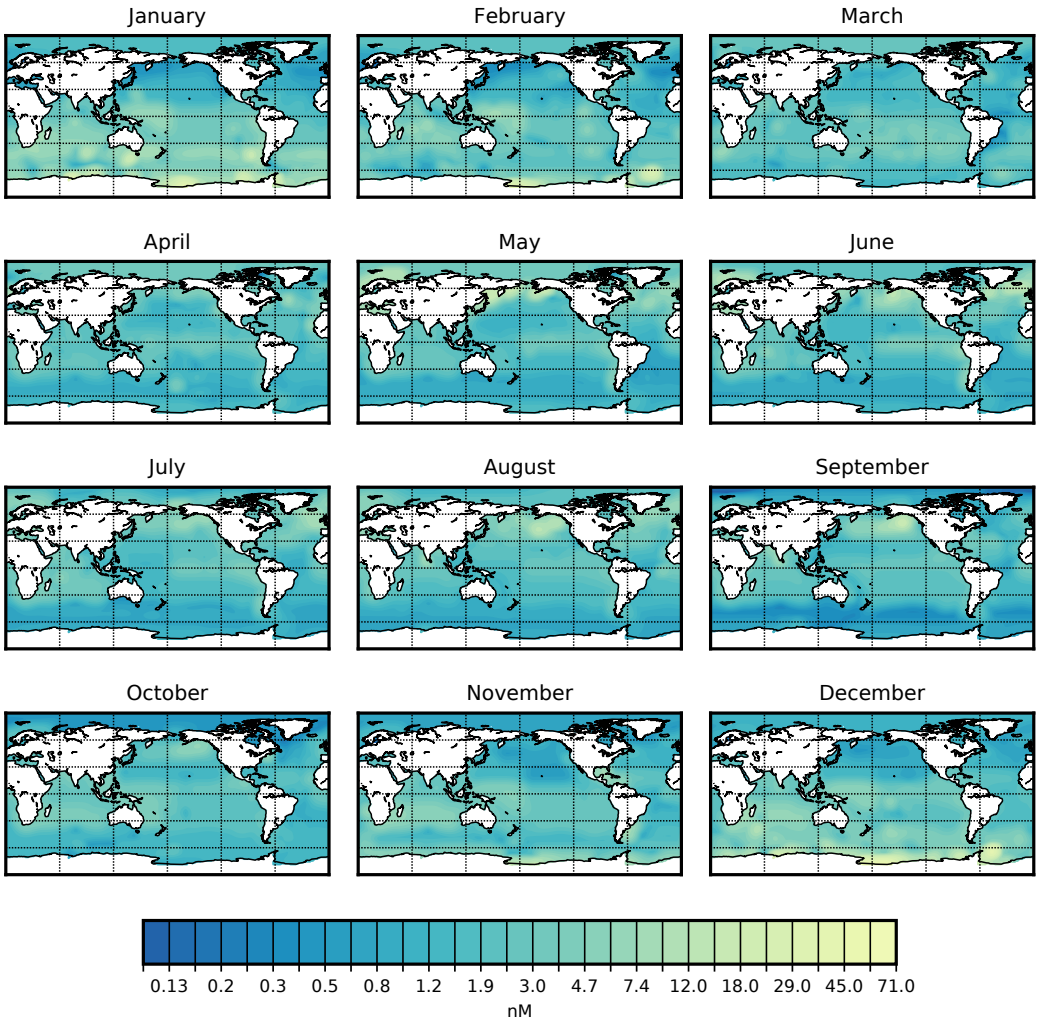


Figure 2.7: The monthly Lana et al. (2011) $DMS_w$ climatology on the original 1x1° grid, used as the benchmark DMS field in this thesis. Note that $DMS_w$ is plotted on a log scale, in nM

In an effort to improve representation of $DMS_w$, a number of studies have parameterised global oceanic $DMS_w$ (or DMSP) concentrations. Methods include using primary productivity, insolation, SSTs, mixed boundary layer depth (oceanic) and other fields as predictors (Anderson et al., 2001; Simó and Dachs, 2002; Belviso et al., 2004b; Galí et al., 2015) with the Lana et al. (2011) or Kettle and Andreae (2000) climatology as a reference. However, numerous issues arise when trying to parameterise oceanic $DMS_w$, including the lack of observations as mentioned, but also that DMS production is species dependent and predictors are not uniformly

relevant across marine biota. Halloran et al. (2010) found that the Anderson et al. (2001) and Simó and Dachs (2002) parameterisations of $DMS_w$ concentrations perform little better than the Kettle and Andreae (2000) climatology when compared to an independent set of observations (observations post 2000).

More recently, Galí et al. (2018) has developed a non-linear parameterisation of $DMS_w$ using satellite estimated DMSP from a previous publication (Galí et al., 2015) and photosynthetically available radiation at the sea surface. Although biases still exist in this study when compared to the Lana et al. (2011) climatology, the authors note that the parameterisation performs with significantly better skill than previous attempts. In light of this, Galí et al. (2018) highlight the need for the climate community to 'move beyond' the fixed monthly climatological representation of $DMS_w$, towards time-varying databases in order to fully capture the importance of this major source of atmospheric sulfur, especially in a changing climate. Gabric et al. (2018) and Hopkins et al. (2016) make similar statements in their respective studies. However, it is noted that parameterisations such as Galí et al. (2018) still do not specifically represent $DMS_w$ from coral reef sources.

### 2.2.3 DMS ocean-atmosphere flux

Stefels et al. (2007) estimate that 10% of $DMS_w$ is released into the atmosphere via sea-air flux. The majority (90%) of DMS in the ocean is removed by bacterial and abiotic processes, including photochemical and biological oxidation as well as biological consumption (Stefels et al., 2007). Sea-air fluxes of DMS ($flux_{DMS}$) are poorly understood, have large variability over space and time and are difficult to measure, subsequently causing large uncertainties in parameterisation (Nightingale et al., 2000; Kloster et al., 2006; Lana et al., 2012; Elliott, 2009; Tesdal et al., 2016b). Parameterisation of $flux_{DMS}$ relies on wind speed, sea surface temperatures and the contrast in DMS concentration between the ocean and atmosphere, allowing a func-

tion of gas exchange to be inferred. A full description of a common parameterisation will be provided at the end of this Section.

Several parameterisations of $\text{flux}_{\text{DMS}}$ exist (eg. Liss and Merlivat, 1986; Wanninkhof, 1992; Nightingale et al., 2000), resulting in a large range of annual global $\text{flux}_{\text{DMS}}$ estimates, for example, 15-35 $\text{Tg}\,\text{year}^{-1}$ of sulfur (Elliott, 2009) or 9-35 $\text{Tg}\,\text{year}^{-1}$ of sulfur (Tesdal et al., 2016b). A summary of the most common $\text{flux}_{\text{DMS}}$ parameterisations, $\text{DMS}_{\text{w}}$ climatologies and the resultant $\text{flux}_{\text{DMS}}$ can be found in Table 2.1 where global flux estimations are compared. Tesdal et al. (2016b), based on an analysis of empirical and prognostic models and observation, recommend a range of 18-24 $\text{Tg}\,\text{year}^{-1}$ of sulfur as a reasonable estimate. Tesdal et al. also note that the global $\text{flux}_{\text{DMS}}$ is primarily dependent on the mean $\text{DMS}_{\text{w}}$ concentrations with spatial variance and the gas exchange coefficient (or the piston velocity - see equations described below) being of secondary importance. Furthermore, Vlahos and Monahan (2009) and Bell et al. (2017) show that current parameterisations overestimate the $\text{flux}_{\text{DMS}}$ at high wind speeds and suggest that annual global $\text{flux}_{\text{DMS}}$ is likely to be in the lower range of current estimates.

Given the large amount of literature evaluating flux sensitivities, no sensitivity tests regarding flux parameterisations were performed for this thesis. The parameterisation used in this project (for both ACCESS-UKCA and WRF-Chem), is the Liss and Merlivat (1986) method and is described in detail below. The Liss and Merlivat (1986) parameterisation is considered a conservative method, inline with the recommendations by Vlahos and Monahan (2009), Tesdal et al. (2016b) and Bell et al. (2017).

Table 2.1: Global $\text{flux}_{\text{DMS}}$ (in $\text{Tg}\,\text{year}^{-1}$ of Sulfur) as reported by the literature, including the $\text{flux}_{\text{DMS}}$ parameterisation and $\text{DMS}_{\text{w}}$ climatology. Note the $\text{flux}_{\text{DMS}}$ is dependent on wind-speeds, so numbers can vary between studies

| Study | $\text{Flux}_{\text{DMS}}$ parameterisation | $\text{DMS}_{\text{w}}$ climatology | $\text{Flux}_{\text{DMS}}$ |
|---|---|---|---|
| Kettle and Andreae (2000) | Liss and Merlivat (1986) | Kettle and Andreae (2000)$^{m}$ | 15.3 |
| Kettle and Andreae (2000) | Wanninkhof (1992) | Kettle and Andreae (2000)$^{m}$ | 32.6 |
| Kettle and Andreae (2000) | Erickson (1993) | Kettle and Andreae (2000)$^{m}$ | 21.8 |
| Anderson et al. (2001) | Wanninkhof (1992) | Anderson et al. (2001)$^{p}$ | 32.4 |
| Anderson et al. (2001) | Nightingale et al. (2000) | Anderson et al. (2001)$^{p}$ | 27.6 |
| Simó and Dachs (2002) | Liss and Merlivat (1986) | Simó and Dachs (2002)$^{p}$ | 17 |
| Simó and Dachs (2002) | Wanninkhof (1992) | Simó and Dachs (2002)$^{p}$ | 34.6 |
| Simó and Dachs (2002) | Nightingale et al. (2000) | Simó and Dachs (2002)$^{p}$ | 23.3 |
| Kloster et al. (2006) | Wanninkhof (1992) | Kloster et al. (2006)$^{b}$ | 28 |
| Elliott (2009) | Liss and Merlivat (1986) | Elliott (2009)$^{b}$ | 16.8 |
| Elliott (2009) | Wanninkhof (1992) | Elliott (2009)$^{b}$ | 29.3 |
| Elliott (2009) | Nightingale et al. (2000) | Elliott (2009)$^{b}$ | 23.6 |
| Elliott (2009) | Elliott (2009) | Elliott (2009)$^{b}$ | 17.3 |
| Vogt et al. (2010) | Wanninkhof (1992) | Vogt et al. (2010)$^{b}$ | 24 |
| Lana et al. (2011) | Liss and Merlivat (1986) | Kettle and Andreae (2000)$^{m}$ | 15 |
| Lana et al. (2011) | Wanninkhof (1992) | Kettle and Andreae (2000)$^{m}$ | 29.4 |
| Lana et al. (2011) | Nightingale et al. (2000) | Kettle and Andreae (2000)$^{m}$ | 24 |
| Lana et al. (2011) | Liss and Merlivat (1986) | Lana et al. (2011)$^{m}$ | 17.6 |
| Lana et al. (2011) | Wanninkhof (1992) | Lana et al. (2011)$^{m}$ | 34.4 |
| Lana et al. (2011) | Nightingale et al. (2000) | Lana et al. (2011)$^{m}$ | 28.1 |
| Tesdal et al. (2016a) | Nightingale et al. (2000) | Lana et al. (2011)$^{m}$ | 28.9 |
| Tesdal et al. (2016a) | Nightingale et al. (2000) | Kettle et al. (1999)$^{m}$ | 25.9 |
| Tesdal et al. (2016a) | Nightingale et al. (2000) | Kettle and Andreae (2000)$^{m}$ | 24.7 |
| Average | | | 24.8 |

$^{b}$ denotes a DMS climatology modelled using a biogeochemistry model
$^{p}$ denotes a parameterised DMS climatology
$^{m}$ denotes a DMS climatology generated from direct measurements

**Liss and Merlivat (1986) flux parameterisation**

$$flux_{\mathrm{DMS}} = k\left(DMS_{\mathrm{w}} - \frac{DMS_{\mathrm{a}}}{\alpha}\right) \tag{2.1}$$

$$DMS_{\mathrm{a}} \rightarrow 0 \tag{2.2}$$

$$flux_{\mathrm{DMS}} = kDMS_{\mathrm{w}} \tag{2.3}$$

For:

$$w_{10} < 3.6\mathrm{m\,s^{-1}} : k = 0.17w_{10}\left(\frac{\mathrm{SC_{DMS}}}{600}\right)^{\frac{2}{3}} \tag{2.4}$$

$$3.6\mathrm{m\,s^{-1}} < w_{10} < 13\mathrm{m\,s^{-1}} : k = (2.85w_{10} - 9.65)\left(\frac{\mathrm{SC_{DMS}}}{600}\right)^{\frac{1}{2}} \tag{2.5}$$

$$w_{10} > 13\mathrm{m\,s^{-1}} : k = (5.9w_{10} - 49.3)\left(\frac{\mathrm{SC_{DMS}}}{600}\right)^{\frac{1}{2}} \tag{2.6}$$

$$\mathrm{SC_{DMS}} = 2674.0 - (147.12 \times T) + (3.726 \times T^2) - (0.038 \times T^3) \tag{2.7}$$

$$\alpha = e^{-10.1794+3761.33\times\frac{1}{T}} \tag{2.8}$$

The Liss and Merlivat (1986) $\mathrm{flux_{DMS}}$ parameterisation is described in Eq. 2.1 where $k$, the piston velocity, is parameterised under three wind induced sea surface regimes: smooth (Eq. 2.4) and rough (Eq. 2.5) gas transfer, and a wave breaking/bubble-bursting regime (Eq. 2.6). $\alpha$ is calculated by Equation 2.8, according to Dacey et al. (1984), $w_{10}$ = 10 m wind speed ($\mathrm{m\,s^{-1}}$). It is assumed that the concentration of $\mathrm{DMS_a}$ is negligible, as it is orders of magnitude smaller than that of seawater. The Schmidt Number of DMS ($\mathrm{SC_{DMS}}$), a measure of viscosity/diffusion and a function of sea surface temperature, is determined following the Saltzman et al. (1993) method and is shown in Equation 2.7, where $T$=SST. The

denominator in this function is the Schmidt Number of $CO_2$ in fresh water at 20 °C, $SC_{CO_2} = 600$, which is used to normalise the numerator ($SC_{DMS}$).

### 2.2.4 DMS in the atmosphere

Once DMS is released into the atmosphere, its oxidative pathway is a further source of uncertainty (von Glasow and Crutzen, 2010). Primarily, atmospheric DMS ($DMS_a$) is oxidised by hydroxyl (OH) and nitrate ($NO_3$) radicals, leading to the production of methane sulfonic acid (MSA) and $SO_2$, which then oxidise further into $H_2SO_4$. The dominant chemical reactions of $DMS_a$ are shown schematically in Figure 2.8. Studies have noted that ozone and halogen oxide radicals, as well molecular chlorine also react with $DMS_a$ (Boucher et al., 2002; Kloster et al., 2006; Khan et al., 2016), which are currently difficult to quantify and often not considered in modelling studies. von Glasow and Crutzen (2010) and Khan et al. (2016) have shown that inclusion of halogen chemistry increases $DMS_a$ oxidation rates, reducing $DMS_a$ lifetime, the efficiency of the conversion of DMS to $SO_2$ and thereby, the global sulfur burden. In addition, von Glasow and Crutzen (2010) show that conversion efficiency of $DMS_a$ to $SO_2$ is significantly reduced under cloudy conditions, impacting cloud droplet number and cloud albedo in stratiform clouds. $DMS_a$ has an atmospheric lifetime of approximately 1-2 days (Korhonen et al., 2008; Kloster et al., 2006; Khan et al., 2016). After oxidation into $H_2SO_4$, aerosol formation can occur via heterogeneous or homogeneous nucleation as discussed in Section 2.1.

### 2.2.5 The Charlson, Lovelock, Andreae and Warren (CLAW) hypothesis

The importance of DMS in the natural sulfur cycle was first proposed by Lovelock et al. (1972) after the sulfur budget was unable to be balanced and observations of

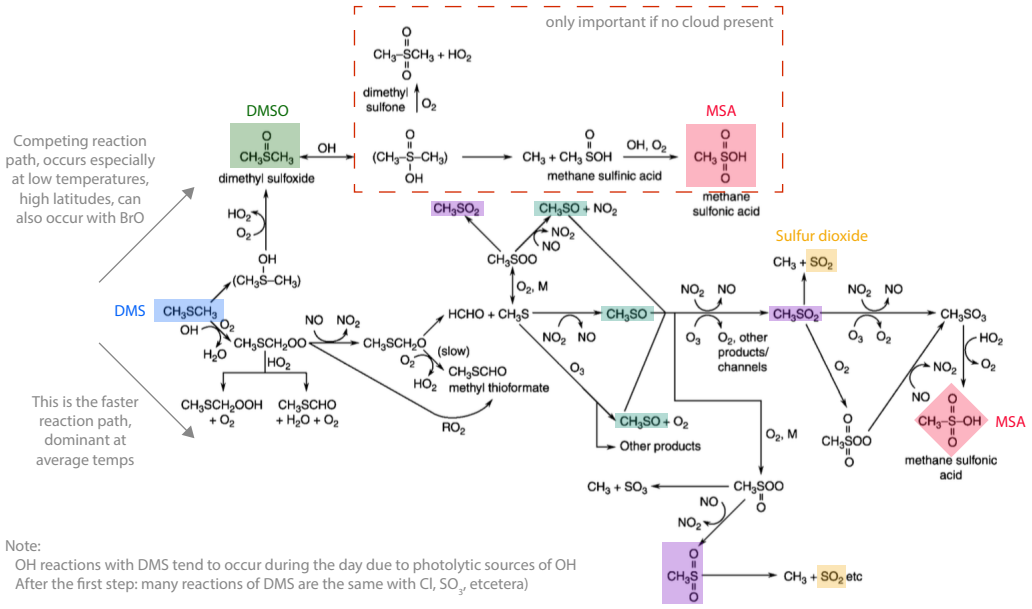


Figure 2.8: The oxidation of DMS by OH. Figure adapted from Finlayson-Pitts and Pitts (2000) and von Glasow and Crutzen (2010)

large-scale biological DMS production became available. As further measurements were made connecting DMS to marine algae (Bigg and Turvey, 1978) and to sulfate aerosol (Parungo et al., 1986), it was suggested that oceanic DMS could be responsible for up to 30% of the sulfur budget (Nguyen et al., 1978). Shaw (1983) hypothesised that the sulfur cycle could be a more effective form of biothermostasis than that of the carbon cycle as suggested by Lovelock and Whitfield (1982), in response to the Gaia theory (Lovelock and Margulis, 1974).

The CLAW hypothesis builds upon Shaw's (1983) work, bringing with it the evidence that Shaw lacked (Charlson et al., 1987). The hypothesis relies on three key assumptions:

- Most species of phytoplankton excrete DMS, which is later oxidized in the atmosphere to form MSA or sulfate aerosol

- These non-sea-salt (NSS) sulfate aerosol are found throughout the marine boundary layer (MBL)

- Aerosol that act as CCN are perhaps almost exclusively NSS-sulfate aerosol.

From this, the CLAW hypothesis was proposed as follows (see Figure 2.9): marine plankton produce significant amounts of DMS; plankton are affected by sea surface temperatures (SSTs) and sunlight. DMS, when released into the atmosphere, affects cloud albedo via the formation of CCN from sulfate aerosol. This in turn influences the temperature and sunlight at the surface, thus setting up a mechanism by which marine plankton, in producing DMS, can influence their environment.

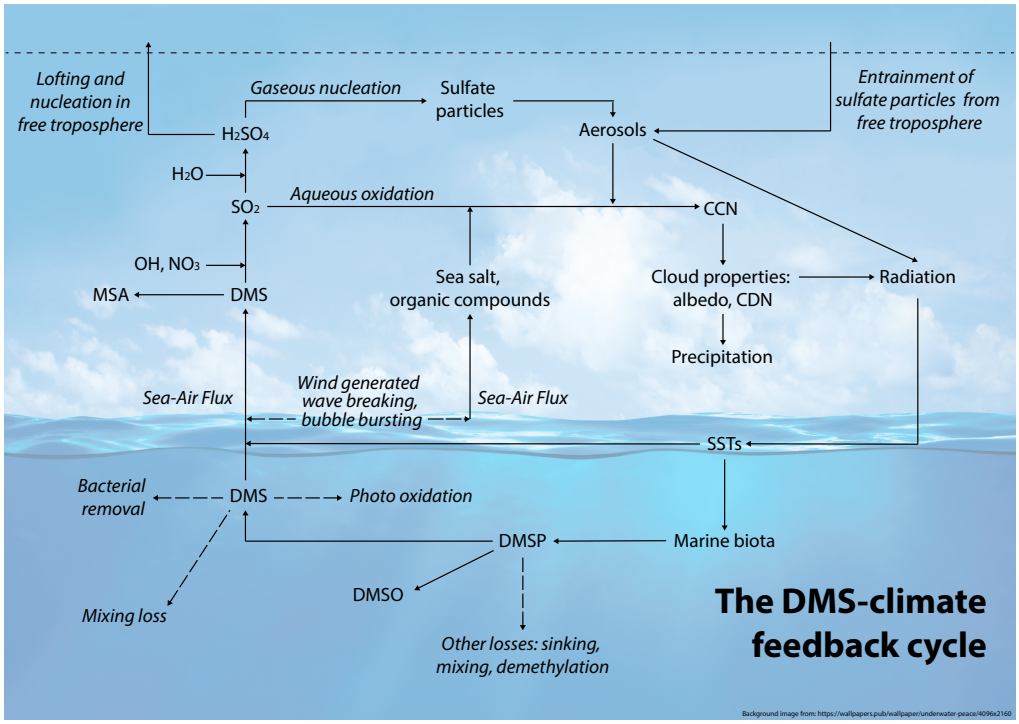


Figure 2.9: Schematic diagram showing the ocean-atmosphere DMS life cycle and climate-relevant processes

### 2.2.6 Evidence of the influence of DMS on the climate system

The primary evidence for the DMS-sulfur feedback presented by Shaw (1983) was based on the assumption that most sulfur derived aerosol were of the size 0.1 $\mu$m, believed at the time to be the most effective particle size for solar radiation scattering (direct effect). The most effective particle size for solar radiation scattering was later found to be 0.08-1 $\mu$m (Murphy, 1998). Furthermore, understanding of the contribution of sea-salt aerosol at this point was poor, and was unaccounted for in Shaw's (1983) theory. Charlson et al. (1987) later assumed that NSS-sulfate made up the majority of MBL CCN, dismissing sea salt as a major source of CCN due to low concentrations at marine cloud height. However, the authors conceded that the role of DMS in CCN formation was poorly understood (Charlson et al., 1987). More recent research has found that these assumptions are incorrect and that the DMS-CCN picture is much more complex (Quinn and Bates, 2011; Green and Hatton, 2014).

Despite sulfates dominating submicrometer particle number concentrations, particle number concentration and CCN variability is difficult to attribute to sulfates in the remote or coastal MBL. Understanding is further limited due to the very few observations of sulfate particle formation (homogeneous nucleation) in the MBL (Ayers et al., 1991; Modini et al., 2009; Humphries et al., 2015). However, studies have shown that CCN variability cannot be fully explained without the inclusion of DMS, especially in the mid-latitudes (Korhonen et al., 2008) and Southern Ocean (Vallina et al., 2006). Modelling shows that the standard deviation of CCN in response to changing $\text{flux}_{\text{DMS}}$ (of -50 to +100%) is 44% higher under pre-industrial conditions than today, implying difficulty in capturing the true nature of DMS forced climate variability in today's polluted conditions (Carslaw et al., 2013). Somewhat understandably then, Woodhouse et al. (2010) and Woodhouse et al. (2013) find

very little change in CCN concentrations in relation to changes in global $\text{flux}_{\text{DMS}}$ or to small regional perturbations in $\text{DMS}_{\text{w}}$ in today's climate.

Sea salt and organic aerosol are important and dominant particles for aerosol and CCN formation in clean marine air providing an important reaction site for heterogeneous nucleation of precursor gases (Murphy, 1998; O'Dowd et al., 2004; Leck and Bigg, 2005; Bigg, 2007; Twohy and Anderson, 2008). Sea salt particle concentrations are logarithmically related to wind speed (O'Dowd et al., 1993), and are large enough to act as CCN with little additional growth required. Consequently, when sea salt particles dominate the MBL, Quinn and Bates (2011) argue that $\text{DMS}_{\text{a}}$ has little impact on CCN concentrations, although it remains difficult to separate the contribution of sea salt and sulfate to CCN formation. However, in later research, Quinn et al. (2017) found that sea spray aerosol make up approximately 30% of CCN over the majority of the world's oceans, with the majority of aerosol made up from NSS aerosol, attributed in part to entrainment from the free troposphere. Entrainment of sulfate aerosol nucleated in the free troposphere can account for 43-65% of summer time remote Southern Hemispheric CCN concentrations, reduced to 7-20% in the winter time (Korhonen et al., 2008). The importance of entrainment from the free troposphere implies DMS derived aerosol can have far reaching impacts, not just at the local scale, as suggested by Raes (1995).

In summary, current understanding of the DMS-climate system implies that no bio-regulatory feedback exists as proposed by the CLAW hypothesis (Quinn and Bates, 2011; Woodhouse et al., 2013). However, observations show that seasonal CCN variability cannot be explained without a contribution from DMS (Korhonen et al., 2008; Vallina et al., 2006), implying DMS is important for global and local climate (Green and Hatton, 2014). Complicating this problem is our limited understanding of the global distribution of DMS, as well as the difficulty in separating the influence of of sea salt and organic matter aerosol from NSS sulfate aerosol within

the MBL. Green and Hatton (2014) suggest that the original CLAW hypothesis oversimplifies a complex process and must be rejected in its original form. However, Green and Hatton allow that marine biogenic activity nevertheless has an influence on the long-term climate and suggest that a revised theory taking into account our greater understanding of the system and all of its complexity may be of merit.

### 2.2.7 Global DMS-climate modelling

The importance of DMS in large-scale climate has been examined by numerous global modelling studies. Mahajan et al. (2015) (using the Lana et al., 2011, $DMS_w$ climatology) and Thomas et al. (2010) (using the Kettle et al., 1999, $DMS_w$ climatology) found DMS to have a radiative effect of -1.79 $W\,m^{-2}$ and -2.03 $W\,m^{-2}$ at the top of the atmosphere (TOA) respectively. Thomas et al. (2011) doubled $DMS_w$ concentrations, finding a TOA radiative effect of -3.42 $W\,m^{-2}$. These studies perturbed DMS in the climate system in order to quantify the effect on climate, and noted that the largest changes in radiation and cloud microphysics occurred in the Southern Ocean and southern Pacific and Indian Oceans.

Other modelling studies have explored the impact of anthropogenic climate change on marine DMS production, often with contradictory conclusions, making it unclear whether marine DMS production would increase or decrease with warming temperatures (e.g. Bopp et al., 2004; Gabric et al., 2004; Kloster et al., 2007; Cameron-Smith et al., 2011). Six et al. (2013) found DMS emissions were reduced by 17% by the end of the century, primarily due to decreasing ocean pH caused by rising anthropogenic $CO_2$ emissions. The reduced $flux_{DMS}$ was found to cause an additional 0.23-0.48 K of warming by the end of the century (Six et al., 2013). Reduced $flux_{DMS}$ due to ocean acidification was also modelled by Schwinger et al. (2017), who found under the Representative Concentration Pathway (RCP) 8.5 to the year 2200, DMS production decreases by 48% assuming a strong sensitivity of

DMS production to changes in pH. Schwinger et al. (2017) calculated a temperature sensitivity to DMS of -0.041 K per $\mathrm{Tg\,year^{-1}}$ of sulfur. It is noted that RCP 8.5 is a high-emissions, business as usual scenario, along which the society is currently tracking, and will likely continue to unless drastic mitigation is undertaken.

Grandey and Wang (2015) attempted to determine if a significant artificial increase of marine DMS production (due to, for example, ocean fertilisation or significant aquaculture) in the oceanic ecosystem could offset future warming trends. Under a scenario where $\mathrm{flux_{DMS}}$ is increased to 46.1 $\mathrm{Tg\,year^{-1}}$ of sulfur, Grandey and Wang found global temperature increases due to anthropogenic climate change under RCP 4.5 were partially offset, primarily due to low and mid-level cloud feedbacks, resulting in a radiative flux perturbation of -2.0 $\mathrm{W\,m^{-2}}$. Regional changes in precipitation of both signs were also noted, up to as much as 30%.

Many DMS-climate modelling studies consider DMS under future scenarios (Bopp et al., 2004; Gabric et al., 2004; Kloster et al., 2007; Cameron-Smith et al., 2011; Six et al., 2013; Grandey and Wang, 2015; Schwinger et al., 2017). However, it is clear that our understanding of DMS in the current climate is not yet fully established, considering both modelling and observational uncertainties. Studies exploring DMS changes under current climate conditions (Thomas et al., 2010; Woodhouse et al., 2010; Gabric et al., 2013; Mahajan et al., 2015) have completed short simulations (at approximately one year are too short to be indicative of a true climatological response), use simplified climate models (without detailed chemistry) or chemical transport models (which cannot provide climate response information). Furthermore, uncertainties related to DMS emission and fate in the atmosphere are not the only barriers to the DMS-climate question. Climate model uncertainties and biases, such as those surrounding aerosol-cloud interactions discussed in Section 2.1.3, should be considered, yet have not been previously.

### 2.2.8 Regional DMS-climate modelling

While there have been numerous studies quantifying the global influence of DMS on climate (as discussed above), this is not the case for impacts of DMS on regional climate. Regional modelling studies specifically targeting DMS in the atmosphere and its interactions with local weather and climate are very limited. DMS has been included in regional climate modelling through models such as WRF-Chem, since the early 2000s with the incorporation of the Georgia Tech/Goddard Global Ozone Chemistry Aerosol Radiation and Transport (GOCART) model (Chin et al., 2000). GOCART (and later schemes) uses the (Kettle et al., 1999) $DMS_w$ concentrations and the Liss and Merlivat (1986) flux parameterisation. With this availability, DMS is often included in regional climate simulations using WRF-Chem as a simple option to switch on or off. However DMS is rarely the field of interest, with little attention being paid to the effects of DMS on the climate, let alone an evaluation of the model's performance. This gap in research is concerning given that DMS has been found in observational studies to explain a significant part of aerosol variability in clean marine areas (see Section 2.2.6). Additionally, some high resolution models are cloud-resolving, hence have the possibility to quantify the DMS-climate system in a different way to what has currently been done.

One exception is the major campaign VAMOS (Variability of the American Monsoon Systems) Ocean-Cloud-Atmosphere-Land Study Regional Experiment (VOCALS-REx), which took a large range of measurements in the Southeast Pacific stratocumulous deck (off the coast of Chile and Peru) and later compared these to modelling. VOCALS-REx had two main themes to explore: i) links between aerosol, clouds, precipitation and radiative properties within marine stratocumulous decks; and ii) how the coupling between the ocean-atmosphere can affect the above atmospheric properties (Wood et al., 2011). Whilst DMS was not the main focus, Yang et al. (2011) and Saide et al. (2012) provide two of the few regional scale mod-

elling studies to evaluate DMS in WRF-Chem (V3.3) relative to observations. Both these studies suggest that the $flux_{DMS}$ is overestimated in the model when compared to ship based measurements. Yang et al. (2011) used a simplified Nightingale et al. (2000) parameterisation producing a much larger $flux_{DMS}$ than Saide et al. (2012), who used the Liss and Merlivat (1986) parameterisation. The overestimation of the $flux_{DMS}$ was further reflected in $DMS_a$ concentrations. Whilst these overestimations of $flux_{DMS}$ were considerable, both Yang et al. and Saide et al.'s focus was not on sensitivity testing of DMS (rather on other model features), and hence both studies stop short of evaluating how DMS alone may affect aerosol-cloud interaction.

More recently, Muñiz-Unamunzaga et al. (2018) show the importance of including marine halogens and DMS on air quality monitoring for large coastal cities (in this case, Los Angeles). Using the Community Multiscale Air Quality (CMAQ) chemical transport model, with meteorology driven by WRF (V3.7), the authors note that these inclusions can decrease ozone and nitrogen dioxide levels and can cause large changes in oxidants (OH, $HO_2$ and $NO_3$) and the composition of particulate matter. Studies such as this highlight the importance of DMS not only on clean marine areas, such as those explored in VOCALS-REx, but also in more polluted urban environments. However, Muñiz-Unamunzaga et al. (2018) provide no evaluation of the impact of DMS on the local climate.

In this thesis, the sensitivity of the Queensland climate to DMS, as simulated by the WRF-Chem model, is tested and evaluated against ship based observations. In Chapter 7 it is noted that due to a lack of research, the default WRF-Chem-$DMS_w$ field is not up to date (using the Kettle and Andreae (2000) climatology), with implications for studies that include DMS chemistry.

## 2.3 Coral reefs and DMS

Coral reefs have been found to produce large amounts of DMS, comparable to regions of high primary productivity. The coral reef source of DMS has not been included in modelling studies to date. With coral reefs globally under significant threat due to anthropogenic climate change (discussed in Section 2.3.1), how this loss of aerosol will affect the climate system is currently unknown. In the last two decades, numerous observational (field and laboratory) studies have identified corals as an important source of DMS (Section 2.3.2). A number of studies have also tried to link coral reef-derived aerosol to aerosol and cloud formation locally (Section 2.3.3). However, as described in Sections 2.1 and 2.2, this is a complex system and observational results alone may not be able to provide conclusive evidence of such interaction. For this reason, this thesis combines specific field campaign data (Section 2.3.4) with modelling studies to better understand the system.

### 2.3.1 Coral reefs

Warm water coral reefs, although making up only 0.1% of the Earth's surface (just 284,300 $km^2$) in today's climate (Figure 2.10), are the most biodiverse marine habitats per unit area and are estimated to support between 0.6 - 9 million species (Plaisance et al., 2011). Coral reefs also provide numerous benefits to human society, both economically and culturally. A valuation of Australia's GBR, a UNESCO Wonder of the World, suggested its economic, social and icon asset value sat at $AUD56 ($US40) billion in 2017 (Deloitte Access Economics, 2017). The GBR was found to support 64,000 jobs directly and indirectly and contribute $AUD6.4 ($US4.5) billion to Australia's economy in 2015/2016 via tourism, commercial fishing and aquaculture, recreational activity and scientific research and management. Spalding et al. (2017), in a more direct valuation of on reef or reef adjacent ac-

tivities only, estimate the economic value of global coral reefs to be worth $US36 ($AUD51) billion. Despite the estimated economic value of global coral reefs and their ecological and social importance, their very existence is under threat.

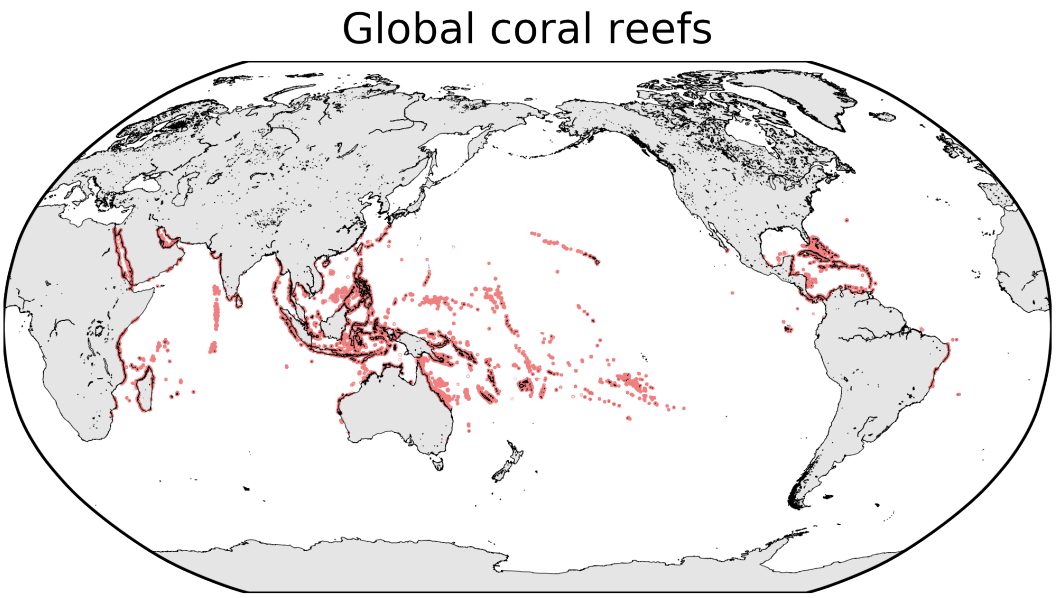


Figure 2.10: Map of the global warm water coral reef distribution provided by UNEP-WCMC et al. (2010)

Globally, coral reef ecosystems are facing dire risk due to anthropogenic climate change (Hughes et al., 2017, 2018). The IPCC special report on climate change (IPCC, 2018) states with 1.5 °C global mean warming, 70-90% of coral reefs will be extinct. The climate risk to coral reefs is multifaceted including increased sea surface temperatures causing more frequent mass coral bleaching events (Hughes et al., 2017; King et al., 2017) and increased ocean acidification causing decreasing calcification and growth of coral species (Hoegh-Guldberg et al., 2017; Magnan et al., 2016). In addition, changing weather patterns, sea level rise and modified coastal habitats are identified as severe risks (Great Barrier Reef Marine Park Authority, 2014). In July 2019 the GBR Marine Park Authority declared climate change to be the greatest threat to the GBR (Great Barrier Reef Marine Park Authority, 2019). Coastal development, land use-runoff, invasive species and over/illegal fishing also

pose severe risk to marine ecosystems (Great Barrier Reef Marine Park Authority, 2014). Whilst the extinction of global coral reefs due to anthropogenic climate change will have clear impacts on the ecosystems and economies they support, a lesser known, and as of yet unquantified, impact is upon the climate itself.

### 2.3.2 Coral reef-derived DMS observations

Since the 2000s, numerous studies, both in situ and in the laboratory, have shown that corals, coral symbionts, coral by-products (eg. mucus and mucus ropes - stringy lines of mucus separating from coral) and coral carbonate sediments in the GBR also produce large amounts of DMSP and DMS (Broadbent et al., 2002; Broadbent and Jones, 2004; Jones and Trevena, 2005; Jones et al., 2007; Deschaseaux et al., 2019). Many of these studies suggest that the contribution of DMS from coral reefs is a significant and yet unaccounted for source of marine aerosol, and may have some climatic relevance. A summary of these findings in the literature is provided in Table 2.2 (in-situ measurements) and 2.3 (laboratory or controlled measurements including bubble chambers, benthic chambers on the sea bed and samples taken from in-situ coral reefs, eg - mucas ropes). From field measurements, an average of 3 nM of $DMS_w$ is found, varying from non-detectable limits to 54 nM. It can be seen that measurements from ship campaigns tend to be lower than measurements taken directly over coral reefs, as noted in Jones et al. (2018). For $DMS_a$, an average of 2.2 $nmol\,m^{-3}$ ranging from non-detectable to 45.9 $nmol\,m^{-3}$ is found.

Of note to this thesis, Jones et al. (2018) recently summarised reports of $flux_{DMS}$ values of 0-153 $\mu mol\,m^{-2}\,day^{-1}$ (0-4906 $\mu g\,m^{-2}\,day^{-1}$), mean 6.4 $\mu mol\,m^{-2}\,day^{-1}$ (205 $\mu g\,m^{-2}\,day^{-1}$), through summer and 0.02-15 $\mu mol\,m^{-2}\,day^{-1}$ (0.6-481 $\mu g\,m^{-2}\,day^{-1}$), mean 2.4 $\mu mol\,m^{-2}\,day^{-1}$ (77 $\mu g\,m^{-2}\,day^{-1}$), through winter over the GBR. Jones et al. (2018) also suggest that total emissions from the GBR are equivalent to 0.64 $Gmol\,year^{-1}$ (0.02 $Tg\,year^{-1}$ of sulfur). This estimate has been made from

Table 2.2: The average and the range (in brackets) of $DMS_w$ and $DMS_a$ measurements taken in-situ over coral reefs as reported by the literature

| Study | Location | Date | $DMS_w$ (nM) | $DMS_a$ ($nmol\,m^{-3}$) |
|---|---|---|---|---|
| Broadbent and Jones (2004) | One Tree Reef (23.4S, 152.1E) | Oct 1995 | 8 (5-11) | |
| Broadbent and Jones (2004) | One Tree Reef (23.4S, 152.1E) | Mar 1996 | 3 (0.5-6) | |
| Jones and Trevena (2005) | Ship campaign (18.5-10S, 146-149E) | Jul 1997 | 1.54 (0.34-5.67) | 2.38 (0.22-6.87) |
| Broadbent and Jones (2006) | One Tree Reef (23.4S, 152.1E) | Oct 1994 - Mar 1996 | 3.8 (0.36-25) | 6.5 (0.12-23) |
| Jones et al. (2007) | Orpheus Island (18.6S, 146.5E) | Dec 1992 - Jul 1994 | 2 (ns) | 0.2 (nd-1.3) |
| Jones et al. (2007) | Orpheus Island (18.6S, 146.5E) | Feb 1993 | 7 (1.6-54) | ns (nd-0.53) |
| Jones et al. (2007) | Orpheus Island (18.6S, 146.5E) | May 1993 | 1.4 (0.8-1.9) | |
| Jones et al. (2007) | Orpheus Island (18.6S, 146.5E) | Aug 1993 | 0.4 (nd-1.0) | 0.1 (nd-0.4) |
| Jones et al. (2007) | Magnetic Island (19.2S, 146.8E) | Nov 1993 - May 1994 | 1.3 (nd -3.9) | 1 (0.13-3.4) |
| Swan et al. (2012) | Heron Island (23.4S, 151.9E) | May - Jun 2011 | | 2.3 (nd-13.1) |
| Swan et al. (2017) | Heron Island (23.4S, 151.9E) | Mar 2012 | | 3.9 (0.6-11.5) |
| Swan et al. (2017) | Heron Island (23.4S, 151.9E) | Jul - Aug 2013 | | 1.3 (0.2-45.9) |
| Jones et al. (2018) | Ship campaign* (16.9-27.4S, 145.9-154.1E) | Sep - Oct 2016 | 1.5 (0.1-2.7) | |
| Average | | | 3.0 (nd-54) | 2.2 (nd-45.9) |

[a] nd indicates non-detectable
[a] ns indicates not stated
* R2R campaign data also used in this thesis

measurements both over coral reefs and in the GBR lagoon, and also includes an estimate of the additional flux from tropical cyclones. The tropical cyclone emission has been calculated (not observed) using the Liss and Merlivat (1986) flux parameterisation, taking into account average wind speeds of tropical cyclones and accounting for approximately five cyclone days per year in the region. However, it has been noted that many parameterisations overestimate the flux at high wind speed.

In addition to measuring the background $DMS_w$ concentrations over coral reefs, laboratory and observational studies have studied what influences the production of DMSP and DMS by corals. For example, recent work has shown a sensitivity of DMS production by corals when stressed due to tidal exposure, warming temperatures, rainfall events and light exposure (Swan et al., 2012; Fischer and Jones, 2012; Hopkins et al., 2016; Swan et al., 2017). Of interest to this thesis are the findings from Hopkins et al. (2016), where the effect of tidal exposure on the coral species *Acropora cf.horrida* was studied in the laboratory. From their results, Hopkins et al. (2016) extrapolate a $flux_{DMS}$ of 9-35 $\mu mol\, m^{-2}\, day^{-1}$ over coral reefs. This estimate is equivalent to 288.6-1122.3 $\mu g\, m^{-2}\, day^{-1}$ of sulfur, and in this thesis is further extrapolated to global coral reef coverage, giving 0.024-0.12 $Tg\, year^{-1}$ of sulfur. Whilst these extrapolations are highly speculative in terms of estimated exposure time, coverage of coral reefs and account for just one species of coral and only DMS produced during tidal stress, the Hopkins et al. (2016) estimations were the first to attempt to quantify the large-scale impact of coral reef-derived DMS.

The measurements summarised above and in Tables 2.2 and 2.3 of $DMS_w$ imply that our estimations of $DMS_w$ in tropical reef regions may be of equivalent importance to that produced by other marine organisms, warranting further research. In addition, it is found that the DMS production by coral reefs (and likely also phytoplankton, although that is not discussed here) has a much more complex cycle, both

spatially and temporally, than the standard fixed concentrations used in current modelling studies.

### 2.3.3 Applying the CLAW hypothesis to coral reefs

Links to coral DMS, aerosol formation, cloud cover and/or SSTs have been made in numerous studies over the last decade (Modini et al., 2009; Deschaseaux et al., 2012; Leahy et al., 2013; Swan et al., 2017; Jones et al., 2017; Cropp et al., 2018; Jackson et al., 2018, 2019). For example, Jackson et al. (2018) show a positive correlation between the aerosol optical depth (AOD) and SSTs and irradiance, suggesting the source of volatile sulfur compounds coming from the GBR to be the mechanism behind this result. Similarly, Cropp et al. (2018) also find a positive correlation between AOD and coral stress indices taking into account irradiance, tidal activity, and water clarity. Both of these studies (and others), rely on linear correlations which cannot take into account the complexity of the DMS-climate system and its significant non-linearities. Furthermore, studies that rely on observational products cannot easily separate the many influences on aerosol loading found in complex coastal regions, for example the influence of sea salt aerosol or continental air mass.

Coral reefs provide the ideal opportunity to detect evidence of bioregulatory feedback, being a large, stationary (both in time and space) source of DMS. Jones (2013), Jones et al. (2017) and Cropp et al. (2018) indeed postulate that coral reefs participate in bioregulatory feedback as suggested by the CLAW hypotheses. However, once again, these postulations are based purely on observational evidence. Many of the DMS-climate complexities, including the significant chemical non-linearities, interaction with other air masses, and intricate coastal meteorology, can be addressed through modelling studies. However, no modelling studies have yet been performed on this subject, let alone included coral reef-derived DMS as a source of sulfur to date. For this reason, the main goal of this thesis is to conduct model simulations

Table 2.3: The average and the range (in brackets) of $DMS_w$ and $DMS_a$ from coral reef laboratory studies as reported by the literature

| Study | Experiment | $DMS_w$ (nM) | $DMS_a$ ($nmol\,m^{-3}$) |
|---|---|---|---|
| Broadbent and Jones (2004) | Coral mucus ropes | 17,909 (16,970-18,665) | |
| Broadbent and Jones (2004) | Coral mucus ropes | 132 (61-203) | |
| Deschaseaux et al. (2012) | Chamber experiments on coral branches | ns (0-300) | 5.5 (ns) |
| Fischer and Jones (2012) | Chamber experiments (control) on coral nubbins | | 3.5 (2.3-2.9) |
| Fischer and Jones (2012) | Chamber experiments (increased light intensity) on coral nubbins | | 0.45 (0.4-0.5) |
| Fischer and Jones (2012) | Chamber experiments (2°C increase) on coral nubbins | | 0.24 (0.08-0.46) |
| Hopkins et al. (2016) | Chamber experiments on exposed coral mucus | ns (279-577) | |
| Hopkins et al. (2016) | Chamber experiments on exposed coral mucus ropes | 373 (ns) | |
| Hopkins et al. (2016) | Chamber experiments on submerged coral nubbins | | ns (0.1-0.3) ppm |
| Hopkins et al. (2016) | Chamber experiments on exposed coral nubbins | | ns (0.5-1.5) ppm |
| Hopkins et al. (2016) | Chamber experiments on re-submerged coral nubbins | | ns (0.02-0.1) ppm |
| Deschaseaux et al. (2019) | Coral reef sediments benthic chamber experiments | 1.5 (0.1-2.7) | |

[a] ns indicates not stated

to quantify the role of coral reef-derived DMS on aerosol, clouds and climate.

### 2.3.4 The Reef to Rainforest Field Campaign

In austral spring 2016 a major field campaign was undertaken titled 'GBR as a significant source of climatically relevant aerosol particles' (Ristovski, 2015) and nicknamed 'Reef to Rainforest' (R2R). The R2R campaign was a result of a successful Australian Research Council (ARC) Discovery Project (DP15010164), awarded in 2015. It involved groups from Queensland University of Technology, the Commonwealth Scientific Industry and Research Organisation (CSIRO), Southern Cross University, The University of Melbourne and the National Institute for Water and Atmospheric Research, New Zealand, as well as several other international partners. The R2R campaign aimed to determine if marine aerosol produced by the GBR could affect CCN concentrations, cloud formation and subsequently the hydrological cycle, providing the essential observational evidence for assessing DMS-climate interaction. A leading motivation for this field campaign came from observations by Modini et al. (2009), who observed new particle formation occurring during clean, marine air mass conditions nearby the GBR, which was attributed to sulfate and organic precursor gases.

The field campaign took place on two fronts, the first on board the CSIRO Marine National Facility RV Investigator (RVI) which navigated a path around the GBR from the 28th September - 22nd October 2016, shown in Figure 2.11. The RVI is Australia's purpose-built scientific research vessel. At 94 meters long it is equipped to support up to 60 scientists, technicians and crew to undertake biological, oceanographic, geological and atmospheric research for up 300 days a year. In addition to the permanent air chemistry lab on the RVI, a number of guest instruments were on board for the voyage to measure multiple aspects of the DMS-climate cycle. More information about the RVI, including information about its air

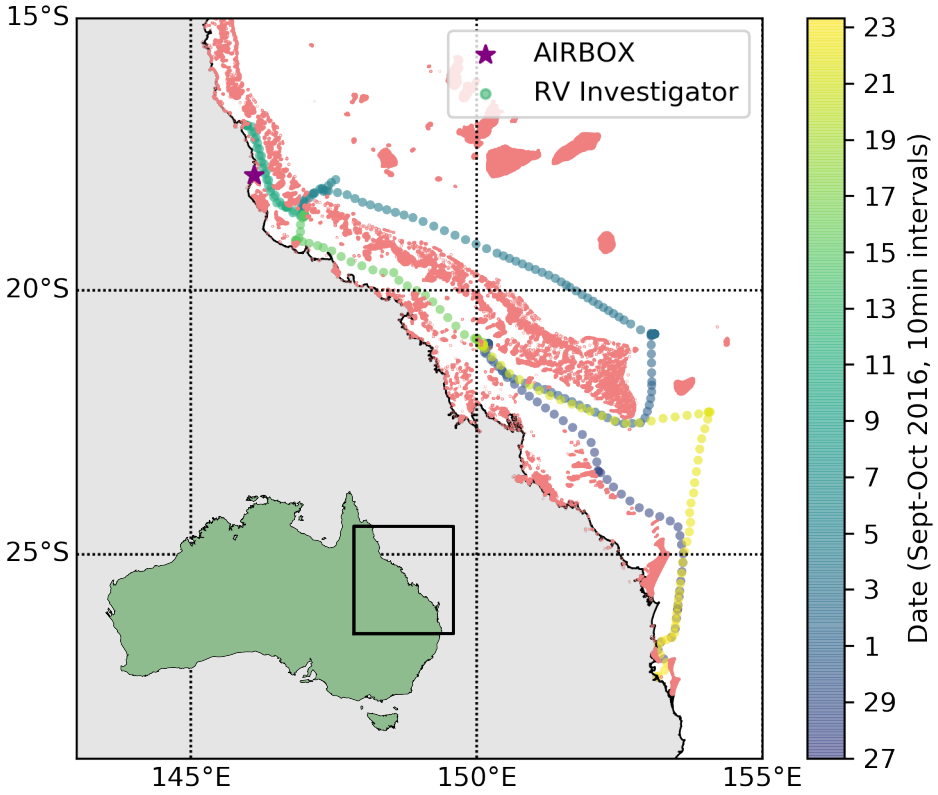


Figure 2.11: Map of the R2R field campaign off the north-east coast of Australia including the ship track of the RV Investigator (circles coloured at 10 min intervals from the 27th Sept to the 23rd Oct 2016) and the location of the mobile atmospheric chemistry lab AIRBOX (purple star). Pink colours show coral reefs

chemistry lab can be found here https://mnf.csiro.au/en/RV-Investigator.

The second aspect of this campaign was the University of Melbourne's Atmospheric Integrated Research Facility for Boundaries and Oxidative Experiments (AIRBOX) mobile atmospheric chemistry lab, stationed at Mission Beach, QLD from the 20th September to the 16th October 2016. AIRBOX is an ARC Linkage Infrastructure Equipment Facility project managed by the University of Melbourne. Nine partner organisations collaborate to manage and maintain the equipment within AIRBOX: CSIRO, the University of Wollongong, the Australian Nuclear Science and Technology Organisation, Queensland University of Technology, Macquarie University, Monash University, University of Tasmania and the Australian Antarctic Division as well as the University of Melbourne. For this campaign, AIRBOX

was also fitted out with a number of guest instruments. More information about AIRBOX can be found on the website: https://airbox.earthsci.unimelb.edu.au/.

Observations collected both on the RVI and at AIRBOX comprised measurements of meteorology and atmospheric chemical and aerosol composition, including $DMS_a$, aerosol number and mass. These observations aimed to capture each step of the DMS cycle, as described in Section 2.2, over the GBR for the first time. A full list of instruments used in this thesis from the R2R campaign is found in Section 3.2.5.

Post campaign, a R2R workshop (at the Atmospheric Composition & Chemistry Observations & Modelling meeting at CSIRO, Aspendale, December 2018), concluded that the observations taken during this campaign were unable to provide direct evidence of DMS-atmosphere interaction. Specifically, no clear new particle formation events, as reported by Modini et al. (2009), were observed. Whether that is due to bad timing (possible, as the campaign was in continental air-mass for much of the time) or because the source of sulfur is too weak, was unable to be determined at that stage.

The R2R campaign focused on observing the DMS-climate system and much work remains to understand the measurements. This thesis aims to contribute to the overall findings by adding a modelling component.

## 2.4 Summary

This Section has summarised the relevant processes and literature that link aerosol-climate interactions to coral reefs. In addition, several gaps in the literature have been highlighted, most prominently being the lack of modelling studies exploring coral reef-derived DMS, and regional-scale DMS-climate modelling. Without such

studies, low confidence is placed in the findings of current literature linking coral reef DMS to climate. In the next Chapter, the model descriptions of both ACCESS-UKCA and WRF-Chem are provided, as well as the methods employed to address the objectives outlined in Chapter 1.2.

# Chapter 3

# Methods and data

Two coupled atmospheric-chemistry models are used in this thesis to explore the impacts of DMS on the atmosphere at different scales. The first, ACCESS-UKCA, is a global climate-chemistry model operating over coarse time and spatial resolutions. ACCESS-UKCA is used to examine the overall importance of DMS and the mechanisms linking it to climate and to assess the impact of the loss of coral reef -derived DMS on a global-regional scale. The model description, setup, input fields, experiment setup, evaluation and analysis methods are discussed in Section 3.1. The second model used in this thesis is WRF-Chem, a weather-chemistry model. WRF-Chem operates at a regional scale making it suitable to study the short term influence of DMS on local weather. Section 3.2 describes the WRF-Chem model, including the chemistry and physics options, the input files, experimental setup and evaluation methods. This Chapter concludes with Section 3.3 describing the statistical methods used throughout this thesis.

# 3.1 ACCESS-UKCA

The ACCESS-UKCA coupled climate-chemistry model is used to evaluate the influence of DMS on the global climate. This Section describes the model set up and key modelling processes relevant to this thesis (Sections 3.1.1 and 3.1.3), the $DMS_w$ climatologies needed for the two studies performed with ACCESS-UKCA (Section 3.1.4), as well as the experimental setup for those studies (Section 3.1.5). Finally, the methods and data used for performing the evaluation and analysis of ACCESS-UKCA are discussed in Section 3.1.6 and 3.1.7.

## 3.1.1 Model setup

The physical atmospheric component in the ACCESS model is the United Kingdom Met Office's Unified Model (UM). In this case, UM version 8.4 is used (and described in Section 3.1.2), in conjunction with the UKCA chemistry model (Abraham et al., 2012), which includes the GLObal Model of Aerosol Processes GLOMAP-mode aerosol scheme described in Section 3.1.3.

All ACCESS-UKCA simulations presented in this thesis are run for the years 1999-2009, with the year 1999 discarded as spin up. Horizontal grid resolution is 1.25° latitude x 1.875° longitude, with 85 vertical levels, with the model top at 85 km. Monthly mean SST and sea ice coverage are prescribed as per the Atmospheric Model Intercomparison Project (AMIP) (Taylor et al., 2015).

The UKCA model is coupled to the ACCESS radiation scheme via $O_3$, $CH_4$, $N_2O$ and aerosol (direct scattering and absorption). Aerosol further influence the large-scale cloud and precipitation schemes via the CDN concentration, allowing changes in the the chemical/aerosol fields to affect the meteorology.

### 3.1.2 ACCESS

The atmospheric component of ACCESS-UKCA is the UM8.4. The 'new dynamics' dynamical core includes a semi-implicit, semi-Lagrangian, predictor corrector scheme solving non-hydrostatic, deep atmosphere equations and is described in Staniforth et al. (2006). The UM employs the Arakawa C grid in the horizontal and a Charney-Phillips grid in the vertical.

The radiation scheme in ACCESS-UKCA is described in Edwards et al. (2013). Shortwave radiation considers absorption in the stratosphere by ozone and in the troposphere, by water vapour and to a lesser degree carbon dioxide and oxygen. Scattering by aerosol, water droplets and ice crystals are considered, as is Rayleigh scattering by molecules and reflection from the surface. In the longwave, emission from the Earth's surface and atmosphere are considered as are the absorption and emission from water vapour, $CO_2$, ozone, clouds and other gas species.

The microphysics scheme is an updated version of the Wilson and Ballard (1999) 3B scheme, which includes water vapour, liquid water droplets, rain, aggregate (large) and crystal (small) ice and graupel and is compatible with the prognostic cloud and condensate scheme (PC2). The more recent scheme (3D) is described in Wilkinson (2012) and includes updates to a number of prognostics, the autoconversion mechanisms, ice nucleation processes, latent heat and cloud fraction calculations, ice and rain fall speeds, among others.

PC2 predicts cloud fraction and condensate prognostically following that of Tiedtke (1993) and described in Wilson et al. (2011). The convective scheme, originally developed from Gregory and Rowntree (1990), considers diagnostics from the boundary layer scheme to trigger shallow or deep convection, where the respective mass flux schemes are called. A mid-level convection scheme may also be called if the respective grid points are above the boundary layer, or above the termination level

of shallow or deep convection (Stratton et al., 2009). Environmental modification is allowed and is followed by the subsequent diagnoses of convective cloud.

The boundary layer scheme (Lock and Edwards, 2012) parameterises vertical turbulent transport of heat, moisture and horizontal momentum and includes a free troposphere component. It considers surface heating, wind shear, radiative and evaporate cooling and local instabilities driven by wind shear. This scheme is closely coupled to the convective scheme and the land surface scheme. The land surface scheme, Joint UK Land Environment Simulator (JULES) considers land surface-atmosphere fluxes of carbon, water, energy and momentum (Best et al., 2011; Clark et al., 2011).

### 3.1.3 UKCA

#### GLOMAP-mode

The GLOMAP-mode aerosol scheme uses two-moment pseudo-modal aerosol dynamics to simulate aerosol mass and number distributions (Mann et al., 2010, 2012). Within GLOMAP-mode, aerosol size distribution is represented across four soluble modes (corresponding to nucleation, Aitken, accumulation and coarse modes) and, in this work, one insoluble mode (Aitken), though up to three insoluble modes are available. The aerosol dry particle diameter size ranges can be found in Table 3.1. Each mode is considered to be internally mixed and has a fixed geometric standard deviation. Growth within the modes can happen via condensation, coagulation or cloud processing. Inter-modal coagulation can occur at larger aerosol sizes, and between soluble and insoluble modes (resulting in soluble aerosol). Similarly, insoluble aerosol age into soluble aerosol via condensation. Once the geometric standard deviation is exceeded for a specific mode, then a fraction of aerosol mass and number is transferred to the next largest mode. GLOMAP-mode includes particle composi-

tions of sulfate, sea-salt and elemental and organic carbon (Mann et al., 2010).

Coagulation in GLOMAP-mode occurs both within modes and between modes following Seinfeld and Pandis (1998) and Spracklen et al. (2005). Condensation of $H_2SO_4$ and secondary organics on aerosol across all modes is calculated according to Fuchs and Sutugin (1971). New particle formation of sulfate aerosol occurs via two mechanisms in GLOMAP-mode: free tropospheric binary homogeneous nucleation (Kulmala et al., 1998) and organic-mediated boundary layer nucleation (Metzger et al., 2010). The nucleation and condensation schemes compete for $H_2SO_4$ through substeps within each timestep. In grid boxes with low-level clouds, the GLOMAP-mode aqueous chemistry scheme calculates the dissolution of $SO_2$ and $H_2O_2$ into cloud droplets within the soluble accumulation and coarse modes (Mann et al., 2010). Aerosol dry deposition is calculated following Slinn (1982), Zhang (2001) and Binkowski and Shankar (1995), representing Brownian diffusion, impaction, interception and sedimentation (Mann et al., 2010). Aerosol scavenging is calculated based on large-scale and convective rain rates. The DMS oxidative pathway parameterisation used in GLOMAP-mode and the reaction rate coefficients at a constant temperature (T) are shown in Table 3.2 (Abraham et al., 2012). A full description of GLOMAP-mode can be found in Mann et al. (2010) with improvements detailed in Mann et al. (2012).

Table 3.1: The four modal size distributions used by GLOMAP-mode. Note that all four soluble aerosol modes and the insoluble Aitken mode are parameterised

| Mode | Particle dry diameter range (nm) |
|---|---|
| Nucleation (soluble) | $< 5$ |
| Aitken (soluble and insoluble) | 5 to 50 |
| Accumulation (soluble) | 50 to 500 |
| Coarse (soluble) | $> 500$ |

**Emissions**

GLOMAP-mode simulates precursor gas emissions including DMS (via Liss and Merlivat, 1986, see Section 2.2.3), $SO_2$ (from fossil fuels, volcanoes and biomass burning, see details below) and secondary organic carbon precursors (assumed to be monoterpenes, GLOMAP-mode does not require isoprene). Sea salt emissions are calculated online and occur following the Gong (2003) parameterisation. The Gong (2003) parameterisation is a function of wind speed and particle dry diameter and emits particles into the soluble accumulation and coarse modes while neglecting the primary emission of marine organics. Recent literature has found that the (Gong, 2003) parameterisation overestimates sea spray flux, especially at high wind speeds (Revell et al., 2019). Dust is treated outside of GLOMAP-mode according to the scheme detailed in Woodward (2001).

Anthropogenic emissions are prescribed pre-2000 from the Atmospheric Chemistry and Climate Model Intercomparison Project (ACCMIP) (Lamarque et al., 2010), and post-2000 from the Representative Concentration Pathway 6.0 (van Vuuren et al., 2011). Surface concentrations of methane and nitrous oxide are similarly prescribed from ACCMIP and RCP6.0. Ozone depleting substances are prescribed by WMO (2010). Biomass burning emissions are from the Global Fire Emission Database Version 4 (GFED4, van der Werf et al., 2017) and are based on observed burning for the simulated years. Terrestrial biogenic emissions are from MEGAN-MACC (Model of Emissions of Gases and Aerosols from Nature - Monitoring Atmospheric Composition and Climate) (Sindelarova et al., 2014) and oceanic emissions of CO, ethane and propane are taken from the POET (Precursors of Ozone and their Effects in the Troposphere) data base (Olivier et al., 2003; Granier et al., 2005). Lightning $NO_x$ emissions are calculated online.

Table 3.2: The DMS oxidation pathways as parameterised in the UKCA and the reaction rate coefficient values at constant temperature T (Abraham et al., 2012)

| Reaction | Reaction Rate |
|---|---|
| $DMS + OH \longrightarrow CH_3SO_2$ | $1.12 \times 10^{-11} \exp \frac{-250}{T}$ |
| $DMS + OH \longrightarrow CH_3SO_2$ | $0.9 \times \frac{9.3\times10^{-39} \exp \frac{5270}{T}[O_2]}{1+\left(7.4\times10^{-29} \exp \frac{5610}{T}[O_2]\right)}$ |
| $DMS + OH \longrightarrow MSA$ | $0.1 \times \frac{9.3\times10^{-39} \exp \frac{5270}{T}[O_2]}{1+\left(7.4\times10^{-29} \exp \frac{5610}{T}[O_2]\right)}$ |
| $DMS + NO_3 \longrightarrow CH_3SO_2$ | $1.9 \times 10^{-3} \exp \frac{-520}{T}$ |
| $CH_3SO_2 + O_3 \longrightarrow CH_3SO_3$ | 100.1 |
| $CH_3SO_2 + NO_2 \longrightarrow CH_3SO_3$ | $6.3 \times 10^{-12}$ |
| $CH_3SO_2 \longrightarrow SO_2 + CH_3$ | $2.2 \times 10^{-11}$ |
| $CH_3SO_3 + HO_2 \longrightarrow MSA$ | $5.0 \times 10^{-11}$ |
| $CH_3SO_3 \longrightarrow SO_2 + CH_3$ | $1.2 \times 10^{-3}$ |

**GLOMAP-mode evaluation**

In this thesis, an evaluation of ACCESS-UKCA has been performed with respect to cloud, radiation and precipitation fields. The evaluation methods are provided in Section 3.1.6. An evaluation of chemistry and aerosol fields in ACCESS-UKCA has not been performed in this thesis as numerous other studies have already performed such evaluation with respect to GLOMAP-mode. Although these evaluations have used differing atmospheric or chemical transport models in conjunction with GLOMAP-mode, in most cases the meteorology has been nudged or driven by reanalysis fields, minimising the impact of meteorology on the chemical response. In addition, apart from the chemical transport model in Mann et al. (2010) and Mann et al. (2012), the remaining evaluations presented here use atmospheric models within the Unified Model family. These evaluations are summarised below.

Mann et al. (2010) evaluated GLOMAP-mode within a chemistry transport model driven by ERA-40 reanalysis fields. Compared to a selection of high-quality point observations, surface $SO_4$, sea salt and dust aerosol mass were found to be well captured, while black carbon and primary organic matter were underestimated. Condensation nuclei were found to be well simulated in marine areas, but underestimated in continental and coastal regions, suggested to be due to underestimated primary emissions and new particle formation in these regions. CCN was found to be well captured over a range of environments.

An updated version of GLOMAP-mode, again run within a chemical transport model driven by ERA-40 reanalysis, was presented in Mann et al. (2012) and evaluated against observations. GLOMAP-mode was found to have good agreement with the DMS annual cycle at three Southern Hemisphere observational stations, with a positive bias at Cape Grim, whilst a negative bias at Amsterdam Island and Dumont D'Urville. Marine $SO_2$ was underestimated at Amsterdam Island and heavily overestimated at Cape Grim, attributed to the observation of only clean-marine conditions in this location and model resolution. Continental $SO_2$ was well captured, however a high bias was found over Europe in summer. Surface $SO_4$ in GLOMAP-mode compares well to North American and European observations, although with a negative winter bias and a positive summer bias. Marine $SO_4$ was well represented in terms of annual cycle and magnitude. Sea salt was found to be improved in the updated version of GLOMAP-mode. Black carbon over North America was well correlated to the model, with a small negative bias, while organic carbon showed a strong negative bias in winter and a moderate negative bias in summer. Low correlations to marine condensation nuclei number concentrations were found despite only a small negative bias. Similarly, for Aitken mode aerosol, a negative correlation was found between the model and observations, with underestimated aerosol number concentrations in the Southern Hemisphere and overestimated concentrations in the Northern Hemisphere. Good correlations were found for the accumulation

mode aerosol number concentration. The modelled concentration of ultrafine particles agreed well with aircraft observations in the Pacific and for larger particles over Germany. Finally, Mann et al. (2012) found good agreement with CCN, with a weak high bias, although marine sites were less well simulated.

Bellouin et al. (2013) evaluated GLOMAP-mode within the Hadley Centre Global Environmental Model (HadGEM) against a mass based aerosol scheme CLASSIC (Coupled Large-scale Aerosol Simulator for Studies in Climate) and both reanalysis AOD products and observations. Although the simulations using CLASSIC and GLOMAP-mode used different versions of the HadGEM model (GLOMAP-mode uses the updated version three, compared to two), both simulations were nudged to the ERA-Interim reanalysis, as were the simulations evaluated in this thesis. Bellouin et al. (2013) find that globally averaged AOD in GLOMAP-mode correlates better to reanalysis compared to CLASSIC. Both aerosol schemes generally underestimate AOD by about 30%, although with different spatial biases. The largest differences between the two aerosol schemes were found in relations to dust treatment, sea salt in the Southern Ocean, in regions of significant biomass burning and over the Northern Hemisphere continents. Compared to observations, a negative bias was found to be generally smaller in GLOMAP-mode and the correlations higher.

Woodhouse et al. (2015) compare a similar ACCESS-UKCA setup used in this thesis to observations of CO, $O_3$ and AOD. CO is found to be well simulated against two Northern Hemisphere observational sites at Mauna Loa and Minamitorishima, while in the Southern Hemisphere (Cape Grim), the model overestimated CO especially in the first half of the annual cycle. $O_3$ is under-predicted at all three sites, although the annual cycle is reasonably well captured. Once again, at Cape Grim the model performs to a lower standard than at its Northern Hemisphere counterparts. Finally, Woodhouse et al. (2015) evaluated ACCESS-UKCA against four

AOD observation sites across Australia. Moderate correlation between modelled and observed AOD was found, while the average AOD was found to be reasonably captured in all but one site on the south-west coast.

Finally, Revell et al. (2019) have evaluated HadGEM3 over the Southern Ocean. The AOD was found to be overestimated in winter, while underestimated in summer. Revell et al. (2019) attribute the winter AOD bias to overestimated sea spray at high wind speeds. After applying a correction to the sea spray flux however a compensating error in DMS was found. Revell et al. (2019) then modified the DMS chemistry representation within the UKCA, resulting in a 20% increase in CCN and CDN and improved agreement with observations.

The studies presented here indicate that the GLOMAP-mode model provides an improved representation of aerosol processes compared to its predecessors. While biases remain within the aerosol scheme, improvement of the specific components causing these biases is an active area of research (eg. for the sea spray flux presented in Revell et al., 2019).

### 3.1.4 DMS climatologies and perturbations

#### The Lana $DMS_w$ climatology

The Lana et al. (2011) gridded $DMS_w$ climatology (subsequently referred to as L11 and shown in Figure 2.7) has been used in this thesis as the baseline climatology. This climatology is commonly used across the literature (see Section 2.2) making comparisons to other work possible. In addition to this, as the L11 climatology consists of very few observations over coral reefs (see Figure 2.6), the L11 climatology is used as an example of a possible world in which all coral reefs have become extinct in Chapter 6. The original L11 climatology, on a 1x1° grid, can be downloaded from `https://www.bodc.ac.uk/solas_integration/implementation_`

`products/group1/dms/` (NERC, 2014). Three $DMS_w$ climatologies have been created for this research, in addition to L11, to explore the importance of $DMS_w$ in the global climate system. These climatologies are summarised in Table 3.3 and discussed below.

Table 3.3: Summary of the four $DMS_w$ climatologies used in the ACCESS-UKCA simulations and the annual mean (2000-2009) total global $flux_{DMS}$

| Simulation | DMS Climatology | $flux_{DMS}$ ($Tg\,year^{-1}$ of sulfur) |
|---|---|---|
| L11 | The Lana et al. (2011) climatology | 17.41 |
| Z | All marine $DMS_w$ set to zero | 0.72 |
| L11MX | Zonal maximum $DMS_w$ from the L11 climatology | 37.05 |
| L11C50 | Weighted 50nM $DMS_w$ over coral reef regions added to the L11 climatology | 17.72 |

**Large-scale DMS perturbations**

In Chapter 5 of this thesis, the sensitivity of the global climate to large perturbations in $DMS_w$ concentrations is explored with two experiments using the Z and L11MX climatologies compared to the L11 climatology. In the Z climatology, all marine DMS was set to zero, resulting in a $flux_{DMS}$ of $0.72\,Tg\,year^{-1}$ of sulfur, derived from terrestrial sources (for example Jardine et al., 2015). By comparing the Z simulation to the L11, the role ocean-derived DMS plays in shaping current climate can be determined and enhance understanding of how the physical processes underpinning the DMS-climate system operate. This knowledge may further aid understanding of how natural aerosol interact with the global radiation budget.

In the L11MX climatology, the $DMS_w$ field was set to each latitude's monthly zonal maximum value (at the model resolution of 1.25°), following a similar method to Grandey and Wang (2015). The January and July climatology can be seen in

Figure 3.1, while the full climatology can be seen in Appendix A. This climatology allows exploration of how the climate responds to large increases in $DMS_w$, the non-linearities in the system and comparison to other work. In this simulation, the global $flux_{DMS}$ more than doubles to 37.05 Tg year$^{-1}$ of sulfur, from 17.41 Tg year$^{-1}$ of sulfur.

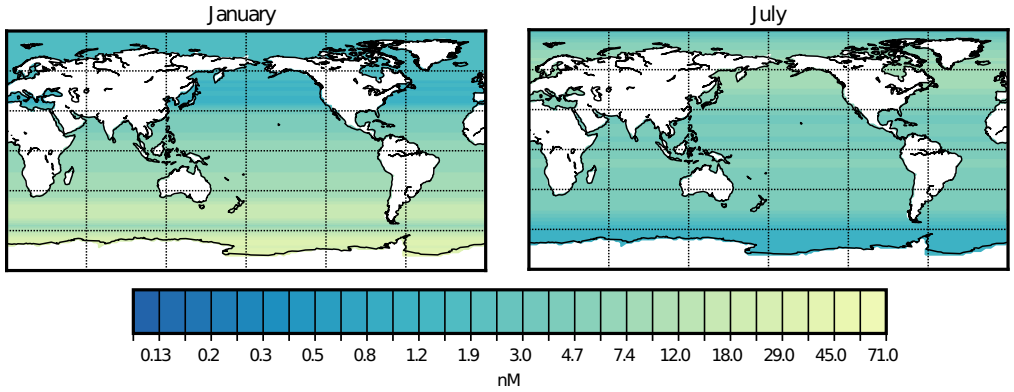


Figure 3.1: The January and July zonal maximum of the L11 $DMS_w$ climatology (L11MX). Note that $DMS_w$ is plotted on a log scale, in nM

### Coral reef DMS perturbations

Chapter 6 aims to determine the impact of mass coral extinction on climate. In this thesis, the L11 climatology is considered to have no contribution of $DMS_w$ from coral reefs. For that reason, a 'coral' climatology was created by adding $DMS_w$ attributed to coral reefs to the L11 climatology. To determine the amount of $DMS_w$ to be added to the L11 climatology, the areal fraction of each ACCESS-UKCA grid box covered by warm water coral reefs was calculated using the UNEP-WCMC et al. (2010) data and is shown in Figure 3.2. The maximum percent of grid box coral reef coverage was 15.6% in the northern GBR.

The areal extent fraction of coral reefs was then used to weight the amount of $DMS_w$ to be added to the L11 $DMS_w$ climatology. A number of different $DMS_w$ concentrations were tested, ranging from 10 nM to 500 nM (if 100% reef coverage is

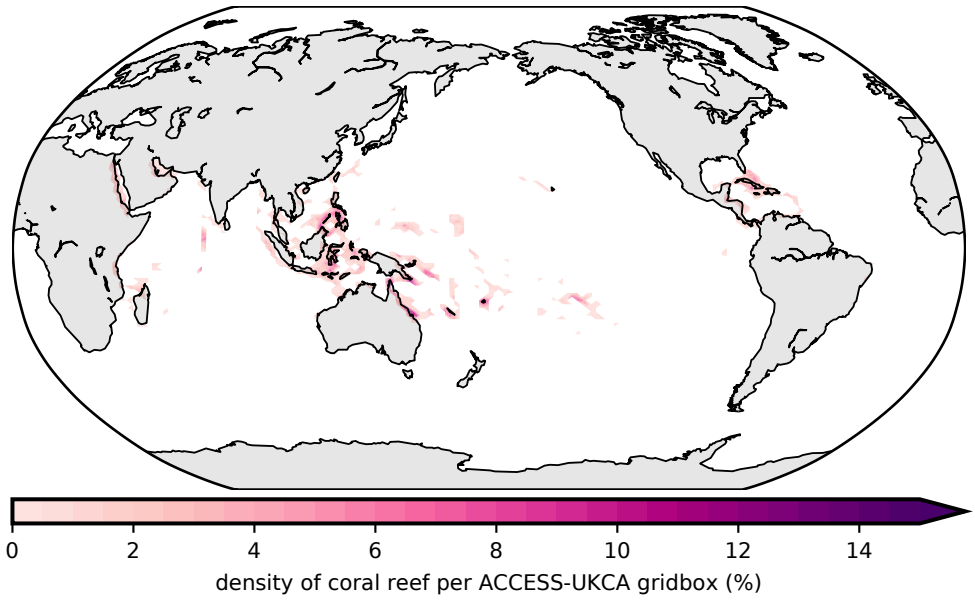


Figure 3.2: The areal fraction of each ACCESS-UKCA grid box covered by warm water coral reefs as indicated by UNEP-WCMC et al. (2010)

assumed). The weighted addition of 50 nM of $DMS_w$ caused a global average increase of 0.03 nM and an additional $flux_{DMS}$ of 0.3 Tg year$^{-1}$ S. These amounts do not significantly impact the global sulfur budget, contributing only 1.7% of additional sulfur to the global $flux_{DMS}$. The 50 nM assumption adds a mean of 0.74 nM and a maximum of 7.8 nM to coral reef regions. The $DMS_w$ climatology with the weighted 50 nM is referred to as L11C50. The January and July L11C50 climatology can be seen in Figure 3.3, while the full climatology can be seen in Appendix A.

The additional average daily $flux_{DMS}$ simulated by ACCESS-UKCA is shown in Figure 3.4. The average daily $flux_{DMS}$ (with a maximum of 621.9 $\mu$g m$^{-2}$ day$^{-1}$ S) is comparable to that of the Hopkins et al. (2016) estimations of $flux_{DMS}$ due to one coral species *Acropora* in response to tidal stress (288.6-1122.3 $\mu$g m$^{-2}$ day$^{-1}$ S). Furthermore, Jones et al. (2018) suggest that the total $flux_{DMS}$ from the GBR and surrounding lagoon is approximately 0.002 Tg year$^{-1}$ S. If this number is extrapolated to global coral reef regions then an annual $flux_{DMS}$ of 0.12 Tg year$^{-1}$ S is estimated. The values from the Hopkins et al. (2016) and Jones et al. (2018) both

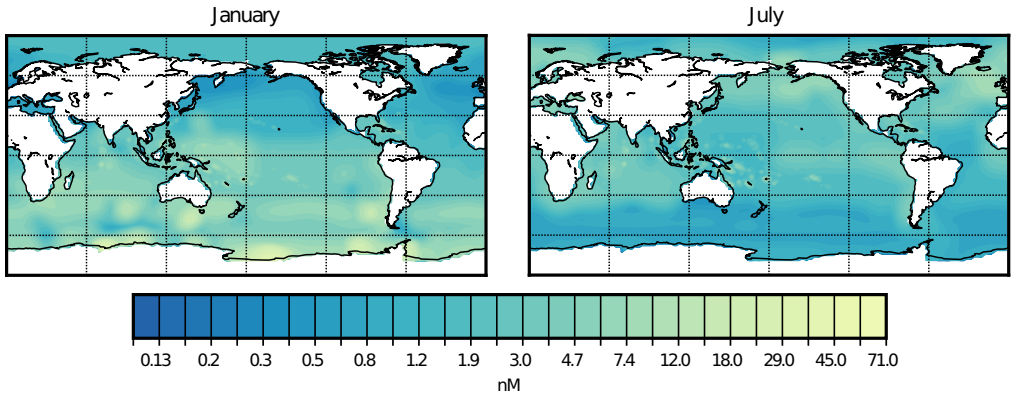


Figure 3.3: The January and July L11 climatology with an additional weighted 50 nM of $DMS_w$ (L11C50). Note that $DMS_w$ is plotted on a log scale, in nM

suggest that the amount of $DMS_w$ attributed to coral reefs in this thesis at the upper range of what is currently expected from observations.

However, it is noted that the values stated here are averages over large grid-boxes, and so may overestimate the extent of coral reef influence. Nevertheless, the 50 nM perturbation was chosen in part to ensure that if no significant changes in the atmosphere were found it would not be because the additional coral reef-DMS was too small.

### 3.1.5 Experiment setup

For the two studies performed with ACCESS-UKCA, different model setups were employed to best answer the respective questions: what is the global importance of total marine DMS and does the contribution of coral-reef DMS have any influence in the global-regional context? The two set-ups are described below.

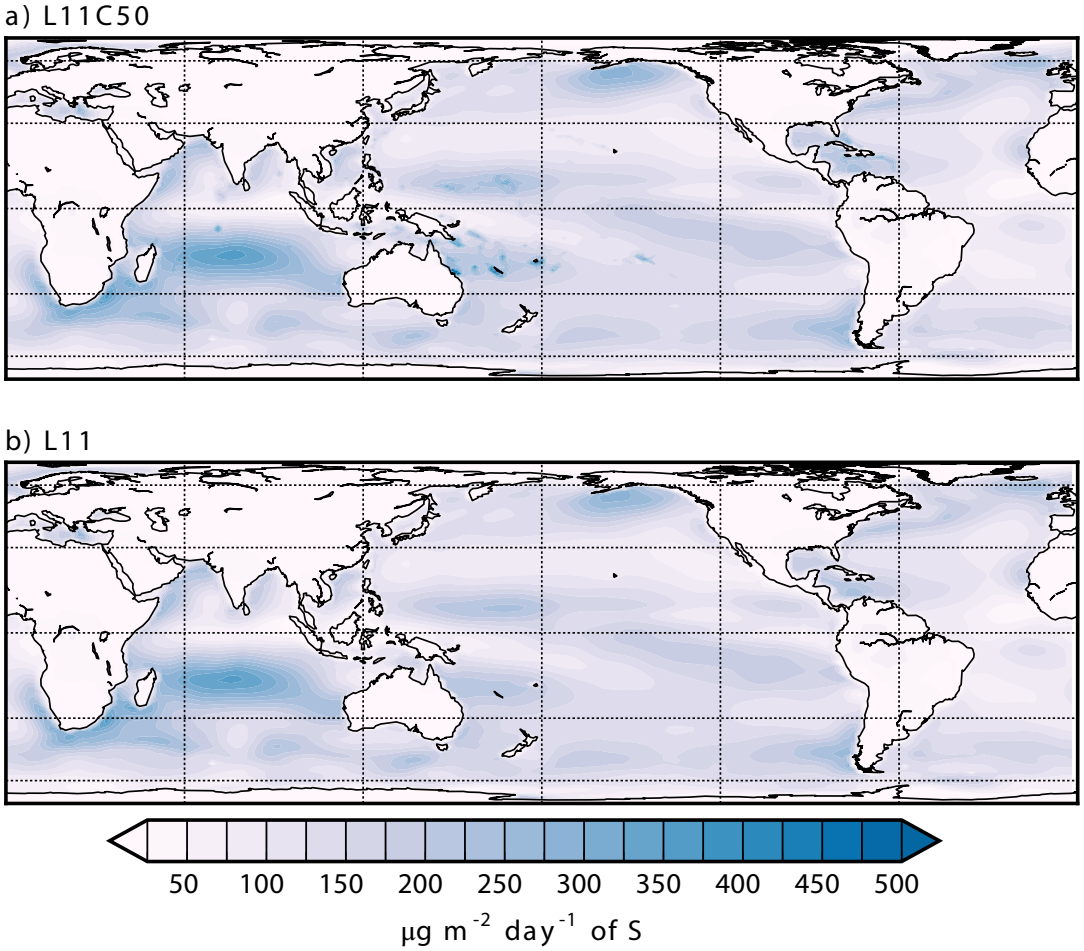


Figure 3.4: The annual average $\text{flux}_{\text{DMS}}$ using the L11C50 climatology (a) with an additional weighted 50 nM of $\text{DMS}_{\text{w}}$ and (b) that for the L11 climatology in $\mu\text{g m}^{-2}\,\text{day}^{-1}$ S.

### Setup for Chapters 4 and 5: ACCESS evaluation and large-scale DMS perturbation

For the analysis of model sensitivity to DMS in ACCESS-UKCA, presented in Chapter 5 of this thesis, three simulations are performed: the L11 is run as a control and the Z and L11MX as experimental simulations. Each of the simulations are nudged to ERA-Interim (Dee et al., 2011), using the horizontal wind components and potential temperature, at 6 hourly intervals in the free troposphere. The use of nudging does not allow aerosol and cloud responses to perturbed DMS to affect synoptic scale meteorology, hence the results here represent instantaneous responses in the climate

system. Nudging was deemed desirable for this study to limit computational expense, allowing single runs of 10 years. Due to nudging, responses in the simulation may be dampened (i.e. feedbacks are restricted by wind and temperature) but can be attributed directly to the DMS perturbations and not internal model variability.

For the analysis in Chapters 4 and 5, three regions of interest are defined and averaged over for their relevance to the broader Australian community or are of particular interest in the DMS-climate system. They are the Australian region: 45°S to 10°S, 110°E to 160°E, the Southern Ocean (SO): ocean grid points south of 40°S and the South Eastern Pacific (SEP) which represents an area of significant stratiform cloud decks: 240°E to 270°E, 25°S to 0°. These regions are shown in Figure 3.5a.

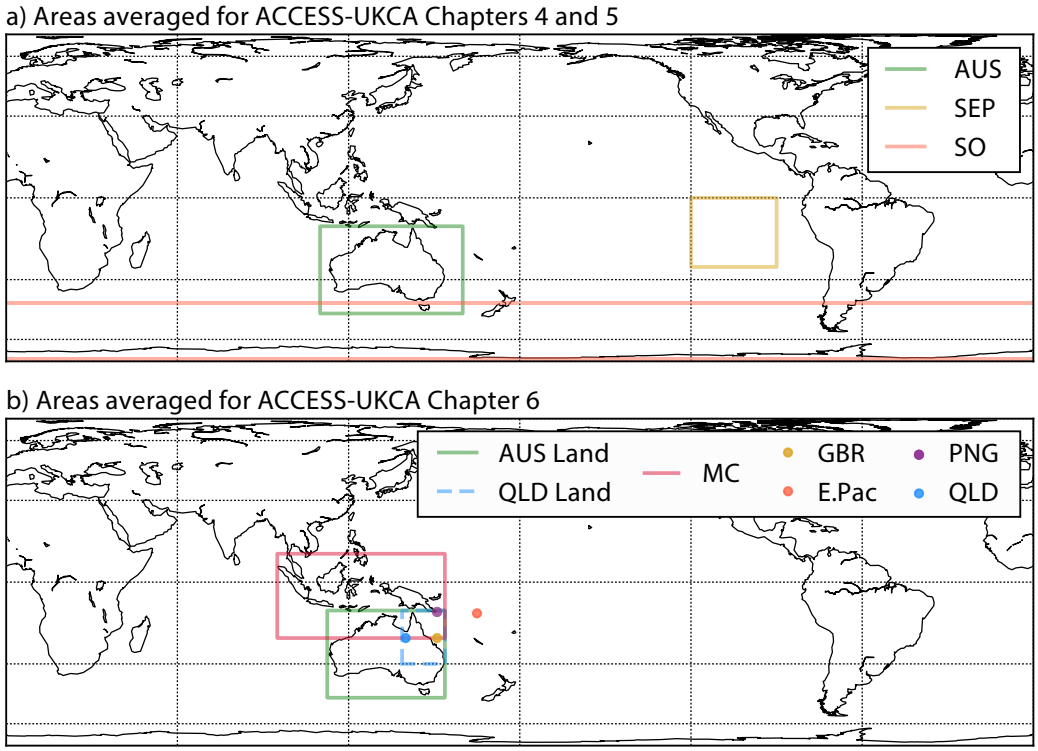


Figure 3.5: The areas used for averaging over fields for Chapters 4 and 5 (a) and Chapter 6 (b). In b), selected points of interest are also shown. Specific locations are described in text in Sections 3.1.5 and 3.1.5

**Setup for Chapter 6: coral reef-derived DMS**

To analyse the importance of coral reef -derived DMS in ACCESS-UKCA, two sets of simulations were performed, both of which include a simulation without coral reef-derived DMS (L11 evaluated in Chapter 4) and a simulation with coral reef-derived DMS (L11C50). The first setup follows the methods described above (Section 3.1.5) in which the L11 and L11C50 simulations were nudged to the ERA-Interim data set. In the second setup the model was allowed to run freely, with no nudging applied. Without nudging, feedbacks within the meteorology, such as changes in wind fields, can manifest within the model. With this method, much greater model variability occurs and differentiating between a true signal from the perturbed DMS fields and internal model variability was difficult. For this reason, seven sets of simulations (for both the L11 and L11C50), each of ten years, were performed with the free running setup to provide an ensemble. Each set of simulations used different atmospheric initial conditions; the start dumps from UTC000, January 1 for 1996, 1998, 1999, 2000, 2001, 2002 and 2003. Whilst this exercise was computationally expensive it provides sufficient data to perform statistical analysis.

For Chapter 6, the following regions were defined for averaging: the Maritime Continent - Australian (MC-Aus) region from 17.4°S to 10°N, 95.625°E to 153.75°E; the Queensland (QLD) land only region from 30°S to 10°S, 138.75°E to 153.75°E and the Australian land only region from 45°S to 10°S, 112.5°E to 153.75°E. Four grid points were selected for analysis of aerosol size distribution: a location off the coast of Papua New Guinea (PNG) at 10.5°S, 151°E, a point in the East Pacific (E.Pac) at 10.5°S, 165°E, a location over the GBR at 20°S, 151°E and a point in inland QLD at 20°S, 140°E. These regions and points are shown in Figure 3.5b. In addition the boundary of the South Pacific Convergence Zone (SPCZ) is defined as the area within the $6\,\mathrm{mm\,day^{-1}}$ or greater threshold (Vincent et al., 2011).

### 3.1.6 Evaluation

A comparison of ACCESS-UKCA to satellite observations was performed in Chapter 4 to provide a model evaluation and to put the results from this thesis into context with other literature. Global means at the surface were calculated over the 2000-2009 period, except for the cloud climatologies, of which were available from 2006-2009.

The following global data sets were compared to the model output: low, medium and high cloud fractions from the GCM-Oriented Cloud-Aerosol Lidar and Infrared Pathfinder Satellite Observation Cloud Product (CALIPSO-GOCCP) (Chepfer et al., 2010), radiation fluxes from the Clouds and the Earth's Radiant Energy System - Energy Balanced and Filled (CERES-EBAF)-TOA Edition 4.0 (Loeb et al., 2009) and CERES-EBAF-Surface Edition 4.0 (Kato et al., 2013) and precipitation from the Tropical Rainfall Measuring Mission (TRMM) (Huffman et al., 2007). Cloud level fraction is defined according to the CALIPSO-GOCCP: high cloud is between 50-440 hPa, medium between 440-680 hPa and low between 680-1000 hPa. Direct comparison of cloud fractions between model output and satellites cannot take into account satellite measurement biases, which can be resolved using a cloud satellite simulator such as the Cloud Feedback Model Intercomparison Program (CFMIP) Observation Simulator Package (COSP). Unfortunately, COSP was not available in the version of ACCESS-UKCA used here and hence these measurement biases must be considered throughout the subsequent analysis.

### 3.1.7 Global energy balance model

Due to prescribed SSTs and the nudging of ACCESS-UKCA to ERA-Interim (described in Section 3.1.5), a direct estimate of how global temperatures might respond to $DMS_w$ perturbations is not possible. For this reason, a simple energy balance model has been used to estimate the effects of the $DMS_w$ perturbations on global

mean temperatures, a useful metric for comparison to some previous studies.

The climate component of the Finite Amplitude Impulse Response (FAIR) model has been used in this thesis. This model is based on one first proposed by Boucher and Reddy (2008) and subsequently used in the IPCC Fith Assessment Report for equivalent emission metric calculations (Myhre et al., 2013b). FAIR's climate component is a simple impulse response model which emulates the behaviour of more complex Earth System Models, given a certain radiative forcing (in this case due to DMS). FAIR has been designed to determine temperature responses to radiative forcing of similar magnitudes to the DMS radiative effect (Millar et al., 2017). FAIR's temperature response is calculated as the sum of two components, approximately representing the response of the upper mixed layer and deep ocean to a change in radiative forcing (Millar et al., 2017). Due to its simplicity, FAIR in this application does not capture the non-linearities and feedbacks of the climate system, and hence the temperature response calculated must be taken as an estimate only.

In this work, we are only using FAIR's component which represents the temperature response to radiative forcing. This component is represented by Equation 3.1, where $T_j$ is the global mean surface temperature anomaly response (K), $F$ is the radiative effect (ie. forcing, $\mathrm{W\,m^{-2}}$) and $j$ = 1,2 representing the deep ocean and mixed layer responses. Subsequently, $q_1 = 0.33\,\mathrm{K\,W^{-1}\,m^{-2}}$, $q_2 = 0.41\,\mathrm{K\,W^{-1}\,m^{-2}}$ and $d_1 = 239\,\mathrm{years}$, $d_2 = 4.1\,\mathrm{years}$. After solving for $T_j$ in Equation 3.1, we then sum the ocean temperature responses to find the total temperature anomaly $T$ (Equation 3.2).

$$\frac{dT_j}{dt} = \frac{q_j F - T_j}{d_j} \tag{3.1}$$

$$T = \sum_j T_j \tag{3.2}$$

The radiative effect due to increasing or decreasing $DMS_w$ ($R_{DMS}$) is defined as the difference between the TOA energy balance (Q*) of an experimental run (eg. Z or L11MX) from the control (L11). The TOA radiation fields can be taken directly from ACCESS-UKCA to calculate Q*. By providing this radiative effect to FAIR's climate component, the difference in temperature expected across the ten year period under Z or L11MX $DMS_w$ conditions can be estimated.

The FAIR model is used in this study to provide an estimate only of the possible temperature response due to the radiative forcing of DMS over the 10-year period and does not consider any possible feedbacks. The radiative forcing provided by ACCESS-UKCA also does not take into account feedbacks due to both the nudged meteorology restricting their occurrence and the lack of a coupled ocean. Similar simulations, with free-running meteorology and a fully coupled chemistry-climate (atmosphere and ocean) may yield differing results.

## 3.2 WRF-Chem

WRF-Chem is a regional weather-chemistry model that is freely available and has wide ranging applications (Grell et al., 2005; Fast et al., 2006). The modelling suite can be run at both high temporal and spatial resolution at the user's discretion. WRF, as the name implies, is routinely used for weather forecasting services, as well as for case studies of extreme weather events and testing of new parameterisations or model sensitivities. Coupling this model to a chemistry scheme allows for detailed air-pollution transport and atmospheric chemistry research to be performed. Here WRF-Chem version 3.9 is used to determine the influence of coral reef DMS on the local weather around the GBR. Several simulations have been performed to explore this question, each having the same following characteristics unless otherwise stated.

The Advanced Research WRF (ARW) dynamical core is used in this work to

ensure compatibility with the chemistry schemes. The ARW is an Eulerian mass dynamical core which employs mass based terrain-following vertical coordinates and is fully compressible. ARW represents basic dynamical equations including high-order advection, pressure gradients, Coriolis, buoyancy and diffusion as well as finite differencing including numerical filters, Arakawa C-grid staggering structure and a 3rd-order Runge-Kutta time integration scheme. This core also allows for one or two way nesting, nudging and full physics.

Each simulation is run for the period: 1st October 2016, at 1200UTC to the 25th October 2016, 1200 UTC, to align with the R2R campaign. Three nested domains have been chosen (see Figure 3.6). The outer (D01) covers the majority of the Australian continent and the Coral Sea and is run at a 27km horizontal resolution with a 120 second time step. The middle domain (D02) runs at a 9km horizontal with a 60 second time step and covers the state of Queensland and the majority of the Great Barrier Reef. The inner domain (D03), is run at 3km with a 20 second time step and focuses on an area of dense coral reef and the location of the fourth station of the RVI campaign (see Figure 3.6). All simulations have 41 vertical levels in the troposphere (up to 20.4km), and produce instantaneous hourly output for each domain.

The chemistry and physics options, experiment set up, DMS climatologies and methods of evaluation are described in the following Sections. In many instances, the choice of the chemistry-aerosol scheme used in this study dictated the physics options. These chemistry and physics options have been selected to not only best represent the aerosol processes examined in this thesis, but to also align with previous studies such as Saide et al. (2012); Yang et al. (2012) and as advised by Dr Steve Utembe and the WRF-Chem tutorials.

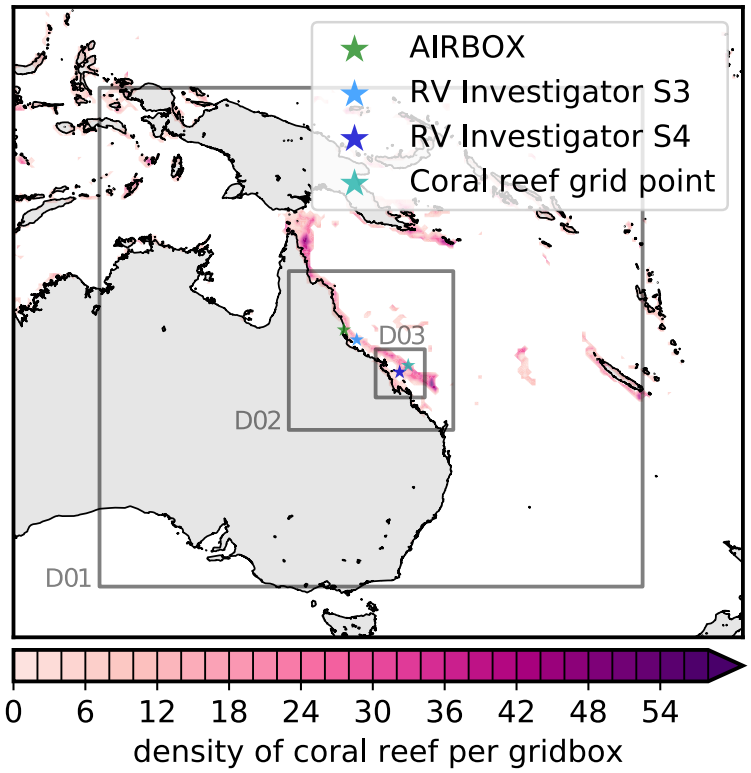


Figure 3.6: The three WRF domains used in this thesis, Domain 1 (D01) at 27km resolution, Domain 2 (D02) at 9km resolution and Domain 3 (D03) at 3km resolution, with the contours showing the density of coral reefs per grid box for the outer domain (D01). AIRBOX and two of the RVI stations are shown by green and blue stars respectively

### 3.2.1 Chemistry and aerosol options

In this thesis the Carbon Bond Mechanism Z (CBMZ) chemical mechanism with aqueous chemistry and DMS is used in conjunction with the Model for Simulating Aerosol Interactions and Chemistry (MOSAIC) aerosol scheme. The full chemistry namelist is provided in the Appendix B, Table B.1 and is described below. This combination of chemistry and aerosol schemes was chosen because of its ability to represent DMS and its pathways through the climate system as well as providing an eight bin aerosol scheme.

All WRF-Chem simulations have been restarted every four days, where the chemistry is reinitialised to the global chemical conditions (see the description of

the initial and boundary conditions in the next paragraph). This was advised to ensure consistency in the chemical and aerosol fields with conditions that have been evaluated globally (Emmons et al., 2010) and to compare with observations. The restart, which begins every fourth day at 0000, includes a 12 hour spin up that is discarded, with the previous time period running up to 1200 on the day of restart ensuring a continuous simulation. Subsequent analysis has revealed that this set-up limits the ability for the model to respond to changes in the aerosol fields and I suggest that continuous runs, without reinitialisation, are performed in the future.

The chemical boundary and initial conditions are provided by the Model for Ozone and Related Chemical Tracers (MOZART-4, Emmons et al., 2010). MOZART-4 is a global chemical transport model driven by meteorology from the Goddard Earth Observing System Model, Version 5. MOZART-4 includes 85 gas phase species, 147 gas phase reactions and 39 photolysis reactions and 12 bulk aerosol species. Terrestrial biogenic and sea salt emissions are calculated online while anthropogenic, biomass burning, volcanic and DMS emissions are provided by global databases, for details see Emmons et al. (2010). MOZART-4 has been specifically made available for use as boundary/initial conditions in models such as WRF-Chem and can be downloaded from `https://www.acom.ucar.edu/wrf-chem/mozart.shtml`.

In WRF-Chem, MOZART-4 provides the boundary/initial conditions for thirty three gas phase species and eight bulk aerosol species mass, including $SO_4$, $NH_4$, $NH_4NO_3$, secondary organic aerosol, black carbon, organic carbon, dust and sea salt. Dust is represented across four size ranges while sea salt across three. For the aerosol species, WRF-Chem is required to approximate the aerosol mass and number to the eight simulated bin sizes from the bulk aerosol mass provided by MOZART-4. Aerosol mass for each of the eight bins is a fractional approximation of the relevant bulk aerosol species mass. For the aerosol number, the sum of the fractional masses

of the aerosol species relevant to each bin size is calculated. For example, dust and sea salt are not included in the smallest bin. The namelist detailing these approximations can be found at `https://github.com/CohenBerkeleyLab/MOZBC/blob/master/src/CBMZ-MOSAIC_8bins.inp`.

### Chemistry

The CBMZ scheme (Zaveri, 1999) is a lumped-structure mechanism where the chemistry is categorised by reactions of similar carbon bonds. This scheme built upon CBM-IV (Gery et al., 2008) by updating the treatment (explicit or parameterised) of many species, increasing the over all number of species considered, whilst also making the mechanism suitable for longer simulations over larger areas. The CBMZ scheme includes 73 species and 237 chemical reactions. Dry deposition of gases and aerosol are turned on, as is wet scavenging (including convective wet scavenging). In-cloud chemistry, turbulent mixing and subgrid convective transport is also switched on. The FTUV (Fast Tropospheric UltravioletVisible) photolysis scheme (Tie, 2003) is used.

### Aerosol

MOSAIC was developed to overcome numerous issues including computing expense and oscillatory solutions (Zaveri et al., 2008). MOSAIC includes eleven specific aerosol species ($SO_4^-$, $HSO_4^-$, $CH_3SO_3$, $NO_3$, Cl, $CO_3$, $NH_4$, Na, Ca, black carbon (BC), primary organic matter (OC) and water and treats other unspecified aerosol species as a lumped mass or through substitutions of equivalent species. Some gas phase species, including sulfuric acid and MSA, are allowed to partition to the particle phase. The MOSAIC scheme uses an augmented selection of prognostic species (67) and reactions (164) from the CBMZ scheme which have been partitioned into four subroutines: background (occurring at all times), urban, biogenic and

DMS (occurring where appropriate) (Zaveri et al., 2008). The atmospheric DMS chemistry is not a part of the CBMZ scheme, but was added with the development and coupling of MOSAIC (Zaveri et al., 2008). The DMS chemistry is based on that of Zaveri (1997) and is shown in Table 3.4. It includes eleven species and 30 reactions.

MOSAIC represents aerosol via a sectional approach with eight discrete sized bins. Table 3.5 shows the bin sizes for this thesis and Figure 3.7 provides a visual representation. For each bin, the number and mass of particles are simulated: defined by the lower and upper limit of the dry particle diameter (Zaveri et al., 2008). Particle growth is calculated in a Lagrangian manner and transfer of particles between bins is calculated using a two-moment approach (Simmel and Wurzler, 2006). Coagulation of aerosol is calculated according to Jacobson et al. (1994) using a Brownian coagulation kernel. Homogeneous nucleation of $H_2SO_4$-$H_2O$ in MOSAIC is calculated via the Wexler et al. (1994) scheme. Zaveri et al. (2008) note that homogeneous nucleation is a complex mechanism with many issues including both under prediction and over prediction of nucleation rates. In MOSAIC, growth to Aitken mode particles is simulated implicitly as newly nucleated particle sizes are smaller than the smallest simulated aerosol size in the model. Heterogeneous nucleation in MOSAIC is partitioned into two schemes, treating condensation of non-volatile gases ($H_2SO_4$ and MSA) and condensation and evaporation of semi-volatile gases ($HNO_3$, HCl and $NH_3$) separately (Zaveri et al., 2008).

**Emissions**

The Liss and Merlivat (1986) parameterisation described in Section 2.2.3 is used to calculate the $\text{flux}_{\text{DMS}}$ emissions inWRF-Chem. Sea salt emissions are calculated online via either the Gong et al. (1997) parameterisation or the Fuentes et al. (2010) adaptation which includes a large addition of marine organic matter. All sea salt

Table 3.4: The DMS oxidation pathways as parameterised in the CBMZ-MOSAIC chemistry-aerosol scheme (Zaveri, 1997; Zaveri et al., 2008)

| Reaction | Reaction Rate |
|---|---|
| $DMS + OH \longrightarrow CH_3SCH_2OO + H_2O$ | $9.6 \times 10^{-12} \exp \frac{-234}{T}$ |
| $DMS + NO_3 \longrightarrow CH_3SCH_2OO + HNO_3$ | $1.4 \times 10^{-13} \exp \frac{500}{T}$ |
| $DMS + O(^3P) \longrightarrow CH_3SO_2 + CH_3O_2$ | $1.3 \times 10^{-11} \exp \frac{409}{T}$ |
| $DMS{+}OH \longrightarrow \alpha CH_3SO_2{+}\alpha CH_3O_2{+}(1{-}\alpha)DMSO{+}(1{-}\alpha)HO_2$ | $1.7 \times 10^{-12}$ [a] |
| $CH_3SCH_2OO + NO \longrightarrow CH_3SO_2 + HCHO + HO_2$ | $8.0 \times 10^{-12}$ |
| $CH_3SCH_2OO + CH_3O_2 \longrightarrow CH_3SO_2 + 2\,HCHO + HO_2$ | $1.8 \times 10^{-13}$ |
| $DMSO + OH \longrightarrow \beta CH_3SO_2H + \beta CH_3O_2 + (1{-}\beta)DMSO_2 + (1{-}\beta)HO_2$ | $5.8 \times 10^{-11}$ [b] |
| $DMSO_2 + OH \longrightarrow CH_3S(O)_2CH_2OO$ | $1.0 \times 10^{-14}$ |
| $CH_3S(O)_2CH_2OO + NO \longrightarrow CH_3SO_2 + HCHO + NO_2$ | $5.0 \times 10^{-12}$ |
| $CH_3S(O)_2CH_2OO + CH_{23}O_2 \longrightarrow CH_3SO_2 + 2\,HCHO + HO_2$ | $1.8 \times 10^{-13}$ |
| $CH_3SO_2H + HO_2 \longrightarrow CH_3SO_2 + H_2O_2$ | $1.0 \times 10^{-15}$ |
| $CH_3SO_2H + NO_3 \longrightarrow CH_3SO_2 + HNO_3$ | $1.0 \times 10^{-13}$ |
| $CH_3SO_2H + CH_3O_2 \longrightarrow CH_3SO_2 + CH_3OOH$ | $1.0 \times 10^{-15}$ |
| $CH_3SO_2H + OH \longrightarrow CH_3SO_2 + H_2O$ | $1.6 \times 10^{-11}$ |
| $CH_3SO_2H + CH_3SO_3 \longrightarrow CH_3SO_2 + MSA$ | $1.0 \times 10^{-13}$ |
| $CH_3SO_2 \xrightarrow{M} SO_2 + CH_3O_2$ | $2.5 \times 10^{13} \exp \frac{-8686}{T}$ |
| $CH_3SO_2 + NO_2 \longrightarrow CH_3SO_3 + NO$ | $1.0 \times 10^{-14}$ |
| $CH_3SO_2 + O_3 \longrightarrow CH_3SO_3 + O_2$ | $5.0 \times 10^{-15}$ |
| $CH_3SO_2 + HO_2 \longrightarrow CH_3SO_3 + OH$ | $2.5 \times 10^{-13}$ |
| $CH_3SO_2 + CH_3O_2 \longrightarrow CH_3SO_3 + HCHO + HO_2$ | $2.5 \times 10^{-13}$ |
| $CH_3SO_2 + OH \longrightarrow MSA$ | $5.0 \times 10^{-11}$ |
| $CH_3SO_2 + O_2 \xrightarrow{M} CH_3S(O)_2OO$ | $2.6 \times 10^{-18}$ |

[a] $\alpha = 5 \times 10^5 / (5 \times 10^5 + O_2 \times 3 \times 10^{-12})$
[b] $\beta = 1.5 \times 10^7 / (1.5 \times 10^7 + O_2 \times 1.2 \times 10^{-12})$

Table 3.4: The DMS oxidation pathways as parameterised in the CBMZ-MOSAIC chemistry-aerosol scheme (Zaveri, 1997; Zaveri et al., 2008) (continued)

| | |
|---|---|
| $CH_3S(O)_2OO \xrightarrow{M} CH_3SO_2 + O_2$ | 3.3 |
| $CH_3S(O)_2OO + NO \longrightarrow CH_3SO_3 + NO_2$ | $1.0 \times 10^{-11}$ |
| $CH_3S(O)_2OO + CH_3O_2 \longrightarrow CH_3SO_3 + HCHO + HO_2$ | $5.5 \times 10^{-12}$ |
| $CH_3SO_3 \xrightarrow{M} H_2SO_4 + CH_3O_2$ | $2.0 \times 10^{17} \exp \frac{-12626}{T}$ |
| $CH_3SO_3 + NO_2 \longrightarrow MSA + HNO_3$ | $3.0 \times 10^{-15}$ |
| $CH_3SO_3 + NO \longrightarrow MSA + HNO_2$ | $3.0 \times 10^{-15}$ |
| $CH_3SO_3 + HO_2 \longrightarrow MSA + O_2$ | $5.0 \times 10^{-11}$ |
| $CH_3SO_3 + HCHO \xrightarrow{O_2} MSA + HO_2 + CO$ | $1.6 \times 10^{-15}$ |

Table 3.5: The eight bins used by MOSAIC (Fast et al., 2006)

| Bin | Particle dry diameter range ($\mu$m) |
|---|---|
| 1 | $3.90625 \times 10^{-2}$ to $7.8125 \times 10^{-2}$ |
| 2 | $7.8125 \times 10^{-2}$ to $1.5625 \times 10^{-1}$ |
| 3 | $1.5625 \times 10^{-1}$ to $3.125 \times 10^{-1}$ |
| 4 | $3.125 \times 10^{-1}$ to $6.25 \times 10^{-1}$ |
| 5 | $6.25 \times 10^{-1}$ to $1.25 \times 10^{0}$ |
| 6 | $1.25 \times 10^{0}$ to $2.50 \times 10^{0}$ |
| 7 | $2.50 \times 10^{0}$ to $5.00 \times 10^{0}$ |
| 8 | $5.00 \times 10^{0}$ to $10.0 \times 10^{0}$ |

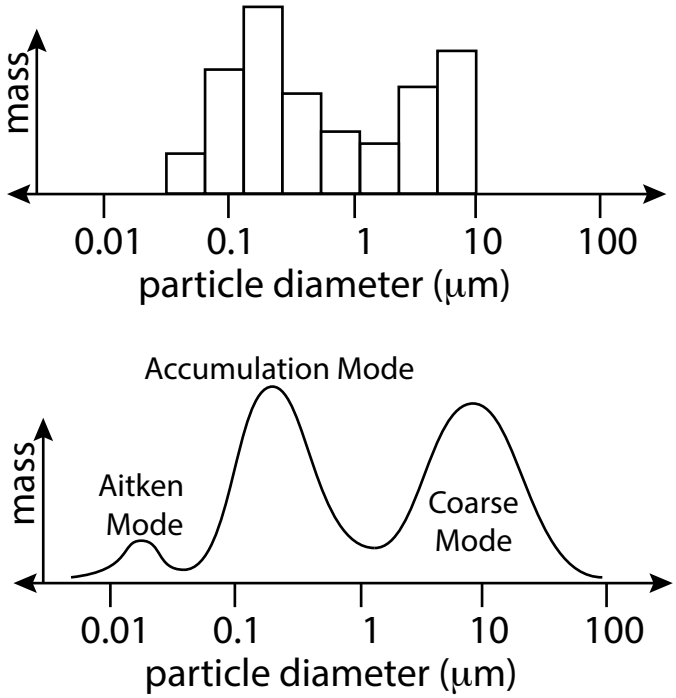


Figure 3.7: A visual representation of the aerosol bins used in the WRF-Chem model (top) compared to a modal distribution (bottom). Figure adapted from Bath (2018)

schemes have been found to overestimate sea salt emissions in WRF-Chem (eg. in Saide et al., 2012) and the Fuentes method especially so. Hence for simulations using the Fuentes high organics option the sea salt emission was halved, as was the sea salt mass within the MOZART-4 boundary and initial conditions.

Dust emissions are calculated via the Shao et al. (2011) scheme. The scheme was tested in an Australian environment by Shao et al. (2011) and found to be satisfactory. Wet deposition of dust has been turned on and follows the Jung and Shao (2006) method. For daily biomass burning emissions, fire location data is provided by FIRMS (Fire Information for Resource Management System) via the MODIS (Moderate Resolution Imaging Spectroradiometer) Collection 6 platform operated by NASA and available from `https://earthdata.nasa.gov/firms`. The fire location is provided to Prep-Chem (Preparative-Chemistry) which calculates the respective emissions and plume rise at daily resolution via the Brazilian Biomass Burning scheme (Longo et al., 2010). Plume rise frequency is set to 120, 30 and 10 seconds

for each domain respectively. Biogenic emissions are calculated online using the Guenther scheme (Guenther et al., 1994; Simpson et al., 1995) and anthropogenic emissions are provided via the Emissions Database for Global Atmospheric Research (EDGAR) V4.2, available at `https://edgar.jrc.ec.europa.eu/` (European Commission Joint Research Centre and Netherlands Environmental Assessment Agency, 2012). Aircraft and volcanic emissions are not included.

### 3.2.2 Meteorology and physics options

All WRF-Chem simulations have been meteorologically nudged to provide the best comparison to the R2R field campaign and to ensure that the responses found in the model are attributable to the $DMS_w$ perturbations and not internal model variability. The Australian Bureau of Meteorology (BoM) Atmospheric high-resolution Regional Reanalysis for Australia - Regional domain (BARRA-R) has been used to perform nudging at six hour intervals (Su et al., 2018). The BARRA-R data set is currently available at a 12km horizontal resolution with 70 vertical levels and hourly time steps for the years 1990-2018 inclusive. More information can be found here `http://www.bom.gov.au/research/projects/reanalysis/`. Nudging has been applied to temperature and water vapour above the planetary boundary layer and to wind above vertical level 19 (above 3km) at six hourly intervals.

The physics options selected for this study are the recommended options for use in conjunction with the CBMZ-MOSAIC chemistry-aerosol scheme, ensuring that aerosol-climate interaction via both direct and indirect aerosol effects are permitted within the model (this will be discussed in Section 3.2.2). All simulations in this thesis use the Morrison double moment cloud microphysics scheme (Morrison et al., 2008). This scheme predicts the mixing ratios and number concentrations of cloud droplets, cloud ice, snow, rain, and graupel. The RRTMG (Rapid Radiative Transfer Model for General circulation models) radiative transfer model for longwave and

shortwave radiation were used (Iacono et al., 2008), including the Monte Carlo Independent Column Approximation method for random cloud overlap (Barker et al., 2003). This scheme, in combination with the Morrison scheme, allows for indirect aerosol effects. In D01 and D02 cumulus parameterisation was performed using the Grell 3D scheme, similar to the Grell-Devenyi Ensemble Scheme (Grell and Dévényi, 2002), a multi-closure, multi-parameter, ensemble method that includes cloud and ice detrainment. In addition, cumulus radiation effects are switched on, allowing interaction of the radiation scheme and parameterised convective clouds (Gustafson et al., 2007). Cloud fractions are calculated using the Xu and Randall (1996) method, while cumulus and aerosol radiative feedbacks are permitted. Aerosol optical properties (Mie calculations) are approximated using the volume averaging method, in which refractive indices (a unitless number describing how light propagates through a particle) are averaged over a volume depending on its composition. The refractive indices for seven species (including dust) are defined by literature with some species having wavelength dependence.

The Noah Land Surface Model is used, with soil temperature and moisture in four layers, fractional snow cover and frozen soil physics (Chen and Dudhia, 2002). The boundary layer scheme used is the Mellor-Yamada-Janjic scheme (Janjić, 1994), a prognostic turbulent kinetic energy scheme with local vertical mixing. The boundary layer scheme operates in conjunction with the surface layer physics scheme, Eta (Janjic, 1996), based on the similarity theory of Monin and Obukhov (1954), with separate parameterisations over land (Zilitinkevich, 1995) and water (Janjić, 1994). The namelist for the physics options is provided in Appendix B, Table B.2.

**Aerosol effects**

In WRF-Chem, with the chemistry and physics namelist options described above, aerosol direct and indirect effects are permitted via the radiative, photolysis and

cloud microphysical schemes. For direct aerosol effects, the size, number and composition of aerosol and aerosol water, refractive indices of aerosol types (based on literature) and the Mie calculations (Bohren and Huffman, 1998) update the AOD, the single scattering albedo and the asymmetry factor used in the RRTGM radiation scheme. Aerosol water has a large impact, and hence the relative humidity must also be considered when direct effects are being examined. In this thesis, water vapour has been nudged to the BARRA-R reanalysis, hence should not change significantly between experiments. It is noted that in MOSAIC, aerosol water is a prognostic aerosol for which the hysteresis effect is taken into account. Additionally, aerosol can also impact photolysis rates (in the FTUV scheme) and photochemistry via the direct effect.

For indirect aerosol effects, the CCN number and composition is used to calculate the CDN in aerosol activation modules (Abdul-Razzak and Ghan, 2000, 2002). Activation of an aerosol requires the environmental supersaturation of an air mass entering a cloud to be greater than the critical supersaturation of that aerosol. Hence activation depends on the composition and size of the particle (i.e. their hygroscopic properties), as well as the vertical and turbulent velocities of the air mass. The hygroscopic properties of the aerosol are computed in the chemistry module, after which the bulk hygroscopic volume is passed to the physics module, where the CDN is able to interact with cloud properties. For the first indirect effect, CDN and the cloud water mixing ratio is used to calculate the cloud particle size and effective radius, which then informs the cloud albedo. The second indirect effect is simulated within the cloud physics routines (Morrison et al., 2008), which are informed by the CDN and subsequently updates the autoconversion rate, rain mixing ratio and precipitation of the module. Lastly, for the semi-direct effect, the cloud optical properties are influenced by the absorption of solar ultra-violet and infrared fluxes altering the heating rate of cloud liquid water. It must be noted that the indirect effects can only be simulated via the microphysics and hence at non-cloud

resolving scales care must be taken in the interpretation. For this reason the third WRF-Chem domain in this thesis is performed at cloud resolving scales.

### 3.2.3 DMS climatologies

At the beginning of this research it was found that the default $DMS_w$ climatology provided by WRF-Chem is the older Kettle and Andreae (2000) climatology on a 1x1.25° grid. This climatology has been updated by Lana et al. (2011). In addition, the interpolation performed by WRF-Chem (via Prep-Chem) was deemed unsatisfactory (creating unphysical patterns around the coastlines and generally a very coarse interpolation). For this reason, the L11 climatology for October was interpolated to each WRF-Chem domain using the python (v3.5) basemap bilinear interpolation (see Figure 3.8a, b and c), overriding the default WRF-Chem $DMS_w$ climatology. Further smoothing around the coastlines was performed. All fields that pass through Prep-Chem underwent the same interpolation to a higher resolution for consistency.

Four $DMS_w$ climatologies were subsequently made for the WRF-Chem model, to evaluate the model against the R2R observations and to explore the influence of DMS on the local climate. These experiments were designed to test whether relationships reported in the literature (Section 2.3.3) could be captured by the model and are provided in Table 3.6 and below.

#### Scaled DMS climatology

The L11 climatology was initially planned to be used as a the control $DMS_w$ climatology. However, after initial testing, it was found that L11 was overestimating $DMS_w$ observations taken during the R2R campaign (this finding will be described in further detail in Chapter 7). For this reason, a scaled $DMS_w$ climatology was

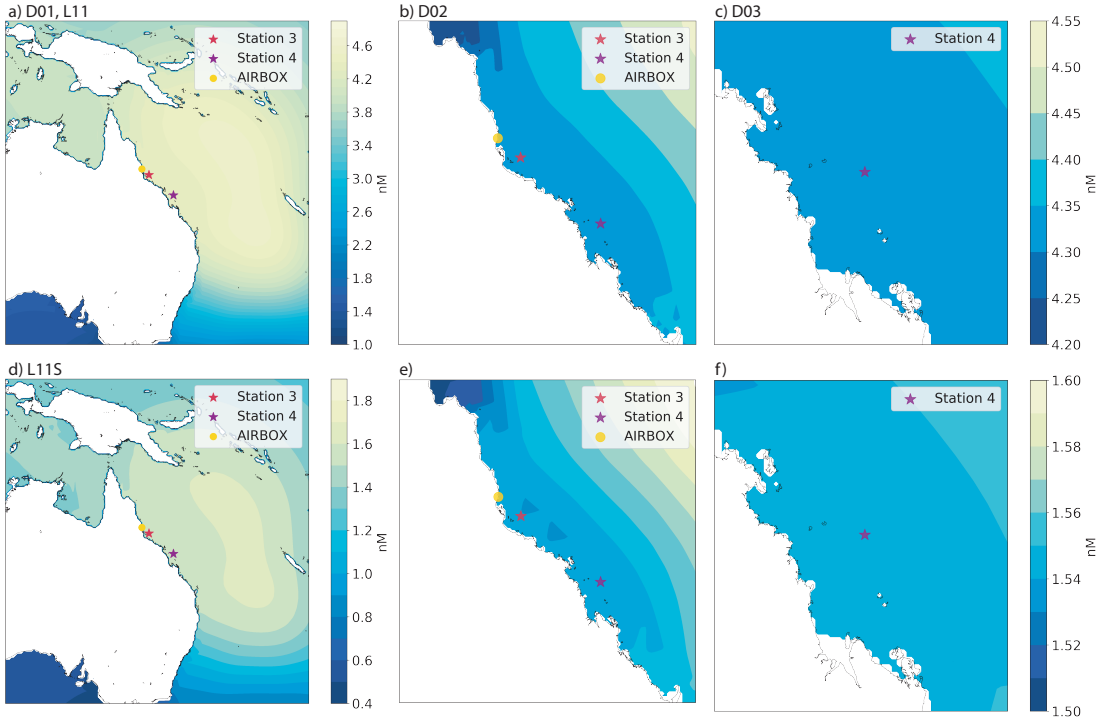


Figure 3.8: The L11 October climatology (top) and scaled L11 climatology for WRF-Chem D01 (a,d), D02 (b,e) and D03 (c,f). Note the different scales of $DMS_w$. Markers represent the locations of AIRBOX and two of the RVI stations

created, where L11 was divided by 2.8 to match the average observations taken during the R2R campaign. This climatology (referred to as L11S) was subsequently used as the control climatology and considered, like L11 to be a climatology with no contribution from coral reef -derived $DMS_w$.

### Coral DMS climatology

To test if coral reef -derived $DMS_w$ can influence the local weather, three climatologies were created with additional amounts of $DMS_w$ over reef regions, representing a low, high and very high coral reef sources. The creation of these climatologies follows a similar method to that described in Section 3.1.4 for ACCESS-UKCA: a fixed amount of $DMS_w$, weighted by the density of coral reefs per grid box was added to the L11S climatology. The DMS scaling by areal coral reef fraction was

Table 3.6: Summary of the four $DMS_w$ climatologies used for the WRF-Chem simulations

| Short name | DMS Climatology |
|---|---|
| L11 | The Lana et al. (2011) climatology |
| L11S | The scaled Lana et al. (2011) climatology |
| L11SCL | Weighted 2 nM $DMS_w$ in coral reef regions added to the L11S climatology |
| L11SCH | Weighted 8 nM $DMS_w$ in coral reef regions added to the L11S climatology |
| L11SCVH | Weighted 50 nM $DMS_w$ in coral reef regions added to the L11S climatology |

performed for each WRF-Chem domain separately, using the UNEP-WCMC et al. (2010) global coral reef data to inform the weighting.

The amount of $DMS_w$ added was informed by $DMS_w$ measurements taken directly over reefs (not ship based), averaging 3.4 nM (summarised in Table 2.2) and the $flux_{DMS}$ estimated by Jones et al. (2018) (winter and summer means (ranges) of 2.4 (0.002-15) and 6.4 (non-detectable-153) $\mu mol\,m^{-2}\,day^{-1}$ respectively) and Hopkins et al. (2016) (9-35 $\mu mol\,m^{-2}\,day^{-1}$). The resulting $DMS_w$ additions were 2, 8 and 50 nM, which are referred to as the L11SCL, L11SCH and L11SCVH climatologies respectively. These values are within those provided in the literature and reflect a plausible range as shown in Figure 3.9.

After this scaling had been applied, the L11SCL climatology was deemed too low to warrant a simulation, as it made very little impact on the $DMS_w$ field and was unlikely to impact the subsequent aerosol and climate fields (as shown in Figure 3.9). The remaining L11SCH and L11SCVH climatologies are shown in Figure 3.10.

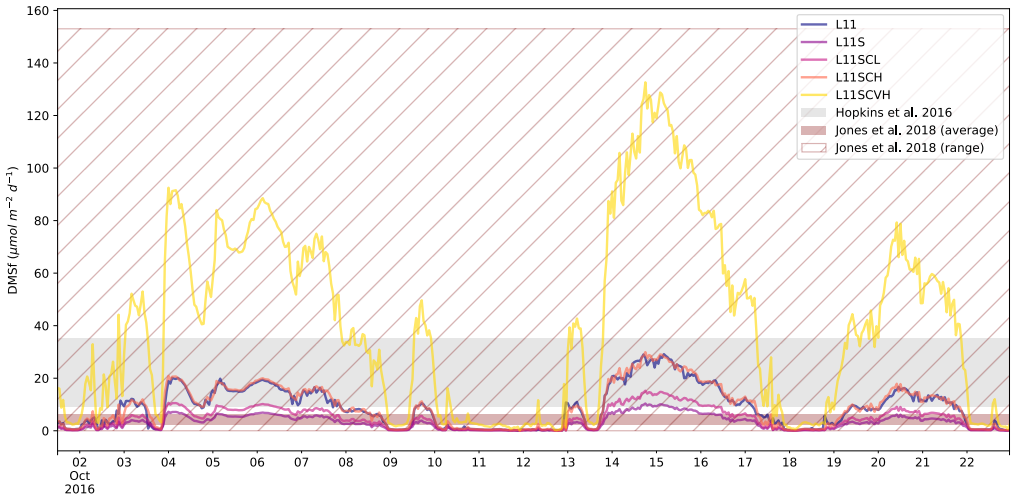


Figure 3.9: The $\text{flux}_{\text{DMS}}$ timeseries in ($\mu\text{mol}\,\text{m}^{-2}\,\text{day}^{-1}$) for a representative coral reef grid point for the L11S (blue), L11SCL (pink) and L11SCH (yellow) simulations. The grey shaded area shows the estimated $\text{flux}_{\text{DMS}}$ by Hopkins et al. (2016) from corals after tidal exposure, the pink shaded area shows the winter-summer average estimates from Jones et al. (2018), and the hatched area shows the full range of observations from Jones et al. (2018)

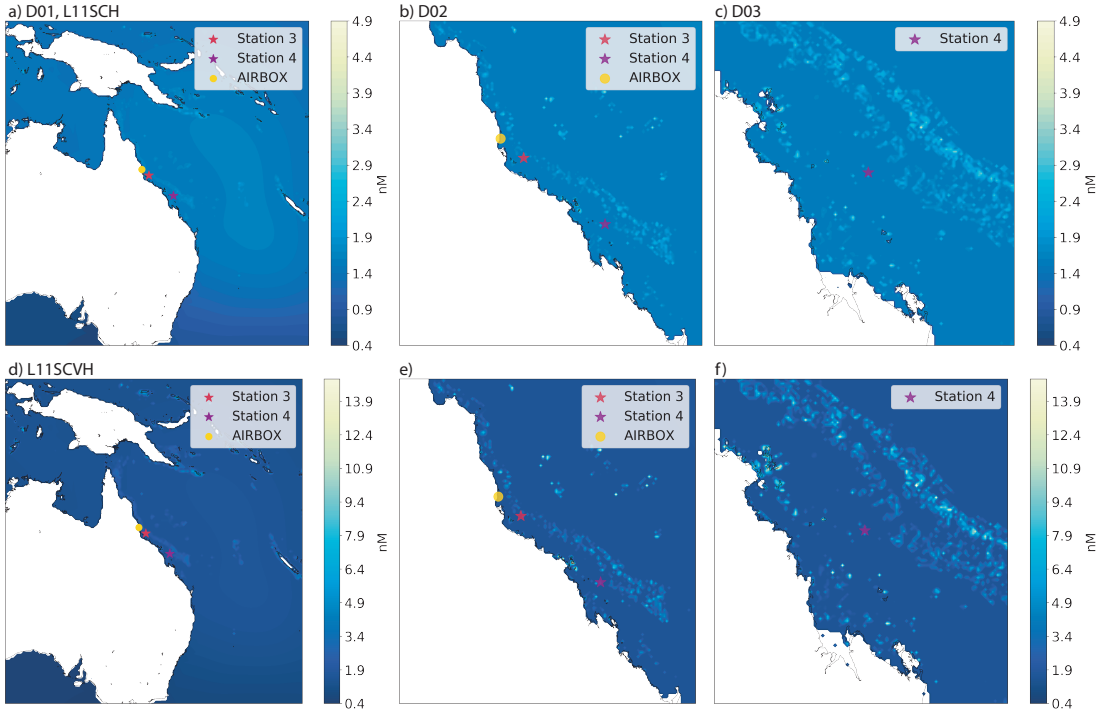


Figure 3.10: The L11SCH climatology (top) and L11SCVH climatology for WRF-Chem D01 (a,d), D02 (b,e) and D03 (c,f). Note the different scales of $\text{DMS}_{\text{w}}$. Markers represent the locations of AIRBOX and two of the RVI stations

Table 3.7: Summary of the four WRF-Chem simulations, the $DMS_w$ climatology (see Section 3.2.3) and the differences in setup

| Simulation | DMS Climatology | Namelist options |
|---|---|---|
| C1 | L11 | No biomass burning or dust, Gong et al. (1997) sea salt emissions (opt 2) |
| C7 | L11S | Includes biomass burning and dust, Fuentes et al. (2010) sea salt emissions (opt 4), with halved sea salt flux and initial and boundary mass |
| CRH | L11SCH | Same as C7 |
| CRVH | L11SCVH | Same as C7 |

### 3.2.4 Experiment setup

Four WRF-Chem simulations are presented in this thesis and are summarised in Table 3.7. Two simulations were compared against the R2R data to evaluate the WRF-Chem model in Chapter 7. The first control simulation (C1) used the L11 climatology, with no biomass burning or dust and with the Gong et al. (1997) sea salt emissions. The second control climatology, C7, used the L11S DMS climatology and the Fuentes et al. (2010) sea salt parmeterisation with high organics, where the sea salt flux and the sea salt mass in the initial and boundary conditions were halved. Biomass and dust emissions were also included.

C7 is subsequently used as the control simulation to examine the impact of coral reef DMS in the simulations presented in Chapter 8. For the two coral reef simulations the same setup as C7 was used. CRH used the high estimated of coral reef DMS (L11SCH) while CRVH used the very high estimate of coral reef DMS L11SCVH.

### 3.2.5 Evaluation

WRF-Chem has been evaluated against data collected during the R2R field campaign. Timeseries comparisons, correlations and a bias factor metric have been used (see Section 3.3), evaluating equivalent model fields to the observations taken during R2R (see Figure 2.11). Evaluation focused on D02 as this encompasses the entire ship track, and little difference was notable between D01, D02 and D03. For aerosol comparisons, particle size bins were not equivalent to observed particle sizes so the a linear interpolation was made, assuming aerosol bins are internally mixed. The nearest neighbour method was used to locate the ship track within the gridded model data. Tables 3.8 and 3.9 provide a summary of observational fields used, the institute responsible for the collection/processing of the observation, the instrument used, references linking to methods where available and how this data may be accessed. Below, brief descriptions of how the data was collected and processed are provided. Where possible, literature that provides full description of these instrument's methods have been cited for the readers reference. In some instances where this literature is not available, greater detail has been provided. Parts of the methods described in this Section have been contributed by the parties responsible for the measurement and processing of the data, including Yuko Omori, Sarah Lawson, Hilton Swan, Joel Alroe, Luke Cravigan, Simon Alexander and Zhenyi Chen.

#### DMS observations

$DMS_w$ observations were taken by the RVI for the duration of the voyage. Seawater samples (from between 0-5 m depth) were pumped through to the wet chemistry laboratory as part of the ship's routine underway measurements every minute. For the first half of the voyage (up until the 14th October) a Shimadzu gas chromatograph (GC-2010) (employing purge and trap gas chromatography) was used to detect $DMS_w$. After the 14th October, due to competing demands for the GC,

Table 3.8: List of all RVI observations used in the WRF-Chem evaluation, the institute responsible for data collection and processing, details on the instrument used and literature relevant to the data processing methods and information on how this data can be accessed. More information can also be found here https://mnf.csiro.au/en/RV-Investigator/Underway-science/Atmospheric-sampling

| Field | Institute | Instrument | Methods* | Data Avail. |
|---|---|---|---|---|
| $DMS_w$ | University of Tsukuba | GC-2010-FPD & EI-PTRMS | (Omori et al., 2013, 2017; Kameyama et al., 2009) | Upon request |
| $DMS_a$ | CSIRO | PTR-MS | NA | Upon request |
| $SO_4$ | QUT | ACSM | (Fröhlich et al., 2013) | Upon request |
| Organics | QUT | ACSM | (Fröhlich et al., 2013) | Upon request |
| $NO_3$ | QUT | ACSM | (Fröhlich et al., 2013) | Upon request |
| $NH_4$ | QUT | ACSM | (Fröhlich et al., 2013) | Upon request |
| Black Carbon | CSIRO/QUT | MAAP | Kanaya et al. (2013) | Upon request |
| CN10 | QUT | CPC (TSI, Model 3772) | NA | Upon request |
| CCN | CSIRO/QUT | CCNc | NA | Upon request |
| Radon | ANSTO/CSIRO | Radon detector | (Chambers et al., 2015) | Upon request |
| Wind speed & direction | CSIRO | | CSIRO (2016) | CSIRO (2016) |
| RH | CSIRO | | CSIRO (2016) | CSIRO (2016) |
| Temperature | CSIRO | | CSIRO (2016) | CSIRO (2016) |
| Pressure | CSIRO | | CSIRO (2016) | CSIRO (2016) |
| BLH | BoM/AAD | Leosphere R-MAN510 Raman UV polarization lidar | (Alexander and Protat, 2018, 2019; Baars et al., 2008) | BoM data base TBD |

[a] *Refer to in text data description for full methods

Table 3.9: List of all AIRBOX and satellite observations used in the WRF-Chem evaluation, the institute responsible for data collection and processing, details on the instrument used and literature relevant to the data processing methods and information on how this data can be accessed. For AIRBOX, more information can also be found here https://airbox.earthsci.unimelb.edu.au

| Field | Institute | Instrument | Methods | Data Avail. |
|---|---|---|---|---|
| $DMS_a$ | Southern Cross University | GC-PFPD | (Swan et al., 2015) | Swan (2017) |
| $SO_4$ | QUT | AMS | Drewnick et al. (2005) | Upon request |
| Organics | QUT | AMS | Drewnick et al. (2005) | Upon request |
| $NO_3$ | QUT | AMS | Drewnick et al. (2005) | Upon request |
| $NH_4$ | QUT | AMS | Drewnick et al. (2005) | Upon request |
| Black Carbon | CSIRO/QUT | MAAP | Kanaya et al. (2013) | Upon request |
| CN10 | QUT | CPC (TSI, Model 3772) | NA | Upon request |
| Radon | ANSTO | Radon detector | (Chambers et al., 2015) | Upon request |
| Wind speed and direction | UoM | Thompson WS800 | NA | Upon request |
| RH | UoM | Thompson WS800 | NA | Upon request |
| Temperature | UoM | Thompson WS800 | NA | Upon request |
| Pressure | UoM | Thompson WS800 | NA | Upon request |
| BLH | UoM/Chinese Academy of Sciences | Sigma Space MiniMPL-532-C Micro, | (Chen et al., 2019; Xiang et al., 2019) | Upon request |
| CTH | BoM | Himawari | Heidinger (2013) | Upon request |
| $\alpha_{Cld}$ | BoM | Himawari | Pavolonis (2010) | Upon request |

[a] Refer to in text data description for full methods

$DMS_w$ was measured using an Equilibrator Inlet (EI) - Proton Transfer Reaction Mass Spectrometry (PTRMS) system (Kameyama et al., 2009; Omori et al., 2013, 2017). The seawater samples pumped by the ship system were flowed continuously into a 10-L glass equilibrator at $1\,L\,min^{-1}$. Pure nitrogen flowed from the bottom to the upper outlet of the equilibrator at 120 sccm. Dissolved DMS was extracted into the $N_2$ gas phase and introduced into the PTRMS (Ionicon Analytik GmbH, Innsbruck, Austria). The mass signal of DMS in the sample gas was obtained at 10 second integration to obtain a mass signal at 1 minute intervals. The $DMS_w$ concentrations were calculated from concentrations in the sample gas extracted from the equilibrator with Henry's law constant (Kameyama et al., 2009). Comparison between the $DMS_w$ observations taken by the two techniques show excellent agreement ($r^2 = 0.999$) with high confidence ($p < 0.001$).

Accompanying the $DMS_w$ measurements on board the RVI were $DMS_a$ observations. A commercially available high sensitivity PTRMS (Ionicon Analytik GmbH, Innsbruck, Austria) was used to measure $DMS_a$. The PTRMS sampled via a 30 m 3/8 inch ID PFA line with an inlet at the top of the mast on the foredeck 17 m above water level at a flow rate of $5\,L\,min^{-1}$. The PTRMS scanned masses from m/z 21 to 160 giving a full mass scan approximately every 10 minutes. $DMS_a$ was measured at m/z 63 corresponding to the protonated parent molecule ($C_2H_6SH^+$). The PTRMS drift tube was operated with an applied voltage of 600V, pressure of 2.2 mbar (E/N = 133 Td) and an average primary ion signal (m/z 19) of 1.78 E+07 cps. Data was filtered to remove periods of instrument instability. The PTRMS was operated with a CSIRO custom built auxiliary system which controlled whether the PTRMS sampled VOC-free air to determine instrument background, calibration gas to determine instrument response or ambient air. Zero air measurements occurred twice daily (0100-0200 AM and 1300-1400 UTC) and an interpolated zero signal was subtracted from the reported ambient and calibration measurement signals. Once per day (1400 to 1500 UTC) calibration measurements occurred by diluting a certified

calibration gas standard containing 997 ppb $DMS_a$ (Apel -Reimer Environmental Inc, Colorado, USA) (stated accuracy ±5%) into VOC-free air. The instrument sensitivity to $DMS_a$ was 11.3 normalised cps $ppb^{-1}$ (rel. stdev ±3%). The minimum detectable limit (MDL) for a single 5 sec measurement at m/z 63 ($DMS_a$) was 0.029 ppb determined using principles of ISO 6879 (ISO 1995). Values less than the MDL were removed.

At AIRBOX, $DMS_a$ was measured using an automated gas chromatograph (GC) - pulsed flame photometric detector (PFPD). Measurements were taken every 20 minutes via an auto-sampler programmed to control the GC-PFPD. Full details on the instrumentation and data processing, including uncertainties, can be found in Swan et al. (2015). The $DMS_a$ data from AIRBOX is available at Swan et al. (2017).

**Aerosol and radon observations**

At AIRBOX, the total number concentrations of aerosol with diameters larger than 10 nm were measured with a series of condensation particle counters (CPCs). Sampling was initially performed with a TSI Model 3787 CPC. This unit failed on 1st October 2016 and was replaced on the 3rd October with a TSI Model 3782 CPC. In the intervening period, aerosol concentrations were calculated from size distributions measured by a TSI 3080 scanning mobility particle sizer (SMPS). The SMPS was operated with a TSI Model 3782 CPC and a custom-made differential mobility analyser, which allowed measurement of aerosol with diameters from 11-600 nm. From 11th October 2016 onwards, a newly calibrated TSI Model 3772 CPC was operated in parallel with these instruments, providing reference measurements that were used to correct the counting efficiencies of SMPS and Model 3782 CPC. In turn, the counting efficiency of the Model 3787 CPC was calibrated against the Model 3782 based on co-located measurements taken at the beginning of the campaign. The measurements were averaged to a 3-minute time resolution.

On board the RVI, total number concentrations of aerosol with diameters larger than 10 nm were measured with a TSI model 3772 (TSI, Shoreview, MN) CPC. Aerosol size distributions were measured at diameters from 14 to 685 nm the using a TSI 3080 SMPS. The SMPS was operated with a TSI Model 3772 CPC and a TSI 3081 differential mobility analyser, with a sheath flow of 3 L/min and aerosol flow of 0.3 L/min.

The number concentration of CCN was measured on the RVI using a continuous-flow streamwise thermal-gradient CCN counter (CCNc, model CCN-100, Droplet Measurement Technologies, Longmont,CO, USA). The instrument was configured to run continuously at 0.5 % supersaturation and the flow rate was set to 0.5 L/min. The CCNc and CPC measured from approximately the same point on the sampling line. At AIRBOX, CCN measurements were unavailable due to instrument failure.

Mass concentrations of black carbon (BC) at AIRBOX and on the RVI were obtained with a Thermo Scientific Model 5012 multi-angle absorption photometer (MAAP). The MAAP sampled through a dedicated PM10 inlet, which was heated to minimise the influence of humidity on the BC measurements (Kanaya et al., 2013). Samples were acquired at 5 s time intervals and have been averaged to a 10 minute time resolution.

An Aerodyne compact Time-of-Flight Aerosol Mass Spectrometer (AMS) provided the non-refractory chemical composition of submicron aerosol at AIRBOX (Drewnick et al., 2005). The AMS sampled through a membrane dryer (Nafion MD-700) and a silica gel diffusion dryer which maintained sample relative humidities below 40%. Daily measurements through a high-performance particle filter were used to calculate detection limits and correct for concentrations of background air species (Allan et al., 2004). Samples were averaged to 10-minute intervals. At this time resolution, the campaign-average detection limits were 54 ng $m^{-3}$ (Organics), 5 ng $m^{-3}$ ($SO_4$), 4 ng $m^{-3}$ ($NO_3$) and 46 ng $m^{-3}$ ($NH_4$).

On board the RVI, an Aerodyne Time of Flight Aerosol Chemical Speciation Monitor (ACSM) was used to obtain chemical composition of the non-refractory submicron aerosol. A full description of its design and operation is given in (Fröhlich et al., 2013). The ACSM inlet efficiency is at a maximum for vacuum aerodynamic diameters between 100-450 nm (Jayne et al., 2000; Liu et al., 2007) and therefore the composition measurements best represent accumulation mode aerosol. The AMS sampled through a membrane dryer (Nafion MD-700) and a silica gel diffusion dryer which maintained sample relative humidities below 40 %. Samples were averaged to 10-minute intervals, and at this time resolution the campaign-average detection limits were 127 ng $m^{-3}$ (Organics), 18 ng ng $m^{-3}$ ($SO_4$), 11 ng $m^{-3}$ ($NO_3$) and 151 ng $m^{-3}$ ($NH_4$).

In addition, atmospheric radon-222 concentrations were measured both at AIRBOX and on the RVI using dual-flow-loop two-filter atmospheric radon detectors. Radon concentrations have been shown to be an accurate, independent measure of residual terrestrial influence within an airmass. Radon can subsequently be used to determine if an airmass has a marine or terrestrial origin, and can be satisfactorily used to detect 'baseline' airmass at locations such as Cape Grim (Chambers et al., 2015). While at Cape Grim, the baseline radon concentration is considered to be 30 mBq or below, on board the RVI and at AIRBOX, terrestrial influence over the airmasses was much higher given their coastal location and the prevailing wind directions. For the RVI, a threshold of 300 mBq was used to determine marine from terrestrial airmass. At AIRBOX no satisfactory threshold of radon could be determined to separate marine and terrestrial influences.

**Meteorological observations**

On board the RVI, meteorological observations were taken as part of the routine observations. Observations are available at 5 or 10 second, or 5 minute intervals.

The five minute interval has been used in this study. Where port and starboard observations were available, an average over the two was taken. These observations have been processed by the Marine National Facility and can be downloaded from the Marlin Metadata System (CSIRO, 2016), where more information can also be found. At AIRBOX, wind speed and direction, RH, temperature and pressure observations were taken using a Thompson WS800 weather station. Observations were taken every 15 seconds. These observations have undergone basic visual checks.

On the RVI, a Leosphere R-MAN510 Raman UV polarization (RMAN) lidar provided one minute vertical profiles of aerosol back scatter. The RMAN lidar is able to receive both elastic aerosol backscatter (Rayleigh) and in-elastic backscatter (Raman) by transmitting in both 355 and 387 nm wavelengths. This allows lidar equations to be solved at both day and night time. Due to the inclusion of Raman backscatter, profiles are retrieved up to 4 km. Full instrument details, including setup, calibration and data processing can be found in Alexander and Protat (2018, 2019). In this thesis, the RMAN lidar observations were used to detect the boundary layer height (BLH) using a wavelet covariance transform method as described by Baars et al. (2008). Alexander and Protat (2019) show that this method, using the same instrument as in this thesis, performs well when compared to the lifting condensation level retrieved by radiosondes. This data will be made publicly available at a location to be determined (personal communication S. Alexander).

The BLH at AIRBOX was estimated from observations by a scanning Mini Micro Pulse lidar -532-C Micro (MiniMPL) System (Sigma Space Corporation, Lanham, MD, USA). The MiniMPL operates at 532 nm wavelength and retrieves elastic aerosol backscatter every 10-20 seconds between 30-9,990 m. More information about the MiniMPL, including the set-up, calibration and data processing can be found in Chen et al. (2019). To detect the PBLH an extension of the gradient method of lidar backscatter was employed, which is explained in Xiang et al. (2019).

Finally, satellite observations of cloud top height, spherical albedo and cloud type were provided by the Himawari-8 geostationary satellite (maintained by the Japanese Meteorological Agency). The cloud fields examined were processed and provided by the BoM using algorithms developed by the National Oceanic and Atmospheric Administration (NOAA) National Environmental Satellite, Data, and Information Service (NESDIS) Center for Satellite Applications and Research (Pavolonis, 2010; Heidinger, 2013). The WRF-Chem output was further processed to retrieve fields comparable to observational data, such as cloud effective radius, cloud albedo, cloud optical thickness, updraft velocity and liquid water path. Code to perform this was provided by Dr Steve Utembe.

## 3.3 Statistical methods

### Bootstrapping

A moving block bootstrap (Wilks, 2011) has been used to provide a measure of model uncertainty in a given field where ensemble experiments have not been performed (for example, those described in Section 3.1.5). By selecting, with replacement, blocks of size 2 (as determined by the timeseries auto-correlation) to create 1000 alternate timeseries, the 10th and 90th percentile confidence intervals of mean change of a given field are provided. This method has been applied in Chapter 5 to the Q* field and used in the calculated temperature response as described in Section 3.1.7, as well as for the $\text{flux}_{\text{DMS}}$ for comparison to other studies.

### Statistical testing and correlations

To test the significance of differences in a given field where enough data points are available (for example the ensemble described in Section 3.1.5), the two-tailed Stu-

dent T-test (Wilks, 2011) and the respective field significance (Wilks, 2011) are used. Both of these methods have been evaluated at confidence levels of the 95th percentile ($p < 0.05$) unless otherwise stated. In addition to this, ensemble agreement, where at least five out of the seven ensemble members agree on the change in sign, has been provided as a further indicator of confidence for Chapter 6. In Chapters 7 and 8, correlation analysis has been performed using Spearman's rank correlation methods (Wilks, 2011). This method is a non-parametric test that quantifies the monotonicity of the relationship between two variables.

**Model performance**

To evaluate WRF-Chem against field observations in Chapter 7, the Normalised Mean Bias Factor (NMBF, Yu et al., 2006) is used and described below where $M$ represents modelled values and $O$ measured values. The NMBF is a symmetric metric, i.e. negative biases are not bound by zero, and remains viable when measured values are much smaller than model values. This metric is an improvement on other model performance metrics, as described by Yu et al. (2006), and is commonly used for air quality and aerosol studies (eg. Woodhouse et al., 2019).

If $\overline{M} > \overline{O}$:

$$NMBF = \left( \frac{\sum (M_i - O_i)}{\sum O_i} \right) \tag{3.3}$$

If $\overline{O} > \overline{M}$:

$$NMBF = \left( \frac{\sum (M_i - O_i)}{\sum M_i} \right) \tag{3.4}$$

To ensure clarity of this metric across both positive and negative biases, the NMBF has been converted into a bias factor (BF), where:

If $NMBF > 0$:

$$BF = NMBF + 1 \tag{3.5}$$

If $NMBF < 0$:

$$BF = 1 - NMBF \tag{3.6}$$

## 3.4 Summary

This Chapter has provided the model descriptions, methods and observational data used for this thesis. Whilst the ACCESS-UKCA model is under licence and hence not available publicly, it is hoped that the model description provided here provides enough information for other users. WRF-Chem is freely available and for that reason the chemistry and physics namelists have been provided in Appendix B for reproducibility. Both models have inherent biases and limitations which I have highlighted throughout this Chapter and will be examined more closely in the respective evaluation chapters (Chapters 4 and 7). In addition, this Chapter has described the processes undertaken to evaluate the sensitivities of ACCESS-UKCA and WRF-Chem to DMS, and to estimate coral reef -derived $DMS_w$ and its subsequent atmospheric influence. The influence of these DMS perturbations are examined in Chapters 5, 6 and 8.

# Chapter 4

# ACCESS-UKCA Model Evaluation

This Chapter evaluates the ACCESS-UKCA model against available satellite data. Annual average and annual cycles of ACCESS-UKCA cloud, radiation and precipitation fields are compared to satellite-derived observations. The satellite data used in this Chapter are described in Section 3.1.6. In order to give context to this evaluation, the ACCESS-UKCA output is also compared to that of the CMIP5 (GCMs) and uncertainties surrounding these GCMs are highlighted. Area averages are presented to quantify biases in regions of interest (see Figure 3.5 for area locations). Significant parts of this Chapter are based on the results of the paper: Fiddes, S. L., Woodhouse, M. T., Nicholls, Z., Lane, T. P., & Schofield, R. (2018). Cloud, precipitation and radiation responses to large perturbations in global dimethyl sulfide. ACP https://doi.org/10.5194/acp-18-10177-2018.

## 4.1 Cloud evaluation

The cloud fraction comparison is performed for the years 2006-2009, aligning with the availability of CALIPSO-GOCCP data. ACCESS-UKCA simulates too little low level cloud fraction (Figure 4.1a-c) over the majority of the globe (mean bias of -0.16), which is consistent with findings for the CMIP5 GCMs (Cesana and Chepfer, 2012; Nam et al., 2012; Klein et al., 2013). Areas of large stratiform cloud decks in eastern ocean basins are significantly underestimated, by a fraction larger than 0.5, consistent with other CMIP5 and CFMIP Phase 1 and 2 findings (Bony and Dufresne, 2005; Cesana and Chepfer, 2012; Klein et al., 2013). Low level marine clouds have an large impact on the global radiation budget (Leon et al., 2009) and have been identified as the primary source of uncertainty in tropical cloud-climate feedbacks (e.g., the effects of the cloud albedo) in GCMs (Bony and Dufresne, 2005). These biases have been attributed to poor vertical distribution of clouds in the models, difficulty capturing overlapping cloud layers, the misrepresentation of cloud structures, deficiencies with the statistical parameterisation of clouds and problems with the cloud microphysics (Nam et al., 2012). Low level clouds over the polar regions and some areas of northern Asia and America are slightly overestimated. The ACCESS-UKCA low level cloud biases over the Arctic are within the range of biases found for the CMIP5 GCMs studied in Cesana and Chepfer (2012). It should be noted that satellite observations are subject to biases in detecting low clouds, particularly over the Southern Ocean.

ACCESS-UKCA reproduces the medium level cloud fraction (Figure 4.1d-f) reasonably well, within $\pm 0.1$ in most regions (global mean bias of -0.01). The largest discrepancies are overestimated medium level cloud fraction over the Southern Ocean and Antarctica, where the simulated medium cloud fraction is at its highest globally. The Antarctic bias is of opposite sign to the CMIP5 models compared in Cesana and Chepfer (2012). Bodas-Salcedo et al. (2014) note that issues within GCMs around

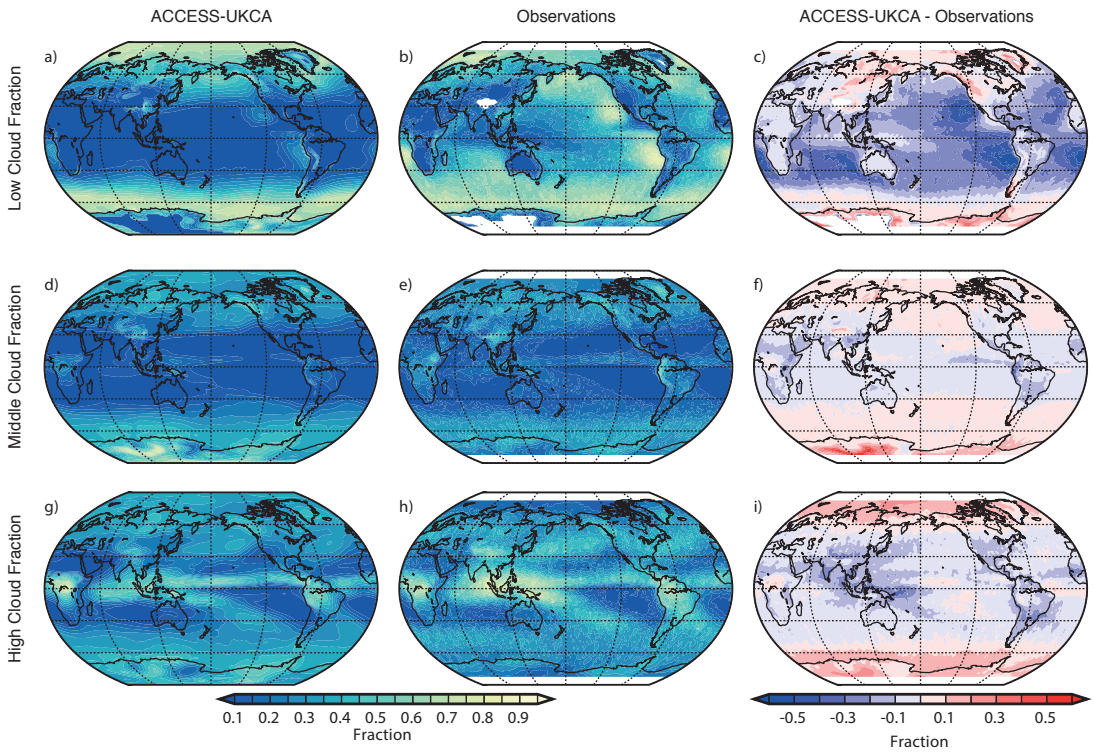


Figure 4.1: The 2006-2009 annual mean of the ACCESS-UKCA Ctl (first column) compared to the CALIPSO-GOCCP (Chepfer et al., 2010) climatology (second column), with the relative differences between the two shown in the third column (model - observations). The top row shows the low level cloud fraction, the middle row shows the middle level cloud fraction and the bottom row the high level cloud fraction

distinguishing between clouds with tops at actual mid level and low level clouds contribute to such biases.

The biases in high level cloud fractions (Figure 4.1g-i) show similar spatial patterns to that of the low level cloud fraction, where underestimation occurs over most of the tropics and mid-latitude. The global mean bias is 0.05 for high level clouds. The largest negative biases, of up to 0.3, occur over the Maritime Continent. Moderate overestimation of high level cloud is noted over the polar regions. These biases are within the range of those found for the CMIP5 models studied in Cesana and Chepfer (2012).

Interestingly, Nam et al. (2012) noted that due to underestimated low level cloud fraction in the tropics, the CMIP5 models over compensate by making optically thick and too bright low clouds and produce more high clouds, impacting the radiation budget. In this research, an underestimation of low clouds is also found in ACCESS-UKCA, although there is no evidence of an over-compensation of high clouds. A small underestimation of high cloud fraction is found in this simulation at tropical to mid latitudes (Figure 4.1i). The optical properties of low clouds have not been analysed.

The annual cycles for cloud fractions are displayed in Figure 4.2, for both the Australian region (green) and the Southern Ocean (blue), as defined in Section 3.1 and Figure 3.5. The low and middle level cloud fractions (Figure 4.2a-b) show little seasonality in the observed climatologies for both the Australian region and the Southern Ocean, whilst high level cloud fraction shows strong seasonality for the Australian region only. For the Southern Ocean, simulated cloud fractions are within at most 0.1 of the observed, though this varies from month to month, and the annual cycle is inverted compared to the observations. Over the Australian region, consistent underestimation of the low level cloud fraction by over 0.1 exists throughout the year, though the annual cycle is well captured. The high level cloud fraction (Figure 4.2c) over the Australian region is underestimated the most (by approximately 0.2) during the summer months, when persistent tropical convection to the north of the country is experienced. Over the rest of the year, high level cloud fraction is within 0.1 of observations.

## 4.2 Radiation evaluation

The remaining analyses for this Chapter consider means over the period of 2000-2009. The comparison of the observed and simulated outgoing longwave radiation

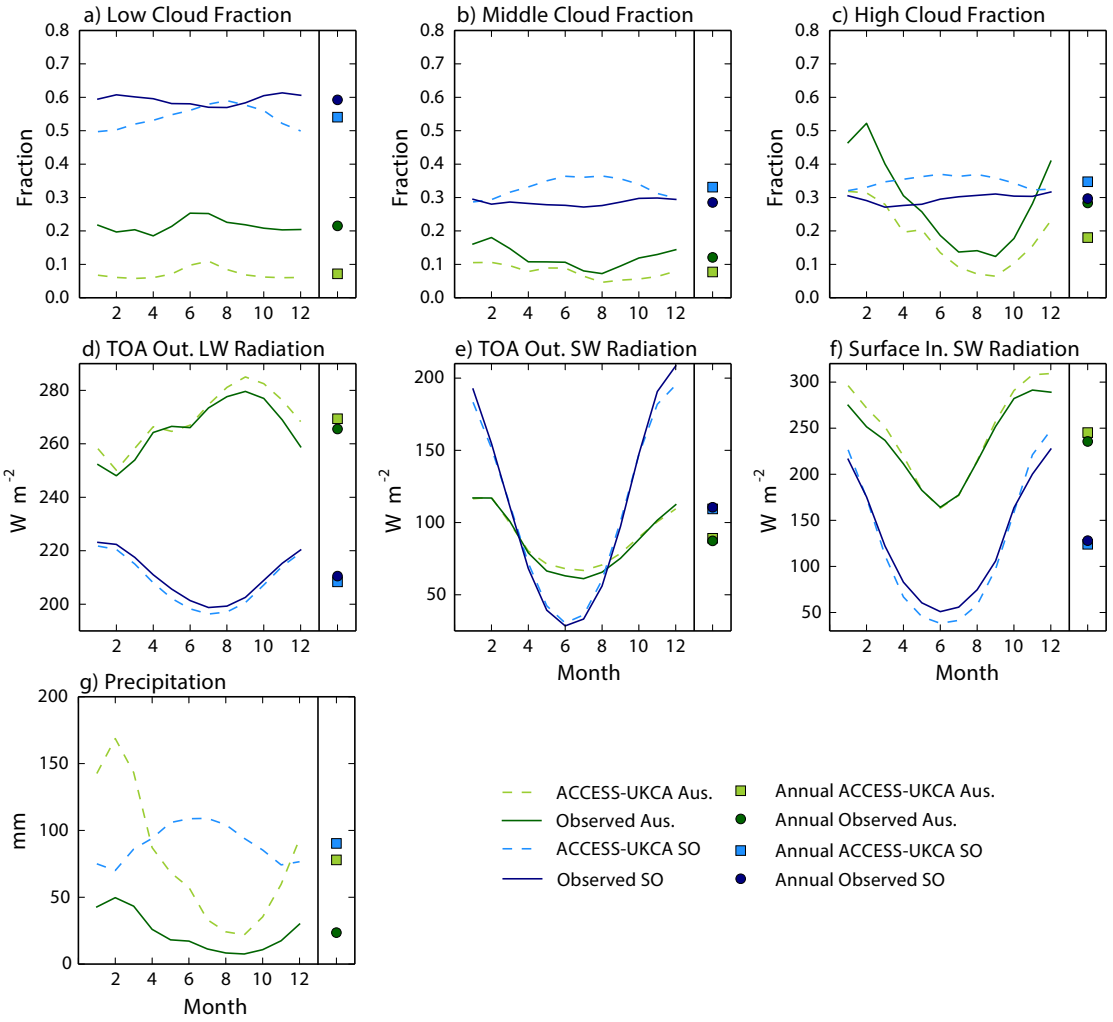


Figure 4.2: Monthly means (averaged over 2000-2009) displayed as an annual cycle (lines) and the annual average (dots/squares on right) for the eight fields compared above: a) low level cloud fraction, b) middle level cloud fraction, c) high level cloud fraction, d) LW$\uparrow_{\mathrm{TOA}}$, e) SW$\uparrow_{\mathrm{TOA}}$, f) SW$\downarrow_{\mathrm{Surf}}$, g) total precipitation. The solid, darker lines represent the observed climatology; dashed, lighter lines the ACCESS-UKCA climatology. Green colours represent the average over the Australian (Aus) region; blues the average over the Southern Ocean (SO). Note that no observed precipitation was plotted for the Southern Ocean in g) due to lack of coverage by observed climatology

at the top of the atmosphere (LW$\uparrow_{\mathrm{TOA}}$) is shown in Figure 4.3a-c. The observed global mean of 239.7 W m$^{-2}$ is closely matched by the simulated 241.0 W m$^{-2}$. Compared to the CMIP5 ensemble, which tends to underestimate LW$\uparrow_{\mathrm{TOA}}$, 238.6 W m$^{-2}$ from Stephens et al. (2012) and 238.9 W m$^{-2}$ from Wang and Su (2013), LW$\uparrow_{\mathrm{TOA}}$

in ACCESS-UKCA is slightly overestimated. The regions with the largest biases (both positive and negative) occur in regions of deep convection (Figure 4.3c), and align well spatially with the biases in high cloud fractions shown in Figure 4.1c. Underestimation by -3 W m$^{-2}$ of LW$\uparrow_{\mathrm{TOA}}$ occurs over the polar oceans which may partly result from an overestimation of cloud fraction at all levels, especially the mid-level clouds (Figure 4.1f) in this region.

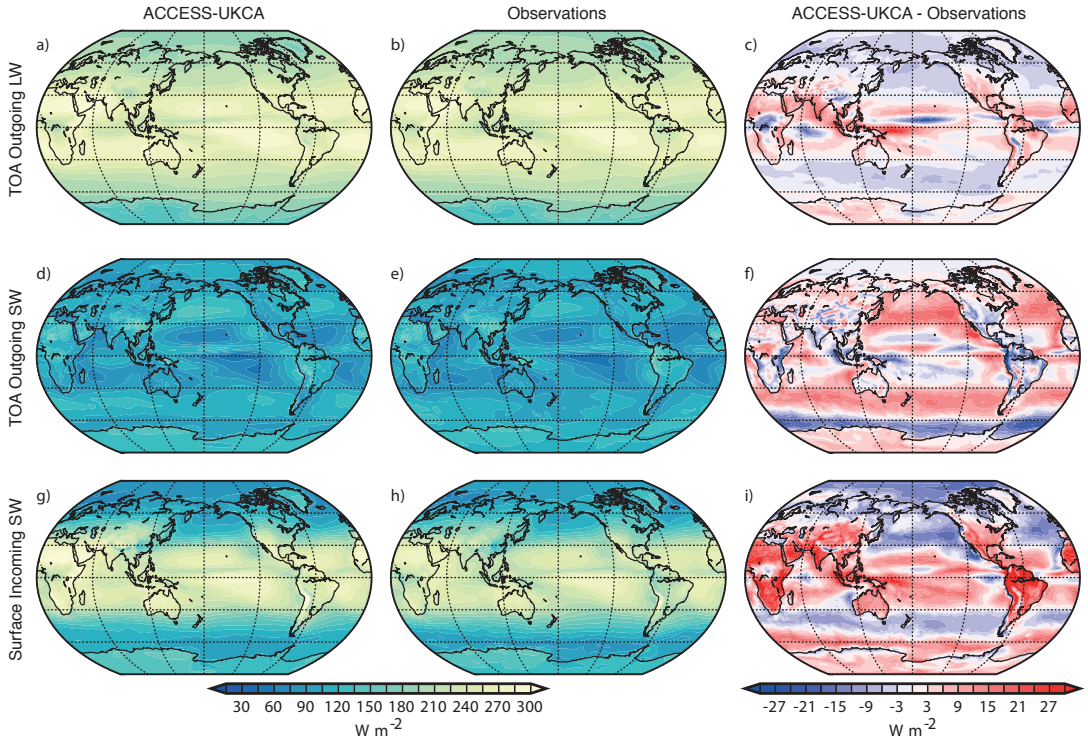


Figure 4.3: As for Figure 4.1 but for annual means for 2000-2009, where the top row shows the LW$\uparrow_{\mathrm{TOA}}$ and the second row: SW$\uparrow_{\mathrm{TOA}}$ and the third row: SW$\downarrow_{\mathrm{Surf}}$. The observations are from the CERES-EBAF - TOA and Surface Ed. 4.0 (Loeb et al., 2009; Kato et al., 2013); all units are in W m$^{-2}$

Spatial biases in the outgoing shortwave radiation at the top of the atmosphere (SW$\uparrow_{\mathrm{TOA}}$) (Figure 4.3d-f) are of greater magnitude than that of the LW$\uparrow_{\mathrm{TOA}}$. In most regions the sign of the SW$\uparrow_{\mathrm{TOA}}$ bias is opposite to that of the LW$\uparrow_{\mathrm{TOA}}$. The same processes that block LW$\uparrow_{\mathrm{TOA}}$ from escaping the atmosphere also reduce incoming shortwave radiation at the surface (SW$\downarrow_{\mathrm{Surf}}$), hence reflecting more sunlight and enhancing the albedo at the top of the atmosphere. Globally, ACCESS-UKCA

performs reasonably well, simulating the global mean $SW\uparrow_{TOA}$ of 101.8 $W\,m^{-2}$ compared to the observed 99.6 $W\,m^{-2}$, consistent with the multi-model mean of GCM ensembles from previous studies (Stephens et al., 2012; Wang and Su, 2013). In Figure 4.3f, an abrupt change in sign of $SW\uparrow_{TOA}$ at 60°S is found, which is also present in the CFMIP comparisons (Bodas-Salcedo et al., 2014). In the Southern Ocean, wrongly assigned mid-level cloud types have been found to be a leading cause of the model underestimation of $SW\uparrow_{TOA}$ (Bodas-Salcedo et al., 2014). In addition, poor representation of the physical processes surrounding super-cooled liquid water in the Southern Ocean has been found to account for 27-38% of the total reflected solar radiation (Bodas-Salcedo et al., 2016). Over the Antarctic ice sheets, both $SW\uparrow_{TOA}$ and $SW\downarrow_{Surf}$ are overestimated, due to an underestimation of low clouds, which allows the high albedo to reflect too much $SW\uparrow_{TOA}$ back out to space.

Globally, ACCESS-UKCA overestimates $SW\downarrow_{Surf}$ (Figure 4.3g-i), with 202.4 $W\,m^{-2}$ compared to observations of 198.3 $W\,m^{-2}$. This overestimation is in agreement with that found for CMIP5 GCMs of $2\pm6$ $W\,m^{-2}$ (Stephens et al., 2012). Nevertheless, large regional biases of over $\pm30$ $W\,m^{-2}$ exist. The most notable features, apart from those discussed above, are too much $SW\downarrow_{Surf}$ over the continents and the tropical regions, which can be attributed in part to the underestimated cloud cover. The northern Pacific and Atlantic Oceans, the Arctic Ocean and parts of the Southern Ocean all receive too little $SW\downarrow_{Surf}$, consistent with overestimated cloud cover.

For each of the radiation fields shown in Figure 4.2d-f, the seasonality is captured with reasonably good skill. Some biases exist at times of highest or lowest radiation. The $SW\downarrow_{Surf}$ experiences the largest biases for both regions of up to $\pm20$ $W\,m^{-2}$, which are likely to have a strong impact on surface temperatures.

## 4.3 Precipitation evaluation

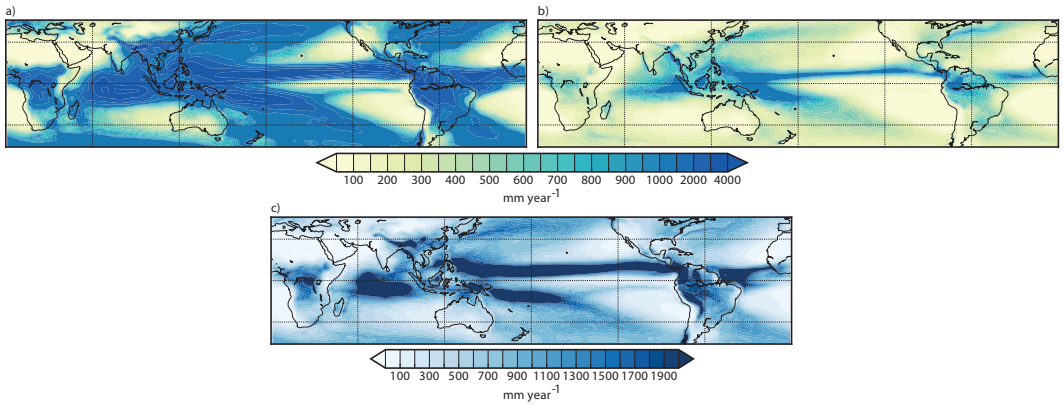


Figure 4.4: The mean (2000-2009) annual total precipitation of a) the ACCESS-UKCA climatology b) the satellite climatology from TRMM (Huffman et al., 2007) and c) the difference between ACCESS-UKCA and the TRMM product (model - observations). Units are in mm year$^{-1}$

Precipitation in ACCESS-UKCA (Figure 4.4) has large positive biases in regions that receive the most annual rainfall and align with the Intertropical and South Pacific Convergence Zones (ITCZ/SPCZ). These regions overestimate precipitation by over 2000 mm year$^{-1}$. Poor performance of GCMs in this region are not unusual however (Stephens et al., 2010), with the current CMIP5 GCM ensemble overestimating precipitation in a similar region by more than 1000 mm year$^{-1}$ (Flato et al., 2013). Stephens et al. (2010) found that models in these regions produce light rain too frequently and suggest that convective processes are poorly simulated. Two of Australia's CMIP5 GCMs, ACCESS 1.0 and 1.3, both overestimate precipitation in this region by similar amounts to that of the ACCESS-UKCA model (Bi et al., 2013). If biases of precipitation are considered as a percentage (not shown), the largest differences occur in the eastern basins of the South Pacific (493% over the SEP region) and South Atlantic Oceans (275% from 0-25°S, 330-10°E).

Finally, large biases in precipitation (Figure 4.2g) are found in ACCESS-UKCA for the Australian region, though these are consistent with those noted for other CMIP5 models as discussed above. Insufficient rainfall observations exist over the

Southern Ocean region to provide a satisfactory analysis. Over Australia, too much rainfall is simulated, especially for the summer months, coinciding with the northern region's wet season. Late winter rainfall shows the least biases. It must be noted however, that the TRMM observational data set underestimates Australian rainfall, with station based 2000-2009 average annual total reported as $487\,\mathrm{mm\,year^{-1}}$ (Bureau of Meteorology, 2017), compared to that of $282\,\mathrm{mm\,year^{-1}}$ for TRMM and $935\,\mathrm{mm\,year^{-1}}$ for ACCESS-UKCA. However, even compared to the station-based rainfall observations, ACCESS-UKCA overestimates precipitation by almost a factor of two.

## 4.4 Discussion

The ACCESS-UKCA chemistry-climate model, which includes a detailed microphysical aerosol module, has been evaluated against satellite observations of cloud fraction, radiation and precipitation. The ACCESS-UKCA model has been found to perform with comparable skill to current CMIP5 GCMs.

Of particular interest, this evaluation of ACCESS-UKCA shows a large underestimation of high, medium and low clouds over tropical regions. These biases have large impacts on the radiation budget for the region, with $\mathrm{SW}{\downarrow_{\mathrm{Surf}}}$ significantly overestimated especially around the Maritime Continent regions, and for precipitation, which is also heavily overestimated. In the Australian region, the high and low cloud annual cycles are not well captured, leading to the larges biases occurring in the austral summer for both radiation and precipitation. In addition, an underestimation of large stratiform cloud decks located in the eastern mid-latitude basins of the Earth's oceans is found. These are regions of extensive low cloud that produce little rainfall (which is overestimated by the model) and are often regions of high primary productivity.

Many of these biases have not been attributed to a single cause (multiple theories have been proposed, as discussed in Section 2.1.3 and within this Chapter), indicating a gap in understanding of atmospheric processes in these regions (Nam et al., 2012).

Numerous DMS-climate studies do not consider the performance of the model alongside their studies, potentially limiting their understanding and application. The evaluation performed here provides crucial context to inform the results discussed in the next two Chapters, Chapter 5 where the large-scale sensitivity of ACCESS-UKCA to DMS is considered, and Chapter 6 that examines the influence of coral reef-derived DMS.

# Chapter 5

# Sensitivity of the current climate to large perturbations in global marine DMS

Natural aerosol emission represents one of the largest uncertainties in understanding of the radiation budget (Carslaw et al., 2013). Sulfur emitted via DMS by marine organisms constitutes at least one-fifth of the global sulfur emissions (Flato et al., 2013) and yet the distribution, fluxes and fate of DMS remain poorly constrained. Numerous global modelling studies have evaluated the importance of DMS in large-scale climate, however, few have placed these results into the context of current or future climate uncertainties. In addition, many of the studies discussed in Section 2.2.7 focus on one or two aspects of the DMS-climate system, commonly reporting on the $\text{flux}_{\text{DMS}}$ and its radiative and temperature effects. In this study the whole system is evaluated, examining chemical, aerosol and meteorological changes, including cloud and precipitation effects.

In this Chapter, ACCESS-UKCA is used to test the large-scale sensitivity of the present day climate to prescribed large-scale changes in $\text{DMS}_{\text{w}}$. Here, sensitivities

within the specific context of the DMS climate system are discussed in addition to the broader context of uncertainties in global DMS and climate modelling. The majority of this Chapter is based on the results of the paper: Fiddes, S. L., Woodhouse, M. T., Nicholls, Z., Lane, T. P., & Schofield, R. (2018). Cloud, precipitation and radiation responses to large perturbations in global dimethyl sulfide. ACP https://doi.org/10.5194/acp-18-10177-2018.

Three simulations are performed to explore the chemical, aerosol and meteorological implications of large $DMS_w$ perturbations. In Section 5.1, the L11 simulation is compared to the Z simulation, in which all $DMS_w$ is removed from the system to determine its current contribution to the climate. In Section 5.2, the L11 simulation is compared to L11MX, where $DMS_w$ is increased to the zonal maximum. The results of this section are compared to that of the work by Grandey and Wang (2015). A description of how the $DMS_w$ fields were created can be found in Section 3.1.4.

## 5.1 Removal of global marine DMS

### 5.1.1 Chemistry response

The 2000-2009 annual mean ocean $flux_{DMS}$ from ACCESS-UKCA is 17.41 Tg year$^{-1}$ of sulfur, resulting in an atmospheric $DMS_a$ annual mean surface concentration of 81.9 ppt. Taking all marine $DMS_w$ out of the model (but retaining the terrestrial source of 0.72 Tg year$^{-1}$ of sulfur) results in a 94% reduction in $DMS_a$ at the surface; throughout the troposphere, it results in a 98% reduction of $DMS_a$.

The impact of this reduced $flux_{DMS}$ on atmospheric sulfur can be seen in Figure 5.1a-b, d-e. Globally, there is a net decrease of 15% of $SO_2$ at the surface. The largest absolute differences are in the tropics and mid-latitudes over the oceans. Large relative decreases in $SO_2$ occur in the SO and SEP, 84% and 94% respectively.

Figure 5.2a shows the vertical profile of $SO_2$ for the Australian region (red), the SO (blue) and the SEP (green). The large peak in concentration at approximately 500 m occurring in the Australian profile is attributable to industrial and energy-related emissions of $SO_2$, which is due to lofting by chimneys and smokestacks. The $SO_2$ in Z is consistently lower than that of the L11 throughout the troposphere, though for the regional means, the difference begins to decrease closer to the tropopause.

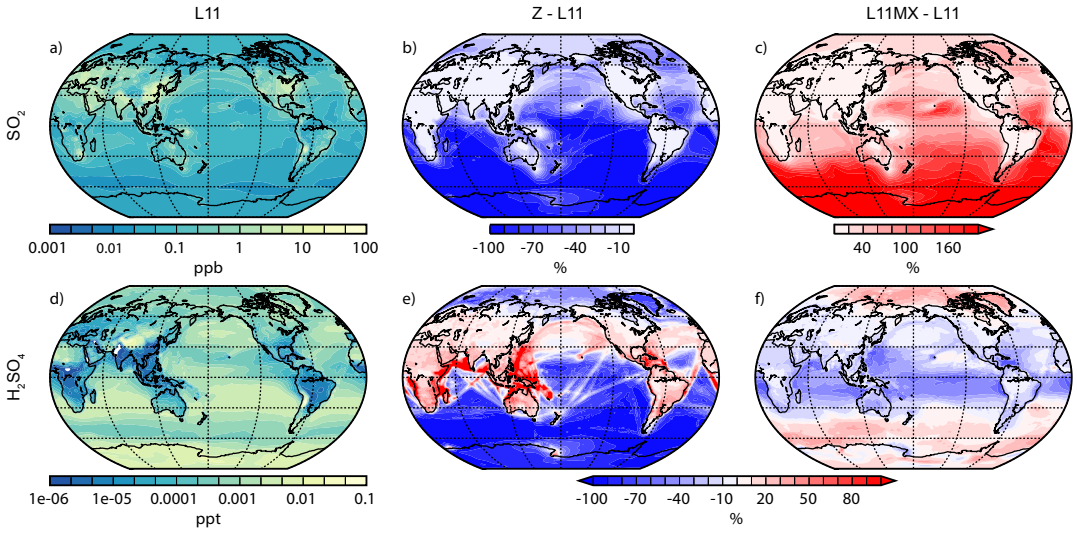


Figure 5.1: Mean (2000-2009) values for the L11 simulation (first column), the difference between Z (zero $DMS_w$) and the L11 (second column) and the difference between L11MX (zonally enhanced $DMS_w$) and the L11 (third column). The first row shows the volume mixing ratio of $SO_2$ in ppb; the second row the volume mixing ratio of $H_2SO_4$ in ppt

Surface $H_2SO_4$ (Figure 5.1d-e) decreases significantly in predominantly clean marine areas; the SO has a 79% decrease and the SEP an 84% decrease, compared to a 49% global mean decrease. Interestingly, heavily polluted regions, especially busy shipping lanes, undergo an increase in $H_2SO_4$. $H_2SO_4$ is an aerosol precursor gas, which can participate in the formation of secondary sulfate aerosol, or it can condense onto pre-existing particles. The increased $H_2SO_4$ concentration in heavily polluted regions results from a decreased condensational sink (not shown). Similar non-linearities have been described in Thomas et al. (2011).

The vertical profiles of $H_2SO_4$ in Figure 5.2b, show that the largest differences between the Z and the L11 occur in the free troposphere (between 1-10 km) for all regions. In all three regions (each considered a relatively clean atmospheric environment), net decreases of $H_2SO_4$ occur.

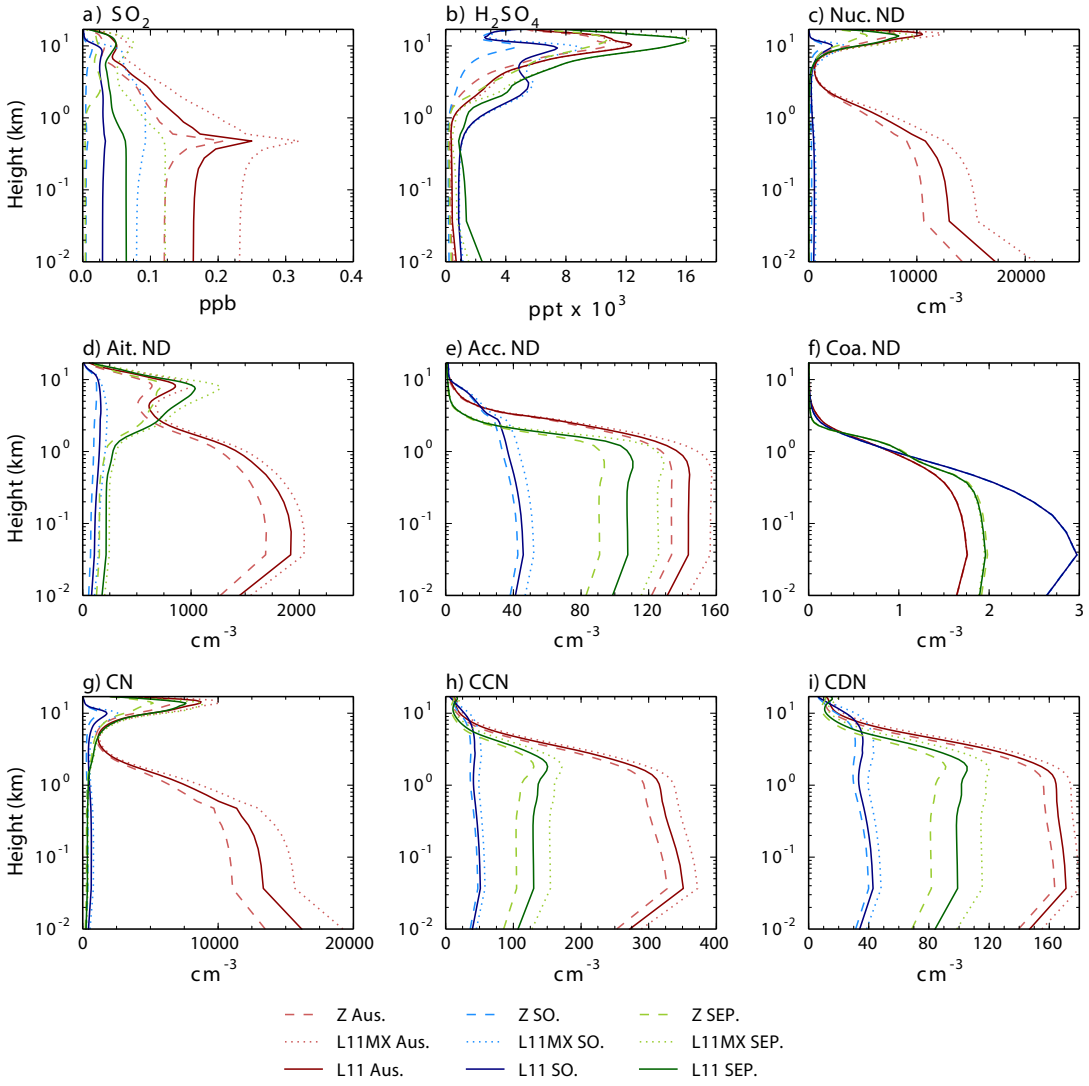


Figure 5.2: The vertical profiles of a) $SO_2$; b) $H_2SO_4$; c) nucleation mode number density; d) Aitken mode number density; e) accumulation mode number density; f) coarse mode number density; g) $N_3$ nuclei number; h) CCN; and i) CDN. The solid lines represent the L11; dashed lines shows Z; and dotted lines show L11MX. Blue lines show the SO mean, red the Australian region mean and green the SEP. All units are $cm^{-3}$, apart from a): ppb and b); ppt x $10^{-3}$

### 5.1.2 Aerosol response

The majority of gaseous $H_2SO_4$ is taken up by aerosol formation (99.99%) as opposed to being removed by dry deposition (0.01%) (Mann et al., 2010). The peak in nucleation mode number density in the free troposphere in Figure 5.2c coincides with the peak concentration of $H_2SO_4$. Surface global nucleation mode number concentration decreases by 9% between Z and the L11 (see Figure 5.2c). While in absolute terms, clean terrestrial regions have the largest decreases, the Australian region only has a relative decrease of 18% in nucleation mode particles. Over the oceans, although few nucleation mode particles exist, there are large relative differences of both signs.

In absolute terms, the differences in the aerosol number concentration are greatest in the smaller aerosol modes, particularly the nucleation mode described above. Figure 5.2d-f show the number concentrations for the Aitken mode, accumulation mode, and coarse mode (global maps not shown). The Aitken mode (Figure 5.2d) shows some differences between the two simulations, with profiles reflecting reduced new particle formation in the free troposphere and reduced condensation-growth of $H_2SO_4$ onto pre-existing particles in the boundary layer. The largest differences are seen over the Australian region. Similar boundary layer differences are also present in the accumulation mode, with the differences between the Z and L11 consistent below 1 km (Figure 5.2e). Little difference is seen in the coarse mode throughout the troposphere (Figure 5.2f), which in marine regions is dominated by sea salt.

As aerosol grow towards the larger end of the Aitken mode, they become relevant to cloud processes. Figure 5.3a shows the L11 condensation number concentration particles with a dry diameter greater than 3 nm ($N_3$). The difference in surface $N_3$ concentration between the L11 and Z shows the largest relative decreases occur in clean, coastal regions, predominantly in the Southern Hemisphere, as well as some regions of the SO. In heavily polluted terrestrial regions a small increase in the $N_3$ number concentration occurs. A decrease of 8% is found globally. For the Australian

region (representative of a clean, terrestrial region), a decrease in $N_3$ of 17% is found.

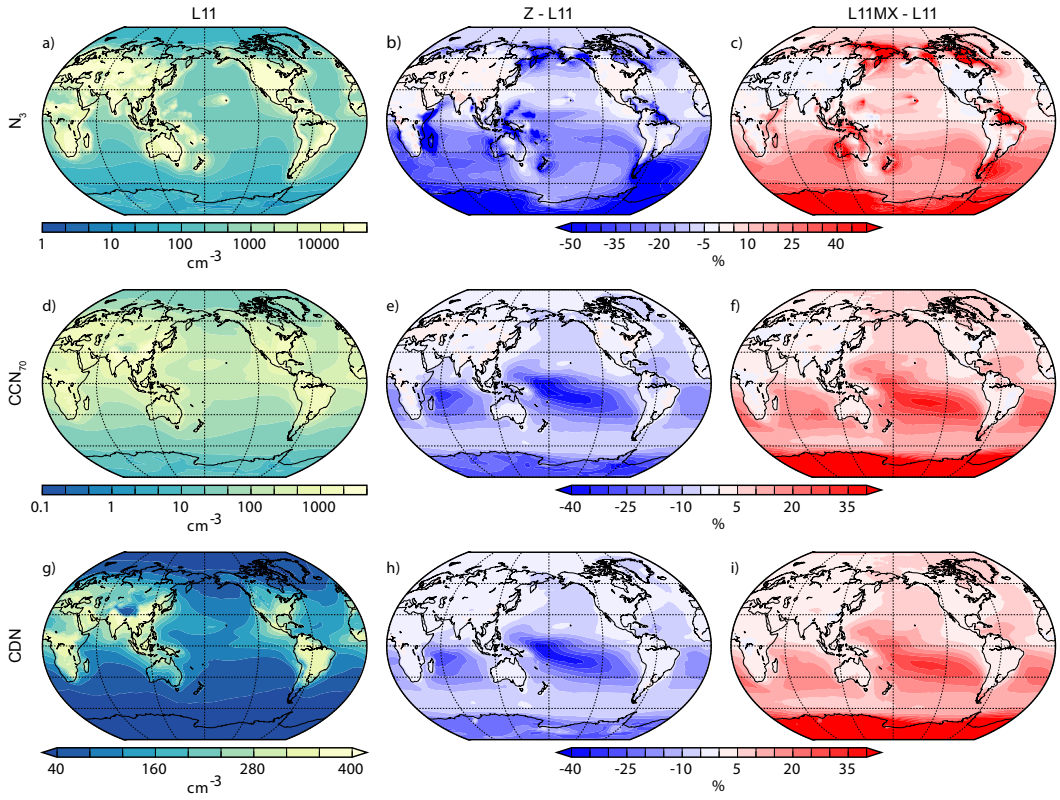


Figure 5.3: As for Figure 5.1, but where the first row shows the number concentration of $N_3$; the second the number of CCN; and the third the CDN concentration. All unitsare in cm$^{-3}$

Over the SO a relative decrease in $N_3$ of 39% occurs at the surface. The SO and the SEP have far fewer aerosol in all modes except the coarse mode (see Figure 5.2c-f), where sea salt dominates. This decrease in number concentration in small aerosol modes represents a large portion of the aerosol loading in the region. The decrease in nucleation mode particles is reflected in the $N_3$ for the SEP region, via a more moderate decrease of 20%.

Figure 5.3d-e show the number concentration of CCN with dry diameters greater than 70 nm ($CCN_{70}$) for the L11 and the differences resulting from Z. The largest absolute differences are in the tropics, which, similarly to the $N_3$, has the highest concentration. Relatively, when all $DMS_w$ is removed, there is a global decrease of 5% in $CCN_{70}$, while decreases of 7% were found over the Australian region, decreases

of 8% over the SO and decreases of 20% over the SEP. Differences in CDN are shown in Figure 5.3g-h. The relative differences in CDN show a similar spatial pattern to that of the $CCN_{70}$. Global mean CDN decreases by 5%. A decrease of 5% is also found for the Australian region, whereas the SO shows an 8% decrease, and the SEP shows an 18% decrease. In both the $CCN_{70}$ and CDN, the marine Southern Hemisphere mid-latitudes have the largest decreases of 14% (averaged between 5-35°S) despite the SO having some of the larger decreases in $SO_2$ and $H_2SO_4$.

The larger differences in concentration of both $CCN_{70}$ and CDN in the oceanic Southern Hemisphere tropics and mid latitudes, compared to the SO, warrant further investigation of how sulfate aerosol are interacting with their background environments, for example cloud processes and pre-existing aerosol. Additionally, in areas of persistent low cloud formation, in-cloud aqueous sulfate oxidation is the dominant reaction (over gaseous nucleation), which allows almost instantaneous growth of existing aerosol, and is temperature dependent. It is speculated that poor representation of low clouds in the SO may have further impacts on atmospheric composition modelling than currently appreciated. A cloud resolving modelling study may be better suited to gain understanding of the complexity of the system described here.

Following the method of Woodhouse et al. (2010, 2013), global and hemispheric sensitivities of $CCN_{70}$ to $flux_{DMS}$ have been calculated (Table 5.1). The results presented here suggest a lower $CCN_{70}$ sensitivity to $flux_{DMS}$ compared to the Woodhouse et al. (2013) study where absolute sensitivities of 94 and 63 $cm^{-3}/mg\,m^{-2}\,day^{-1}$ of sulfur were found globally for June and December respectively. Similar $CCN_{70}$ sensitivities are reported in the Woodhouse et al. (2010) study (63 $cm^{-3}/mg\,m^{-2}\,day^{-1}$ global average). The lower sensitivities in this study are likely the result of the large (near 100%) changes in $flux_{DMS}$ (the denominator), and further show that the DMS-climate system is non-linear. Relative CCN sensitivities calculated here compare well with the Woodhouse et al. (2010) and Woodhouse et al. (2013) studies.

For example Woodhouse et al. (2010) finds mean hemispheric relative $CCN_{70}$ sensitivities of 0.02 for the Northern Hemisphere and 0.07 for the Southern Hemisphere. These results highlight the greater relative importance of DMS in the Southern Hemisphere.

Table 5.1: Global and hemispheric means of the CCN sensitivity to the $flux_{DMS}$ (as defined by Woodhouse et al. (2010, 2013)) in both absolute ($cm^{-3}/mg\,m^2\,day^{-1}$) and relative terms, for Z and L11MX

| Region | Z Absolute | L11MX Absolute | Z Relative | L11MX Relative |
|---|---|---|---|---|
| Global | 16.9 | 12.4 | 0.048 | 0.036 |
| SH | 15.8 | 11.2 | 0.090 | 0.063 |
| NH | 18.6 | 14.5 | 0.029 | 0.023 |

### 5.1.3 Cloud, radiation and precipitation response

Meteorological responses to the DMS perturbations must be considered carefully. As detailed in the methods section, the ACCESS-UKCA simulations are nudged to ERA-Interim potential temperature and horizontal winds, preserving synoptic scale meteorology and limiting any feedbacks. While performing a non-nudged simulation would allow the meteorology to respond to changes in the chemistry and aerosol more freely, it would make comparison of the aerosol and meteorological responses more difficult. Within ACCESS-UKCA, GLOMAP-mode is directly coupled to the large-scale cloud and precipitation schemes via the CDN (Abraham et al., 2012), as well as the radiation scheme via aerosol and some gases (see Section 3.1.3). Convective rainfall and cloud formation are not directly coupled to the aerosol scheme, but can be indirectly influenced via changes in radiation (which can act on temperature, moisture, etc).

Differences in low cloud fraction occur predominantly in areas with large stratiform cloud decks (Figure 5.4a). The largest differences occur in eastern basins of the

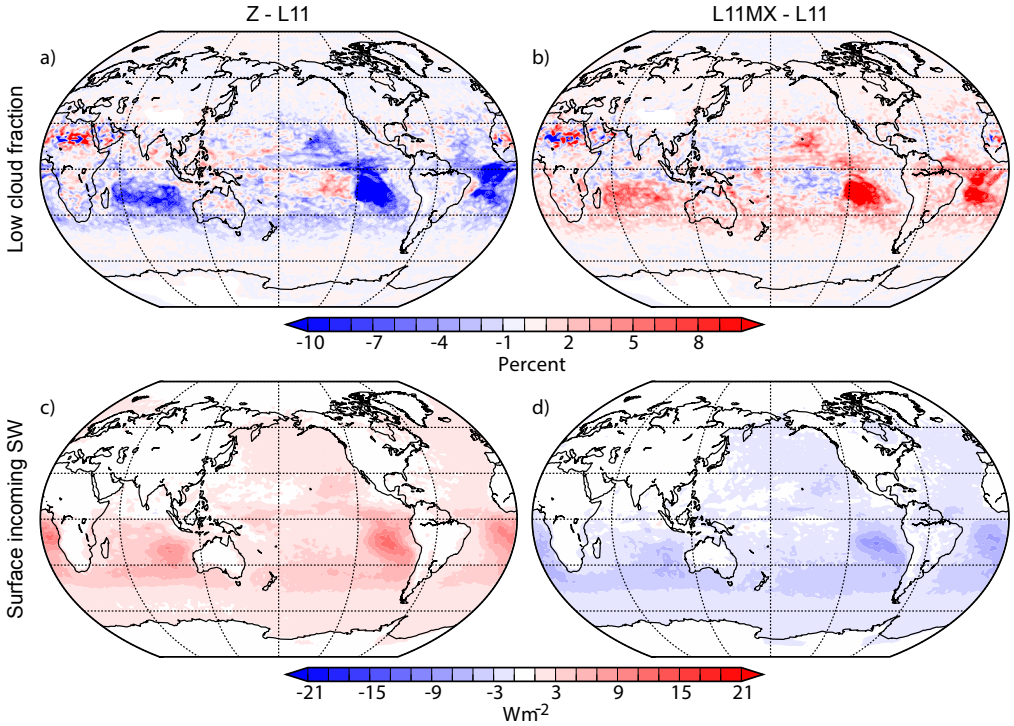


Figure 5.4: Comparisons in of the low cloud fraction (as a percentage) (a-b) and $SW\downarrow_{Surf}$ ($W\,m^{-2}$) c-d) over the 2000-2009 period for Z (first column) and L11MX (second column) minus the L11. The absolute values for the L11 of these fields can be seen in Figure 4.1 and 4.3

Southern Hemisphere's oceans. The SEP region shows an annual mean decrease in low cloud fraction of 9%. In the Northern Hemisphere (including the north eastern Pacific where significant stratiform cloud decks are found) and the SO (where persistent low cloud formation occurs) only small differences are evident, which may in part be due to the modest differences in $CCN_{70}$ and CDN concentrations discussed in Section 5.1.2. Stratiform cloud deck low cloud fractions are consistently underestimated by ACCESS-UKCA and other GCMs (see Chapter 4) in comparison to other areas of significant low cloud formation such as the SO. The mechanism behind the different responses (between the SO and cloud deck regions), and whether the long standing model biases, especially those around the formation of supercooled liquid water, have contributed to the differing responses should be the subject of future investigations.

The decrease in low cloud fraction and aerosol number concentration discussed above lead to an increase in $SW\downarrow_{Surf}$ (Figure 5.4c). This increase in $SW\downarrow_{Surf}$ is highest in the regions of stratiform cloud deck formation. In the SEP region there is a mean increase of 7 W $m^{-2}$.

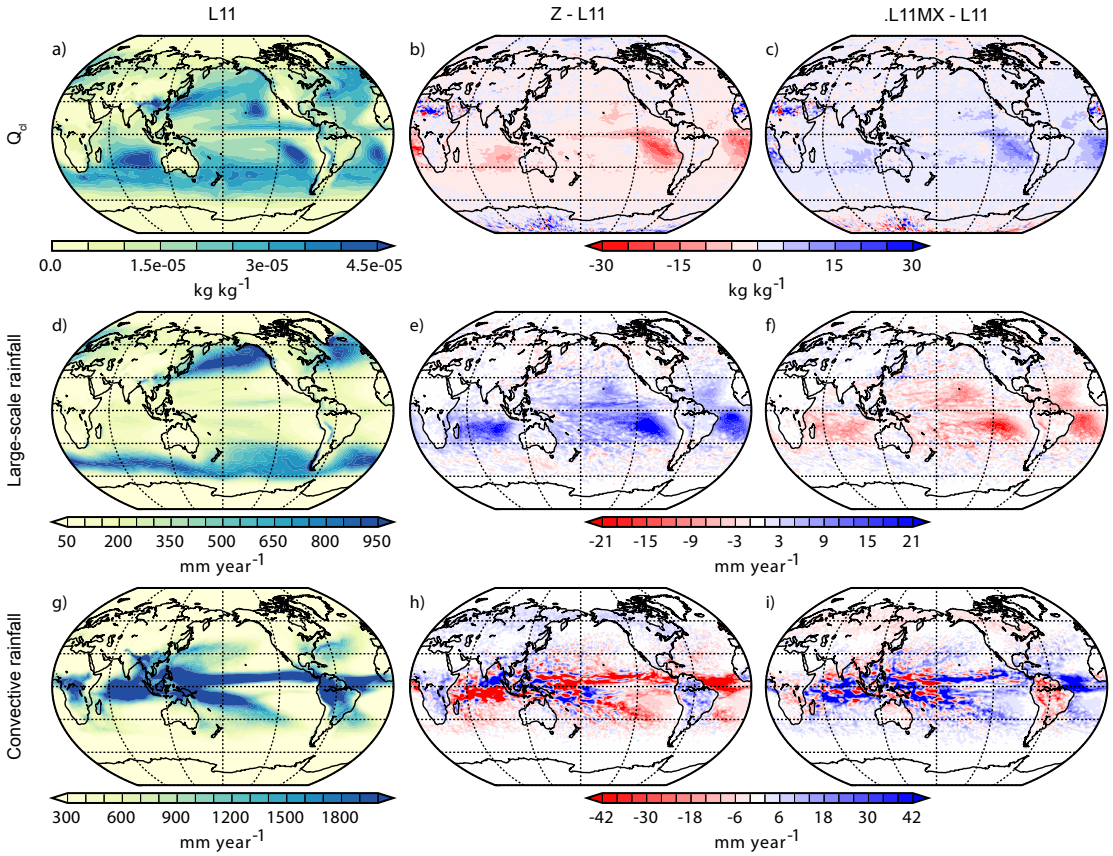


Figure 5.5: Comparisons of the (a-c) $Q_{cl}$ at 1700m height, (d-f) large-scale rainfall, (g-i) convective rainfall over the 2000-2009 period. The L11 absolute values are shown in the first column, and respectively Z and L11MX minus the L11 in the second and third columns. Units are in kg $kg^{-1}$ and mm $year^{-1}$

Decreases of cloud liquid water ($Q_{cl}$) at 1700 m height shown in Figure 5.5a-b are found in the stratiform cloud deck regions. Globally, small differences in $Q_{cl}$ are found to occur at the surface. The decrease in $Q_{cl}$ is coincident with increases in large-scale precipitation in the stratiform cloud decks, regions with very little precipitation (Figure 5.5d-e). In the SEP region large-scale rainfall increases by 17 mm $year^{-1}$ (15%) over the L11 mean of 111 mm $year^{-1}$.

In the Southern Hemisphere stratiform cloud decks, and in particular the SEP region, the model demonstrates a distinct cloud lifetime effect in response to removing DMS in Z. Decreased CDN concentration and the associated increase in cloud droplet size and increased liquid water lead to increased autoconversion and large scale rainfall. The overall impact is to reduce low cloud fraction.

Figure 5.5g-h shows the differences in convective rainfall. While the convective rainfall scheme is not coupled directly to GLOMAP-mode, there are differences between the simulations. Convective rainfall decreases in Z compared to the L11 along the ITCZ (a mean difference of 11 mm year$^{-1}$ between 20°S-20°N). This difference represents a small fraction (less than 1%) of the total convective rainfall. Relatively, (not shown) the largest differences (a 5% decrease in the SEP) are found once again in eastern ocean basins of Southern Hemisphere stratiform cloud decks.

Seifert and Beheng (2006) note that even when convection schemes are coupled to an aerosol scheme, the effects of $CCN_{70}$ on convection, and the resultant precipitation and associated maximum updrafts, differs significantly depending on the cell type and size, making these effects difficult to quantify. Large differences in convective rainfall would not be expected in these results, due to the meteorological nudging used in the experiments.

## 5.2 Increasing DMS to the zonal maximum

This section considers the global response to zonally enhanced $DMS_w$, resulting in a $flux_{DMS}$ of 37.05 Tg year$^{-1}$ of sulfur (relative to 17.41 Tg year$^{-1}$ of sulfur in the L11 simulation). For comparison, the Grandey and Wang (2015) study considered the impact of zonally enhanced $flux_{DMS}$ of 46.1 Tg year$^{-1}$ of sulfur (up from 18.2 Tg year$^{-1}$ of sulfur), under global warming scenarios. Many of the differences resulting from zonally enhancing $DMS_w$ show similar spatial patterns, with similar

magnitude but reversed sign compared to the Z simulation.

Globally, the differences in $SO_2$ (Figure 5.1c) are of comparable magnitude to Z. Increased $SO_2$ concentrations occur over the Australian region, the SO and the SEP: increases of 42%, 172%, 89% respectively. There is a net decrease in $H_2SO_4$ of 14% in Australia, and a larger decrease over the tropical oceans. Over the SO there is an increase of 9%, while in the SEP a decrease of 37% occurs. Similar non-linearities are discussed in terms of doubled $DMS_w$ in Thomas et al. (2011). These differences in $SO_2$ and $H_2SO_4$ are also clear in the vertical profiles shown in Figure 5.2a-b.

Differences in the aerosol modes (see Figure 5.2c-f) are of similar magnitude but opposite sign to those noted in Section 5.1.2. Global mean $N_3$, $CCN_{70}$ and CDN increases by 6%, 4% and 5% respectively (Figure 5.3c,f,i). Larger differences are seen over the SO of 27%, 15% and 13% and the SEP of 14%, 19% and 17% for $N_3$, $CCN_{70}$ and CDN respectively.

Globally, there is little difference in low cloud fraction or $Q_{cl}$, though increases are noted in regions of large stratiform cloud decks (Figure 5.4d), which show similar spatial patterns to that of Z. $SW{\downarrow}_{Surf}$ has a global mean decrease of -1.75 W $m^{-2}$. This decrease is comparable to the Grandey and Wang (2015) finding of -2.2 W $m^{-2}$ (noting the larger $DMS_w$ perturbation by Grandey and Wang, 2015). Lastly, decreases in large-scale precipitation are found, again in regions of stratiform cloud decks (Figure 5.5f), while general increases in convective precipitation over the tropical oceans occur (Figure 5.5i). The Grandey and Wang (2015) study, which analysed a warming climate, also found large relative decreases in precipitation rate predominantly in eastern ocean basins. Under the current climate, the largest relative increase in total precipitation are found in the southeast basins of the Pacific and Atlantic ocean (not shown), however the results presented here are much noisier than the Grandey and Wang (2015) results. Grandey and Wang (2015) find that artificial enhancement of DMS may offset some global warming, which is supported

by this study as implied by the decreases in $SW\downarrow_{Surf}$, however the precipitation responses warrant further study.

## 5.3 Determining the temperature response to changes in radiative forcing

Table 5.2: Summary of the global mean (2000-2009) radiation fields: absolute L11 values for the TOA shortwave (SW) and longwave (LW) outgoing and Q*; and the differences in these quantities resulting from Z and L11MX (from L11) as well as the FAIR temperature response. The ranges shown for Z-L11 and L11MX-L11 indicate the 10th and 90th percentile confidence intervals

| Simulation | TOA SW ↑ ($W\,m^{-2}$) | TOA LW ↑ ($W\,m^{-2}$) | Q* ($W\,m^{-2}$) | FAIR response (K) |
|---|---|---|---|---|
| Ctl absolute values | 101.79 | 241.04 | -1.35 | NA |
| Z - L11 | -1.82 (-2.62 to -1.23) | 0.13 (0.04 to 0.20) | 1.69 (1.13 to 2.43) | 0.45 (0.30 to 0.64) |
| L11MX - L11 | 1.57 (1.08 to 2.48) | -0.12 (-0.20 to -0.04) | -1.45 (-2.33 to -0.98) | -0.38 (-0.61 to -0.26) |

The global 2000-2009 mean of Q*, and its main components are provided in Table 5.2, along with the relevant confidence intervals derived from the bootstrapping technique (see Section 3.3). Due to the nudging used in the simulations, it is not expected that the TOA Q* will be balanced (i.e. Q* = 0). The differences in Q* seen in Z and L11MX, 1.69 $W\,m^{-2}$ (1.13 to 2.43, 10th and 90th confidence intervals) and -1.48 $W\,m^{-2}$ (-2.33 to -0.98, 10th and 90th confidence intervals) respectively, show a substantial radiative effect of DMS on the energy budget. The Q* response found for Z is consistent with the Mahajan et al. (2015) findings of 1.79 $W\,m^{-2}$. Using the FAIR model's climate component (see Section 3.1.7), the 2000-2009 mean temperature response is calculated to be 0.45 K (0.30 to 0.64, 10th and 90th percentile range) for Z and -0.38 K (-0.26 to -0.61, 10th and 90th percentile range) for

L11MX.

Other studies generally consider DMS changes under global warming. To make comparisons, the sensitivity of the estimated global temperature response to changes in the $\text{flux}_{\text{DMS}}$ (see Table 5.3) is used. In this study, a response of 0.027 K per $\text{Tg}\,\text{year}^{-1}$ of sulfur in Z, and 0.019 K per $\text{Tg}\,\text{year}^{-1}$ of sulfur in L11MX is found. These results are of similar magnitude to the Grandey and Wang (2015) study (0.029 K per $\text{Tg}\,\text{year}^{-1}$ of sulfur) and in the range of the lowest impact scenario of Six et al. (2013) (0.03 - 0.060 K per $\text{Tg}\,\text{year}^{-1}$ of sulfur). The other scenarios in the Six et al. (2013) study (0.046 - 0.11 K per $\text{Tg}\,\text{year}^{-1}$ of sulfur) suggest much higher temperature sensitivities to changes in $\text{flux}_{\text{DMS}}$, as does the Schwinger et al. (2017) study (0.041 K per $\text{Tg}\,\text{year}^{-1}$ of sulfur).

Table 5.3: The estimated temperature response to perturbations in the $\text{flux}_{\text{DMS}}$ (K per $\text{Tg}\,\text{year}^{-1}$ of sulfur) for the current study's experiments (Z and L11MX) and those found in the literature. The ranges shown for Z and L11MX indicate the 10th and 90th percentile confidence intervals

| Experiment | K per $\text{Tg}\,\text{year}^{-1}$ of sulfur |
|---|---|
| Z | 0.027 (0.018 to 0.038) |
| L11MX | 0.019 (0.013 to 0.031) |
| Schwinger et al. (2017) | 0.041 |
| Six et al. (2013) - low pH impact scenario | 0.03 - 0.060 |
| Six et al. (2013) - medium pH impact scenario | 0.046 - 0.096 |
| Six et al. (2013) - high pH impact scenario | 0.051 - 0.11 |
| Grandey and Wang (2015) | 0.029 |

## 5.4 Discussion

Globally, removing or enhancing $\text{DMS}_{\text{w}}$ from the climate system leads to significant responses in chemistry and aerosol concentrations. While changes in meteorological parameters (low level cloud fraction, large-scale precipitation, moisture, radiation)

are largest in the Southern Hemisphere stratiform cloud decks, global mean differences were small. DMS in these stratiform regions is found to play an important role in cloud processes and precipitation suppression (as discussed in Thomas et al. (2011) or with regards to anthropogenic pollution in Ackerman et al. (2004)). Furthermore, it has been demonstrated that marine DMS is responsible for increasing low level cloud fraction in stratiform cloud deck regions, a demonstration of the second aerosol indirect (or lifetime) effect (Albrecht, 1989). These results indicate that a greater understanding of natural aerosol and their interaction with cloud processes (both via observations and modelling studies) in these regions may improve model representation, as these regions were found to have considerable model bias in comparison to observations in the Chapter 3.1.6.

In other regions of significant low cloud formation (SO, Northern Hemisphere cloud decks), anthropogenic aerosol and modelling deficiencies may be preventing responses due to changes in DMS-derived aerosol. In the SO, representation of cloud characteristics in global climate models is poor (see Chapter 3.1.6), especially with respect to supercooled liquid water (Bodas-Salcedo et al., 2016). It is likely that these deficiencies are misrepresenting the DMS-climate interactions in the SO. Improvement in the representation of these characteristics, such as cloud height and phase, may yield a greater understanding of how DMS interacts with climate.

In addition, the Northern Hemisphere was found to be less sensitive to changes in marine DMS. The Northern Hemisphere is considered a less 'clean' environment than the Southern Hemisphere. The reduction in sensitivity in polluted conditions is supported by Carslaw et al. (2013), who found a much higher response of CCN to $\text{flux}_{\text{DMS}}$ perturbations under pre-industrial conditions compared to today's conditions. This finding may have important implications for how much coral reef-derived DMS can influence the environment, given many of the world's coral reefs are located near polluted regions (eg. southeast Asia, India and Central America).

By nudging these simulations, the model response to the DMS perturbations is limited to fast aerosol and cloud changes. Similarly, the temperature estimate provided by the FAIR model can only take into account direct changes in temperature due to the radiation forcing provided and cannot account for subsequent feedbacks in the system. It is suggested that free running ensemble experiments be performed to gain insight into the aerosol-cloud-climate processes and the subsequent feedbacks occurring in regions of significant DMS influence. Such experiments should focus on improving microphysical aspects of aerosol-cloud interaction in these regions (and how it differs among regions), improving the representation of aerosol, in particular natural aerosol and on understanding the interconnected nature of the DMS-climate system.

Previous studies examining the role of DMS in the climate system have not identified stratiform cloud decks as regions of particular importance. Instead, these studies focused on cloud feedbacks in the SO (Thomas et al., 2010; Mahajan et al., 2015). Mahajan et al. (2015) estimated the global TOA radiative effect of DMS to be $1.79\,\mathrm{W\,m^{-2}}$, which is consistent with the results of this thesis ($1.69\,\mathrm{W\,m^{-2}}$), but slightly lower than the estimation of $2.03\,\mathrm{W\,m^{-2}}$ estimated by Thomas et al. (2010), who used the previous Kettle and Andreae (2000) $\mathrm{DMS_w}$ climatology.

In this study, the estimated temperature responses per unit change in DMS-derived sulfur flux (0.027 or 0.019 K per $\mathrm{Tg\,year^{-1}}$ of sulfur) are lower than those reported in the Six et al. (2013) (0.046-0.096 K per $\mathrm{Tg\,year^{-1}}$ of sulfur, medium impact scenario) and Schwinger et al. (2017) (0.041 K per $\mathrm{Tg\,year^{-1}}$ of sulfur) studies. The temperature response sensitivities calculated here are comparable to those given in Grandey and Wang (2015) (0.029 K per $\mathrm{Tg\,year^{-1}}$ of sulfur). Without further information, it is difficult to speculate on the cause of the discrepancy between the results presented here and those in Six et al. (2013) and Schwinger et al. (2017). One such cause could be the relative simplicity of the FAIR model in comparison

to fully coupled climate models and hence cannot represent all feedbacks. However, we note that the FAIR morel is a GCM emulator and so the results should be superficially comparable (as it is for Grandey and Wang, 2015). Nevertheless, the discrepancy between these results suggests the need for better observational constraints to constrain fully coupled climate simulations and highlights the complexity of the DMS-aerosol-cloud system.

Natural aerosol account for a significant source of uncertainty in climate modelling and radiation budgets (Carslaw et al., 2013). This study uses the Lana et al. (2011) $DMS_w$ climatology with the Liss and Merlivat (1986) flux parameterization. Though this dataset and method are commonplace for DMS-climate studies, both are limited by sparse observations and uncertainties (Tesdal et al., 2016b). Observational deficiencies become particularly relevant when considering the stratiform cloud deck regions. In the Lana et al. (2011) dataset, the SEP region contains only two ship campaigns collecting measurements in January and February. The cloud deck in the Southern Hemisphere eastern basin of the Indian Ocean has no $DMS_w$ observations. The higher susceptibility of cloud and precipitation to changes in DMS in these regions suggest that they should be a priority for future atmospheric composition field campaigns.

To place the conclusions of this study into a broader perspective, the DMS-climate system must be considered within the context of anthropogenic climate change despite the uncertainties discussed above and in Section 2.2.7. A better understanding of current global DMS is essential before future scenarios can be considered with certainty. Nevertheless, Hopkins et al. (2011), Six et al. (2013) and Schwinger et al. (2017) have suggested that global production of DMS by marine phytoplankton is vulnerable to ocean acidification, amongst other oceanic changes expected with global warming, for example impacts on nutrient availability, salinity, mixed layer depths, and light penetration (Kloster et al., 2007). While both the Six

et al. (2013) and Schwinger et al. (2017) temperature responses are much larger than those found here, the results presented here imply a 25% decrease in $\text{flux}_{\text{DMS}}$ would result in an increase of 0.12 K (0.07 to 0.16, 10th and 90th confidence intervals) globally.

Considering the current Paris Agreement target of limiting global warming to 1.5-2.0 K, the sensitivity of ocean-derived sulfate aerosol to warming temperatures and ocean acidification becomes important. Strategies to mitigate anthropogenic climate change must consider not only the effect of increased $CO_2$ on temperatures, but also on ocean pH. Mitigating only temperature increases, (e.g. via solar radiation management) may have short term cooling effects, however, without removing $CO_2$ from the atmosphere, ocean acidification will continue to impact marine life, and as demonstrated here, the climate. Coral reefs are expected to be one of the first major ecosystems to collapse if anthropogenic climate change is unmitigated. How corals contribute to the global sulfur and hence energy budget is currently unquantified. This question is addressed in the forthcoming Chapter.

# Chapter 6

# The atmospheric influence of coral reef-derived DMS globally

At the global scale, Chapter 5 found that DMS from phytoplankton contributed an important cooling effect to the climate (and regional cloud and precipitation changes), without which, the effects of anthropogenic climate change could be exacerbated. Building upon that knowledge, this Chapter asks the question: what climatic effects might be expected if coral reefs no longer contributed to the DMS derived sulfur burden? This question has particular relevance as the extinction of all coral reefs, whilst alarming, is a scenario that is quickly becoming reality (see Chapter 2.3.1).

In this Chapter, a large estimate of coral reef-derived $DMS_w$ (L11C50) has been included in global model simulations for the first time. This allows the possible influence of coral reefs on climate to be explored through comparison with a world without a $DMS_w$ source from coral reefs (L11). All results are presented as the L11 world minus the L11C50 world in order to demonstrate the impact of the loss of coral reef-derived DMS. Differences in the free running ensemble and nudged simulations are presented side-by-side to demonstrate where meteorological responses

are having an impact (see Section 3.1.1 for setup details). In the free running simulations, stippling indicates where at least five of the seven ensemble members agree on the change in sign, and for area averages, the student t-test is used to determine significance, $p$ (see Chapter 3.3).

The inclusion of coral reef-derived $DMS_w$ is found to increase the total global $flux_{DMS}$ by only 1.7% and subsequently has no influence on the global energy balance. Using the temperature-flux sensitivity found in Chapter 5.3, it is estimated that this would translate to a 0.006-0.009 K cooling. These temperature estimates are unlikely to have any impact on global climate. At regional scales, however, the findings are much more nuanced. For this reason, the MC-Aus region is the main region of focus in this Chapter. The areas are defined in Chapter 3.1.5 and summarised in Figure 3.5b, as are the four specific locations used to show aerosol size distributions. Area averages are presented as violin plots to show the range and ensemble spread of these results.

In Section 6.1 the influence of coral reef-derived $DMS_w$ on atmospheric composition and the subsequent direct and indirect effects on radiation in the MC-Aus region are presented. In Section 6.2, the implications these results have for QLD, Australia are examined and Section 6.3 summarises the Chapter and considers the many uncertainties and caveats associated with this work.

# 6.1 Impacts of coral reef-derived DMS over the MC-Aus region

## 6.1.1 DMS and sulfur dioxide

This Section describes the changes in $DMS_a$ when coral reefs are removed (L11 minus L11C50), noting that the results are presented this way in order to demonstrate what the impact of the loss of coral reefs may be on the climate system. The annual differences in $DMS_a$ (with respect to the L11C50 simulation, shown in Figure 6.1a) for the nudged simulations (Figure 6.1b) and the free ensemble (Figure 6.1c) are spatially very similar to each other and to the respective change in $flux_{DMS}$ (shown in Figure 3.4a). Good agreement across the ensemble is found with the free running simulations over reef regions. Figure 6.1d-g shows, for both the free and nudged simulations, a strong seasonal signal over the MC-Aus region in terms of both mean value and the range of values. A seasonal signal is found in both the $DMS_a$ and $flux_{DMS}$ (see Table 6.1), and is in part due to the variation of the L11 $DMS_w$ climatology. In DJF, the range of results from the ensemble are larger than those of any other season and it appears that the free running meteorology is actually dampening the response of $DMS_a$ compared to the nudged runs. This damped response is not surprising as surface wind speeds were found to be stronger in this region at this time in the free ensemble (see Appendix C, Figure C.1). Increased wind speeds (and hence increased $flux_{DMS}$) causes the the decrease in $flux_{DMS}$ and $DMS_a$ expected due to coral reef removal to be less pronounced than in the nudged runs. Such examples of wind driven DMS responses are also found in other locations (and in other seasons), including over the SO at around 60°E and 60°W (see annual plots in Figure 6.1c). These responses highlight the complexity of the DMS-climate system. In addition, wind driven responses in other aerosol sources are found in regions around the globe (eg. from sea salt and dust), but are not discussed further

here.

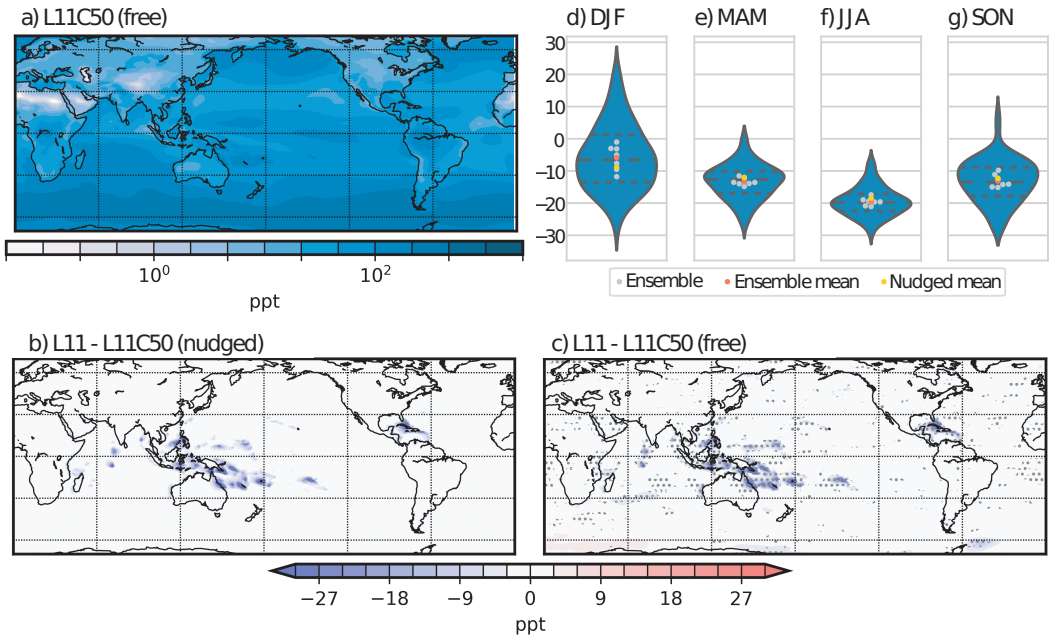


Figure 6.1: The annual $DMS_a$ concentration (ppt) for the L11C50 simulation (a) and the L11-L11C50 difference for the nudged simulations (b) and free running ensemble (c). In c) the model agreement, where at least five of the seven ensemble pairs agree in the sign of the difference, is shown by stippling. d-g) show violin plots of the average seasonal difference (L11-L11C50) in $DMS_a$ over the MC-Aus region as a percentage, where all years in the ensemble is shown by the distribution, the dashed lines represent the 25, 50 and 75th percentiles, the grey dots show each pair of models mean difference, red represents the ensemble average and yellow represents the nudged average

Figure 6.2 shows changes in $SO_2$ that are spatially similar to that of $DMS_a$. However the reductions around smaller coral reefs, such as those in the central Pacific, Indian or Caribbean oceans, are of lesser magnitude to that of the coral reefs in the MC-Aus region. This is true for both the nudged (Figure 6.2b) and the free simulations (Figure 6.2c) which implies that these areas of lower reef density are unlikely to have a significant impact on regional climate. In terms of seasonality, Table 6.1 and Figure 6.2d-g indicate less $SO_2$ variability compared to $DMS_a$ throughout the year for both the free and nudged simulations. MAM has the smallest, statistically insignificant change (-0.9% and -1.3% for the free and nudged simulations

Table 6.1: Seasonal changes over the Maritime Continent-Australian region as a percent (except for $SW\downarrow_{Surf,CS}$, $SW\uparrow_{TOA,CS}$ and $SW\downarrow_{Surf}$ which are an absolute change in $W\,m^{-2}$ and w in $cm\,s^{-1}$) for both the free running ensemble (F) and the nudged simulations (N)

| Field | Run | DJF | MAM | JJA | SON |
|---|---|---|---|---|---|
| $flux_{DMS}$ | F | -5.1$^{95}$ | -13.7$^{95}$ | -19.2$^{95}$ | -13.5$^{95}$ |
| (%) | N | -8.8$^{95}$ | -12.2$^{95}$ | -18.6$^{95}$ | -11.4$^{95}$ |
| $DMS_a$ | F | -6.1$^{95}$ | -14.2$^{95}$ | -22.3$^{95}$ | -14.3$^{95}$ |
| (%) | N | -8.9$^{95}$ | -12.6$^{95}$ | -20.6$^{95}$ | -13.3$^{95}$ |
| $SO_2$ | F | -3.2$^{95}$ | -0.9 | -3.8$^{95}$ | -2.4$^{95}$ |
| (%) | N | -2.7 | -1.3 | -2.2 | -1.5 |
| $N_3$ | F | -0.1 | -4.6$^{95}$ | -5.2$^{95}$ | -5.3$^{95}$ |
| (%) | N | -3.3 | -3.8$^{90}$ | -5.1 | -3.6$^{90}$ |
| Nuc. ND | F | -0.2 | -5.2$^{95}$ | -6.0$^{95}$ | -6.2$^{95}$ |
| (%) | N | -3.8 | -4.4$^{90}$ | -6.1 | -4.6$^{95}$ |
| Nuc. MS | F | -1.4 | -6.4$^{95}$ | -6.5$^{95}$ | -6.6$^{95}$ |
| (%) | N | -4.3 | -5.8$^{95}$ | -5.5 | -4.3$^{95}$ |
| Ait. ND | F | 0.0 | -1.9$^{95}$ | -2.1$^{95}$ | -1.5 |
| (%) | N | -1.3 | -1.2 | -2.3$^{95}$ | -1.1 |
| Ait. MS | F | -1.6 | 0.0 | -3.1$^{95}$ | -2.0 |
| (%) | N | -2.4 | -1.2 | -1.3 | -1.2 |
| Acc. ND | F | -1.4 | 0.1 | -1.8 | -1.3 |
| (%) | N | -0.5 | -0.8 | -0.7 | -0.7 |
| Acc. MS | F | -4.3$^{90}$ | 1.1 | -4.3$^{95}$ | -2.0 |
| (%) | N | -1.9 | -1.5 | -1.1 | -0.6 |
| Coa. ND | F | 1.8 | -1.3 | 0.0 | -1.9 |
| (%) | N | -0.4 | 0.2 | 0.2 | -0.4 |
| Coa. MS | F | -2.3$^{95}$ | -0.7 | -3.1$^{95}$ | -3.4$^{95}$ |
| (%) | N | -0.9 | -1.8 | -0.4 | -0.7 |
| CCN | F | -0.7 | 0.3 | -1.4$^{90}$ | -1.4 |
| (%) | N | -0.6 | -0.8 | -0.9 | -0.9 |

$^{95}$ Statistical significant at the 95th percentile, $p < 0.05$
$^{90}$ Statistical significant at the 90th percentile, $p < 0.1$

Table 6.1: Seasonal changes over the Maritime Continent-Australian region as a percent (except for $SW\downarrow_{Surf,CS}$, $SW\uparrow_{TOA,CS}$ and $SW\downarrow_{Surf}$ which are an absolute change in $W\,m^{-2}$ and w in $cm\,s^{-1}$) for both the free running ensemble (F) and the nudged simulations (N) (continued)

| Field | Run | DJF | MAM | JJA | SON |
|---|---|---|---|---|---|
| AOD | F | -1.4 | 0.0 | -1.6$^{90}$ | -1.7 |
| (%) | N | -1.1 | -1.1 | -0.6 | -0.6 |
| $SW\uparrow_{TOA,CS}$ | F | -0.04 | 0.00 | -0.06 $^{90}$ | -0.11 $^{90}$ |
| ($W\,m^{-2}$) | N | -0.05 | -0.04 | -0.03 | -0.04 |
| $SW\downarrow_{Surf,CS}$ | F | 0.12 | 0.00 | 0.11 | 0.03 |
| ($W\,m^{-2}$) | N | 0.07 | 0.06 | 0.01 | 0.05 |
| CDN | F | -0.6 | 0.1 | -0.9$^{90}$ | -0.9 |
| (%) | N | -0.4 | -0.6 | -0.4 | -0.6 |
| $TQ_{cl}$ | F | 0.3 | -0.8 | 0.4 | 0.4 |
| (%) | N | -0.1 | -0.2 | 0.3 | 0.2 |
| HuS | F | -1.0 | 0.0 | -0.1 | 1.0 |
| (%) | N | 0.1 | 0.1 | -0.1 | -0.1 |
| CldL | F | 0.7 | -0.6 | 0.9 | 1.7 |
| (%) | N | 0.1 | -0.1 | -0.4 | 0.2 |
| CldH | F | -1.0 | -0.6 | 0.5 | -0.1 |
| (%) | N | -0.1 | 0.0 | -0.1 | -0.1 |
| Pr | F | -0.3 | -0.4 | 0.2 | 0.8 |
| (%) | N | -0.2 | -0.2 | 0.4 | 0.2 |
| PrL | F | 0.9 | -0.7 | -0.8 | 1.0 |
| (%) | N | -0.2 | 0.6 | 0.6 | 0.1 |
| PrC | F | -0.4 | -0.3 | 0.3 | 0.8 |
| (%) | N | -0.2 | -0.3 | 0.4 | 0.2 |
| w500hPa | F | -0.009 | -0.004 | -0.001 | 0.015 |
| ($cm\,s^{-1}$) | N | -0.001 | -0.001 | 0.003 | -0.001 |
| $SW\downarrow_{Surf}$ | F | 0.56 | 0.23 | 0.01 | -0.14 |
| ($W\,m^{-2}$) | N | 0.11 | 0.25 | 0.01 | 0.09 |

$^{95}$ Statistical significant at the 95th percentile, $p < 0.05$
$^{90}$ Statistical significant at the 90th percentile, $p < 0.1$

respectively), while DJF and JJA show larger changes over the MC-Aus region of -3.2 and -3.8% ($p < 0.05$) in the free ensemble and -2.7 and -2.2% ($p > 0.1$) for the nudged runs. The violin plots indicate there is a similar degree of variability for each of these seasons (compared to $DMS_a$) and the influence of free running meteorology is again noted where changes in $SO_2$ are found outside of coral reef regions.

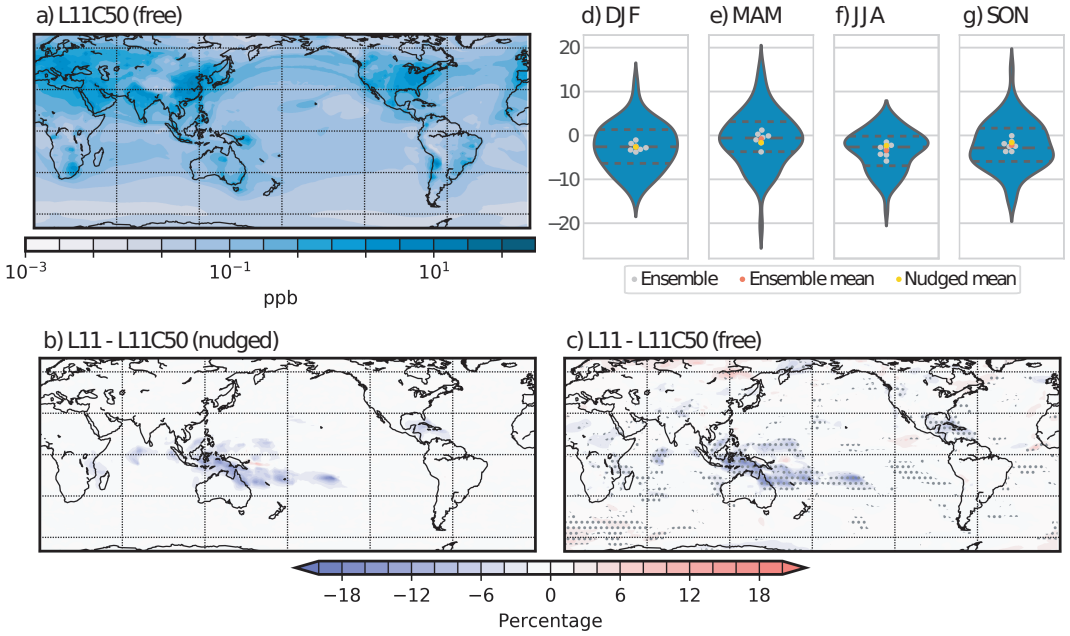


Figure 6.2: As for Figure 6.1 but for $SO_2$ in parts per billion (ppb) (a) and percent (b-g)

Interestingly, in the nudged (b) and, to a lesser degree, the free (c) simulations in Figure 6.2, a small increase in $SO_2$ is found to the west of PNG. This anomaly is larger in both MAM and SON than in JJA and is almost non-existent in DJF (not shown). The localised increase is found to have an impact on the larger (accumulation size) aerosol number concentrations and the sulfate mass, subsequently increasing the AOD. A similar anomaly is noted in the results presented in Chapter 5.1.2 (see Figure 5.1) and in Woodhouse et al. (2019), a study on secondary organics using the same version of ACCESS-UKCA. These similarities indicate that this anomaly is not specific to coral reef DMS, but is instead a sensitivity within the model in this region to changes in secondary aerosol. This anomaly has some

impact on the results in this area and will be kept in mind for the remainder of this Chapter.

### 6.1.2 Aerosol

#### Nucleation and Aitken mode aerosol

The removal of coral reef-derived DMS leads to a significant ($p < 0.05$) decline in nucleation mode aerosol number of -5.1, -6.0 and -6.2% for MAM, JJA and SON respectively in the free ensemble over the MC-Aus region (see Table 6.1). In the nudged simulations, SON decreases by -4.6% ($p < 0.05$) and MAM by -4.4% ($p < 0.1$). Although not statistically significant, JJA continues to show the largest changes (-6.1%), and DJF the smallest (-3.8%), in the nudged runs. The changes in nucleation mode number density are strongly reflected in the $N_3$ concentrations, which are shown annually in Figure 6.3. The violin plots in Figure 6.3d-g show a large range in the response in DJF, while a much smaller range in SON, with many of the individual free running pairs agreeing on the magnitude of the change.

These small aerosol (nucleation mode sized) show a greater response to changes in DMS than the larger aerosol sizes (see Table 6.1) in both the free and nudged simulations, aligning with the results of Chapter 5. This result is likely due to a range of complex interactions. In particular, it indicates that fewer homogeneous nucleation events are occurring in the free troposphere as a result of removing coral-derived DMS. Hence, fewer particles are being entrained back into the boundary layer. This process is confirmed by the vertical profile of $N_3$ showing a decrease in the upper levels of the atmosphere (not shown).

The size distributions shown in Figure 6.4 at four select regions also support this, indicating that most of the decreases are occurring in the nucleation mode and the Aitken mode. The range of locations shown by the size distribution, including

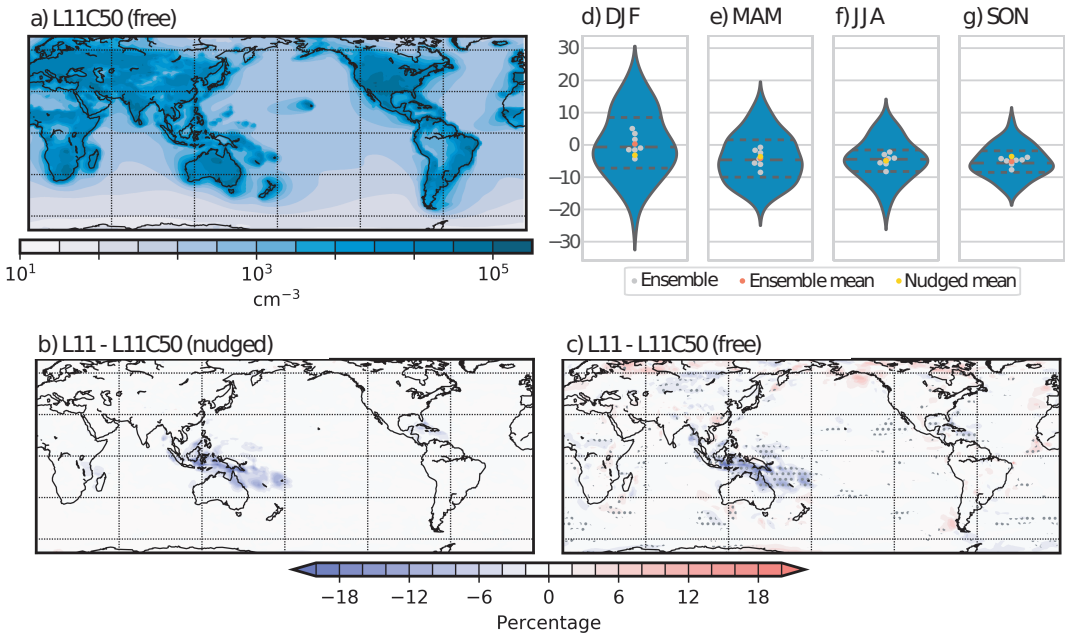


Figure 6.3: As for Figure 6.1 but for condensation number in $cm^{-3}$ (a) and percent (b-g)

directly over coral reefs (GBR and PNG) and removed from coral reefs (East Pacific and QLD) demonstrate that the effect of coral reef-derived DMS loss is not restricted to directly over coral reef regions. This is shown notably at the QLD location for JJA in both the nucleation and Aitken modes and SON for the Aitken mode. Over the MC-Aus region, decreases in the soluble Aitken aerosol number occur in MAM and JJA of -1.9 and -2.1% respectively ($p < 0.05$). The changes in both the nucleation and Aitken mode number concentrations are accompanied by similar changes in aerosol mass at this size (see Table 6.1).

### Accumulation and coarse mode aerosol

At the larger sizes (soluble accumulation and coarse modes) little change in aerosol number is found on average over the MC-Aus region. However, significant ($p < 0.05$) decreases in aerosol mass are found in the coarse mode during DJF, JJA and SON, and in the accumulation mode in DJF ($p < 0.1$) and JJA ($p < 0.05$) for the free

running ensemble (see Table 6.1). Declines of smaller magnitude ($p > 0.1$) are found for the nudged runs. For the free ensemble, the larger change in mass instead of number suggests a reduction in aerosol growth at these sizes as the larger aerosol sizes rely on condensational growth and cloud processing to interact with DMS-derived sulfate. One exception to the observed change in mass instead of number is the region west of PNG, which varies by season (not shown). In this region, a small increase in accumulation mode aerosol number is found, accompanied by a larger increase in the aerosol mass. This increase is more evident in the nudged runs and is linked to the sensitivity of the model to $SO_2$ in this region. Once again, a similar result can be found in the simulations presented in Chapter 5 (Figure 5.3). Subsequently, it is suggested that this positive anomaly is not an effect of coral reef removal and is instead masking some of the effects of removing coral reef-derived DMS when results are averaged across the MC-Aus region, especially in MAM and SON.

**CCN**

At this stage, the results show that the largest response in aerosol due to loss of coral reef-derived DMS occurs over the MC-Aus region. For this reason, all subsequent plots focus on this region. It is noted that there are impacts on aerosol from the free running meteorology outside of this domain, but these can mostly be explained by changes in surface wind speeds (see Appendix C). In addition, the influence of the free running meteorology is found to have a larger impact on the results in subsequent analysis, with greater seasonal variation. Hence Figure 6.5 is provided at a seasonal resolution.

Despite the loss of coral reef-derived aerosol having the largest impact on the nucleation mode aerosol, these small aerosol don't interact with climatic processes via direct or indirect aerosol effects. While the changes are small in the larger sized

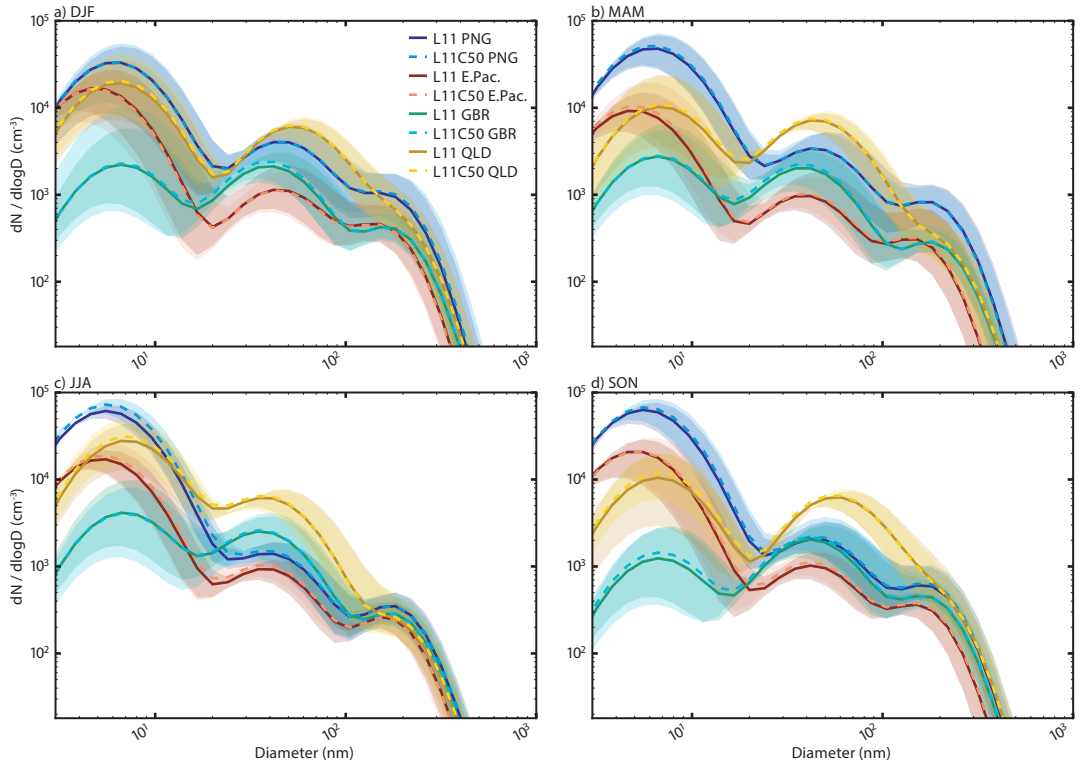


Figure 6.4: Aerosol dry diameter in nm (x-axis) and number concentration (as a function of number over the log of the diameter) in $cm^{-3}$ (y-axis), both in log scales, for four regions: off the coast of PNG (blues), in the East Pacific (reds/oranges), over the GBR (green/turquoise) and inland QLD (yellow/brown), for the L11C50 (dashed lines) and L11 simulations (solid lines) (see Figure 3.5b for regions), for four season DJF (a), MAM (b), JJA (c), SON (d). The lines show the ensemble mean for the free running simulations and the shaded regions show the range of results from all years in the ensemble

aerosol number and mass, a cumulative response to the loss of coral reef-derived sulfur has some interesting impacts. Figure 6.5 shows the column integrated seasonal $CCN_{70}$ response to removal of coral reef-derived DMS. For the nudged simulations in Figure 6.5b, f, j and n, a consistent, yet small and insignificant reduction in $CCN_{70}$ is found over the MC-Aus region (between -0.6 to -0.9%). Interestingly, over the SPCZ region, decreases of -1.0, -0.3, -1.9 and -1.1% are also found in the nudged simulations for each season (DJF, MAM, JJA and SON) respectively. The SPCZ is a relatively clean region, with few $CCN_{70}$ sized aerosol (see Figure 6.5a) and also few coral reefs. This lack of direct aerosol source suggests that changes in aerosol from other regions is affecting this region via transport along the SPCZ.

For the free ensemble, in Figure 6.5c, g, k, and o, the SPCZ region again stands out in MAM, JJA and SON with decreases in $CCN_{70}$ of -2.8, -2.2 and -1.9% for each season respectively (MAM and SON, $p < 0.1$, and JJA, $p < 0.05$). In this region, little change in surface wind speeds are found, suggesting that the changes found here are also likely due to loss of aerosol from coral reefs and their subsequent transport, as seen in the nudged runs.

Over the MC-Aus region in the free running ensemble, JJA and SON have decreases in CCN of -1.4 % ($p < 0.1$ and $p > 0.1$ respectively). In MAM, an increase is observed, demonstrating the anomaly in $SO_2$ processes near PNG discussed earlier, the influence of the free running meteorology and the non-linearity of this system. The violin plots in the far right column of Figure 6.5 indicate large model spread in the $CCN_{70}$ changes. SON (Figure 6.5o) has the most ensemble agreement over the MC-Aus region, while little agreement is observed in other seasons. For this reason, from this point only the SON results will be shown and discussed (although the statistics for all seasons can be found in the continuation of Table 6.1).

Whilst the changes in aerosol discussed in this section are small, it is worth remembering that in Chapter 5, when all marine $DMS_w$ was removed, a global decrease of 8 % of all $N_3$ (17 % for Australia) was found. For $CCN_{70}$, a decrease of just 5 % was found globally (8 % for Australia). It is clear from the perturbation of total marine DMS that global DMS contributes only a small amount to the total aerosol number. Hence local differences from coral reef-derived DMS found in this Chapter could be considered to be relatively large.

### 6.1.3 Direct aerosol radiative effects

Aerosol of greater than 5 nm are used by the ACCESS-UKCA radiation scheme to calculate aerosol direct radiative effects. In Figure 6.6, the SON AOD, clear

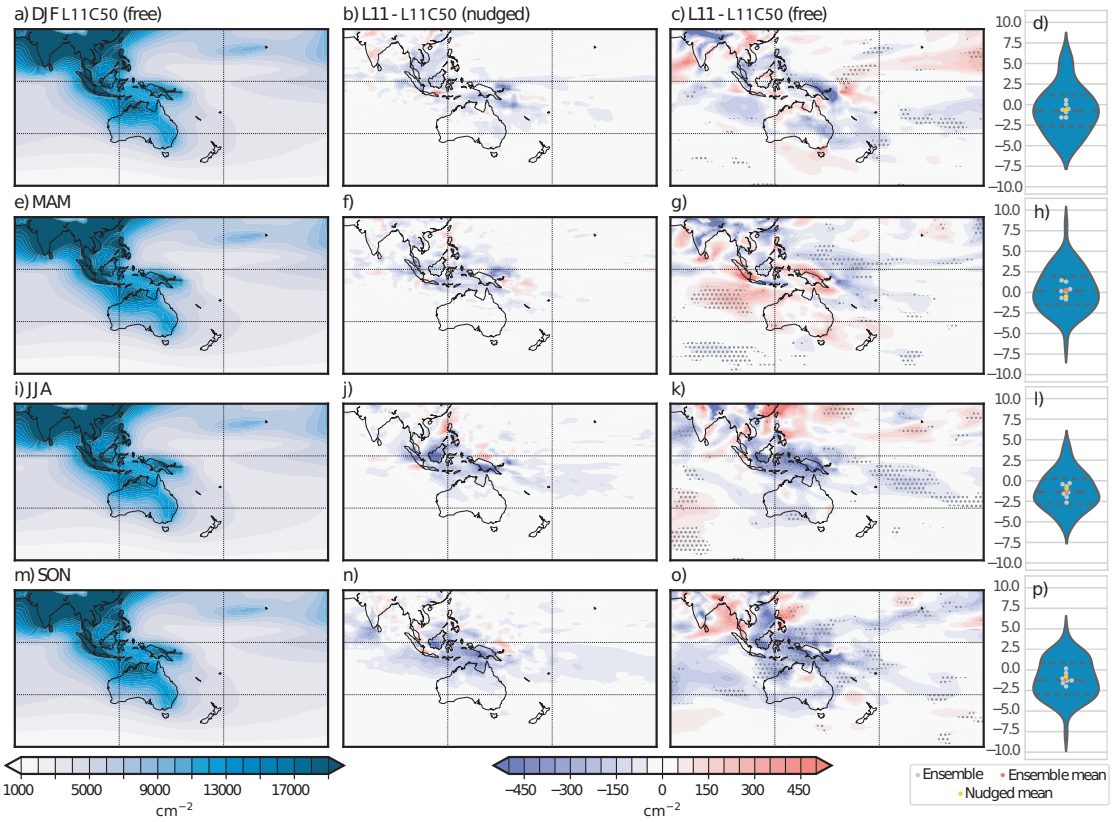


Figure 6.5: The seasonal (DJF - top row, MAM - upper middle row, JJA - lower middle row and SON - bottom row) total column $CCN_{70}$ (particles of dry diameter greater than 70 nm) concentration (in $cm^{-2}$) over the broad MC-Aus region for the free L11C50 simulation (left column); the L11-L11C50 difference for the nudged simulations (middle left column); and the L11-L11C50 difference for the free running ensemble (middle right column) with the model agreement shown by stippling, where at least five of the seven ensemble pairs agree in the sign of the difference. The right column shows violin plots of the average seasonal difference (L11-L11C50) in total column $CCN_{70}$ over the MC-Aus region as a percentage, where all years in the ensemble is shown by the distribution, the dashed lines represent the 25, 50 and 75th percentiles, the grey dots show the mean of each pair of models, the red dots the ensemble average and the yellow the nudged average

sky outgoing shortwave radiation at the top of the atmosphere ($SW\uparrow_{TOA,CS}$) and clear sky incoming shortwave radiation at the surface ($SW\downarrow_{Surf,CS}$) are shown. The clear sky radiation fields are examined in this Section to allow detection of direct effects from aerosol without the influence of clouds. Changes in the all sky fields are dominated by the convective cloud response, which will be discussed in Section 6.2.

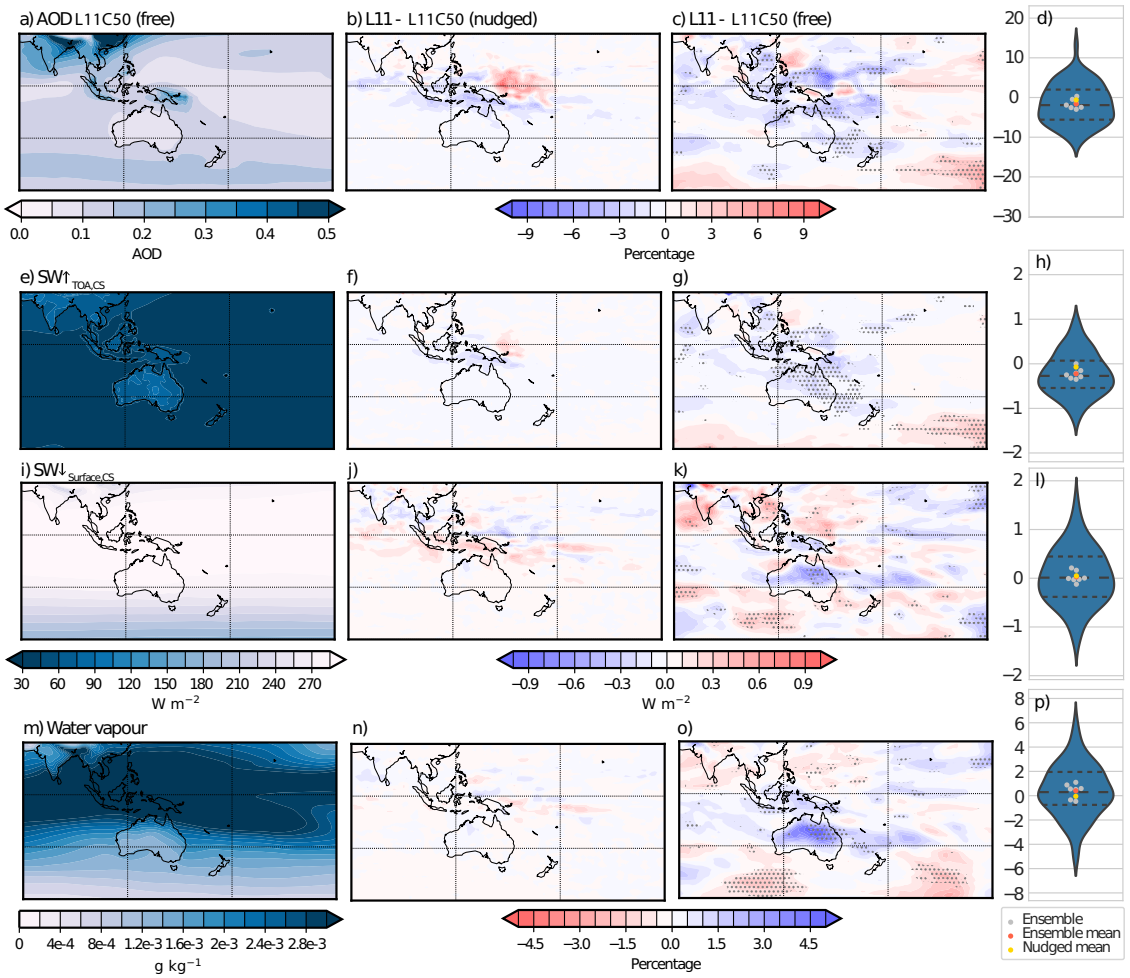


Figure 6.6: SON averages over the MC-Aus region for top row: the AOD (unitless and changes in percentage); upper middle row: $SW\uparrow_{TOA,CS}$ ($W\,m^{-2}$); lower middle row: $SW\downarrow_{Surf,CS}$ ($W\,m^{-2}$); and bottom row: column average specific humidity ($g\,kg^{-1}$ and percent). The left column shows the free L11C50 simulation; the middle left column shows the L11-L11C50 difference for the nudged simulations; the middle right column shows the L11-L11C50 difference for the free running ensemble with the model agreement shown by stippling, where at least five of the seven ensemble pairs agree in the sign of the difference; and the right column shows violin plots of the average seasonal differences (L11-L11C50) as a percentage for AOD and specific humidity and in $W\,m^{-2}$ for $SW\uparrow_{TOA,CS}$ and $SW\downarrow_{Surf,CS}$, where all years in the ensemble are shown by the distribution; the dashed lines represent the 25, 50 and 75th percentiles; the grey dots show each pair of models mean, the red dot the ensemble average and the yellow the nudged average

The spatial response of AOD to changes in aerosol in the nudged simulations (Figure 6.6b) is broadly consistent with the $CCN_{70}$ findings (Figure 6.5n). Decreasing AOD is found over most of the MC-Aus region, while the area to the west of

PNG experiences an increase. The seemingly amplified aerosol response in the PNG region is due to the increased accumulation mode sulfate mass, and to a lesser degree the increased particle concentration numbers once again associated with the $SO_2$ anomaly discussed earlier. This increase is not believed to be associated with coral reef-derived DMS removal but a function of complex non-linearities and model sensitivities in a polluted region. This anomaly is likely to be dampening the area averages over the MC-Aus region.

In Figure 6.6f, the change in nudged $SW\uparrow_{TOA,CS}$ is consistent with the AOD, indicating that there is a weak reduction in the amount of shortwave radiation being reflected out to space at the top of the atmosphere over significant coral reef regions. This decrease in $SW\uparrow_{TOA,CS}$ suggests more shortwave radiation is passing through the atmosphere and reaching the surface. For the nudged runs, this is broadly true, as shown by the $SW\downarrow_{Surf,CS}$ in Figure 6.6j. These results indicate that when no interaction with meteorology is allowed, a weak, statistically insignificant direct aerosol effect is associated with certain regions over the MC under clear sky conditions in austral spring.

For the free running ensemble, however, the result is far less clear, primarily due to interactions with meteorology. The AOD response (Figure 6.6c) is again broadly consistent with the changes in $CCN_{70}$ (Figure 6.5o), where over the MC-Aus region a decrease of -1.7% ($p < 0.1$) is found. The $SW\uparrow_{TOA,CS}$ responds as expected with a decrease of -0.11W $m^{-2}$ over the MC-Aus region ($p < 0.1$, with considerable model agreement). However, the subsequent $SW\downarrow_{Surf,CS}$ response (Figure 6.6k) is not as straightforward. While the SON MC-Aus average suggests a weak, insignificant increase in shortwave radiation reaching the surface, the spatial patterns are not consistent with the AOD, aerosol fields or the $SW\uparrow_{TOA,CS}$.

In ACCESS-UKCA, the shortwave (defined as wavelengths between 0.2-5 $\mu$m) radiative transfer scheme considers not just the scattering and absorption of energy

by aerosol and cloud droplets, but also the absorption of energy by water vapour (Edwards et al., 2013). Water vapour has an effect at wavelengths greater than 0.7 $\mu$m. In Figure 6.6o, the average change in water vapour throughout the column is shown, which is more spatially consistent with the free running $SW\downarrow_{Surf,CS}$ response than that of the AOD or $SW\uparrow_{TOA,CS}$. This consistency is particularly clear over the Australian region. An increase in water vapour in the column would suggest more absorption of radiation throughout the column, and hence less energy is received at the surface, as found in the $SW\downarrow_{Surf,CS}$ results (Figure 6.6k). It is emphasised that this interaction of energy with water vapour is only found in the free ensemble, when meteorology is allowed to vary.

The cause of the change in water vapour is difficult to determine as it is intricately linked to both local and large-scale climate processes. For example, meteorological effects found in this study that could explain the water vapour increase include:

- Warming at upper levels (15-20 km) of the atmosphere over the tropics (not shown), indicating more water vapour can be held in the atmosphere
- Increased in latent heat flux at the surface over the Australian region (not shown), suggesting increased evaporation
- A general increase in vertical motion found for the Southern Hemisphere tropics-mid latitudes (Figure 6.7b), aligning neatly with the regions of increased water vapour (Figure 6.7d). Increased vertical motion is accompanied by decreased southwards transport at upper levels and decreased northwards transport at the surface (Figure 6.7f), suggesting a weakening of the southern branch of the Hadley Cell.
- Increased high level cloud and convective precipitation found over the MC-Aus region, causing increased high cloud cover, an overall decrease in $SW\downarrow_{Surf}$ and

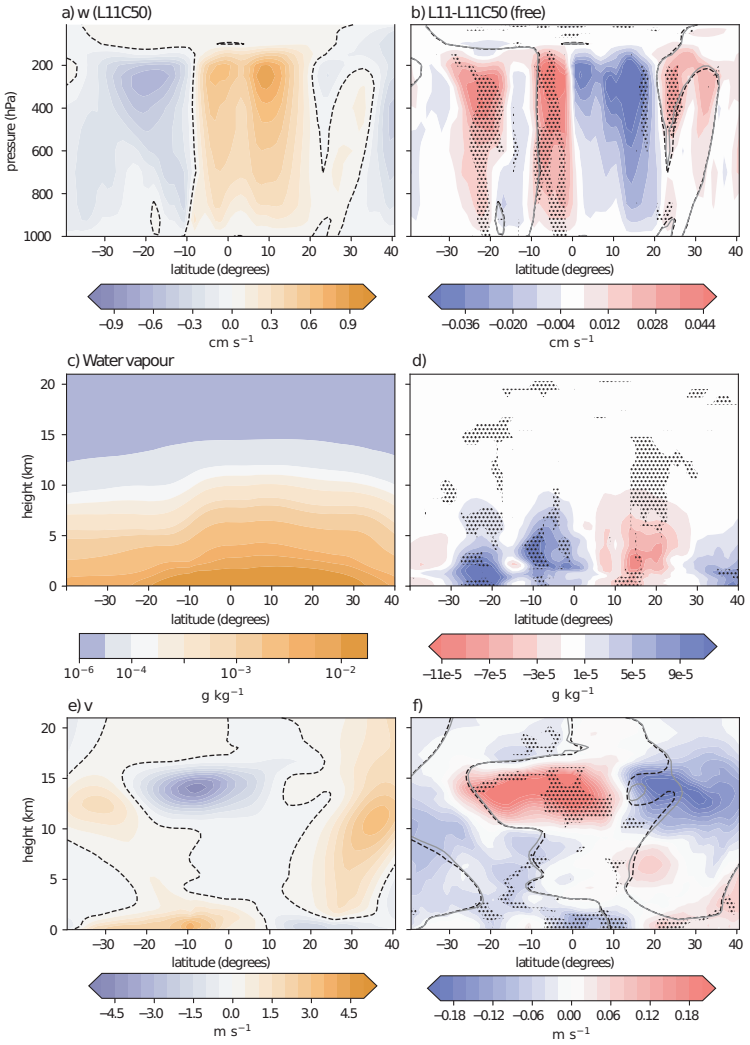


Figure 6.7: The zonal mean vertical profiles over the MC-Aus longitudinal region for vertical velocity (w, top row) in cm s$^{-1}$, water vapour (middle) in g kg$^{-1}$ and the v component of wind (bottom) in m s$^{-1}$) for the free running L11C50 simulation (left column) and the difference in L11-L11C50 the free ensemble (right column), with the model agreement shown by stippling where at least five of the seven ensemble pairs agree in the sign of the difference. For a-b) and (e,f), the black dashed lines in all plots represent the zero contour of the L11C50 field, while in b) and f) the solid grey line indicates the zero contour of the L11 field

increased convective precipitation.

It is hypothesised that the increase in short wave radiation passing through the atmospheric column results in warming, which may cause increased evaporation, vertical transport and convective activity, and subsequently increased water vapour. Despite many of the responses described above having good ensemble agreement,

low confidence is attributed to this hypothesis for three reasons:

- The top of the atmosphere direct radiative effect that is proposed to initiate these responses is small. Furthermore, the changes in aerosol and AOD that have caused the radiative effect are also small and insignificant. Hence it may be unreasonable to suggest such small changes in aerosol could be causing a direct radiative effect.

- Over the MC-Aus region as a whole, little statistical significance is found in these responses, and ensemble agreement can be found in regions that are seemingly not associated with coral reef-derived DMS. Thus, internal model variability cannot be ruled out as the cause for these meteorological responses.

- In Chapter 5, when all marine DMS-derived aerosol were removed from the system, decreases in convective activity were found over the tropics, despite those simulations being nudged (nudging can allow small differences in meteorology if the forcing is large enough). That change is of the opposite sign found here, casting doubt on the legitimacy of these results.

Therefore, despite a weak yet significant ($p < 0.1$) decline in $SW\uparrow_{TOA,CS}$, it is concluded that over the MC-Aus region, no robust impact on climate via the direct radiative effect can be confidently detected. This result may be due to averaging over a large area, as the same processes are found over QLD with generally greater statistical significance and ensemble agreement. This will be discussed further in Section 6.2.

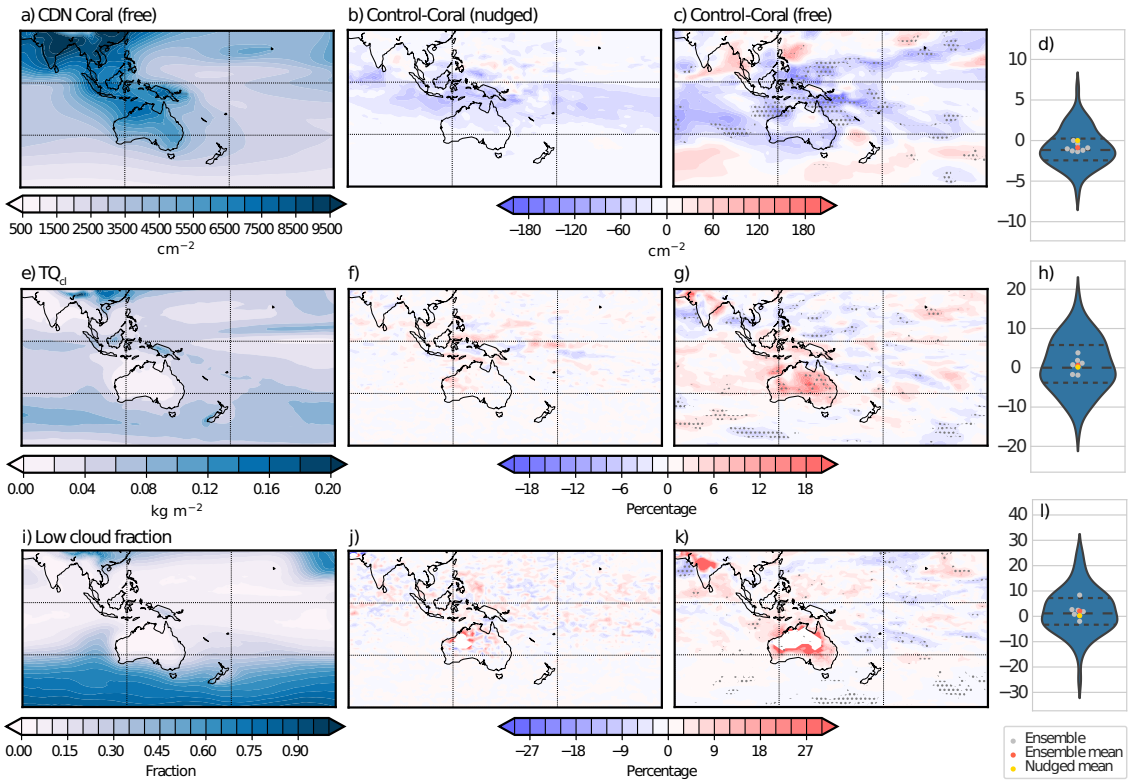


Figure 6.8: As for Figure 6.6 but for CDN (top row) in $cm^{-3}$, $TQ_{cl}$ (middle row) in $kg\,m^{-2}$ and percent and low cloud fraction (bottom row) as a fraction and in percent

### 6.1.4 Indirect aerosol radiative effects in the large-scale cloud and precipitation scheme

Indirect aerosol effects take place as CCN particles activate and become CDN. In ACCESS-UKCA, aerosol activation depends on the size and composition of aerosol as well as the atmospheric supersaturation, which is influenced by the vertical velocity. Thus, the significant increase in smaller size aerosol found earlier may have some influence over indirect aerosol effects in certain conditions, although it is noted that larger aerosol have much greater ability to influence indirect effects. Figure 6.8 shows the responses of CDN, total cloud liquid water ($TQ_{cl}$) and low cloud fraction (noting that only the microphysics scheme can respond to change in CDN). For both the nudged and free simulations, the changes found in CDN are consistent

with, though weaker than, the changes observed in the CCN fields (noting again the vertical integral of CDN through the column is shown). No statistical significance is attributed to the changes in CDN over the MC-Aus region, although reasonable ensemble agreement is found in Figure 6.8c. These weak changes suggest that the reductions in CDN are unlikely to have an effect on cloud properties.

A small decrease in the amount $TQ_{cl}$ is found on average over the MC-Aus region in the free simulations, although Figure 6.8g-h shows a large amount of variability in the region and little model agreement. This change in CDN and $TQ_{cl}$ has had little impact on properties such as low cloud fraction (Figure 6.6k) or large scale precipitation (see Appendix C), as shown in Table 6.1, over the MC-Aus region for each season. In addition there is very little model agreement in these fields. For the nudged simulations, constrained meteorology has meant little response of cloud properties is allowed. Subsequently, these results suggest that the loss of coral reef-derived aerosol has no impact on climate via the indirect aerosol effects.

## 6.2 Implications for Queensland, Australia

A relatively large change in precipitation, of 11 %, has been found over QLD. Although approximately equivalent declines were found in the large-scale and convective precipitation (10.9 %, $p > 0.1$, and 9.4 %, $p < 0.1$), very little large-scale precipitation occurs in this region, with convective precipitation by far the more important of the two. No evidence of indirect aerosol effects are detected within the microphysics (low cloud or large-scale rainfall) over QLD or the MC-Aus region (Section (6.1.4), ruling out indirect aerosol effects as the cause.

At this point, it is worth remembering that the convective scheme is not coupled to the aerosol scheme thus has no knowledge of the removal of coral reef-derived DMS. Hence the increased convective activity must be occurring dynamically, with

possible causes discussed in Section 6.1.3. Specifically, over QLD, a significant decrease in $N_3$ of 5 % is found ($p < 0.05$). Although this does not translate into a meaningful decrease of $CCN_{70}$ (0.5 %), a significant ($p < 0.1$) decline in the AOD is found of 1.6 %, which has resulted in less $SW\uparrow_{TOA,CS}$ of -0.16 W m$^{-2}$, ($p < 0.05$). As for the MC-Aus region, the increased radiation through the atmospheric column has been absorbed by increased water vapour (see Figure 6.6o), resulting in a significant reduction in $SW\downarrow_{Surf}$ of -0.38 W m$^{-2}$ ($p < 0.1$). While high cloud cover has increased by 7.4 % ($p < 0.1$), which in turn has caused a decrease in $SW\downarrow_{Surf}$ of -1.61 W m$^{-2}$ ($p < 0.1$), linking these convective responses to the changes in direct aerosol effect at the top of the atmosphere is not able to be done with confidence.

Interestingly, however, the relatively large change in all sky surface solar radiation is of the opposite sign to what one would expect following the aerosol direct and indirect theories, due to increased high cloud cover. Further, it is noted that the changes in the all-sky radiation is much larger than that of the clear-sky radiation and indicates that the response in cloud cover is much more important for radiative processes in this region than the direct aerosol effects.

Despite the changes presented in this Section having greater statistical significance and more ensemble agreement than over the MC-Aus region, low confidence is still attributed these results due to an unclear physical mechanism (Section 6.1.3) and the existence of similar responses elsewhere that are likely to be model noise (not shown). It is emphasised that the meteorological results discussed above are considered to be a response to a direct aerosol radiative effect, only possible when meteorological feedbacks are allowed. Nevertheless, these results were interesting and unexpected, demonstrating a clear example of how non-linear the DMS-climate system is and how important it is to consider the system as a whole, rather than isolating certain aspects.

## 6.3 Discussion

This Chapter set out to determine if the loss of coral reefs could have any impact on regional or global climate. On the global scale, coral reefs appear to have little influence on the sulfur budget or global energy balance. At regional scales, however, this Chapter has found some interesting and unexpected effects that would not have intuitively been hypothesised.

The MC-Aus region has been found to have the largest aerosol response to removal of coral reef-derived DMS across the globe. This is unsurprising given that this region has the highest density of coral reefs in the world. Over other coral reef regions, the effects of coral-derived DMS are quickly diluted by other influencing factors, such as pollution. Significant decreases in the free running ensemble's small size aerosol (both number and mass) are found over the MC-Aus region. For the larger sized aerosols, small, generally insignificant decreases in sulfate mass are found while little change in number is noted. The nudged simulation shows a more consistent small decrease across all aerosol fields and seasons. The decreases in aerosol have cumulatively lead to an insignificant decrease in SON of AOD in the MC-Aus region, and a significant decrease of AOD over QLD. No significant or robust changes were detected in other seasons.

Despite the weak AOD response over the MC-Aus region, a significant reduction in $SW\uparrow_{TOA,CS}$ of -0.11 $W\,m^{-2}$ was found for SON in the free running ensemble and attributed to the reduction of aerosol in the region. This result appears to be enhanced when compared to the nudged results. Much smaller (or no) reductions were found in all other seasons. In contrast to the nudged simulations, for the free running SON reduction in $SW\uparrow_{TOA,CS}$ does not directly translate to similar increases in $SW\downarrow_{Surf,CS}$ as expected. Here, the leading hypothesis suggests that interaction of shortwave radiation with water vapour causes the opposite $SW\downarrow_{Surf,CS}$ effect, which

is itself a result of complex meteorological feedbacks. The response of water vapour could not be confidently attributed to changes in aerosol (as opposed to internal model variability) and the direct effects at the top of the atmosphere are considered to be weak. For these reasons, this Chapter concludes that no robust direct aerosol effects can be confidently associated with coral reef-derived DMS.

This Chapter has found little to no indirect aerosol effects in any region in response to coral reef DMS. This is unsurprising given the small and insignificant changes found in the CDN and also the results of Chapter 5, where few indirect effects were observed outside of the clean marine regions of the Southern Hemisphere mid-latitudes. However, it may also be a result of the lack of coupling between the convective scheme and aerosol in the model. Coral reefs are located in tropical regions that are dominated by convective processes, with little large-scale meteorological activity. Hence, it is possible that no indirect effects were found in this work simply because such effects are only allowed to occur in the large-scale scheme, which is not particularly active in the regions of interest.

How the convective scheme may interact with changes in aerosol is currently a large source of uncertainty (Tao et al., 2012). Aerosol-induced convective invigoration theories suggest that with less aerosol, CDN would rain out more quickly, reducing the amount of latent heat release caused by condensation, thus, inhibiting convection. This mechanism has been found in both simulations and observations with respect to increased anthropogenic ultrafine aerosol over the Amazon invigorated deep convection Fan et al. (2018). Conflicting the Fan et al. (2018) results, Hassim et al. (2016) found a reduction in deep convection in simulations of a polluted environment over New Guinea, demonstrating the complexity of this problem. Nishant et al. (2019) has demonstrated that while satellite observations correlating high aerosol loading to increased convection, the presence of aerosol may not be the cause of connectivity activity due to the co-variation of aerosol-wind and wind-cloud

processes. Fan et al. (2016) summarise that the influence of aerosol on convection is highly dependent on different kinds of convective systems (eg. the trigger, if it is a super cell) and the environment (eg. wind shear, cloud base temperature). The studies discussed above and the results of this thesis indicate that aerosol interaction with climate is far from linear.

Interestingly, this Chapter has found some unexpected dynamical results in the convective processes, including a significant increase of 10.9% in convective rainfall over QLD, attributed to suppressed downwards motion in the region. However, low confidence is given to the physical cause (weak direct radiative effects) of the changes in vertical motion, especially due to the fact that Chapter 5 found, in nudged simulations, an opposite signal when aerosol was removed from the system. Unfortunately, in the simulations completed for this study, the required model outputs to further investigate this issue are not available (for example fields to calculate the lapse rate), but should be kept in mind for future studies.

It is noted that the weak direct effects discussed above are considering clear sky processes only. The changes in convective processes result in significant changes in high-cloud fraction. Increased cloud cover subsequently has large impacts on the all-sky radiation response (decreased $SW\downarrow_{Surf}$), overwhelming any clear-sky responses. This again highlights the complexity of the system and issues a warning to the oversimplification of aerosol effects in climate models.

The weak - and in some cases unexpected - response of radiation, both at the surface and the TOA, combined with no robust response via indirect effects, have implications for the validity of the CLAW hypothesis, both in respect to coral reefs and other marine organisms. In this work, it has been shown that these processes are far more complex than what has been assumed, even in more recent literature (eg. Quinn and Bates, 2011; Green and Hatton, 2014).

The tool used for this work, ACCESS-UKCA, is able to provide detailed di-

agnostics of the DMS-climate system; however, some important model limitations remain. By conducting a global study, a limitation of this work is resolution in space and in time. The coarse temporal resolution of the output for this model (monthly) has made extracting process information difficult, as the averaging applied at these time steps often overwhelms initial perturbations and the subsequent response. In addition, by allowing the model to run freely, disentangling responses due to coral reef-derived DMS as opposed to internal model variability has been difficult. While an effort to resolve this problem has been made by creating a seven member ensemble (limited by computer resources) and comparing to nudged simulations, there remains a significant likelihood that some of the results presented in the work are purely from internal model variability.

Further limitations of this model are the inherent biases (discussed in Chapter 4) and the inability of the model to represent certain microphysical processes, which can have important effects on how aerosol interact with the climate. For example, Chapter 5 showed that ACCESS-UKCA significantly underestimated all cloud levels, which led to overestimated $SW\uparrow_{TOA}$. The responses found here in cloud and radiation are well within the model uncertainties reported in the literature and are smaller than the model biases themselves. In effect, improved model representation of the climate system may have a larger impact on the energy balance than the small perturbation applied in this work. The sensitivity of GCMs to changes in model structure has been highlighted recently by some CMIP6 GCMs, where the models reportedly have a higher climate sensitivity than CMIP5 in part due to improved representation of cloud feedbacks (Zelinka et al., 2020).

The results presented here indicate that although the loss of coral reef-derived DMS may have small impacts on small sized aerosol, the end result is not as straightforward as the aerosol effects theory suggests. This complexity is highlighted by the difference between the nudged simulations and the free ensemble, where in the lat-

ter, the impact of changing meteorology in response to a weak direct effect has impacts on the radiation budget often opposing what was expected. These results also demonstrate how interdependent this system is and suggests that considering only a few aspects of the DMS-climate cycle, as much literature has done, may be misleading. These results further highlight the costs and benefits of the two modelling methods (free versus nudged simulation) when trying to separate climate responses from climate variability.

This has been the first study to include coral reef-derived DMS in a global climate-chemistry model and to then determine what possible effect the loss of this DMS source may have on climate. It is noted that the amount of $DMS_w$ assumed to be produced by coral reefs in this work (a weighted 50 nm) is likely larger than reality due to area averaging and the far more variable nature of DMS production. That said, no robust evidence of indirect effects and weak evidence of a direct effect over just one season (SON) has been found over the MC-Aus region. These results suggest that with smaller estimates of coral reef $DMS_w$, little to no impact on the climate would be found. These results have significant implications for current coral-DMS-climate literature, effectively signalling that coral reefs have no importance for the climate.

In the proceeding chapters, a similar experiment to quantify the importance of coral reef-derived DMS is performed with a focus on weather at a regional-local geographical scale. However, firstly, an evaluation of the WRF-Chem model is performed in the next Chapter, along with its sensitivity to large changes in $DMS_w$.

# Chapter 7

# WRF-Chem model evaluation and atmospheric sensitivity to large perturbations in DMS

Up to this point in this thesis, the global to regional influence of DMS, and more specifically coral reef-derived DMS, has been analysed. While marine DMS has been shown to be important for the global climate, the role of coral reef-derived DMS in atmospheric processes was found to be small and in most cases insignificant at large scales. In this Chapter and the next, a similar question will be examined but at time scales that may better represent the complex chemistry and meteorology of the DMS-climate system. Instead of detecting the influence of coral reefs at a climate scale, the possibility of a bioregulatory feedback is explored in a broad interpretation: do corals impact local composition or weather? Before addressing this question however, a model evaluation and sensitivity test is performed in order to contextualise the subsequent results.

In this Chapter, WRF-Chem is evaluated over DO2 (9 km, 60 second resolution, see Figure 3.6) against observations of meteorology (Section 7.1), DMS and sulfate

aerosol (Section 7.2) and total aerosol (Section 7.3) from the R2R campaign. In addition, Section 7.4 evaluates WRF-Chem against cloud fields from the Himawari-8 satellite along the RVI track and at AIRBOX. Two configurations of WRF-Chem are evaluated: C1, which uses the original L11 $DMS_w$ climatology and does not include biomass burning or dust; and C7, which uses the scaled L11S $DMS_w$ climatology, and includes biomass burning, dust and a higher marine organic emission. More details about the two control simulations can be found in Section 3.2.4.

Timeseries and distribution plots are used to show the model performance against RVI and AIRBOX while the BF (calculated using the NMBF) and Spearman rank correlation coefficient (R) are calculated as a measure of model skill (see Chapter 3.3). It is noted that little difference was found between D01, D02 and D03 in the evaluated fields, even considering cloud characteristics (noting that D03 resolves convective cloud and D01 and D02 parameterise convective cloud). The differences between the three domains therefore is not discussed. It is further noted that the AIRBOX grid box within WRF-Chem is designated as water, where the adjacent eastwards grid box is designated as land.

## 7.1 Meteorology

Figure 7.1 to Figure 7.4 evaluate the meteorological fields from the C1 and C7 WRF-Chem simulations compared to the observations taken on the RVI and at AIRBOX. In most instances, C1 and C7 are effectively the same due the nudged meteorology. In addition, the observations taken by the RVI have been assimilated into the BARRA-R reanalysis product which nudges the simulations present here. For this reason, only C7 will be discussed in this Section, while the differences between C1 and C7 will be examined more closely in the next Sections.

Figure 7.1a and i show the timeseries and distribution of wind speed for the RVI.

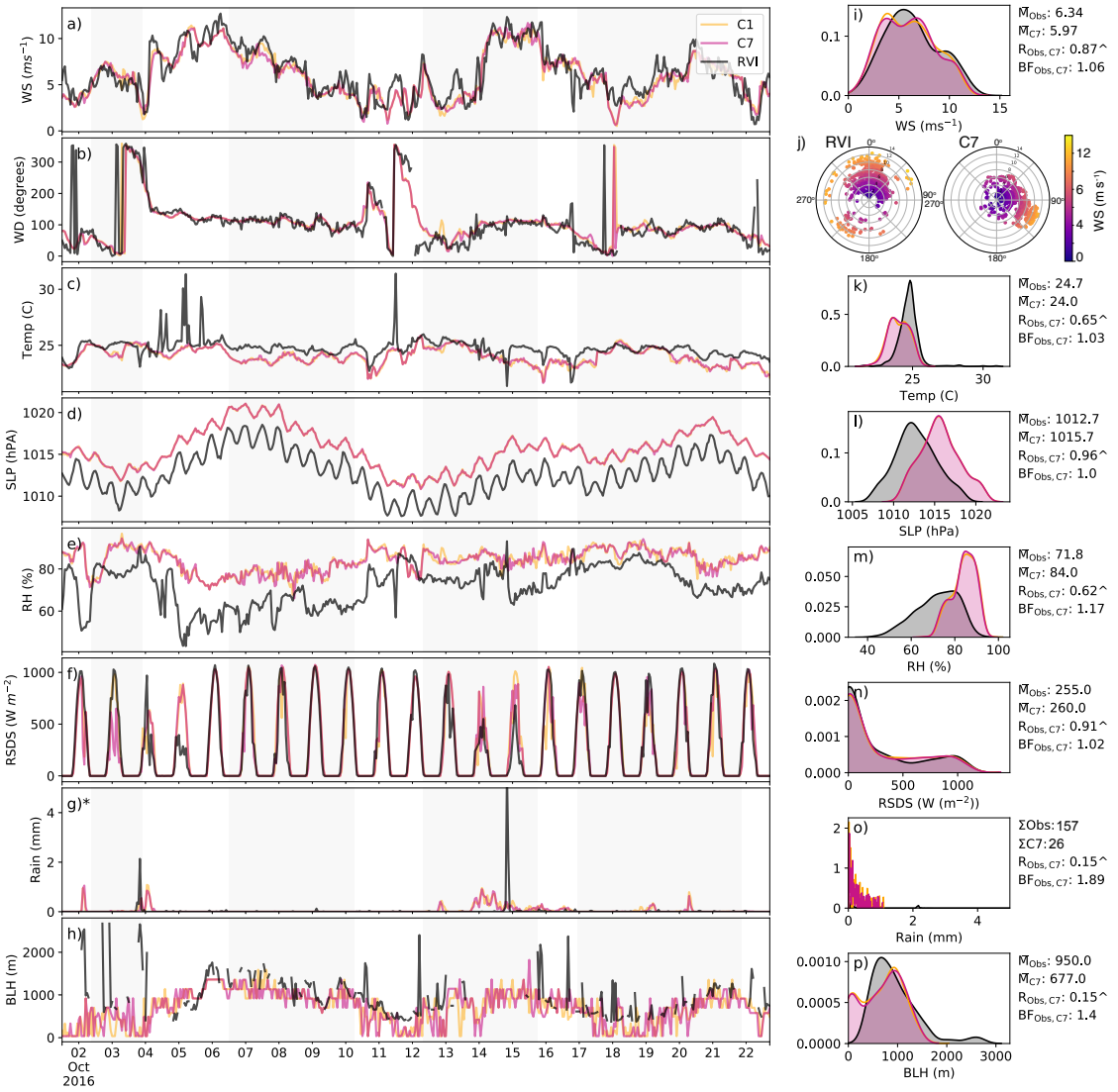


Figure 7.1: Timeseries along the RVI track (in UTC, left) and distributions or wind roses (right) in descending order: wind speed, wind direction, temperature, sea level pressure, relative humidity, surface incoming radiation, rainfall and boundary layer height, comparing WRF-Chem simulations C1 and C7 to observations. Summary statistics are shown for the observations and C7 including the mean ($\bar{M}$) (or sum Σ), the correlation (R) and the BF. ^ indicates where the R values are significant to the 95th percentile. The shaded grey areas in a-h) represent periods when the ship was at station (S2, S3.1, S3.2 and S4). For j), the wind roses of the RVI and C7 are shown instead of a distribution of wind direction and summary statistics. The y-axis in g) and x-axis in o) have been limited to 5 mm for clarity. Observations in h) are flagged by grey dots when cloud was detected, and these points have been excluded for p) and the relevant statistics

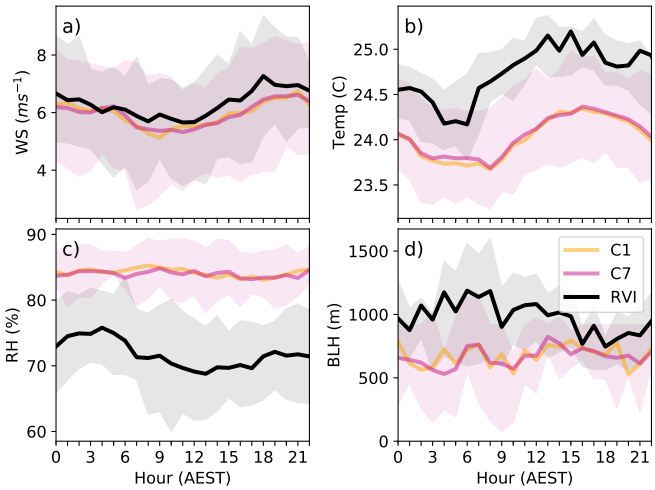


Figure 7.2: The diurnal cycles along the RVI track (in AEST) of a) wind speed, b) temperature, c) relative humidity and d) boundary layer height comparing the WRF-Chem simulations C1 (yellow) and C7 (pink) to the observations taken by the RVI (black). Solid lines indicate the mean, while for C7 and RVI, the 25-75th percentile range is shown by shading. Periods where clouds were observed in for >50% of the hour have been excluded in d)

Overall, the model performs well, with a BF of 1.06, and a correlation coefficient of R=0.87. The diurnal cycle is also well captured (Figure 7.2a), although the model tends to underestimate and delay the peak wind speed. This is attributed to the poor simulation of the sea breeze. For AIRBOX, the wind speed is significantly overestimated, with a BF of 3.63. However, the discrepancy between the model and observations may in part be caused by an underestimation of the observations due to the sheltering of AIRBOX. At Mission Beach, AIRBOX was located on top of a cliff overlooking the beach and surrounded by rainforest, with the meteorological station on top of the container (4 m) and not clearing the tree tops. Hence it is likely that observed AIRBOX wind speeds are lower than what would be expected if the observations were free of interference. Unlike for the RVI, the model shows strong diurnal variation in wind speed at AIRBOX (Figure 7.4a) associated with the land-sea breeze cycle. Little diurnal variation is found in the observations, again likely due to the AIRBOX location. The complexity of the AIRBOX location, for both the observations and simulations is highlighted in many instances in the following

sections.

Figure 7.1b and j show the timeseries of wind direction and the wind rose for both RVI (left) and C7 (right). In the timeseries, the simulated wind direction appears to capture the trends of variability of the observations well. However, comparison of the wind roses indicates that the model has a significant bias of winds from the south-east. This bias reflects the predominant large scale flow over the area for this time of year. It is also likely that the ship's wind direction observations may contain significant amounts of noise and possible biases (for example, lack of observations due north). A similar south-east tendency in the model is found at AIRBOX (Figure 7.3j), although this is somewhat supported by the observations. It is noted in Figure 7.3b that the structure of the sea-land breeze cycle is better represented in the wind direction for the AIRBOX observations than it was for the wind speed.

Both the wind observations for the RVI and AIRBOX show a distinct period of predominantly south-easterly flow during the 4-9th October. This event was caused by a high pressure system moving eastwards across the continent. Back trajectory analysis (Chen et al., 2019) indicates that the airmass originated over the Australian continent and circled anti-cyclonically over the reef, with more of a marine influence towards the end of the period (as the anticyclone moved offshore). Little to no sea-breeze activity was noted for this period (Vincent et al., 2019). These findings indicate that despite the wind direction coming from the marine sector, considerable continental influence remained in the airmass.

The model's temperature along the RVI track shows a consistent underestimation in both the timeseries and distributions in Figure 7.1c and k, of approximately 0.7$^{\circ}$C. C7 and the observations correlate moderately well, with R=0.65. However, as shown in Figure 7.2b, the timing of the minimum temperature lags by about 3 hours, while the maximum is timed relatively well, though underestimated. At AIR-

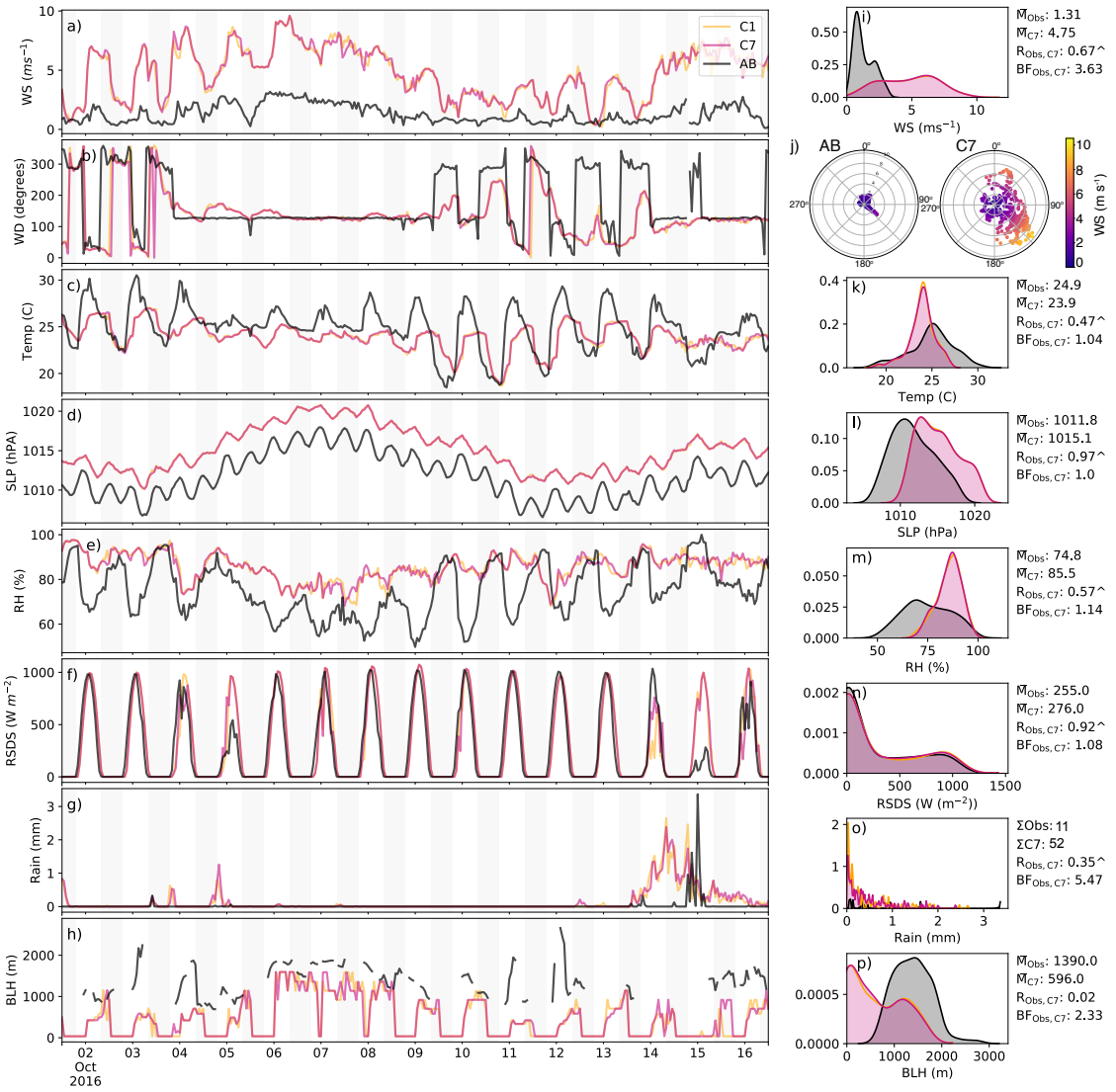


Figure 7.3: Timeseries for AIRBOX (in UTC, left) and distributions or wind roses (right) in order of top to bottom of wind speed, wind direction, temperature, sea level pressure, relative humidity, surface incoming radiation, rainfall and boundary layer height, comparing the WRF-Chem simulations C1 and C7 to the observations. Summary statistics are shown for the observations and C7 including the mean ($\bar{M}$) (or sum $\Sigma$), the correlation (R) and the BF. ^ indicates where the R values is significant to the 95th percentile. The shaded grey areas in a-h) represent nocturnal periods. For j), the wind roses of AIRBOX and C7 are shown instead of a distribution of wind direction and summary statistics

BOX, a similar underestimation by C7 of 1 °C and a correlation of R=0.47 is shown (Figure 7.3c,k and Figure 7.4b). The model at AIRBOX is unable to correctly reproduce the structure of the diurnal cycle, where the maximum peak is significantly

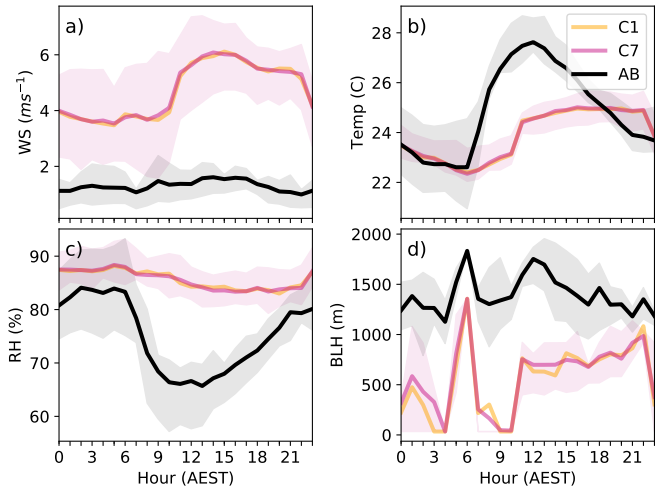


Figure 7.4: The diurnal cycles for AIRBOX (in AEST) of wind speed a), temperature b), relative humidity c) and boundary layer height d) comparing the WRF-Chem simulations C1 (yellow) and C7 (pink) to the observations taken by the AIRBOX (black). Solid lines indicate the mean, while for C7 and AIRBOX, the 25-75th percentile range is shown by shading

underestimated and the timing is late (Figure 7.4b). This is likely due to the model struggling with the coastal nature of this location, where there is a strong influence of the marine environment (where as WRF-Chem registers this location as ocean). Conversely, the AIRBOX minimum temperature is relatively well simulated in terms of both magnitude and timing.

Following the temperature deficiencies, WRF-Chem systematically overestimates the sea level pressure by about 3 hPa for both the RVI and AIRBOX (Figure 7.2d, Figure 7.4d). However, the model captures the variability and trends well (R=0.96 and R=0.97 for RVI and AIRBOX), as well as the diurnal cycle (not shown). The overestimation for both locations may reflect the reality that the ship's observations are not taken at sea level but at a height of 17 m and that AIRBOX was located approximately 10 m above sea level on a cliff overlooking the beach.

For the RVI, the mean bias factor for C7 relative humidity is 1.17, where the model is overestimating the observations by approximately 12 % (absolute value) and has a narrower distribution (Figure 7.2e and m). The variability in the timeseries

is captured to a degree, with R=0.62; however, the diurnal cycle (Figure 7.2c) is poorly captured, with little to no change throughout the day. At AIRBOX, the model overestimates the observations by approximately 11% (absolute), with a BF of 1.14 (Figure 7.3e and m). A moderate correlation between the two timeseries is found (R=0.57); however, the model is unable to reproduce the structure of the diurnal cycle appropriately, missing the daytime minimum completely, again likely due to a strong marine influence (Figure 7.4c).

For both RVI and AIRBOX, incoming surface solar radiation ($SW\downarrow_{Surf}$) is modelled well, with BFs of 1.02 and 1.08 and correlation coefficients of 0.91 and 0.92 (Figure 7.1h and n and Figure 7.3h and n). It is only during periods of cloudy conditions (as indicated by the rainfall in plot g in both Figure 7.1 and Figure 7.3) that the model overestimates surface radiation. How well the model captures cloud formation is discussed further in Section 7.4.

Rainfall in both the observations and WRF-Chem is highly variable, and we note that the rainfall shown for WRF is the mean over the nine gridboxes centred over the ship/AIRBOX. Figure 7.1h and Figure 7.3h indicate that the model does produce rain during more persistent observed rainfall events; however, fails to capture the magnitudes correctly. For example, for the RVI, over the entire time period, a total of 157 mm of rain was observed compared to just 25 mm modelled. Conversely, at AIRBOX, 64 mm was observed, while 51 mm was simulated.

Lastly, for the RVI, the modelled BLH (Figure 7.1h,p) is simulated better than expected, given generally poor simulation of this field in the literature (eg. Chen et al., 2019, and discussed further in Section 7.5). C7 captures some of the variability in the timeseries, although with a BF of 1.4 and a weak correlation of R=0.15. The lidar observations from the RVI also have limitations, including an inability to detect BLHs below 500m and issues detecting thin clouds. For example, closer examination of the lidar output (not shown) for the period of 1st-5th of October

suggests the existence of cloud which has not been detected by the cloud detection scheme (described by Alexander and Protat, 2019), suggesting that the high BLH observations in this period are not accurate. The 500 m limitation can be seen clearly when comparing the diurnal cycle of the observed BLH to the simulated (Figure 7.2d). Here, the model shows little diurnal variation, while the observations show a peak during mid morning (noting that sunrise is at 0500) and a minimum at sunset (1800).

At AIRBOX, lidar observations were significantly interrupted, with many periods of missing data. Here, the model performs consistently worse compared to the RVI, with a BF of 2.33. Interestingly, the model captures some of the diurnal variability, including the peak at 0600. A similar result is found for a meteorology only simulation of WRF and is described by Chen et al. (2019).

## 7.2 DMS and sulfate aerosol

Figure 7.5 shows the evaluation of WRF-Chem for $DMS_w$, $DMS_a$, $flux_{DMS}$ and $SO_4$ aerosol for the RVI. In Figure 7.5a, the effect of scaling the L11 $DMS_w$ climatology can clearly be seen, where C7 represents a much more realistic value for the GBR region with a BF of 1.02 compared to C1 of 2.74. Figure 7.5b and f indicate that despite the model not having any variability in $DMS_w$, it is able to do a comparatively good job representing the average $flux_{DMS}$, with a BF of 1.37 for C7, compared to 2.07 for C1 (noting the the RVI $flux_{DMS}$ is calculated from observed fields as per Chapter 2.2.3). This skill is predominantly due to the well captured marine wind speeds discussed in Section 7.1. Figure 7.5f indicates that C7 tends to have a bi-modal distribution, likely due to the nature of the flux parameterisation that calculates the $flux_{DMS}$ as a function of effectively binned wind speed regimes. Visually, the C7 $flux_{DMS}$ timeseries appears to follow that of the observations relatively

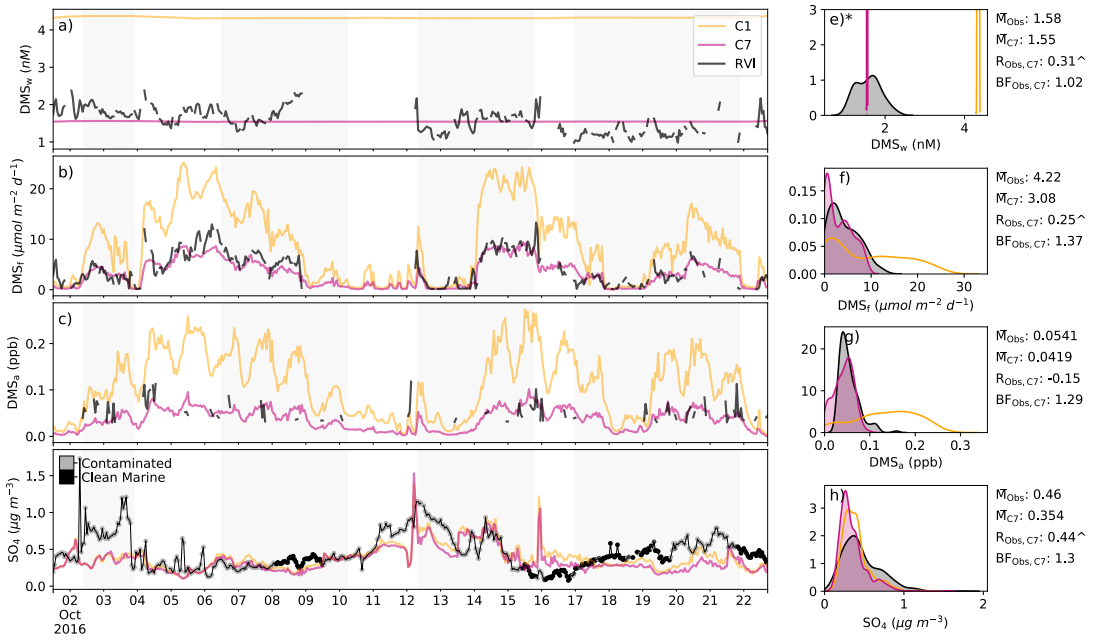


Figure 7.5: Timeseries along the RVI track (left) and distributions (right) in order of top to bottom of $DMS_w$, $flux_{DMS}$, $DMS_a$ and $SO_4$ aerosol mass comparing the WRF-Chem simulations C1 and C7 to the observations. Summary statistics are shown for the observations and C7 including the mean ($\bar{M}$), the correlation (R) and the BF. ^ indicates where the R values is significant to the 95th percentile. The shaded grey areas in a-d) represent periods when the ship was at station (S2, S3.1, S3.2 and S4). Observations in d) are flagged by grey dots when then airmass was considered to be contaminated; however, the flagged values have not been excluded for h) or the statistics shown. *The distribution in e) has been limited in the y-axis to ensure clarity

closely, with a well captured variance (where $\sigma_{C7} = 3.08$, $\sigma_{Obs} = 3.16$), although the weak R value of 0.25.

Figure 7.5c and g, showing $DMS_a$ observed from the RVI, tells a similar story to that of the $flux_{DMS}$, where the average is reasonably well captured (slight underestimation) by C7 (a BF of 1.29) although the distribution is less bimodal. A weak and insignificant R value (-0.15) is found between the two timeseries. At AIRBOX, a similar overestimation of $DMS_a$ is found (Figure 7.6a and c, where the BF is 1.42. A weak correlation of -0.12 is found between C7 and AIRBOX, implying that the model is not reproducing variability in $DMS_a$ well. Both the RVI and AIRBOX correlations show weak negative values suggesting that the model may be missing

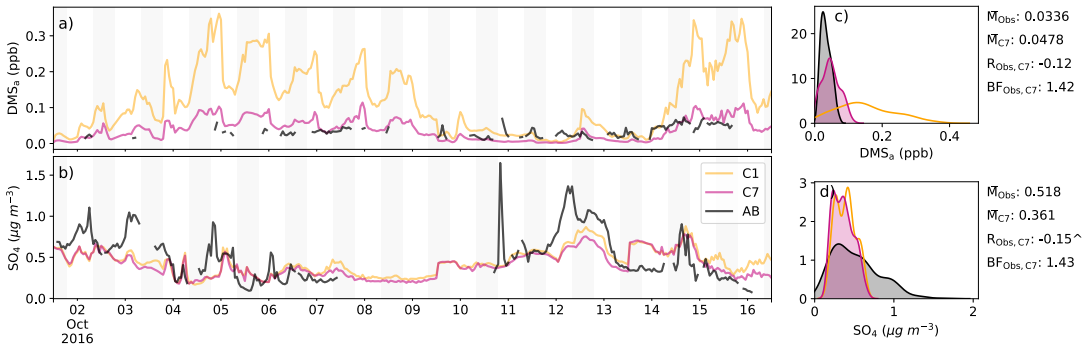


Figure 7.6: Timeseries for AIRBOX (left) and distributions (right) in order of top to bottom of $DMS_w$, $flux_{DMS}$, $DMS_a$ and $SO_4$ aerosol mass comparing the WRF-Chem simulations C1 and C7 to the observations. Summary statistics are shown for the observations and C7 including the mean ($\bar{M}$), the correlation (R) and the BF. ^ indicates where the R values is significant to the 95th percentile. The shaded grey areas in a-d) represent nocturnal periods

an important aspect of $DMS_a$ variability, such as a sink via particular chemical mechanisms. While WRF-Chem has more robust DMS chemistry, comprising 30 DMS oxidation pathway reactions, compared with other chemical models (such as the UKCA, described in Chapter 3.1.4, comprising only eleven DMS reactions), it is possible that it is still missing an important component. For example, the importance of DMS removal by BrO or $Cl_2$ has been highlighted in the literature (Khan et al., 2016; Muñiz-Unamunzaga et al., 2018). Specifically, Khan et al. (2016) note that without these inclusions, the variability of $DMS_a$ is not well modelled.

Finally, Figure 7.5d and h show the observed and simulated sulfate aerosol mass for the RVI. For C7, over the entire timeseries, the model underestimates the observations by approximately 0.11 $\mu g\,m^{-3}$, with a BF of 1.3. A moderate correlation of R=0.44 suggests that the model is capturing some of the observed trends and variability. For AIRBOX, the underestimation of the observations by C7 increases to 0.16 $\mu g\,m^{-3}$ and the BF is 1.43 (Figure 7.6b and d). In addition, a significant, though inconsequential, negative relationship is found between the two timeseries (R=-0.15), reflecting the negative relationships found in the $DMS_a$ at AIRBOX. This may also be due to a number of local sulfate sources observed by AIRBOX

that were unable to be included in the model, for example, vehicle emissions.

Importantly, it is clear from both the RVI and AIRBOX that the difference between sulfate aerosol mass in C1 (with the L11 $DMS_w$) and C7 (with the L11S $DMS_w$) is small. It is possible that this is because C7 also included biomass burning, which C1 did not; however, for the RVI results, this was not expected to be a strong influence in a marine environment. Additional experiments (not shown) testing the inclusion of biomass burning also support this conclusion, where by little differences in $SO_4$ mass was found.

The mean difference of $SO_4$ surface concentration for C1 and C7 over the entire RVI timeseries is -0.039 $\mu g\,m^{-3}$, or a decrease of 10 % of the C1 mean. When periods of contaminated air (airmasses that contained high levels of black carbon, terrestrial influence or were flagged for other reasons) are filtered out of the calculations, the means became 0.298 and 0.249 $\mu g\,m^{-3}$ for C1 and C7 respectively, with a difference of -0.049 $\mu g\,m^{-3}$, or -15%. The difference between the filtered and unfiltered means suggests that the inclusion of biomass burning has offset the reduction in $DMS_w$ only marginally (by about 5 %).

## 7.3 Total aerosol

WRF-Chem simulates too many particles in both the $N_{10}$ (aerosol greater than 10 nm) and $CCN_{70}$ fields compared to the RVI, as shown in Figure 7.7. For $N_{10}$, the model overestimates the observations with a BF of 2.07. The overestimation shown here however may in fact be underestimated. The limited size range of particles simulated by WRF-Chem, down to approximately 39 nm, means that the smaller particles represented in the observations are not captured by the model, suggesting that the overestimation of $N_{10}$ may actually be much larger. For $CCN_{70}$, a larger overestimation is found, where the BF is 4.0. In both $N_{10}$ and $CCN_{70}$, some

interesting features are captured by the model, including a peak in the late stages of the 15th October, which is attributed to a peak in nitrate aerosol (see Appendix D). For AIRBOX (Figure 7.8), the modelled $N_{10}$ is captured similarly to the RVI, with a BF of 1.38. Unfortunately, $CCN_{70}$ observations at AIRBOX are unavailable due to failed instrumentation.

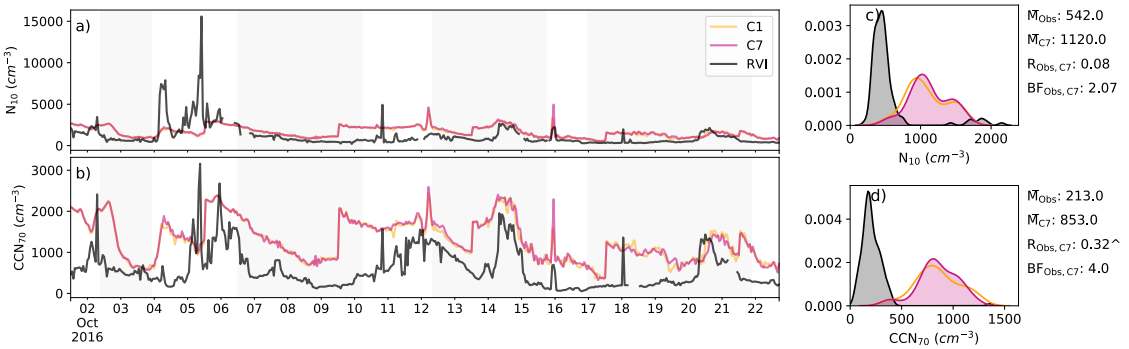


Figure 7.7: Timeseries along the RVI track (left) and distributions (right) of $N_{10}$ (top) and $CCN_{70}$ (bottom) comparing the WRF-Chem simulations C1 and C7 to the observations. Summary statistics are shown for the observations and C7 including the mean ($\bar{M}$), the correlation (R) and the BF. ^ indicates where the R values is significant to the 95th percentile. The shaded grey areas in a-b) represent periods when the ship was at station (S2, S3.1, S3.2 and S4)

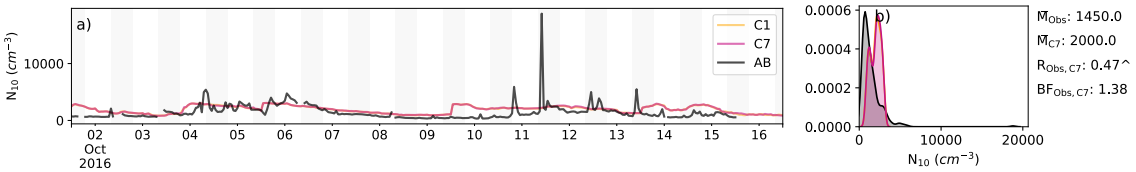


Figure 7.8: Timeseries at AIRBOX (left) and distributions (right) for $N_{10}$ comparing the WRF-Chem simulations C1 and C7 to the observations. Summary statistics are shown for the observations and C7 including the mean ($\bar{M}$), the correlation (R) and the BF. ^ indicates where the R values is significant to the 95th percentile. The shaded grey areas in a) represent nocturnal periods

Analysis of other terrestrial and anthropogenic aerosol species (black carbon, ammonium, nitrate and organics - see Appendix D) mass concentrations cannot explain the overestimation in aerosol number. All species but black carbon (slightly overestimated) and organics (captured very well) were underestimated under clean

marine conditions from the RVI and under the coastal conditions at AIRBOX. Sea salt is known to be overestimated in WRF-Chem, especially at high wind speeds. Unfortunately model comparison to observations is unable to be performed due to further data processing requirements (personal communication Joel Alroe). In this study, the sea salt flux was halved in an attempt to mitigate its overestimation.

Due to the model set-up, where the re-initialisation of the chemical fields occurs every four days (at 0000 UTC, followed by a 12 hour spin-up), step changes can be found in both the $N_{10}$ and $CCN_{70}$ fields at both locations on October 5, 9, 13, 17 and 21 at 1200 UTC. The step changes are more pronounced in the marine environment. After the re-initialisation, the model tends towards the observations, suggesting that the boundary and initial conditions used here (derived from MOZART-4) are overestimating aerosol number in this region, especially for the marine environment. Similar step changes were not observed for the aerosol species mass concentrations ($SO_4$ and others - see Appendix D), implying that the species examined here (many of them with online flux calculations) are not the cause of this overestimation. It is suggested here that the WRF-Chem approximation of aerosol number from the bulk aerosol mass provided by MOZART-4 may be the cause. The implications of this approximation are discussed further in Section 7.5.

Lastly, insignificant differences in aerosol number concentrations are found between C1 and C7 for both the RVI track and at AIRBOX. For the RVI, insignificant differences of less than 3 % are found for the $N_{10}$, in both marine only conditions and over the entire timeseries. For $CCN_{70}$, the difference is less than 1 %. At AIRBOX, while the magnitude of $N_{10}$ is higher, the same result is found, with insignificant differences of less than 1 % between C1 and C7. Effectively no difference between C1 and C7 suggests that, in this study, large changes in $DMS_w$ has little impact on total aerosol numbers in WRF-Chem.

This lack of sensitivity may be a result of the overestimation of total aerosol

number enforced by the four day restarts, as described above. It may also be because the area of study in this work is a predominantly coastal-marine environment. As Chen et al. (2019) showed, much of the airmass measured at AIRBOX had strong terrestrial influence, with signatures of biomass burning. Strong terrestrial influence was also found for this work, where radon concentrations were consistently high at AIRBOX (above 1000 mBq). For the RVI, despite periods of low radon concentrations of below 300 mBq (which in this case is considered to be 'clean marine' when coupled with low black carbon measurements), this concentration is far from what is considered 'clean marine' in other regions (eg. 30 mBq at Cape Grim). In addition to unfavourable synoptic conditions (such as those described in Section 7.1), one such cause of a lack of clean marine periods is the influence of sea-land breeze coupling. Over coastal-marine regions, recycling of air masses over the land and ocean can occur and have far reaching impacts. For example, Vincent et al. (2019) found for the RVI campaign, under favourable conditions, the sea-land breeze influence was detected up to 150 km offshore.

## 7.4 Cloud height and albedo

Figure 7.9 and Figure 7.10 examine the model performance of cloud top height and cloud albedo compared to observations derived from the Himawari-8 satellite, at points along the ship track and at AIRBOX. It is noted that for all the distribution plots and statistics discussed below, only points where both the Himawari-8 observed and the model simulated cloud are considered. Furthermore, spatial maps of these fields were also produced, but did not add extra information to his analysis and hence have not been included.

For the cloud top height along the RVI track (Figure 7.9a,c), the model can be seen to preferentially simulate low and high level clouds, with few occasions

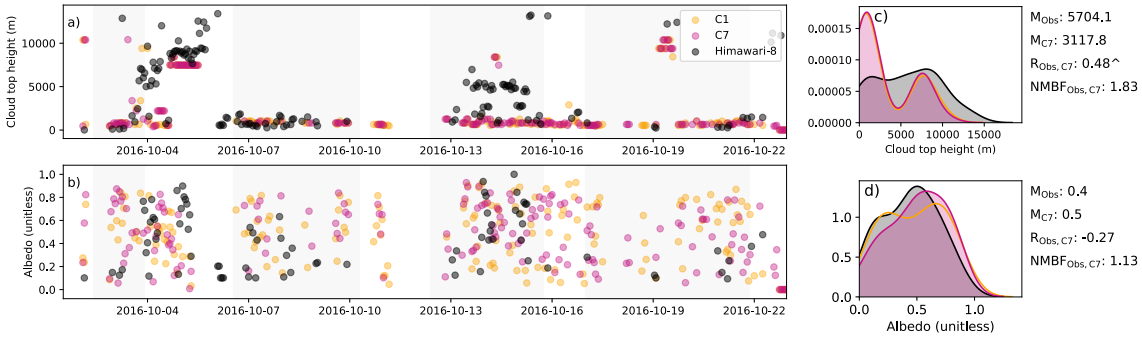


Figure 7.9: Timeseries along the RVI track (left) and distributions (right) of cloud top height (top) and cloud albedo (bottom) comparing the WRF-Chem simulations C1 and C7 to the Himawari-8 satellite. Summary statistics are shown for the observations and C7 including the mean ($\bar{M}$), the correlation (R) and the BF. ^ indicates where the R values is significant to the 95th percentile. The shaded grey areas in a-b) represent periods when the ship was at station (S2, S3.1, S3.2 and S4)

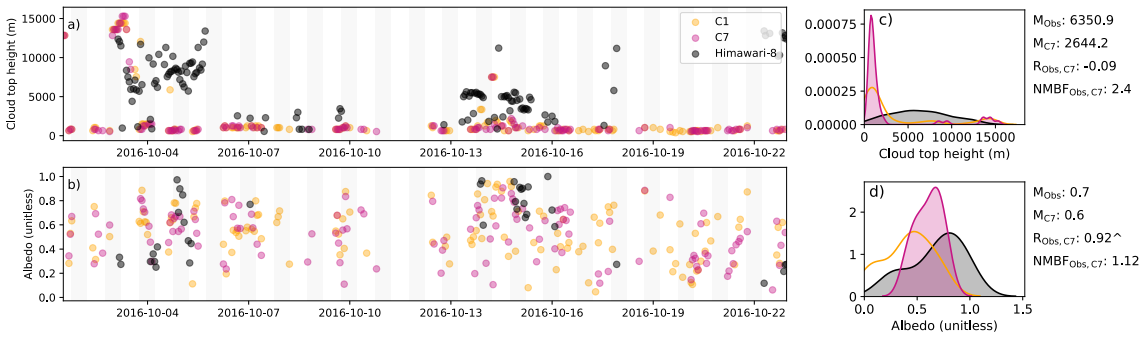


Figure 7.10: Timeseries (left) and distributions (right) at AIRBOX of cloud top height (top) and cloud albedo (bottom) comparing the WRF-Chem simulations C1 and C7 to the Himawari-8 satellite. Summary statistics are shown for the observations and C7 including the mean ($\bar{M}$), the correlation (R) and the BF. ^ indicates where the R values is significant to the 95th percentile. The shaded grey areas in a-b) represent nocturnal periods

of mid-level clouds simulated in the timeseries. This bias is clearly seen in the strongly bimodal distributions of the model. Nevertheless, the model does appear to be capturing some cloud features appropriately (although the period between the 13-16th October is poorly simulated), with a correlation of R=0.48. Overall, the model underestimates the cloud top height, with a BF of 1.83. At AIRBOX (Figure 7.10a,c), a similar result is found, with an increased BF of 2.4, although

with much less coherence between the two timeseries (R=-0.09, insignificant).

For cloud albedo (Figure 7.9b, d and Figure 7.10b, d), for both the RVI track and at AIRBOX, the results are much more noisy, with large variability in both the model and observations and significant amounts of missing data points. Despite this, the model performs better than the cloud top height for both locations in terms of BFs (1.13 and 1.12 respectively), with the RVI results in particular capturing the distribution well. An insignificant correlation of R=-0.27 is found for the RVI, while at AIRBOX, R=0.92. While visually, C1 and C7 appear to be different in the timeseries shown for cloud albedo, it is noted that C7 does present an improved distribution for both cases. However, given the amount of missing data, it is not felt that this is a robust result.

## 7.5 Discussion

This Chapter evaluated WRF-Chem against observations taken during the R2R field campaign. In terms of meteorology (excluding clouds) along the RVI track, the model performs reasonably well, in part due to the assimilation of the ship's observations into BARRA-R, which was then used to nudge the model. At AIRBOX, the meteorology is less well simulated, especially when considering the structure of the diurnal cycle. However, issues with the placement of the instruments, and the complexity of the location (right on the coastline) is likely to play a role in this poorer performance.

Many of the biases found in the meteorology, and especially those noted in the diurnal cycle, can be in part attributed to the performance of the PBL scheme. Rahn and Garreaud (2010) in particular note that the Mellor-Yamada-Janjic (MYJ) boundary layer scheme used in this thesis underestimates the BLH the most in coastal marine areas, which then improves further offshore. This appears to be sup-

ported by the results of this study. Hariprasad et al. (2014) found at a tropical location that the MYJ scheme could represent moderately deep convective layers appropriately and a stable morning layer. While some deep boundary layers have been simulated in this work, significant issues are found in particular for the afternoon BLH. Other studies at mid-latitude location have found that the MYJ scheme tends to be too moist and cool overnight, resulting in problems with the nocturnal BLH (Hu et al., 2010; Shin and Hong, 2011).

In terms of $DMS_a$ and the calculated $flux_{DMS}$, the model performs reasonably well once the $DMS_w$ was scaled to an appropriate level, in part due to the well captured marine wind speeds along RVI track. However, the large differences between simulations with scaled $DMS_w$ and the original was not carried through to the sulfate aerosol mass concentrations at either location. A small difference (-15 %) in sulfate aerosol mass is found between C1 and C7, with at least 10 % attributed to the halving of $DMS_w$. Therefore, it is concluded that DMS has only a small influence over sulfate aerosol mass in this study.

The reduction in sulfate mass due to halved $DMS_w$ was found to have effectively no influence on $N_{10}$, which was significantly overestimated. This lack of influence by $DMS_w$ could be a result of the four day restart interval causing a step change of number concentration to higher values which then slowly track towards the observations. Thus, the re-initialisation may overwhelm any possible aerosol number response to changes in DMS. However, it is noted that towards the end of each four-day period, no change in the difference between C1 and C7 is found, implying that the boundary/initial conditions, despite being the likely cause of the overestimation, may not be the reason for this lack of sensitivity to $DMS_w$ changes. In future studies, we suggest both limiting nudging to only the outer domain in addition to letting the chemistry run freely (no re-initialisation). Alternatively, methods such as 'piggy backing' as described in Grabowski (2014, 2015), in which two sets of diagnostic

outputs are built into a model, one representing control conditions and the other 'piggy backing' the experiment, may be of use in applications such as this.

In addition, problems with restart intervals were only apparent for aerosol number concentration (both $N_{10}$ and $CCN_{70}$) and not for the aerosol mass of any species analysed here. Aerosol mass was found to be simulated better than aerosol number even though speciated aerosol mass was also provided by boundary/initial conditions, and approximated into respective bin sizes by WRF-Chem. For this reason, the overestimation of total aerosol number found in this Chapter is attributed to the calculations performed within WRF-Chem to convert the bulk aerosol species given by the boundary/initial conditions to number concentrations at the aerosol bin size ranges.

An additional limitation of WRF-Chem to be considered is the binned aerosol scheme only representing aerosol of Aitken mode sizes and larger. The DMS-climate cycle is in part dependant on nucleation sized aerosol, as found in Chapters 5 and 6, where nucleation in the free troposphere has an important role. Approximating this processes, rather than directly resolving nucleation sized aerosol may have a significant impact on the results, especially when considering the response in aerosol mass while no response in aerosol number found here. The respective changes to aerosol mass and number are similar to what was found in Chapter 6 for the larger aerosol sizes (accumulation and coarse mode) in ACCESS-UKCA. The equivalent changes in the smaller size aerosol number found in ACCESS-UKCA are not represented in WRF-Chem, which may also help explain the lack sensitivity to aerosol to changes in DMS. This suggestion is supported by Zaveri et al. (2008) who state that the Wexler et al. (1994) homogeneous nucleation parameterisation used in this work under predicts binary homogeneous nucleation. An aerosol scheme that captures smaller sized aerosol would be desirable for future studies.

A further reason for the lack of influence by DMS is the study location. Ter-

restrial sources of aerosol were found to dominate the aerosol concentration for the majority of the study period due to the proximity to the coast and prevailing synoptic conditions, both in the model and observations, at both locations (also found by Chen et al., 2019, at AIRBOX). When there is an abundance of aerosol (such as from anthropogenic sources), low volatility gases (such as $DMS_a$) will more likely condense onto these particles rather than nucleate. Hence under these conditions, changes to precursor gases may manifest in the larger particle sizes, rather than at smaller sizes, where the growth, coagulation and deposition of particles may be altered. In this work, while sulfate mass decreased with reduced $DMS_a$, suggesting less condensation, marginally higher CCN concentrations (statistically insignificant insignificant) were found, possibly indicating reduced coagulation processes. A similar study in a clean marine environment (devoid of anthropogenic sources) would be of interest in the future.

In comparison to other WRF-Chem marine based aerosol-cloud interaction studies, this work has found lower sensitivity of cloud properties to changes in aerosol (Yang et al., 2011, 2012; Saide et al., 2012). However, it is likely that this is due to the constraining of the model both chemically and meteorologically. Yang et al. (2011) found that accurate modelling of aerosol number, mass and optical properties lead to improved simulation of cloud properties. Interestingly, Yang et al. (2012) found a large indirect aerosol response to a five times increase in anthropogenic emissions over a relatively clean marine region of the southeast Pacific. This result suggests that such clean marine regions are particularly sensitive to transported anthropogenic emissions, as found in this work. Yang et al. (2012) further stress that the accurate simulation of natural aerosol emissions is essential in understanding the impact of anthropogenic emissions.

To summarise, this Chapter has found that WRF-Chem simulates DMS processes and speciated aerosol mass reasonably well, yet significantly overestimating

aerosol number. While the aerosol number was found to be insensitive to changes in DMS, sulfate aerosol mass responded in a manner that fits with our understanding. Model limitations including four day restart intervals and the inability to explicitly resolve small aerosol are likely to be causing some of the apparent lack of sensitivity to total aerosol found. However, it is also suggested that close proximity to the coast and dominant continental airmass has limited the opportunity for aerosol number to respond to changes in marine DMS. It is therefore concluded that over the GBR in October 2016, DMS played no detectable role in marine aerosol formation as simulated by WRF-Chem. This finding has significant implications for the following chapter where the influence of coral reef-derived $DMS_w$ is explored.

# Chapter 8

# The atmospheric influence of DMS derived from the Great Barrier Reef

This Chapter uses WRF-Chem to explore the role of DMS produced by the Great Barrier Reef for local and regional atmospheric composition and weather. The C7 simulation evaluated in the previous chapter is compared to two additional simulations with coral reef-derived DMS representation. As discussed in Chapter 2.3 and Chapter 6, coral reefs are currently under threat of extinction due to anthropogenic climate change and a number of observational studies suggest corals play an important role in the DMS cycle. Thus, understanding the role of coral-derived DMS contribution is important for future climate monitoring and modelling. This is the first modelling study to analyse the atmospheric role of coral reef-derived DMS at short timescales and regional-local spatial scales.

This Chapter, while using a similar method to that of Chapter 6, explores a slightly different question due to the differences in scale (in both time and space) between ACCESS-UKCA and WRF-Chem. The climatic impacts of coral reef loss

cannot be explored within WRF-Chem, due to the three-and-a-half-week simulation period. However, the ability of coral reef-derived DMS to influence the weather can be assessed. This Chapter explores the extent to which DMS is able to influence atmospheric aerosol burden and the subsequent direct and indirect aerosol effects. Thus, in broad terms, this Chapter also attempts to quantify the existence of any bioregulatory feedbacks at the scale for which the CLAW hypothesis was originally proposed.

To do this analysis, the WRF-Chem control simulation (C7 - with L11S $DMS_w$), evaluated in Chapter 7, is compared to simulations that have a high (CRH) and very high (CRVH) estimate of coral reef-derived DMS included in the $DMS_w$ concentrations (a weighted 8 nM and 50 nM respectively - see Chapter 3.2.3). For this Chapter, timeseries analysis over a representative grid box (with approximately 36 % coral reef coverage, seen in Figure 3.6) and comparisons are performed. Statistical testing (student t-test) is used in both instances to detect significance of the signals.

## 8.1 Differences in DMS, sulfate aerosol mass and the aerosol burden

Figure 8.1 shows the timeseries of $DMS_a$, $SO_4$ aerosol mass and $N_{10}$ over a grid point that is representative of significant coral reef coverage. CRVH is shown to have $DMS_a$ concentrations approximately 42 % greater than that of the control (C7), with the entire distribution shifted to the right in Figure 8.1d. In Figure 8.1a, it is evident that the difference between C7 and CRVH is greater during periods of high wind speeds (not shown), while at lower wind speeds little difference is found. For CRH, only an 8 % difference is found between C7 and CRVH, although this is still significant. Only small differences can be seen in Figure 8.1a, again during periods of higher wind speeds.

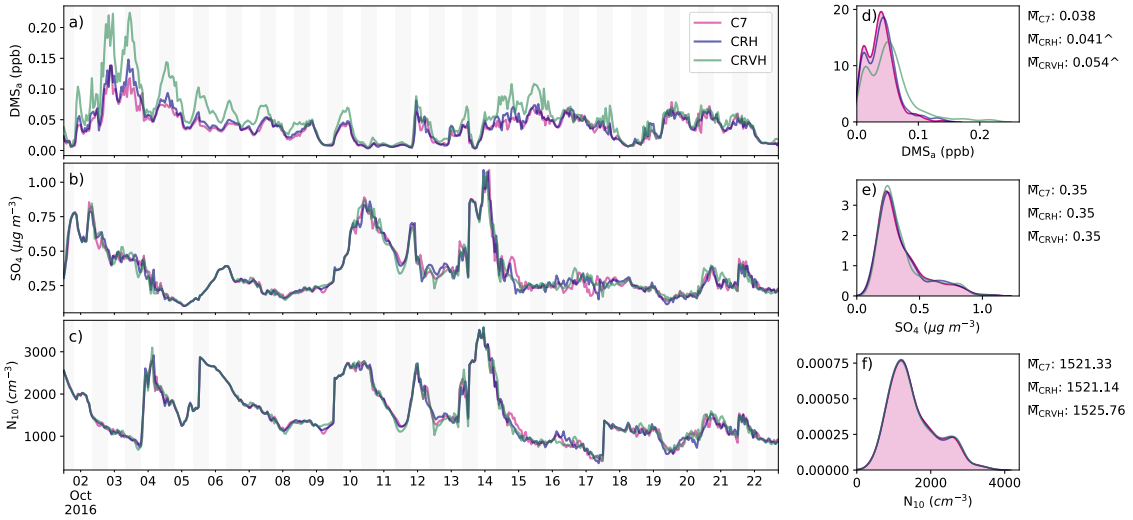


Figure 8.1: Timeseries (left) and distributions (right) for a representative grid box with significant coral reef coverage for surface $DMS_a$, $SO_4$ aerosol mass, $N_{10}$ and incoming solar radiation (RSDS) at the surface comparing the WRF-Chem control simulation C7 to the experimental simulations CRH and CRVH. The means ($\bar{M}$), of each simulations are shown. ^ indicates where the R values is significant to the 95th percentile

Considering now $DMS_a$ across D02, Figure 8.2 indicates that the addition of a weighted 8 nM of $DMS_w$ in CRH has made little difference to the $DMS_a$ over the GBR and QLD generally. Over the entire domain, an insignificant increase of 4 % is found for CRH. The difference between CRVH and C7, however, is larger, with statistical significance found for much of the domain. Interestingly, the increased $DMS_a$ can be seen advecting north-west across the QLD coast, due to the model's tendency to produce south-easterly winds found in Chapter 7. On average, the increase in $DMS_a$ is a significant 12 % over the entire domain. For D03 (see Appendix D), greater detail over the GBR can be seen and reefs dominate most of the marine area. Hence an increase of 28 % in $DMS_a$ is found for CRVH and of approximately 5 % for CRH.

The differences in $DMS_a$ found above, however, have not resulted in meaningful differences in $SO_4$, as shown in Figure 8.1b and e, where the means over the time-series are equal and little difference is visually discernible. The lack of change is also

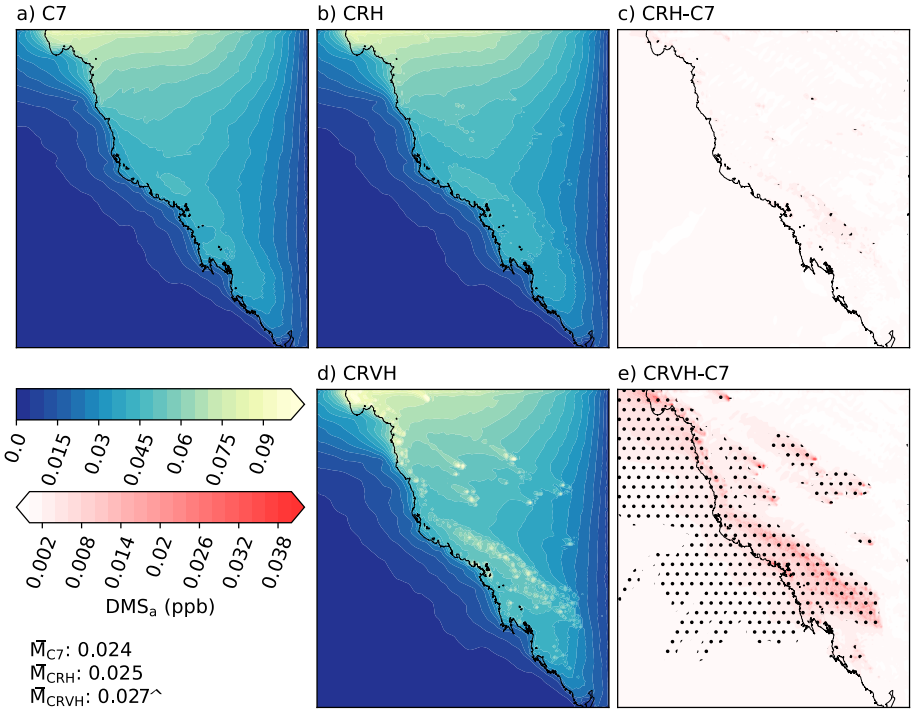


Figure 8.2: Average surface $DMS_a$ concentrations over D02 for a) C7, b) CRH and d) CRVH and the differences between CRH minus C7 in c) and CRVH minus C7 in e). Stippling in c) and e) indicate where the change is statistically significant ($p < 0.05$). In the lower left corner the area mean for each simulation is shown and ^ indicates that the mean is significantly different to C7

evident in Figure 8.3c and e, for which there is no difference in the domain averages (for both D02 here and D03 in Appendix D). The differences found locally cannot be attributed to coral reef $DMS_a$ and are very small (see scales) and hence are likely to be model noise, especially at the boundaries. It is noted that the scales of the difference in Figure 8.3 c and e and in figures throughout the rest of this Section are typically on orders of 1-2 % or less of the actual values given in a, b and d, again indicating that the differences shown are very small.

Figure 8.3a, b and d imply that a large portion of the sulfate aerosol mass is derived from anthropogenic sources. There are coal fired power stations in Gladstone (the largest plant in Queensland) and Stanwell in the south-eastern corner of the domain, and the gas turbine power station in Townsville, in the middle of the domain. Australian power stations currently are not required to use sulfur scrubbers, cat-

alytic converters or other means of pollution reduction, making them a large source of fine particulate matter and other toxic emissions. In addition, the influence of biomass burning can be seen to a lesser extend in some areas also contributing to the sulfate aerosol mass.

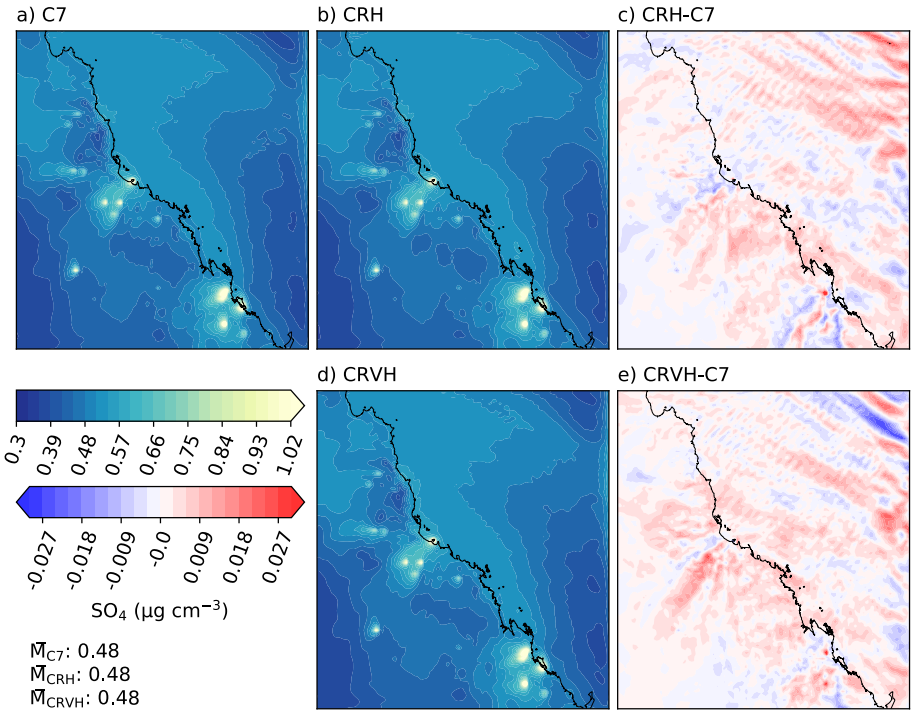


Figure 8.3: As for Figure 8.2 but for surface $SO_4$ aerosol mass concentration

Figure 8.1c and f indicate that the perturbations in $DMS_w$ in CRH and CRVH (compared to C7) have not had any meaningful impact on the total aerosol number concentration $N_{10}$ directly over significant coral reefs. This result is unsurprising given that of Chapter 7. Once again, the lack of response is clearly shown in Figure 8.4. Here, the influence of anthropogenic and biomass burning sources is also evident. A similar result is found for the $CCN_{70}$ (see Appendix D).

The significant lack of response in $N_{10}$ can be attributed to the similar lack of response found in the $SO_4$ aerosol mass. In addition, given that Chapter 7 found an approximately 10 % decline in $SO_4$ mass due to a halving of $DMS_w$, it is unlikely that the small perturbations in coral reef $DMS_w$ presented here would have a large

effect. Chapter 7 also suggested that the overestimation of $N_{10}$ due to four day restart intervals and the inability to simulate small size aerosol explicitly may be reducing the sensitivity of $N_{10}$ to $SO_4$. The lack of change in $SO_4$ found in this Chapter suggest that even if $N_{10}$ were well captured and more sensitive to $SO_4$, no change would be found.

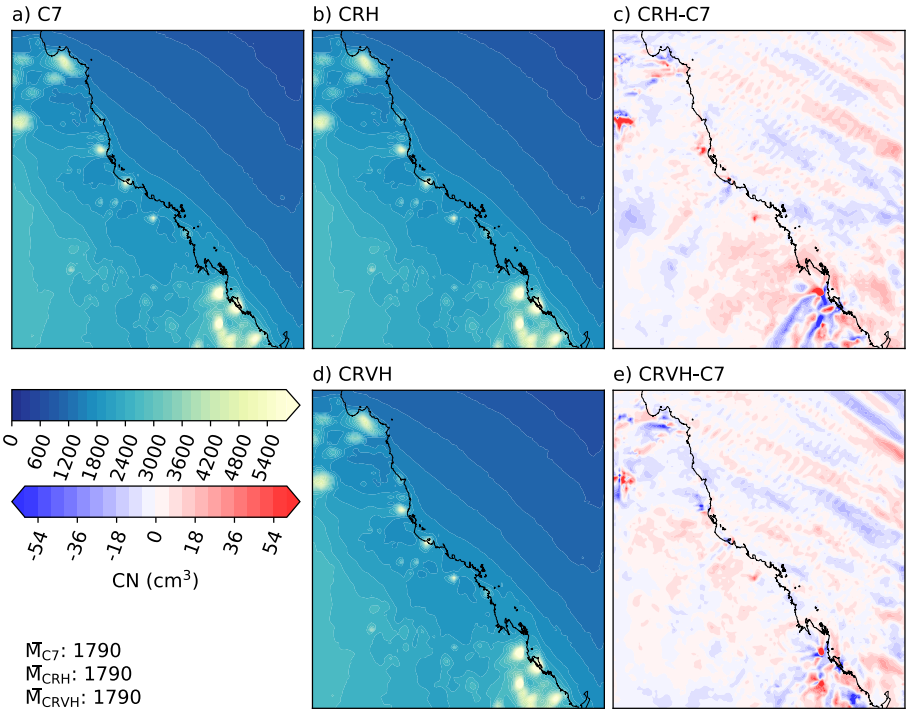


Figure 8.4: As for Figure 8.2 but for surface $N_{10}$ concentration

These results, from $DMS_a$ through to $N_{10}$, imply that when significant amounts of $DMS_w$ are added to the climate system, little to no impact is found on the aerosol burden. With this knowledge alone, it is reasonable to hypothesise that the addition of $DMS_w$ is unlikely to have any influence on the local weather over the GBR. This hypothesis will be explored in the next Section.

## 8.2 Direct and indirect aerosol effects

Figure 8.5 shows the $SW\downarrow_{Surf,CS}$ over D02, which is used in this thesis to assess the direct radiative effects of aerosol burden without the influence of clouds. In this Figure, no change in the $SW\downarrow_{Surf,CS}$ is apparent, with little model noise (see scale of c and e). The lack of response supports the conclusions drawn from the previous section that the inclusion of high estimates of $DMS_w$ has not resulted in a direct aerosol effect, either over the reef, or in the region, due to the lack of change in the $SO_4$ aerosol mass, $N_{10}$ and $CCN_{70}$ (see Appendix D). This is supported by findings for D03 (not shown) and the nudged results of ACCESS-UKCA in Chapter 6, where over the GBR no change in $SW\downarrow_{Surf,CS}$ was found.

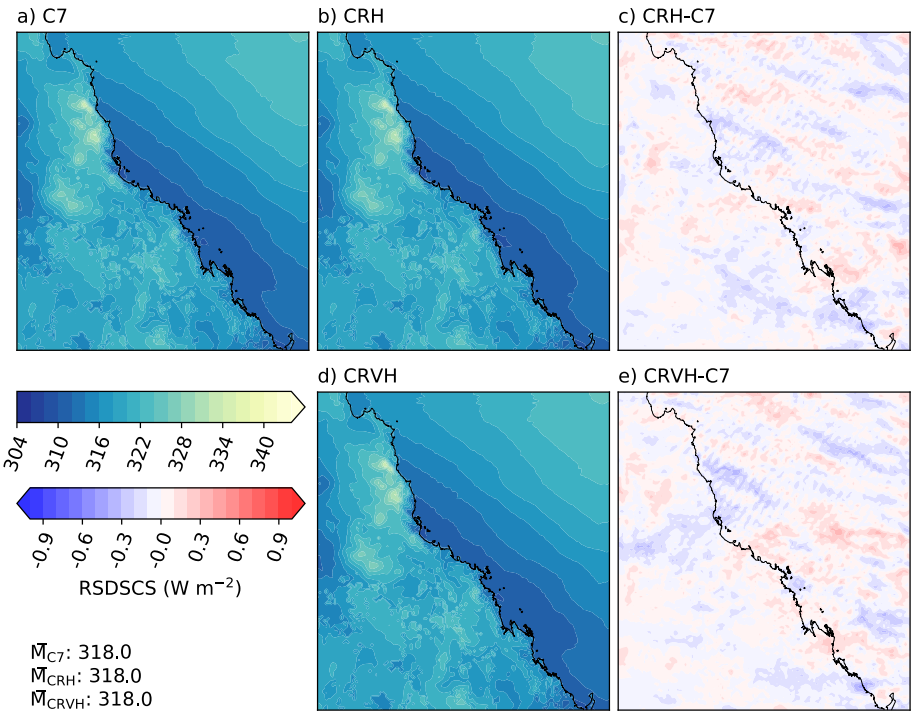


Figure 8.5: As for Figure 8.2 but for $SW\downarrow_{Surf,CS}$

Finally, Figure 8.6 shows that no difference in the liquid water path was found when coral reef $DMS_w$ was included. Analysis of other cloud properties, such as cloud fraction CDN (see Appendix D), cloud albedo and cloud height (not shown) also indicate no significant change attributable to perturbations in DMS. As a result,

the $SW{\downarrow}_{Surf}$ (not shown) and total precipitation over D02, see Figure 8.7 have not changed (the same is found for D03 - not shown). The consistent lack of differences found in cloud fields in this Section provide clear indication that no indirect aerosol effects have occurred as a result of including $DMS_w$ in WRF-Chem. These local-scale results support the conclusions of Chapter 6 at the global scale.

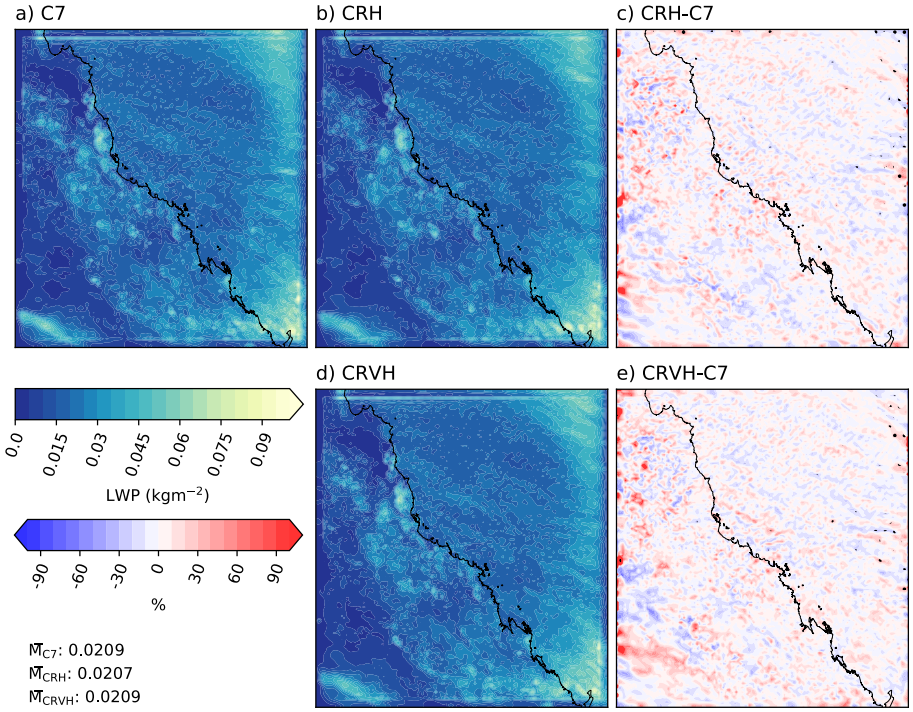


Figure 8.6: As for Figure 8.2 but for the liquid water path

## 8.3 Discussion

This Chapter has analysed the atmospheric effects of including coral reef-derived $DMS_w$ in WRF-Chem simulations. It has been shown that neither the high nor very high estimates of coral reef $DMS_w$ had an influence on atmospheric composition analysed here beyond the $DMS_a$ concentrations. As a result, no differences in meteorological properties were found, including no evidence of direct or indirect aerosol effects. These results are in agreement with what was concluded at the end

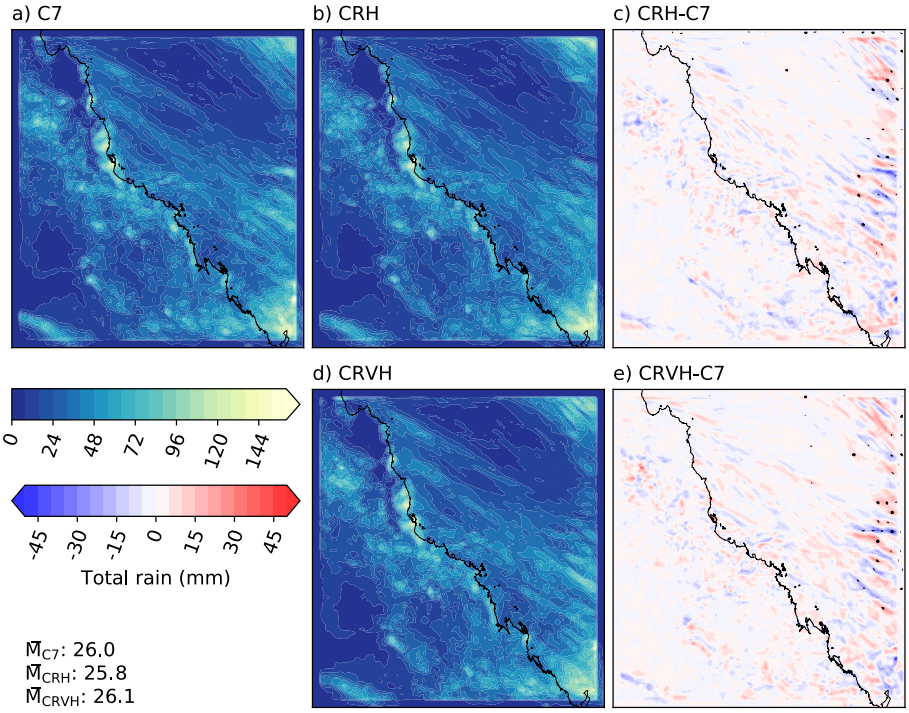


Figure 8.7: As for Figure 8.2 but for the period's total rainfall

of the R2R campaign (personal communication Zoran Ristovski).

These results are not unexpected given the findings from Chapter 7 where the halving of $DMS_w$ was found to have a small impact on sulfate aerosol mass and no impact on aerosol number. Chapter 7 suggested that the airmass in the QLD/GBR region was dominated by continental sources (also noted in this Chapter), despite the predominant south-easterly flow. The influence of these non-marine airmasses make the likelihood of marine aerosol influencing the local atmospheric composition and weather small. A study over more remote marine locations may overcome this influence. However, large coral reefs are inherently located along coastlines, hence limiting the possibility of such work to remote island reefs, which may not be large enough to have any effect as found in Chapter 6. In addition, anthropogenic sources operate year round so it is suggested that studying a different time of year is unlikely to change this finding. As an interesting aside, an experiment testing the impact of cleaning up Australia's anthropogenic pollution from energy generation may yield

interesting results.

Chapter 7 also noted that the four day restart interval and inability to resolve small size aerosol explicitly may have impacted the ability of WRF-Chem to respond to changes in $DMS_w$. However, in this Chapter, the significant lack of response at the $SO_4$ stage of the atmospheric DMS cycle suggest that no response would be expected even if these issues were overcome.

The results of this Chapter also agree well with the nudged ACCESS-UKCA results presented in Chapter 6, where no significant direct or indirect aerosol effects attributable to coral reefs were found over the QLD region. It is possible that repeating these experiments with free running meteorology, as done for ACCESS-UKCA, may yield different results due to the allowance of meteorological feedbacks, and in particular, that of water vapour. As found in the ACCESS-UKCA results however, the interaction of water vapour with shortwave radiation makes detecting the influence of aerosol difficult. Given the consistent lack of differences in $SO_4$, $N_{10}$ and $CCN_{70}$ found in this Chapter, it is postulated that a robust direct radiative response due to aerosol is unlikely if WRF-Chem were allowed to run freely.

Little difference is found between the results of D02 and D03, despite D03 being of a cloud resolving resolution. Possible future work to explore this further could include identification of particular convective periods to perform a case study. However, it is noted that in the current simulations, the nudging of water vapour may inhibit potentially interesting results. Hence it is suggested that such an analysis should be done with free running simulations.

It is therefore concluded that coral reef-derived DMS has little influence over $SO_4$ aerosol mass or total aerosol number. Subsequently, coral reefs are suggested to play no role in the balancing of the energy budget at short time scales over QLD and the GBR. This result does not support postulations from much of the observational literature discussed in Chapter 2.3 that coral reef-derived DMS is important for

climate/weather. These studies, unlike this one, could only examine aspects of the atmospheric DMS system that are relatively removed from each other (for example, comparing coral stress indices to the AOD). By examining the atmospheric DMS system from sea-air flux to cloud and radiation properties, this study has considered the significant complexities and non-linearities of this system. This method, in addition to the satisfactory skill of WRF-Chem to reproduce $DMS_a$ and $SO_4$ aerosol mass found in Chapter 7, has meant high confidence is given to the results of this Chapter.

Of particular note, the lack of difference in composition and meteorology when coral reef DMS was included at high concentrations further suggests that little potential for a bioregulatory feedback mechanism exists, especially as in reality the DMS produced by corals is highly variable and of lower magnitude.

# Chapter 9

# Conclusions

This thesis aimed to quantify the influence of coral reef-derived DMS on the atmosphere, both compositionally and meteorologically, across temporal and spatial scales. This has been done using two atmospheric-chemistry models running at different spatial and temporal resolutions to simulate the DMS-climate system from the ocean-atmosphere flux to changes in the energy balance and hydrological cycle. In order to contextualise the results, evaluation of model performance and consideration of how sensitive each model is to large perturbations in total marine $DMS_w$ was also performed. The results of this thesis and their implications for the state of knowledge are presented below.

DMS produced by phytoplankton was found to cool the Earth by approximately 0.45 K when total marine $DMS_w$ was removed from nudged ACCESS-UKCA simulations, demonstrating the importance of marine DMS for the global climate. In addition to this, DMS was found to play an important role in cloud formation and precipitation in regions of significant stratiform cloud decks in the Southern Hemisphere.

Southern Hemisphere stratiform cloud decks were found to have significantly

underestimated low level clouds and overestimated precipitation. DMS was found in this work to play an important role in low level cloud formation and the suppression of precipitation in these cloud decks. These results highlight the importance of accurately simulating natural aerosol emissions, especially in clean marine environments.

Interestingly, other regions of significant low level cloud formation, such as the Southern Ocean or Northern Hemisphere stratiform cloud decks, showed less response to the removal of marine DMS. It is hypothesised that poor representation of cloud characteristics, such as cloud phase and structure, may be preventing the expected climate response to changes in DMS in the Southern Ocean. In the Northern Hemisphere, high levels of pollution is suggested to overwhelm the small influence that DMS may have. The lack of sensitivity in these regions has important implications for climate modelling and highlights the need for improved aerosol and aerosol-cloud process representation.

Of note for this work, little influence of DMS on large-scale cloud and precipitation fields were found in tropical regions, where coral reefs are found. Tropical regions are dominated by convective processes with little large scale activity. However, current aerosol-climate modelling does not consider how convective processes may respond to changes in aerosol. This omission places a significant limitation on atmospheric models and on the results of this thesis. Despite this however, in nudged simulations, small and noisy decreases in convective processes are found around the tropics when all marine DMS is removed.

With knowledge of how the climate within ACCESS-UKCA responds to large perturbations in DMS, the importance of the much smaller contribution of DMS by global coral reefs was examined for the first time. To do this a nudged simulation pair and a seven-pair free-running ensemble of ACCESS-UKCA simulations were used. A world with a high-end estimation of global coral reefs (the estimation added to the

Lana et al., 2011, climatology) was compared to a world without (the Lana et al., 2011, climatology). At the global scale, coral reef-derived DMS was found to have effectively no impact on the climate, with an estimation of less than a 0.01 K cooling effect.

Regionally however, coral reefs were found to have a small yet significant contribution to the sulfur burden and nucleation and Aitken mode aerosol numbers, with some seasonal variation. These significant contributions were only found over the MC-Aus region, where the highest density of coral reefs are found globally, and highlight the importance of representing nucleation mode aerosol and subsequent growth explicitly in climate models. In other regions of lower density coral reefs, coral reef-derived DMS was found to be too weak to have any meaningful impact on atmospheric composition.

Responses to coral reef-derived DMS in accumulation and coarse mode aerosol were generally smaller and insignificant compared to those found in the nucleation or Aitken mode, with aerosol mass responding more than aerosol number. As a result, small and generally insignificant responses in $CCN_{70}$, AOD and CDN were found, with the most consistent response in austral spring. Interestingly, for many of the aerosol fields, the results were enhanced by the free-running meteorology, although remained insignificant despite the seven member ensemble.

Small reductions in the $SW\uparrow_{TOA,CS}$ were found in both the nudged simulation and free running ensemble in response to removal of coral reef-derived DMS. While in the nudged simulation the reduced $SW\uparrow_{TOA,CS}$ corresponded to a similar but opposite change in $SW\downarrow_{Surf,CS}$, in the free running ensemble, the influence of water vapour on short wave radiation was clearly demonstrated.

Increases in water vapour were found to overwhelm the aerosol response suggested by the nudged simulations. The water vapour response highlights the importance of meteorological effects on aerosol processes and also the difficulty in sepa-

rating the two. In addition, this research indicates that changes in water vapour could be as important or possibly even more so than small changes in local aerosol to the radiation budget and warrants further investigation.

A physical mechanism explaining how water vapour could be responding to changes in coral reef-derived DMS was unable to be determined with confidence, implying that internal model variability could not be ruled out as the cause. It was subsequently concluded that although coral reefs contribute a small amount of small sized aerosol, the subsequent direct radiative effects are likely to be too small to have any climatic importance. In addition to this, no indirect effects were detected in either CDN, low cloud properties or large-scale precipitation.

While the findings above related to the broader MC-Aus region, over QLD, the meteorological response to coral reef-derived DMS were enhanced. Over this region, statistical significance and greater model agreement than over the MC-Aus region were found with respect to AOD, $SW\uparrow_{TOA,CS}$, $SW\downarrow_{Surf,CS}$ and convective cloud processes.

Interestingly, an unexpected increase in convective precipitation of 11 % was found over QLD when coral reef-derived DMS was removed from the system. This increase must have occurred dynamically as the convective scheme is not explicitly coupled to the aerosol scheme. However, difficulty in detecting a physical cause linking these convective changes to the weak direct effect has meant low confidence is given to this result. In addition, earlier results examining the influence of DMS derived from plankton indicated an opposite response in the convective system. Nevertheless, this result highlights the complexity of the aerosol-climate system and clearly demonstrates why considering the system as a whole, as opposed to a few select parameters, must be analysed to understand aerosol-climate interaction.

The regional scale model WRF-Chem was then used to further understand the effects of coral reef-derived DMS over the QLD region. Nudged WRF-Chem simu-

lations were run over three nested domains, the inner of which, at 3 km horizontal and 20 s temporal resolution, was at a cloud resolving resolution in an attempt to overcome the issue of convective cloud parameterisation not being coupled to aerosol schemes. WRF-Chem was run over the period of October 2016 to coincide with R2R field campaign, the observations of which were used to evaluate the model.

Two high end estimations of coral reef-derived $DMS_w$ were added to a scaled version of the Lana et al. (2011) climatology, reduced by a factor of 2.8 to match with observed $DMS_w$. Many regional and global models include DMS without considering its accuracy or impacts. For this reason, it is crucial to ensure that the climatology used is accurate. I highlight this point, as the default WRF-Chem $DMS_w$ climatology is the Kettle et al. (1999) climatology, not the more recent Lana et al. (2011) climatology.

Using the WRF-Chem simulations, over QLD, and more specifically over the GBR, no influence of coral reef-derived DMS could be detected beyond changes in $DMS_a$. When coral reef-derived DMS was added into the system, despite significant increases in $DMS_a$, no response in $SO_4$ aerosol mass was found. WRF-Chem was found to simulate $DMS_a$ and $SO_4$ aerosol mass satisfactorily when compared to observations and $SO_4$ aerosol mass was found to be sensitive to large-scale changes in $DMS_w$. These two findings suggest that poor model performance or low sensitivity to DMS is not the reason for the lack of response to coral reef-derived DMS in $SO_4$ aerosol mass.

Alternatively, it was suggested that anthropogenic sources of sulfur, associated in this case with energy generation in QLD, may be playing a significant role in $SO_4$ aerosol mass, with a larger effect than marine sources of sulfur. This suggestion is supported by the global results from ACCESS-UKCA and by literature (Carslaw et al., 2013). For the Australian region, the importance of anthropogenic sulfur on local weather warrants further examination, especially considering the transition

towards fossil fuel free energy generation. A future study exploring how low anthropogenic $SO_2$ emissions need to be for coral reef-derived DMS to have a local impact may be of interest.

Furthermore, for the period analysed, significant terrestrial influence was detected throughout (Chen et al., 2019), while literature has also shown that the sea salt aerosol flux in WRF-Chem is overestimated (Saide et al., 2012; Yang et al., 2011). The combination of these two influences over coral reef regions further suggests that a coral reef contribution to aerosol is likely to be too small to have an impact under current conditions.

The significant lack of response in $SO_4$ to coral reef-derived DMS subsequently meant no response in aerosol number ($N_{10}$ or $CCN_{70}$) was found. In these simulations, WRF-Chem was restarted at four day intervals. However, the re-initialisation resulted in significant overestimation of both $N_{10}$ and $CCN_{70}$ at the start of the four day period, likely due to the approximations performed by WRF-Chem in estimating aerosol number from bulk aerosol mass. The influence of the re-initialisation may have had some impact on the sensitivity of WRF-Chem to larger changes in marine DMS. However re-initialisation is not suggested to have influenced the coral reef-derived DMS response due to the lack of response of $SO_4$ aerosol mass. In a similar vein, it is suggested that running WRF-Chem freely, as done for ACCESS-UKCA is unlikely to yield differing results. Finally, the inability of WRF-Chem to explicitly simulate small sized aerosol has also likely played a role in the lack of sensitivity of aerosol number, as small sized aerosol are an important aspect of the DMS-climate system.

As a result, no direct or indirect aerosol radiative effects were found in WRF-Chem in response to coral reef-derived DMS, in any domain (cloud resolving or parameterising), agreeing with the results of the nudged ACCESS-UKCA-coral simulations.

This research has demonstrated that coral reefs have no robust impact on local, regional or global weather or climate. The estimate of coral reef-derived DMS, added to the Lana et al. (2011) $DMS_w$ climatology in ACCESS-UKCA or a scaled version of Lana et al. (2011) in WRF-Chem, was at the high end of the range suggested by observations. In addition, the coral reef-derived DMS estimate, despite being weighted by coral reef density, was an average over grid boxes, likely further overestimating realistic values given relatively low reef surface area. More realistic values of coral reef-derived $DMS_w$ are likely to be not only lower but much more variable than what is considered in this thesis suggesting that little atmospheric influence could be expected with a more realistic representation of coral reef-derived DMS.

The conclusions of this thesis are in contrast to literature postulating that coral reef-derived DMS plays a role in atmospheric composition or meteorological processes (eg. Deschaseaux et al., 2016; Hopkins et al., 2016; Jones et al., 2018; Cropp et al., 2018; Jackson et al., 2018, 2019). All of these studies were based on observations and employed linear statistics to ascertain relationships between coral reefs and local climate. Even with comprehensive observations, attributing a climatic response to a particular aerosol source is difficult and prone to error due to the influence of many aerosol sources, as demonstrated in this thesis.

A combination of modelling and measurement analysis provides the best approach to quantifying the role of DMS in the atmosphere. This thesis provides one of the first examples in DMS-climate literature where this has been achieved. In this work, stepping through the atmospheric DMS pathway from flux to meteorological effects has shown how complex the atmospheric DMS system is. Furthermore, this thesis has demonstrated that assumptions of linearity or even of how the climate responds to aerosol should not be made lightly.

The research presented here suggests that coral reefs are not a significant enough

source of DMS to participate in bioregulatory feedback. This research was the first, to my knowledge, to attempt to find an atmospheric response to DMS from any source at a high time resolution (hours) and at local geographical scale (down to a 3 km grid). This is important as the CLAW hypothesis describes a process that would have to occur over a matter of days (despite having an accumulative climatic effect). While this work does not disprove the CLAW hypothesis as originally proposed by Charlson et al. (1987), it provides no supporting evidence towards its existence.

This thesis is in agreement with the majority of the global DMS-climate literature that suggest no bioregulatory mechanism by DMS-producing marine organisms exists (Woodhouse et al., 2010; Quinn and Bates, 2011; Woodhouse et al., 2013; Green and Hatton, 2014). It must be emphasised however, that these studies and this thesis, do not dispute the long term importance of DMS in the climate system.

Aerosol-climate and in particular aerosol-cloud interaction is the most uncertain component of the global energy balance (Myhre et al., 2013b). Carslaw et al. (2013) suggest that natural aerosol, in particular sulfate aerosol, contribute a large portion of this uncertainty. Sulfates make up a large fraction of the global aerosol mass fraction, with DMS the second largest natural source of sulfur to the atmosphere (Sheng et al., 2015).

Better representation of $DMS_w$ and $flux_{DMS}$ has been highlighted as one important way to improve natural aerosol modelling. Capturing the correct number and mass concentration of aerosol is considered to be another. This was especially clear where nucleation mode sized aerosol are concerned. In this thesis, nucleation mode aerosol were not explicitly resolved in WRF-Chem, while ACCESS-UKCA demonstrated these aerosol played an important role in the DMS-climate system. Better representation of the aerosol size distribution is suggested to be an important aspect of modelling the influence of natural aerosol. Furthermore, the model evaluations

presented in this work showed that the simulation of cloud remains a core problem in both models. The complete coupling of aerosol and cloud processes is an active research area and one which must be guided by measurements and evaluation.

This thesis has explored the atmospheric DMS system, specifically quantifying the role of coral reef-derived DMS across temporal and spatial scales. No robust evidence has been found to indicate that coral reefs have a significant role in climate or weather under present day conditions. In contrast, this work has shown that DMS produced by phytoplankton globally contributes a 0.45 K cooling effect, demonstrating the importance of marine ecosystem health for climate. The possibility remains that in a cleaner world, i.e. one with reduced anthropogenic aerosol emission, DMS may play a larger role in the climate system.

# Definition of terms

$\alpha_{\mathrm{Cld}}$ Cloud albedo.

**ACCESS-UKCA** Australian Community Climate and Earth System Simulator - United Kingdom Chemistry and Aerosol; a global coupled climate-chemistry model.

**AIRBOX** Atmospheric Integrated Research Facility for Boundaries and Oxidative Experiments; a mobile atmospheric chemistry laboratory.

**AOD** Aerosol optical depth.

**BARRA-R** Australian Bureau of Meteorology Atmospheric high-resolution Regional Reanalysis for Australia.

**BF** Bias Factor calculated from the Normalised Mean Bias Factor method.

**BLH** Boundary Layer Height.

**C1** Control 1 WRF-Chem simulation, see Table 3.7 for details.

**C7** Control 2 WRF-Chem simulation, see Table 3.7 for details.

**CALIPSO-GOCCP** GCM-Oriented Cloud-Aerosol Lidar and Infrared Pathfinder Satellite Observation Cloud Product.

**CBMZ** Carbon Bond Mechanism Z.

**$CCN_{70}$** Cloud condensation nuclei with a dry diameter greater than 70 nm.

**CCN** Cloud condensation nuclei.

**CDN** Cloud droplet number.

**CERES-EBAF** Clouds and the Earths Radiant Energy System - Energy Balanced And Filled.

**CFMIP** Cloud Feedback Model Intercomparison Project.

**CLAW** Charlson, Lovelock, Andrea and Warren; the authors of the hypothesis.

**CldH** High level cloud fraction.

**CldL** Low level cloud fraction.

**CMIP5** Coupled Model Intercomparison Project Phase Five.

**COSP** CFMIP Observation Simulator Package.

**CRH** Coral Reef - high estimate WRF-Chem simulation, see Table 3.7 for details.

**CRVH** Coral Reef - very high estimate WRF-Chem simulation, see Table 3.7 for details.

**CSIRO** Commonwealth Scientific and Industrial Research Organisation.

**CTH** Cloud top height.

**$DMS_a$** Atmospheric DMS.

**$DMS_w$** Surface water DMS.

**DMS** Dimethyl sulfide.

**DMSP** Dimethyl sulfoniopropionate.

**ERF** Effective radiative forcing.

**FAIR** Finite Amplitude Impulse Response model.

**$\mathbf{flux_{DMS}}$** Sea-air DMS flux.

**GBR** Great Barrier Reef.

**GCM** General Circulation Model/Global Climate Model.

**GLOMAP-mode** GLObal Model of Aerosol Processes; a modal aerosol scheme.

**GOCART** Georgia Tech/Goddard Global Ozone Chemistry Aerosol Radiation and Transport.

**HuS** Specific humidity.

**IPCC** Intergovernmental Panel on Climate Change.

**ITCZ** Intertropical Convergence Zone.

**L11** The Lana et al. (2011) $DMS_w$ climatology used in both ACCESS-UKCA and WRF-Chem.

**L11C50** The Lana et al. (2011) $DMS_w$ climatology with an additional weighted 50 nM over coral reef regions for ACCESS-UKCA.

**L11MX** The zonal maximum Lana et al. (2011) $DMS_w$ climatology for ACCESS-UKCA.

**L11S** The Lana et al. (2011) $DMS_w$ climatology scaled to the R2R observations for WRF-Chem.

**L11SCH** The scaled Lana et al. (2011) $DMS_w$ climatology with an additional weighted 8 nM over coral reef regions for WRF-Chem.

**L11SCL** The scaled Lana et al. (2011) $DMS_w$ climatology with an additional weighted 2 nM over coral reef regions for WRF-Chem.

**L11SCVH** The scaled Lana et al. (2011) $DMS_w$ climatology with an additional weighted 50 nM over coral reef regions for WRF-Chem.

**LW$\uparrow_{TOA}$** Longwave radiation up-welling at the top of the atmosphere.

**LWC** Liquid water content.

**MBL** Marine boundary layer.

**MOSAIC** Model for Simulating Aerosol Interactions and Chemistry.

**MSA** Methane sulfonic acid.

**$N_{10}$** Condensation nuclei with a dry diameter greater than 10 nm.

**$N_3$** Condensation nuclei with a dry diameter greater than 3 nm.

**NSS** Non-sea salt.

**Pr** Total precipitation.

**PrC** Convective rainfall.

**PrL** Large-scale rainfall.

**$Q_{cl}$** Total cloud liquid water.

**Q*** Top of the atmosphere energy balance.

**$R_{DMS}$** Radiative effect of DMS.

**R2R** Reef to Rainforest field campaign.

**RCP** Representative Concentration Pathway.

**RH** Relative humidity.

**RVI** Research Vessel Investigator.

**SEP** Southeast Pacific.

**SO** Southern Ocean.

**SPCZ** South Pacific Convergence Zone.

**SST** Sea surface temperature.

**SW$\uparrow_{\mathrm{TOA}}$** Shortwave radiation up-welling at the top of the atmosphere.

**SW$\uparrow_{\mathrm{TOA,CS}}$** Clear sky shortwave radiation up-welling at the top of the atmosphere.

**SW$\downarrow_{\mathrm{Surf}}$** Shortwave radiation down-welling at the surface.

**SW$\downarrow_{\mathrm{Surf,CS}}$** Clear sky shortwave radiation down-welling at the surface.

**TOA** Top of the atmosphere.

**$\mathbf{TQ_{cl}}$** Vertically integrated total cloud liquid water.

**TRMM** Tropical Rainfall Measuring Mission.

**VOCALS-REx** VAMOS (Variability of the American Monsoon Systems) Ocean-Cloud-Atmosphere-Land Study Regional Experiment.

**WRF-Chem** Weather Research and Forecasting - Chemistry; a regional coupled weather-chemistry model.

**Z** Zero marine $\mathrm{DMS_w}$ climatology for ACCESS-UKCA.

# Appendix A

# ACCESS-UKCA DMS climatologies

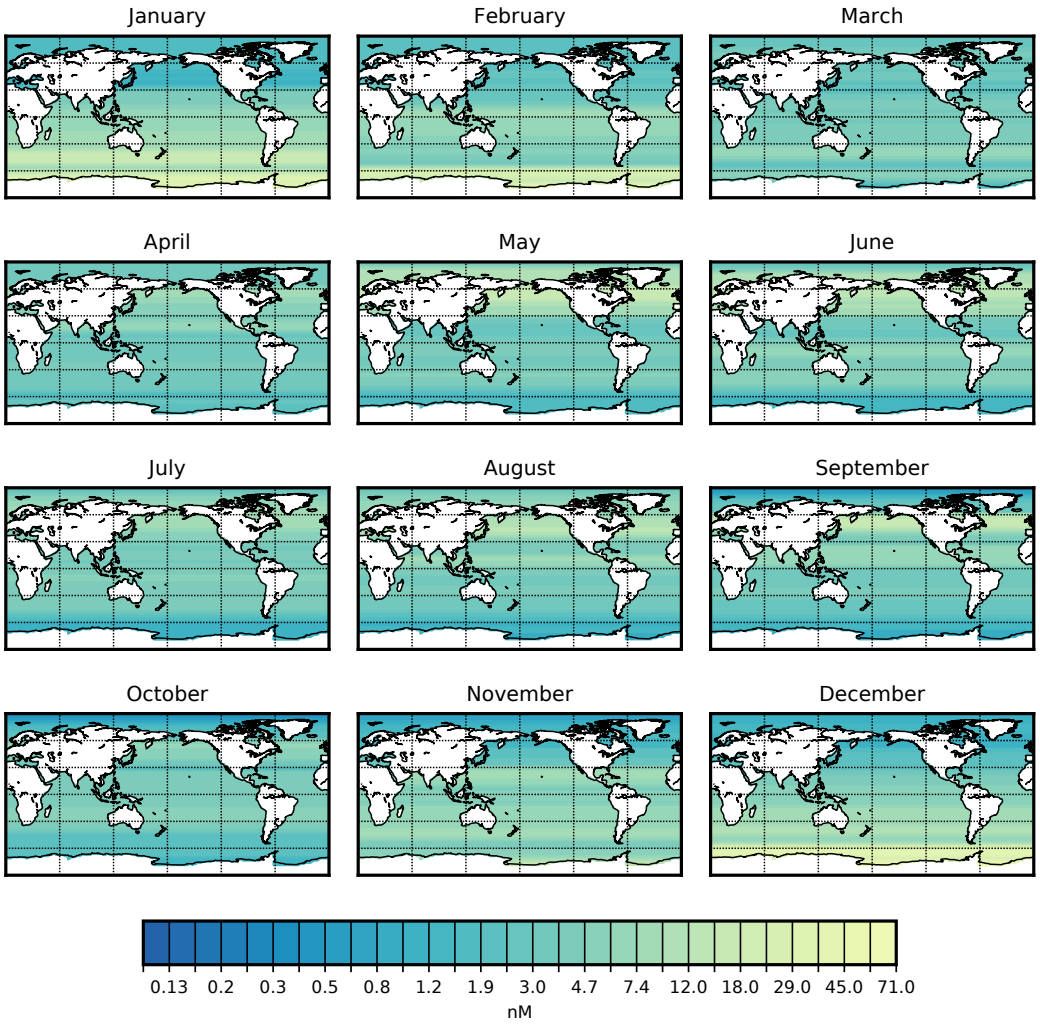


Figure A.1: The January and July zonal maximum of the L11 $DMS_w$ climatology (L11MX). Note that $DMS_w$ is plotted on a log scale, in nM

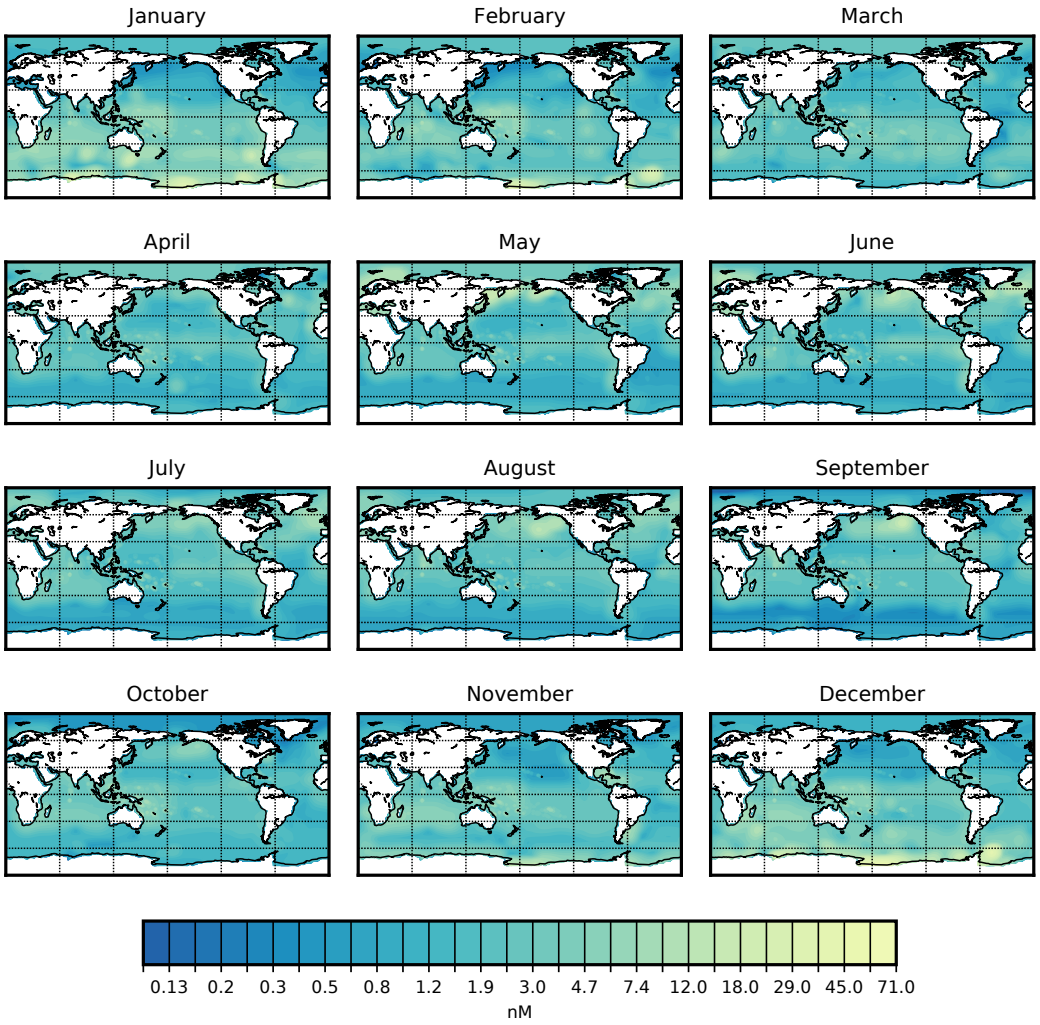


Figure A.2: The monthly L11 climatology with an additional weighted 50 nM of $DMS_w$ (L11C50). Note that $DMS_w$ is plotted on a log scale, in nM

# Appendix B

# WRF-CHEM namelists

The following tables provide the namelist options for the C7 simulations.

Table B.1: The chemistry namelist options selected for WRF-Chem

| &chem | Option |
|---|---|
| kemit | = 9, |
| chem_opt | = 34, 34, 34, |
| bio_emiss_opt | = 1, 1, 1, |
| emiss_opt | = 4, 4, 4, |
| emiss_inpt_opt | = 102, 102, 102, |
| bioemdt | = 30, 30, 30, |
| photdt | = 30, 30, 30, |
| chemdt | = 0, 0, 0, |
| io_style_emissions | = 2, |
| chem_in_opt | = 1, 1, 1, |
| phot_opt | = 3, 3, 3, |
| gas_ic_opt | = 0, 0, 0, |
| gas_bc_opt | = 0, 0, 0, |
| gas_drydep_opt | = 1, 1, 1, |
| aer_drydep_opt | = 1, 1, 1, |
| gaschem_onoff | = 1, 1, 1, |
| aerchem_onoff | = 1, 1, 1, |
| wetscav_onoff | = 1, 1, 1, |
| cldchem_onoff | = 1, 1, 1, |
| vertmix_onoff | = 1, 1, 1, |
| chem_conv_tr | = 1, 1, 1, |
| conv_tr_wetscav | = 1, 1, 1, |
| conv_tr_aqchem | = 1, 1, 1, |
| seas_opt | = 2, (C1) or 4, (C7) |
| dust_opt | = 0, (C1) or 4, (C7) |
| dust_schme | = 2, (C7 only) |
| dustwd_onoff | = 1, (C7 only) |
| dmsemis_opt | = 1, |
| aircraft_emiss_opt | = 0, |
| biomass_burn_opt | = 0, 0, 0, (C1) or 1, 1, 1, (C7) |
| plumerisefire_frq | = 120, 30, 10, (C7 only) |
| have_bcs_chem | = .true., .true., .true., |
| aer_ra_feedback | = 1, 1, 1, |
| diagnostic_chem | = 1, 1, 1, |
| opt_pars_out | = 1, |
| aer_op_opt | = 1, 1, 1, |
| chemdiag | = 1, |
| ne_area | = 240, |

Table B.2: The physics namelist options selected for WRF-Chem

| &physics | Option |
|---|---|
| physics_suite | = 'CONUS' |
| mp_physics | = 10, 10, 10, |
| radt | = 30, 30, 30, |
| bldt | = 0, 0, 0, |
| cudt | = 0, 0, 0, |
| icloud | = 1, |
| num_soil_layers | = 4, |
| num_land_cat | = 24, |
| sf_sfclay_physics | = 2, 2, 2, |
| ra_lw_physics | = 4, 4, 4, |
| ra_sw_physics | = 4, 4, 4, |
| sf_urban_physics | = 2, 2, 2, |
| bl_pbl_physics | = 2, 2, 2, |
| sf_surface_physics | = 2, 2, 2, |
| cu_physics | = 5, 5, 0, |
| cu_diag | = 1, 1, 0, |
| cu_rad_feedback | = .true.,.true.,.false., |
| sst_update | = 1, |
| sst_skin | = 1, |
| progn | = 1, 1, 1, |

# Appendix C

# Additional plots for ACCESS-UKCA

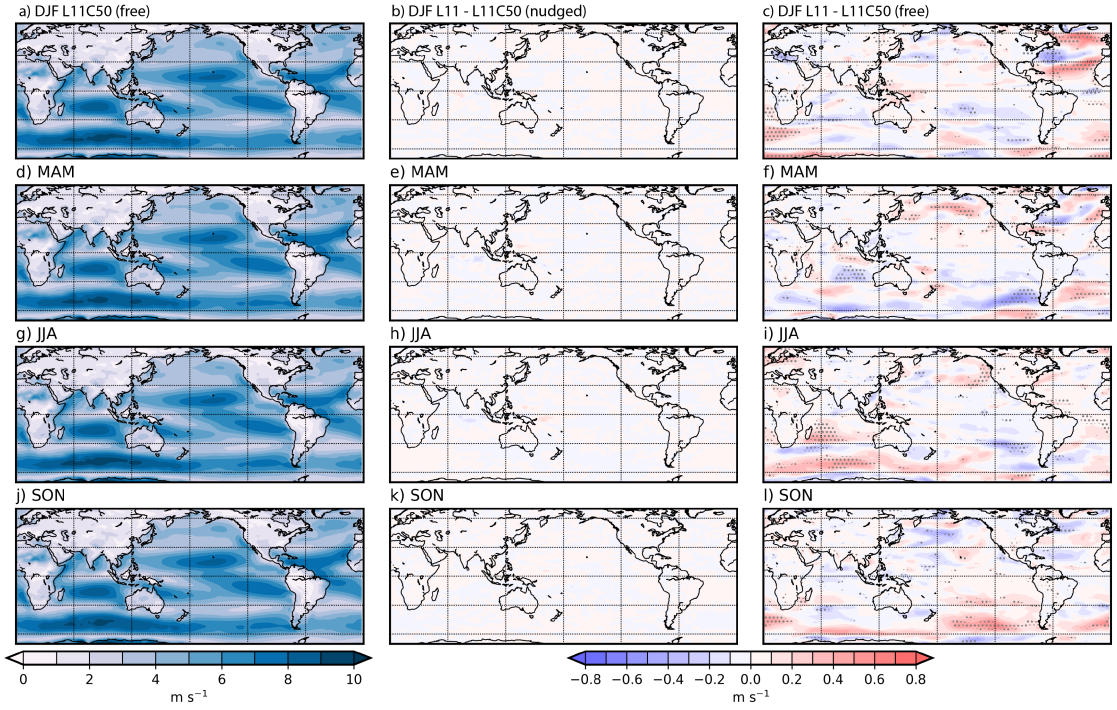


Figure C.1: The seasonal (DJF - top row, MAM - upper middle row, JJA - lower middle row and SON - bottom row) wind speed at the surface (10m) (in $\mathrm{m\,s^{-1}}$) for the free L11C50 simulation (left column); the L11-L11C50 difference for the nudged simulations (middle column); the L11-L11C50 difference for the free running ensemble (right column) with the model agreement shown by stippling, where at least five of the seven ensemble pairs agree in the sign of the difference.

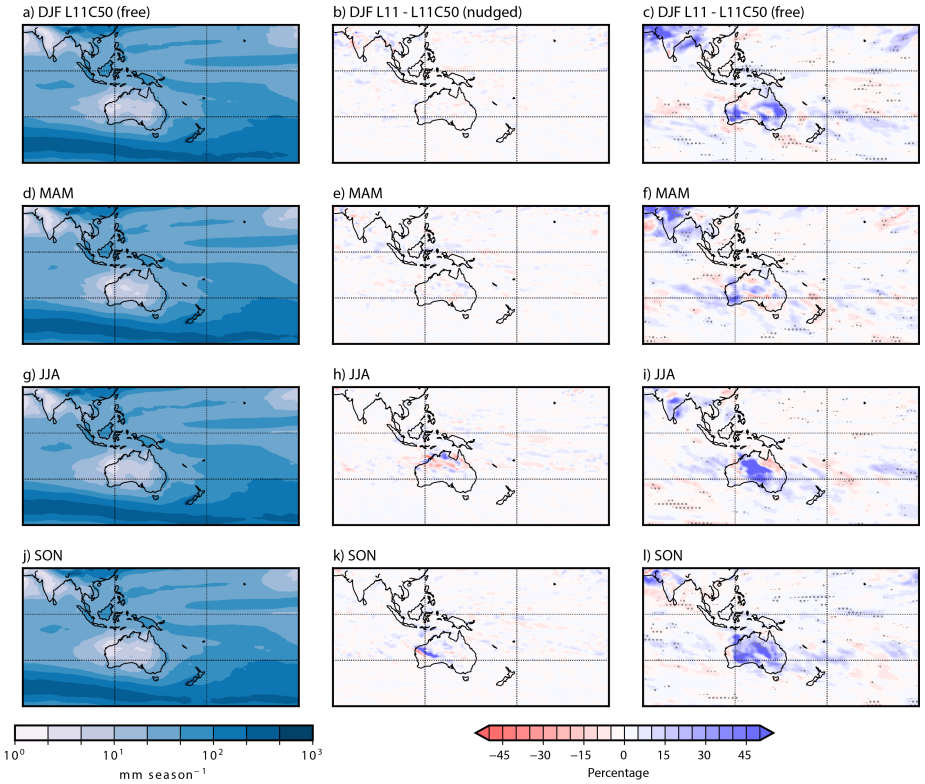


Figure C.2: As for Figure C.1 but for PrC in mm season$^{-1}$

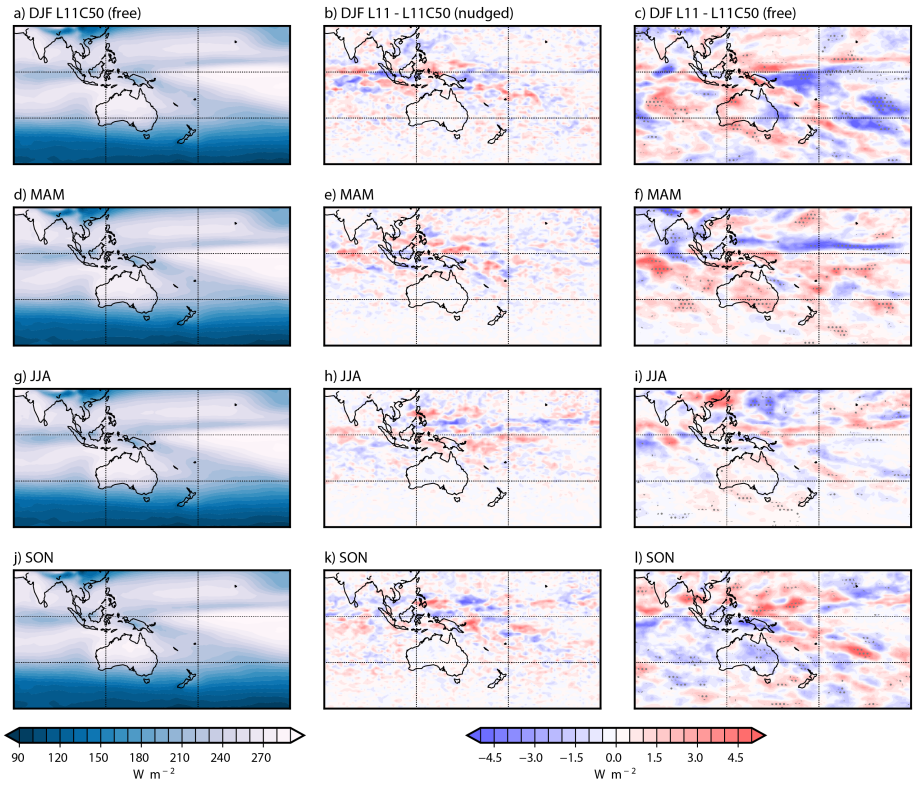


Figure C.3: As for Figure C.1 but for $SW\downarrow_{Surf}$ in W m$^{-2}$

# Appendix D

# Additional plots for WRF-CHEM

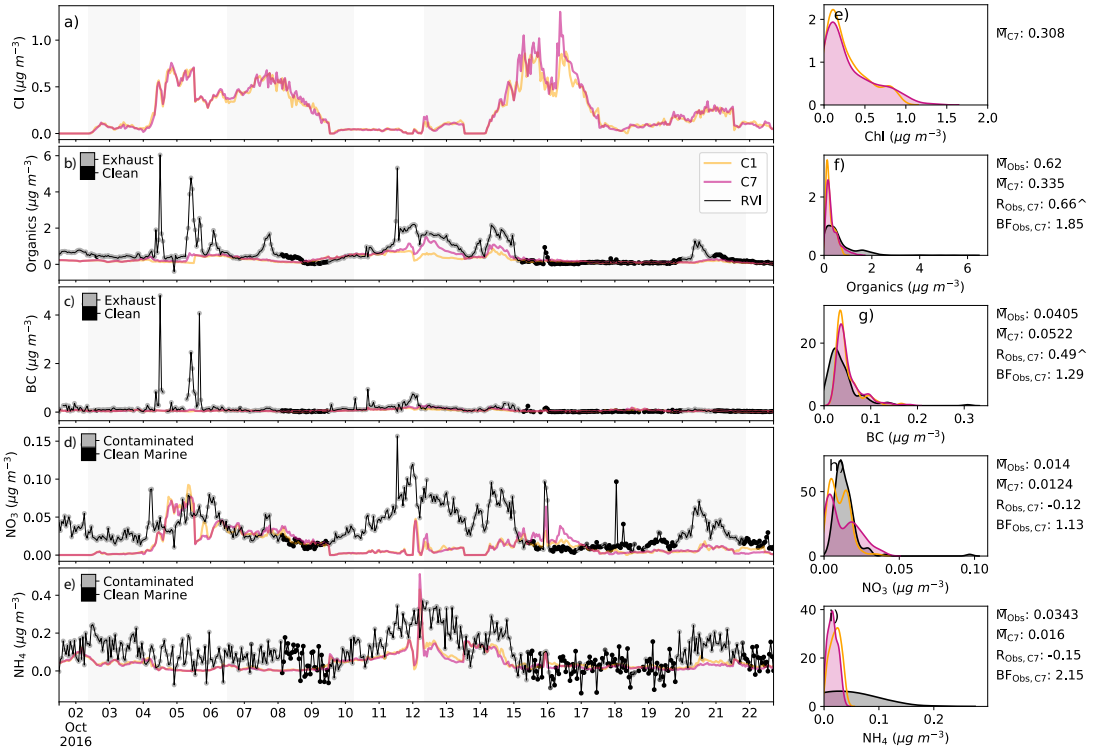


Figure D.1: Timeseries along the RVI track (left) and distributions (right) in order of top to bottom of surface chlorine, organic, BC, $NO_3$ and $NH_4$ aerosol mass comparing the WRF-Chem simulations C1 and C7 to the observations. Summary statistics are shown for the observations and C7 including the mean (M), the Pearson correlation (R) and the BF. îndicates where the R values is significant to the 95th percentile. The shaded grey areas in a-e) represent periods when the ship was at station (S2, S3.1, S3.2 and S4). Observations in the timeseries are flagged by grey dots when then airmass was considered to be influenced by exhaust, terrestrial airmass or both (contaminated), including a log flag. Flagged values have been excluded from the distributions and statistics

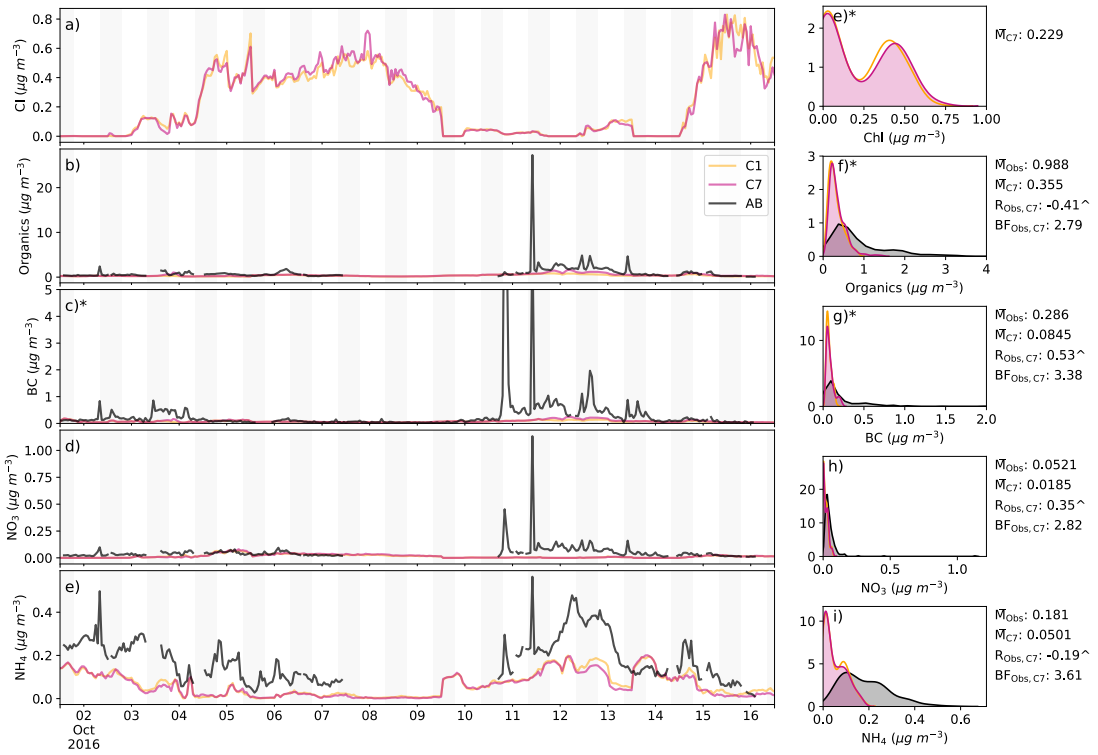


Figure D.2: Timeseries at AIRBOX (left) and distributions (right) in order of top to bottom of surface chlorine, organic, BC, $NO_3$ and $NH_4$ aerosol mass comparing the WRF-Chem simulations C1 and C7 to the observations. Summary statistics are shown for the observations and C7 including the mean (M), the Pearson correlation (R) and the BF. îndicates where the R values is significant to the 95th percentile. The shaded grey areas in a-e) represent nocturnal periods. * indicates where the x-axis has been limited for clarity

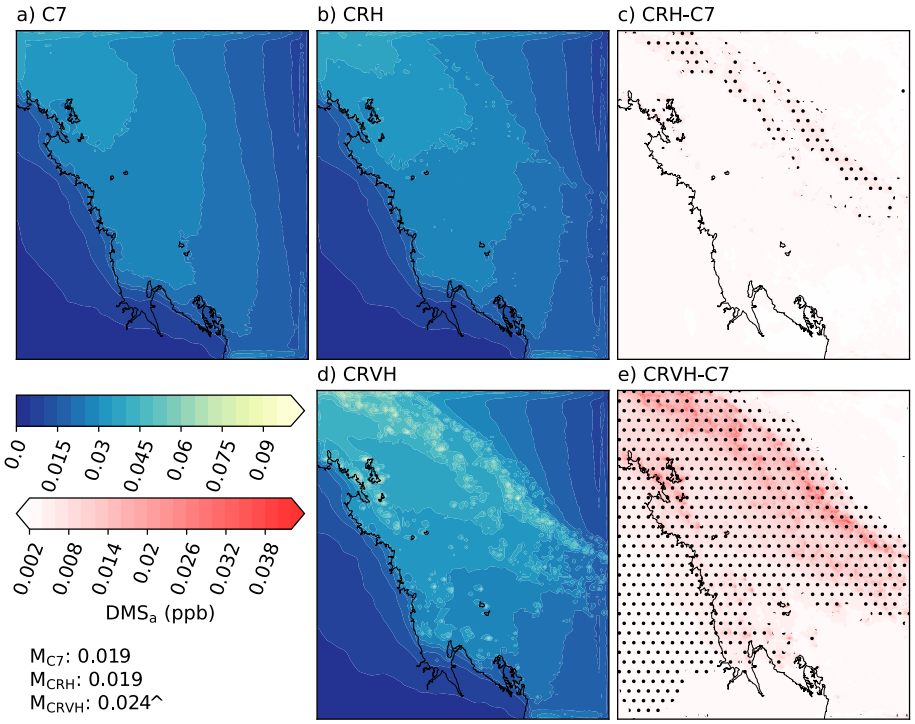


Figure D.3: Spatial timeseries average of surface $DMS_a$ concentrations over D03 for a) C7, b) CRH and d) CRVH and the differences between CRH minus C7 in c) and CRVH minus C7 in e). Stippling in c) and e) indicate where the change is statistically significant ($p < 0.05$). IN the lower left corner the area mean for each simulation is shown and îndicates that the mean is significantly different to C7

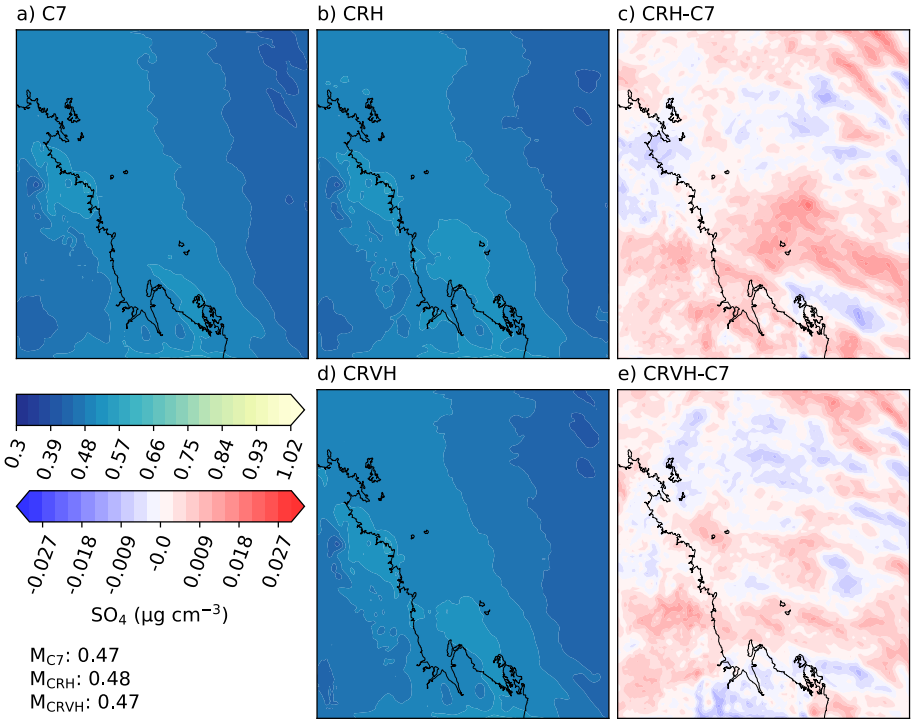


Figure D.4: As for Figure D.3 but for surface $SO_4$ aerosol mass concentration

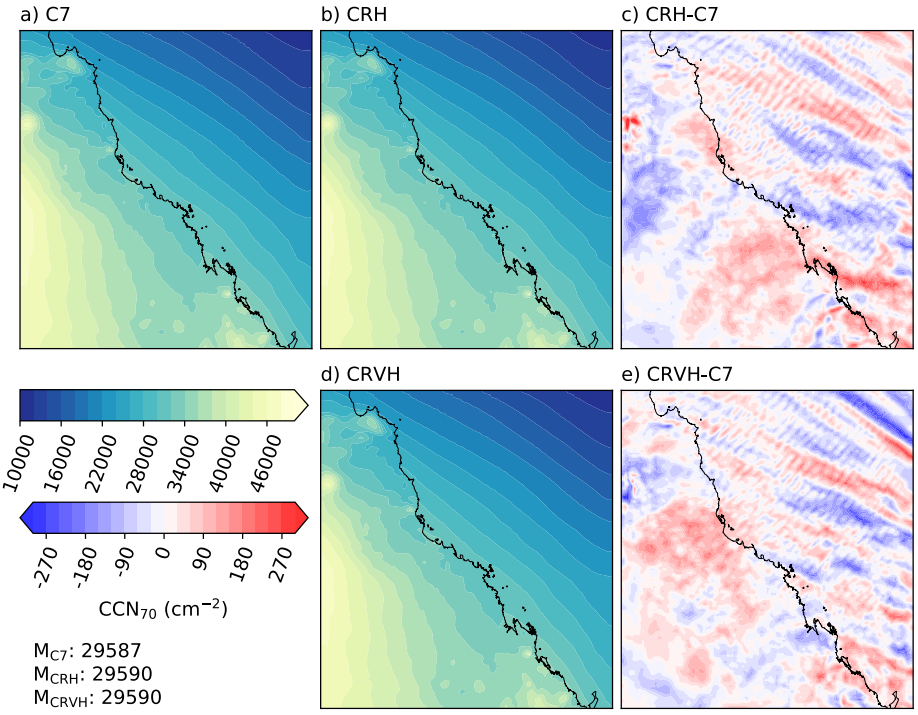


Figure D.5: As for Figure D.3 but for total column $CCN_{70}$ over D02

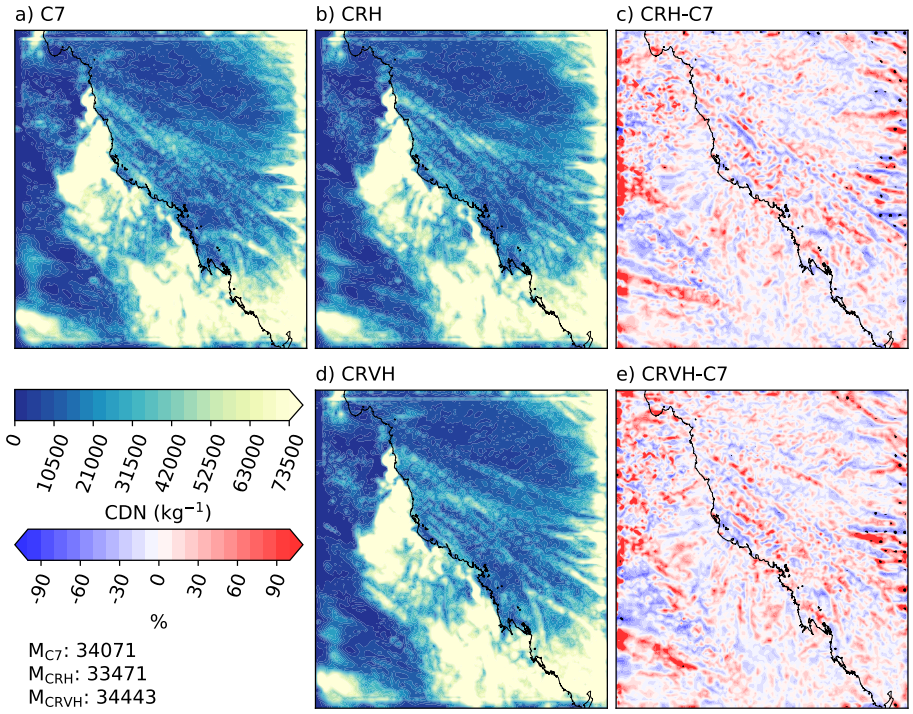


Figure D.6: As for Figure D.3 but for total column CDN over D02

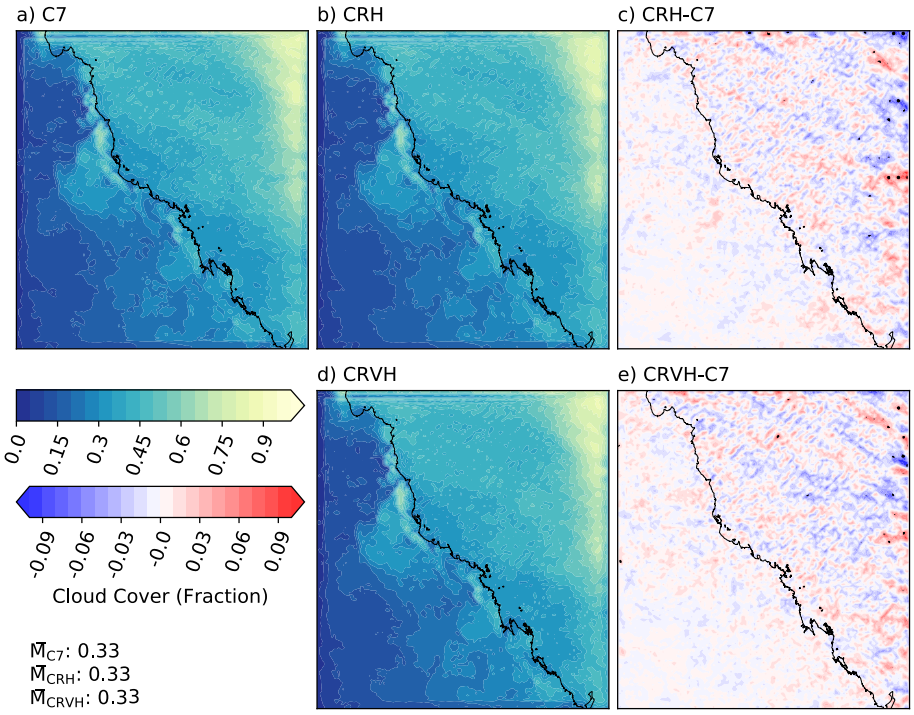


Figure D.7: As for Figure D.3 but for total cloud fraction over D02

# Bibliography

Abdul-Razzak, H. and Ghan, S. J.: A parameterization of aerosol activation: 2. Multiple aerosol types, Journal of Geophysical Research: Atmospheres, 105, 6837–6844, doi: 10.1029/1999JD901161, 2000.

Abdul-Razzak, H. and Ghan, S. J.: A parameterization of aerosol activation 3. Sectional representation, Journal of Geophysical Research Atmospheres, 107, 1–6, doi: 10.1029/2001jd000483, 2002.

Abraham, N. L., Archibald, A. T., Bellouin, N., Boucher, O., Braesicke, P., Bushell, A., Carslaw, K., Collins, B., Dalvi, M., Emmerson, K., Folberth, G., Haywood, J., Johnson, C., Kipling, Z., Macintyre, H., Mann, G., Telford, P., Merikanto, J., Morgenstern, O., Connor, F. O., Ord, C., Osprey, S., Pringle, K., Pyle, J., Rae, J., Reddington, C., Savage, N., Spracklen, D., Stier, P., and West, R.: Unified Model Documentation Paper No. 84: United Kingdom Chemistry and Aerosol (UKCA) Technical Description MetUM Version 8.4, Tech. rep., UK Met Office, 2012.

Ackerman, A. S., Kirkpatrick, M. P., Stevens, D. E., and Toon, O. B.: The impact of humidity above stratiform clouds on indirect aerosol climate forcing., Nature, 432, 1014–1017, doi: 10.1038/nature03137.1., 2004.

Albrecht, B. A.: Aerosols, cloud microphysics, and fractional cloudiness., Science, 245, 1227–1230, doi: 10.1126/science.245.4923.1227, 1989.

Alcolombri, U., Ben-Dor, S., Feldmesser, E., Levin, Y., Tawfik, D. S., and Vardi, A.: Identification of the algal dimethyl sulfide-releasing enzyme: A missing link

in the marine sulfur cycle, Science, 348, 1466–1469, doi: 10.1126/science.aab1586, 2015.

Alexander, S. and Protat, A.: Vertical profiling of aerosols with a combined raman-elastic backscatter lidar in the remote southern ocean marine boundary layer (43S 66S, 132E 150E), Journal of Geophysical Research: Atmospheres, Accepted, 2019.

Alexander, S. P. and Protat, A.: Cloud Properties Observed From the Surface and by Satellite at the Northern Edge of the Southern Ocean, Journal of Geophysical Research: Atmospheres, 123, 443–456, doi: 10.1002/2017JD026552, 2018.

Allan, J. D., Delia, A. E., Coe, H., Bower, K. N., Alfarra, M. R., Jimenez, J. L., Middlebrook, A. M., Drewnick, F., Onasch, T. B., Canagaratna, M. R., Jayne, J. T., and Worsnop, D. R.: A generalised method for the extraction of chemically resolved mass spectra from Aerodyne aerosol mass spectrometer data, Journal of Aerosol Science, 35, 909–922, doi: 10.1016/j.jaerosci.2004.02.007, 2004.

Anderson, T. R., Spall, S. A., Yool, A., Cipollini, P., Challenor, P. G., and Fasham, M. J.: Global fields of sea surface dimethylsulfide predicted from chlorophyll, nutrients and light, Journal of Marine Systems, 30, 1–20, doi: 10.1016/S0924-7963(01)00028-8, 2001.

Ayers, G. P., Lvey, J. P., and Gillett, R. W.: Coherence between seasonal cycles of dimethyl sulphide, methanesulphonate and sulphate in marine air, Nature, 349, 404–406, doi: 10.1038/349404a0, 1991.

Baars, H., Ansmann, A., Engelmann, R., and Althausen, D.: Continuous monitoring of the boundary-layer top with lidar, Atmospheric Chemistry and Physics, 8, 7281–7296, doi: 10.5194/acp-8-7281-2008, 2008.

Barker, H., Pincus, R., and Morcrette, J.-J.: The Monte-Carlo Independent Column Approximation: Application within large-scale models, in: Proceedings of the GCSS/ARM Workshop on the Representation of Cloud Systems in Large-Scale Models, p. 10, May 2002, Kananaskis, Alberta, Canada,, URL `www.met.utah.edu/skrueger/gcss-2002/Extended-Abstracts.pdf`, 2003.

Bath, M.: Aerosol-Radiation-Microphysics Interactions, URL https://ruc.noaa.gov/wrf/wrf-chem/wrf_tutorial_2018/AerosolInteractions.pdf, 2018.

Bell, T. G., Landwehr, S., Miller, S. D., De Bruyn, W. J., Callaghan, A. H., Scanlon, B., Ward, B., Yang, M., and Saltzman, E. S.: Estimation of bubble-mediated air-sea gas exchange from concurrent DMS and CO2 transfer velocities at intermediate-high wind speeds, Atmospheric Chemistry and Physics, 17, 9019–9033, doi: 10.5194/acp-17-9019-2017, 2017.

Bellouin, N., Mann, G. W., Woodhouse, M. T., Johnson, C., Carslaw, K. S., and Dalvi, M.: Impact of the modal aerosol scheme GLOMAP-mode on aerosol forcing in the hadley centre global environmental model, Atmospheric Chemistry and Physics, 13, 3027–3044, doi: 10.5194/acp-13-3027-2013, 2013.

Belviso, S., Bopp, L., Moulin, C., Orr, J. C., Anderson, T. R., Aumont, O., Chu, S., Elliott, S., Maltrud, M. E., and Simó, R.: Comparison of global climatological maps of sea surface dimethyl sulfide, Global Biogeochemical Cycles, 18, doi: 10.1029/2003GB002193, 2004a.

Belviso, S., Moulin, C., Bopp, L., and Stefels, J.: Assessment of a global climatology of oceanic dimethylsulfide (DMS) concentration based on SeaWiFS imagery (1998-2001), Canadian Journal of Fisheries and Aquatic Sciences, 61, 804–816, doi: 10.1139/F04-001, 2004b.

Best, M. J., Pryor, M., Clark, D. B., Rooney, G. G., Essery, R. L. H., Ménard, C. B., Edwards, J. M., Hendry, M. A., Porson, A., Gedney, N., Mercado, L. M., Sitch, S., Blyth, E., Boucher, O., Cox, P. M., Grimmond, C. S. B., and Harding, R. J.: The Joint UK Land Environment Simulator (JULES), model description Part 1: Energy and water fluxes, Geoscientific Model Development, 4, 677–699, doi: 10.5194/gmd-4-677-2011, 2011.

Bi, D., Dix, M., Marsland, S. J., O'Farrell, S., Rashid, H. A., Uotila, P., Hirst, A. C., Kowalczyk, E. A., Golebiewski, M., Sullivan, A., Yan, H., Hannah, N., Franklin, C., Sun, Z., Vohralik, P., Watterson, I., Zhou, X., Fiedler, R., Collier,

M., Ma, Y., Noonan, J., Stevens, L., Uhe, P., Zhu, H., Griffies, S. M., Hill, R., Harris, C., and Puri, K.: The ACCESS coupled model: description, control climate and evaluation, Australian Meteorological and Oceanographic Journal, 63, 41–64, 2013.

Bigg, E. K.: Sources, nature and influence on climate of marine airborne particles, Environmental Chemistry, 4, 155–161, doi: 10.1071/EN07001, 2007.

Bigg, E. K. and Turvey, D. E.: Sources of atmospheric particles over Australia, Atmospheric Environment (1967), 12, 1643–1655, doi: 10.1016/0004-6981(78)90313-X, 1978.

Binkowski, F. S. and Shankar, U.: The Regional Particulate Matter Model: 1. Model description and preliminary results, Journal of Geophysical Research, 100, 26 191, doi: 10.1029/95JD02093, 1995.

Bodas-Salcedo, A., Williams, K. D., Ringer, M. A., Beau, I., Cole, J. N. S., Dufresne, J. L., Koshiro, T., Stevens, B., Wang, Z., and Yokohata, T.: Origins of the solar radiation biases over the Southern Ocean in CFMIP2 models, Journal of Climate, 27, 41–56, doi: 10.1175/JCLI-D-13-00169.1, 2014.

Bodas-Salcedo, A., Hill, P. G., Furtado, K., Williams, K. D., Field, P. R., Manners, J. C., Hyder, P., and Kato, S.: Large contribution of supercooled liquid clouds to the solar radiation budget of the Southern Ocean, Journal of Climate, 29, 4213–4228, doi: 10.1175/JCLI-D-15-0564.1, 2016.

Bohren, C. F. and Huffman, D. R.: Absorption and Scattering of Light by Small Particles, Wiley, Weinheim, Germany, doi: 10.1002/9783527618156, URL `https://onlinelibrary.wiley.com/doi/book/10.1002/9783527618156`, 1998.

Bony, S. and Dufresne, J. L.: Marine boundary layer clouds at the heart of tropical cloud feedback uncertainties in climate models, Geophysical Research Letters, 32, 1–4, doi: 10.1029/2005GL023851, 2005.

Bony, S., Colman, R., Kattsov, V. M., Allan, R. P., Bretherton, C. S., Dufresne, J.-L., Hall, A., Hallegatte, S., Holland, M. M., Ingram, W., Randall, D. A., Soden,

B. J., Tselioudis, G., and Webb, M. J.: How Well Do We Understand and Evaluate Climate Change Feedback Processes?, Journal of Climate, 19, 3445–3482, doi: 10.1175/JCLI3819.1, 2006.

Bopp, L., Boucher, O., Aumont, O., Belviso, S., Dufresne, J.-L., Pham, M., and Monfray, P.: Will marine dimethylsulfide emissions amplify or alleviate global warming? A model study, Canadian Journal of Fisheries and Aquatic Sciences, 61, 826–835, doi: 10.1139/f04-045, 2004.

Boucher, O. and Reddy, M. S.: Climate trade-off between black carbon and carbon dioxide emissions, Energy Policy, 36, 193–200, doi: 10.1016/j.enpol.2007.08.039, 2008.

Boucher, O., Moulin, C., Belviso, S., Aumont, O., Bopp, L., Cosme, E., von Kuhlmann, R., Lawrence, M. G., Pham, M., Reddy, M. S., Sciare, J., and Venkataraman, C.: Sensitivity study of dimethylsulphide (DMS) atmospheric concentrations and sulphate aerosol indirect radiative forcing to the DMS source representation and oxidation, Atmospheric Chemistry and Physics, 2, 1181–1216, doi: 10.5194/acpd-2-1181-2002, 2002.

Boucher, O., Randall, D., Artaxo, P., Bretherton, C., Feingold, G., Forster, P., Kerminen, V. M., Kondo, Y., Liao, H., Lohmann, U., Rasch, P., Satheesh, S. K., Sherwood, S., Stevens, B., Zhang, X. Y., and Zhan, X. Y.: Clouds and Aerosols, in: Climate Change 2013: The Physical Science Basis. Contribution of Working Group I to the Fifth Assessment Report of the Intergovernmental Panel on Climate Change, edited by Stocker, T., Qin, D., Plattner, G.-K., Tignor, M., Allen, S., Boschung, J., Nauels, A., Xia, Y., Bex, V., and Midgley, P., pp. 571–657, Cambridge University Press, Cambridge, United Kingdom and New York, NY, USA, doi: 10.1017/CBO9781107415324.016, 2013.

Broadbent, A. and Jones, G. B.: Seasonal and diurnal cycles of dimethylsulfide, dimethylsulfoniopropionate and dimethylsulfoxide at one tree reef lagoon, Environmental Chemistry, 3, 260–267, doi: 10.1071/EN06011, 2006.

Broadbent, A., Jones, G. B., and Jones, R. J.: DMSP in Corals and Benthic Algae from the Great Barrier Reef, Estuarine, Coastal and Shelf Science, 55, 547–555, doi: 10.1006/ecss.2002.1021, 2002.

Broadbent, A. D. and Jones, G. B.: DMS and DMSP in mucus ropes, coral mucus, surface films and sediment pore waters from coral reefs in the Great Barrier Reef, Marine and Freshwater Research, 55, 849–855, doi: 10.1071/MF04114, 2004.

Bureau of Meteorology: Climate and past weather, URL `http://www.bom.gov.au/climate/`, 2017.

Cameron-Smith, P., Elliott, S., Maltrud, M., Erickson, D., and Wingenter, O.: Changes in dimethyl sulfide oceanic distribution due to climate change, Geophysical Research Letters, 38, 1–5, doi: 10.1029/2011GL047069, 2011.

Carslaw, K. S., Lee, L. A., Reddington, C. L., Pringle, K. J., Rap, A., Forster, P. M., Mann, G. W., Spracklen, D. V., Woodhouse, M. T., Regayre, L. a., and Pierce, J. R.: Large contribution of natural aerosols to uncertainty in indirect forcing., Nature, 503, 67–71, doi: 10.1038/nature12674, 2013.

Cesana, G. and Chepfer, H.: How well do climate models simulate cloud vertical structure? A comparison between CALIPSO-GOCCP satellite observations and CMIP5 models, Geophysical Research Letters, 39, 1–6, doi: 10.1029/2012GL053153, 2012.

Chambers, S. D., Williams, A. G., Crawford, J., Griffiths, A. D., Krummel, P. B., Steele, L. P., Law, R. M., van der Schoot, M. V., Galbally, I. E., and Molloy, S. B.: A radon-only technique for characterising atmospheric 'baseline' constituent concentrations at Cape Grim, Baseline Atmospheric Program Australia 20102011, 2015.

Charlson, R. J., Lovelock, J. E., Andreae, M. O., and Warren, S. G.: Oceanic phytoplankton, atmospheric sulphur, cloud albedo and climate, Nature, 326, 655–661, doi: 10.1038/326655a0, 1987.

Chen, F. and Dudhia, J.: Coupling an Advanced Land SurfaceHydrology Model with

the Penn StateNCAR MM5 Modeling System. Part II: Preliminary Model Validation, Monthly Weather Review, 129, 587–604, doi: 10.1175/1520-0493(2001)129⟨0587:caalsh⟩2.0.co;2, 2002.

Chen, Z., Schofield, R., Rayner, P., Zhang, T., Liu, C., Vincent, C., Fiddes, S., Ryan, R. G., Alroe, J., Ristovski, Z. D., Humphries, R. S., Keywood, M. D., Ward, J., Paton-Walsh, C., Naylor, T., and Shu, X.: Characterization of aerosols over the Great Barrier Reef: The influence of transported continental sources, Science of The Total Environment, 690, 426–437, doi: 10.1016/j.scitotenv.2019.07.007, 2019.

Chepfer, H., Bony, S., Winker, D., Cesana, G., Dufresne, J. L., Minnis, P., Stubenrauch, C. J., and Zeng, S.: The GCM-oriented CALIPSO cloud product (CALIPSO-GOCCP), Journal of Geophysical Research Atmospheres, 115, 1–13, doi: 10.1029/2009JD012251, 2010.

Chin, M., Rood, R. B., Lin, S.-J., Müller, J.-F., and Thompson, A. M.: Atmospheric sulfur cycle simulated in the global model GOCART: Model description and global properties, Journal of Geophysical Research: Atmospheres, 105, 24 671–24 687, doi: 10.1029/2000JD900384, 2000.

Clark, D. B., Mercado, L. M., Sitch, S., Jones, C. D., Gedney, N., Best, M. J., Pryor, M., Rooney, G. G., Essery, R. L. H., Blyth, E., Boucher, O., Harding, R. J., Huntingford, C., and Cox, P. M.: The Joint UK Land Environment Simulator (JULES), model description Part 2: Carbon fluxes and vegetation dynamics, Geoscientific Model Development, 4, 701–722, doi: 10.5194/gmd-4-701-2011, 2011.

Cropp, R., Gabric, A., van Tran, D., Jones, G., Swan, H., and Butler, H.: Coral reef aerosol emissions in response to irradiance stress in the Great Barrier Reef, Australia, Ambio, doi: 10.1007/s13280-018-1018-y, 2018.

CSIRO: RV Investigator Voyage IN2016_V05 Underway UWY Data, URL http://www.marlin.csiro.au/geonetwork/srv/eng/search#!65e8e881-dafe-4ca5-8f8a-f69d83596523, 2016.

Curson, A. R., Todd, J. D., Sullivan, M. J., and Johnston, A. W.: Catabolism of

dimethylsulphoniopropionate: Microorganisms, enzymes and genes, Nature Reviews Microbiology, 9, 849–859, doi: 10.1038/nrmicro2653, 2011.

Dacey, J. W. H., Wakeham, S. G., and Howes, B. L.: Henry's law constants for dimethylsulfide in freshwater and seawater, Geophysical Research Letters, 11, 991–994, doi: 10.1029/GL011i010p00991, 1984.

Dee, D. P., Uppala, S. M., Simmons, A. J., Berrisford, P., Poli, P., Kobayashi, S., Andrae, U., Balmaseda, M. A., Balsamo, G., Bauer, P., Bechtold, P., Beljaars, A. C. M., van de Berg, L., Bidlot, J., Bormann, N., Delsol, C., Dragani, R., Fuentes, M., Geer, A. J., Haimberger, L., Healy, S. B., Hersbach, H., Hólm, E. V., Isaksen, L., Kållberg, P., Köhler, M., Matricardi, M., Mcnally, A. P., Monge-Sanz, B. M., Morcrette, J. J., Park, B. K., Peubey, C., de Rosnay, P., Tavolato, C., Thépaut, J. N., and Vitart, F.: The ERA-Interim reanalysis: Configuration and performance of the data assimilation system, Quarterly Journal of the Royal Meteorological Society, 137, 553–597, doi: 10.1002/qj.828, 2011.

Deloitte Access Economics: The economic, social and icon value of the Great Barrier Reef Acknowledgement, Tech. rep., Deloitte Touche Tohmatsu, Brisbane, QLD, Australia, URL `https://www2.deloitte.com/au/en/pages/economics/articles/great-barrier-reef.html`, 2017.

Deschaseaux, E., Jones, G. B., Miljevic, B., Ristovski, Z., and Swan, H.: Can corals form aerosol particles through volatile sulphur compound emissions?, in: Proceedings of the 12th International Coral Reef Symposium, edited by Yellowlees, D. and Hughes, T., James Cook University, Cairns, QLD, Australia, 2012.

Deschaseaux, E., Jones, G. B., and Swan, H.: Dimethylated sulfur compounds in coral-reef ecosystems, Environmental Chemistry, 13, 239–251, doi: 10.1071/EN14258, 2016.

Deschaseaux, E., Stoltenberg, L., Hrebien, V., Koveke, E. P., Toda, K., and Eyre, B. D.: Dimethylsulfide (DMS) fluxes from permeable coral reef carbonate sediments, Marine Chemistry, 208, 1–10, doi: 10.1016/j.marchem.2018.11.008, 2019.

Deutscher Wetterdienst: Particle Size-Distribution, URL http://www.dwd.de/EN/research/observing_atmosphere/composition_atmosphere/aerosol/cont_nav/particle_size_distribution_node.html, 2016.

Drewnick, F., Hings, S. S., DeCarlo, P., Jayne, J. T., Gonin, M., Fuhrer, K., Weimer, S., Jimenez, J. L., Demerjian, K. L., Borrmann, S., and Worsnop, D. R.: A new time-of-flight aerosol mass spectrometer (TOF-AMS) - Instrument description and first field deployment, Aerosol Science and Technology, 39, 637–658, doi: 10.1080/02786820500182040, 2005.

Dutkiewicz, S., Morris, J. J., Follows, M. J., Scott, J., Levitan, O., Dyhrman, S. T., and Berman-Frank, I.: Impact of ocean acidification on the structure of future phytoplankton communities, Nature Climate Change, 5, 1002–1006, doi: 10.1038/nclimate2722, 2015.

Edwards, J. M., Manners, J., Thelen, J.-C., Ingram, W. J., and Hill, P. G.: Unified Model Documentation Paper No. 23: The Radiation Code, Tech. Rep. Model version 8.2, UK Met Office, Exeter, UK, 2013.

Elliott, S.: Dependence of DMS global sea-air flux distribution on transfer velocity and concentration field type, Journal of Geophysical Research: Biogeosciences, 114, 1–18, doi: 10.1029/2008JG000710, 2009.

Emmons, L. K., Walters, S., Hess, P. G., Lamarque, J.-F., Pfister, G. G., Fillmore, D., Granier, C., Guenther, A., Kinnison, D., Laepple, T., Orlando, J., Tie, X., Tyndall, G., Wiedinmyer, C., Baughcum, S. L., and Kloster, S.: Description and evaluation of the Model for Ozone and Related chemical Tracers, version 4 (MOZART-4), Geoscientific Model Development, 3, 43–67, doi: 10.5194/gmd-3-43-2010, 2010.

Erickson, D. J.: A stability dependent theory for air-sea gas exchange, Journal of Geophysical Research, 98, 8471, doi: 10.1029/93JC00039, 1993.

European Commission Joint Research Centre and Netherlands Environmental Assessment Agency: Emission Database for Global Atmospheric Research

(EDGAR), URL `http://edgar.jrc.ec.europe.eu`, 2012.

Fan, J., Wang, Y., Rosenfeld, D., and Liu, X.: Review of aerosol-cloud interactions: Mechanisms, significance, and challenges, Journal of the Atmospheric Sciences, 73, 4221–4252, doi: 10.1175/JAS-D-16-0037.1, 2016.

Fan, J., Rosenfeld, D., Zhang, Y., Giangrande, S. E., Li, Z., Machado, L. A., Martin, S. T., Yang, Y., Wang, J., Artaxo, P., Barbosa, H. M., Braga, R. C., Comstock, J. M., Feng, Z., Gao, W., Gomes, H. B., Mei, F., Pöhlker, C., Pöhlker, M. L., Pöschl, U., and De Souza, R. A.: Substantial convection and precipitation enhancements by ultrafine aerosol particles, Science, 359, 411–418, doi: 10.1126/science.aan8461, 2018.

Fast, J. D., Gustafson, W. I., Easter, R. C., Zaveri, R. A., Barnard, J. C., Chapman, E. G., Grell, G. A., and Peckham, S. E.: Evolution of ozone, particulates, and aerosol direct radiative forcing in the vicinity of Houston using a fully coupled meteorology-chemistry-aerosol model, Journal of Geophysical Research Atmospheres, 111, 1–29, doi: 10.1029/2005JD006721, 2006.

Feingold, G., Kreidenweis, S. M., Stevens, B., and Cotton, W. R.: Numerical simulations of stratocumulus processing of cloud condensation nuclei through collision-coalescence, Journal of Geophysical Research Atmospheres, 101, 21 391–21 402, doi: 10.1029/96jd01552, 1996.

Finlayson-Pitts, B. J. and Pitts, J. N.: Acid Deposition, in: Chemistry of the Upper and Lower Atmosphere, pp. 294–348, Elsevier, San Diego, California, USA, doi: 10.1016/B978-012257060-5/50010-1, 2000.

Fischer, E. and Jones, G. B.: Atmospheric dimethysulphide production from corals in the Great Barrier Reef and links to solar radiation, climate and coral bleaching, Biogeochemistry, 110, 31–46, doi: 10.1007/s10533-012-9719-y, 2012.

Flato, G., Marotzke, J., Abiodun, B., Braconnot, P., Chou, S., Collins, W., Cox, P., Driouech, F., Emori, S., Eyring, V., Forest, C., Gleckler, P., Guilyardi, E., Jakob, C., Kattsov, V., Reason, C., and Rummukainen, M.: Evaluation of Climate

Models, in: Climate Change 2013: The Physical Science Basis. Contribution of Working Group I to the Fifth Assessment Report of the Intergovernmental Panel on Climate Change, edited by Stocker, T., Qin, D., Plattner, G.-K., Tignor, M., Allen, S., Boschung, J., Nauels, A., Xia, Y., Bex, V., and Midgley, P., pp. 741–866, Cambridge University Press, Cambridge, United Kingdom and New York, NY, USA, doi: 10.1017/CBO9781107415324, 2013.

Forster, P., Ramaswamy, V., Artaxo, P., Berntsen, T., Betts, R., Fahey, D., Haywood, J., Lean, J., Lowe, D., Myhre, G., Nganga, J., Prinn, R., Raga, G., Schulz, M., and Dorland, R. V.: Changes in Atmospheric Constituents and in Radiative Forcing, in: Climate Change 2007: The Physical Science Basis. Contribution of Working Group I to the Fourth Assessment Report of the Intergovernmental Panel on Climate Change, edited by Solomon, S., Qin, D., Manning, M., Chen, Z., Marquis, M., Averyt, K., M.Tignor, and Miller, H., pp. 129–234, Cambridge University Press,Cambridge, United Kingdom and New York, NY, USA, 2007.

Fröhlich, R., Cubison, M. J., Slowik, J. G., Bukowiecki, N., Prévôt, A. S. H., Baltensperger, U., Schneider, J., Kimmel, J. R., Gonin, M., Rohner, U., Worsnop, D. R., and Jayne, J. T.: The ToF-ACSM: a portable aerosol chemical speciation monitor with TOFMS detection, Atmospheric Measurement Techniques, 6, 3225–3241, doi: 10.5194/amt-6-3225-2013, 2013.

Fuchs, N. and Sutugin, A.: Highly dispersed aerosols, in: Topics in Current Aerosol Research, pp. 1–86, US Army Foreign Science and Technology Centre, New York, 1971.

Fuentes, E., Coe, H., Green, D., De Leeuw, G., and McFiggans, G.: On the impacts of phytoplankton-derived organic matter on the properties of the primary marine aerosol - Part 1: Source fluxes, Atmospheric Chemistry and Physics, 10, 9295–9317, doi: 10.5194/acp-10-9295-2010, 2010.

Gabric, A., Qu, B., Rotstayn, L., and Shephard, J.: Global simulations of the impact on contemporary climate of a perturbation to the sea-to-air flux of dimethyl-

sulfide, Australian Meteorological and Oceanographic Journal, 63, 365–376, doi: 10.22499/2.6303.002, 2013.

Gabric, A., Matrai, P., Jones, G., and Middleton, J.: The Nexus between Sea Ice and Polar Emissions of Marine Biogenic Aerosols, Bulletin of the American Meteorological Society, 99, 61–81, doi: 10.1175/BAMS-D-16-0254.1, 2018.

Gabric, A. J., Simó, R., Cropp, R. A., Hirst, A. C., and Dachs, J.: Modeling estimates of the global emission of dimethylsulfide under enhanced greenhouse conditions, Global Biogeochemical Cycles, 18, doi: 10.1029/2003GB002183, 2004.

Galí, M., Devred, E., Levasseur, M., Royer, S. J., and Babin, M.: A remote sensing algorithm for planktonic dimethylsulfoniopropionate (DMSP) and an analysis of global patterns, Remote Sensing of Environment, 171, 171–184, doi: 10.1016/j.rse.2015.10.012, 2015.

Galí, M., Levasseur, M., Devred, E., Simó, R., and Babin, M.: Sea-surface dimethylsulfide (DMS) concentration from satellite data at global and regional scales, Biogeosciences, 15, 3497–3519, doi: 10.5194/bg-15-3497-2018, 2018.

Gery, M. W., Whitten, G. Z., Killus, J. P., and Dodge, M. C.: A photochemical kinetics mechanism for urban and regional scale computer modeling, Journal of Geophysical Research, 94, 12 925, doi: 10.1029/jd094id10p12925, 2008.

Gong, S. L.: A parameterization of sea-salt aerosol source function for sub- and super-micron particles, Global Biogeochemical Cycles, 17, n/a–n/a, doi: 10.1029/2003GB002079, 2003.

Gong, S. L., Barrie, L. A., and Blanchet, J.-P.: Modeling sea-salt aerosols in the atmosphere: 1. Model development, Journal of Geophysical Research: Atmospheres, 102, 3805–3818, doi: 10.1029/96jd02953, 1997.

Grabowski, W. W.: Extracting microphysical impacts in large-eddy simulations of shallow convection, Journal of the Atmospheric Sciences, 71, 4493–4499, doi: 10.1175/JAS-D-14-0231.1, 2014.

Grabowski, W. W.: Untangling microphysical impacts on deep convection applying

a novel modeling methodology, Journal of the Atmospheric Sciences, 72, 2446–2464, doi: 10.1175/JAS-D-14-0307.1, 2015.

Grandey, B. S. and Wang, C.: Enhanced marine sulphur emissions offset global warming and impact rainfall., Scientific reports, 5, 13 055, doi: 10.1038/srep13055, 2015.

Granier, C., Lamarque, J., Mieville, A., Muller, J., Olivier, J., Orlando, J., Peters, J., Petron, G., Tyndall, G., and Wallens, S.: POET, a database of surface emissions of ozone precursors, http://www.aero.jussieu.fr/projet/ACCENT/POET.php, 2005.

Great Barrier Reef Marine Park Authority: Great Barrier Reef outlook report 2014: in brief, Tech. rep., Great Barrier Reef Marine Park Authority, Townsville, URL http://elibrary.gbrmpa.gov.au/jspui/bitstream/11017/2856/5/InBrief_accessible_lowres.pdf, 2014.

Great Barrier Reef Marine Park Authority: Position Statment Climate change, Tech. rep., Great Barrier Reef Marine Park Authority, Townsville, URL http://elibrary.gbrmpa.gov.au/jspui/bitstream/11017/3460/1/v0-Climate-Change-Position-Statement.pdf, 2019.

Green, T. K. and Hatton, A. D.: The Claw Hypothesis: A New Perspective on the Role of Biogenic Sulphur in the Regulation of Global Climate, Oceanography and Marine Biology, 52, 315–336, doi: 10.1201/b17143-7, 2014.

Gregory, D. and Rowntree, P. R.: A mass flux convection scheme with representation of cloud ensemble characteristics and stability-dependent closure, doi: 10.1175/1520-0493(1990)118⟨1483:AMFCSW⟩2.0.CO;2, 1990.

Grell, G. A. and Dévényi, D.: A generalized approach to parameterizing convection combining ensemble and data assimilation techniques, Geophysical Research Letters, 29, 38–1, doi: 10.1029/2002gl015311, 2002.

Grell, G. A., Peckham, S. E., Schmitz, R., McKeen, S. A., Frost, G., Skamarock, W. C., and Eder, B.: Fully coupled "online" chemistry within the WRF model,

Atmospheric Environment, 39, 6957–6975, doi: 10.1016/j.atmosenv.2005.04.027, 2005.

Guenther, A., Zimmerman, P., and Wildermuth, M.: Natural volatile organic compound emission rate estimates for U.S. woodland landscapes, Atmospheric Environment, 28, 1197–1210, doi: 10.1016/1352-2310(94)90297-6, 1994.

Gustafson, W. I., Chapman, E. G., Ghan, S. J., Easter, R. C., and Fast, J. D.: Impact on modeled cloud characteristics due to simplified treatment of uniform cloud condensation nuclei during NEAQS 2004, Geophysical Research Letters, 34, 1–5, doi: 10.1029/2007GL030021, 2007.

Halloran, P. R., Bell, T. G., and Totterdell, I. J.: Can we trust empirical marine DMS parameterisations within projections of future climate?, Biogeosciences, 7, 1645–1656, doi: 10.5194/bg-7-1645-2010, 2010.

Hariprasad, K. B., Srinivas, C. V., Singh, A. B., Vijaya Bhaskara Rao, S., Baskaran, R., and Venkatraman, B.: Numerical simulation and intercomparison of boundary layer structure with different PBL schemes in WRF using experimental observations at a tropical site, Atmospheric Research, 145-146, 27–44, doi: 10.1016/j.atmosres.2014.03.023, 2014.

Hassim, M. E. E., Grabowski, W. W., and Lane, T. P.: Impact of aerosols on precipitation over the Maritime Continent simulated by a convection-permitting model, Atmospheric Chemistry and Physics Discussions, -, 1–25, doi: 10.5194/acp-2016-402, 2016.

Heidinger, A.: ABI Cloud Height, NOAA NESDIS Center for Satellite Applications and Research Algorithm Theoretical Basis Document, 3, 79, URL `https://www.star.nesdis.noaa.gov/goesr/docs/ATBD/Cloud_Height.pdf`, 2013.

Hoegh-Guldberg, O., Poloczanska, E. S., Skirving, W., and Dove, S.: Coral Reef Ecosystems under Climate Change and Ocean Acidification, Frontiers in Marine Science, 4, doi: 10.3389/fmars.2017.00158, 2017.

Hopkins, F. E., Turner, S. M., Bakker, D., Steinke, M., Liss, P. S., and Nightingale,

P. D.: Ocean acidification and marine trace gas emissions, Proceedings of the National Academy of Sciences, 107, 760–765, doi: 10.1073/pnas.0907163107, 2010.

Hopkins, F. E., Nightingale, P., and Liss, P.: Ocean acidification, in: Ocean acidification, edited by Gattuso, J.-P. and Hansson, L., p. 326, Oxford Univerity Press, 2011.

Hopkins, F. E., Bell, T. G., Yang, M., Suggett, D. J., and Steinke, M.: Air exposure of coral is a significant source of dimethylsulfide (DMS) to the atmosphere, Scientific Reports, 6, 36 031, doi: 10.1038/srep36031, 2016.

Hopkins, F. E., Nightingale, P. D., Stephens, J. A., Moore, C. M., Richier, S., Cripps, G. L., and Archer, S. D.: Dimethylsulfide (DMS) production in polar oceans may be resilient to ocean acidification, Biogeosciences Discussions, In Review, 1–42, doi: 10.5194/bg-2018-55, 2018.

Hu, X. M., Nielsen-Gammon, J. W., and Zhang, F.: Evaluation of three planetary boundary layer schemes in the WRF model, Journal of Applied Meteorology and Climatology, 49, 1831–1844, doi: 10.1175/2010JAMC2432.1, 2010.

Huffman, G. J., Bolvin, D. T., Nelkin, E. J., Wolff, D. B., Adler, R. F., Gu, G., Hong, Y., Bowman, K. P., and Stocker, E. F.: The TRMM Multisatellite Precipitation Analysis (TMPA): Quasi-Global, Multiyear, Combined-Sensor Precipitation Estimates at Fine Scales, Journal of Hydrometeorology, 8, 38–55, doi: 10.1175/JHM560.1, 2007.

Hughes, T. P., Kerry, J. T., Alvarez-Noriega, M., Alvarez-Romero, J. G., Anderson, K. D., Baird, A. H., Babcock, R. C., Beger, M., Bellwood, D. R., Berkelmans, R., Bridge, T. C., Butler, I. R., Byrne, M., Cantin, N. E., Comeau, S., Connolly, S. R., Cumming, G. S., Dalton, S. J., Diaz-Pulido, G., Eakin, C. M., Figueira, W. F., Gilmour, J. P., Harrison, H. B., Heron, S. F., Hoey, A. S., Hobbs, J.-P. A., Hoogenboom, M. O., Kennedy, E. V., Kuo, C.-Y., Lough, J. M., Lowe, R. J., Liu, G., McCulloch, M. T., Malcolm, H. A., McWilliam, M. J., Pandolfi, J. M., Pears, R. J., Pratchett, M. S., Schoepf, V., Simpson, T., Skirving, W. J.,

Sommer, B., Torda, G., Wachenfeld, D. R., Willis, B. L., and Wilson, S. K.: Global warming and recurrent mass bleaching of corals, Nature, 543, 373–377, doi: 10.1038/nature21707, 2017.

Hughes, T. P., Anderson, K. D., Connolly, S. R., Heron, S. F., Kerry, J. T., Lough, J. M., Baird, A. H., Baum, J. K., Berumen, M. L., Bridge, T. C., Claar, D. C., Eakin, C. M., Gilmour, J. P., Graham, N. A., Harrison, H., Hobbs, J. P. A., Hoey, A. S., Hoogenboom, M., Lowe, R. J., McCulloch, M. T., Pandolfi, J. M., Pratchett, M., Schoepf, V., Torda, G., and Wilson, S. K.: Spatial and temporal patterns of mass bleaching of corals in the Anthropocene, Science, 359, 80–83, doi: 10.1126/science.aan8048, 2018.

Humphries, R. S., Schofield, R., Keywood, M. D., Ward, J., Pierce, J. R., Gionfriddo, C. M., Tate, M. T., Krabbenhoft, D. P., Galbally, I. E., Molloy, S. B., Klekociuk, A. R., Johnston, P. V., Kreher, K., Thomas, A. J., Robinson, A. D., Harris, N. R. P., Johnson, R., and Wilson, S. R.: Boundary layer new particle formation over East Antarctic sea ice - Possible Hg-driven nucleation?, Atmospheric Chemistry and Physics, 15, 13 339–13 364, doi: 10.5194/acp-15-13339-2015, 2015.

Iacono, M. J., Delamere, J. S., Mlawer, E. J., Shephard, M. W., Clough, S. A., and Collins, W. D.: Radiative forcing by long-lived greenhouse gases: Calculations with the AER radiative transfer models, Journal of Geophysical Research Atmospheres, 113, 2–9, doi: 10.1029/2008JD009944, 2008.

IPCC: Summary for Policy Makers, in: Global Warming of 1.5°C. An IPCC Special Report on the impacts of global warming of 1.5°C above pre-industrial levels and related global greenhouse gas emission pathways, in the context of strengthening the global response to the threat of climate change,, edited by Masson-Delmotte, V., Zhai, P., Pörtner, H.-O., Roberts, D., Skea, J., Shukla, P., Pirani, A., Moufouma-Okia, W., C. Péan, R. P., Connors, S., Matthews, J., Chen, Y., Zhou, X., Gomis, M., Lonnoy, E., Maycock, T., Tignor, M., and Waterfield, T., p. 32, World Meteorological Organization, Geneva, Switzerland, 2018.

Jackson, R., Gabric, A., and Cropp, R.: Effects of ocean warming and coral bleaching on aerosol emissions in the Great Barrier Reef, Australia, Scientific Reports, 8, 1–11, doi: 10.1038/s41598-018-32470-7, 2018.

Jackson, R., Gabric, A., Cropp, R., and Woodhouse, M.: Reviews and syntheses : Marine biogenic aerosols and the ecophysiology of coral reefs, Biogeosciences Discussions, Unpublishe, doi: https://doi.org/10.5194/bg-2019-207, 2019.

Jacobson, M. Z., Turco, R. P., Jensen, E. J., and Toon, O. B.: Modeling coagulation among particles of different composition and size, Atmospheric Environment, 28, 1327–1338, doi: 10.1016/1352-2310(94)90280-1, 1994.

Janjić, Z. I.: The Step-Mountain Eta Coordinate Model: Further Developments of the Convection, Viscous Sublayer, and Turbulence Closure Schemes, Monthly Weather Review, 122, 927–945, doi: 10.1175/1520-0493(1994)122⟨0927:TSMECM⟩2.0.CO;2, 1994.

Janjic, Z. I.: The surface layer in the NCEP Eta Model,, in: Eleventh Conference on Numerical Weather Prediction, pp. 354–355, Amer. Meteor. Soc., Boston, MA,, Norfolk, VA, 1996.

Jardine, K., Yañez-Serrano, A. M., Williams, J., Kunert, N., Jardine, A., Taylor, T., Abrell, L., Artaxo, P., Guenther, A., Hewitt, C. N., House, E., Florentino, A. P., Manzi, A., Higuchi, N., Kesselmeier, J., Behrendt, T., Veres, P. R., Derstroff, B., Fuentes, J. D., Martin, S. T., and Andreae, M. O.: Dimethyl sulfide in the Amazon rain forest, Global Biogeochemical Cycles, 29, 19–32, doi: 10.1002/2014GB004969, 2015.

Jarnikova, T. and Tortell, P. D.: Towards a revised climatology of summertime dimethylsulfide concentrations and sea air fluxes in the Southern Ocean, Environmental Chemistry, 13, 364–378, doi: 10.1071/EN14272, 2016.

Jayne, J. T., Leard, D. C., Zhang, X., Davidovits, P., Smith, K. A., Kolb, C. E., and Worsnop, D. R.: Development of an Aerosol Mass Spectrometer for Size and Composition Analysis of Submicron Particles, Aerosol Science and Technology,

33, 49–70, doi: 10.1080/027868200410840, 2000.

Jones, G., Curran, M., Swan, H., and Deschaseaux, E.: Dimethylsulfide and Coral Bleaching: Links to Solar Radiation, Low Level Cloud and the Regulation of Seawater Temperatures and Climate in the Great Barrier Reef, American Journal of Climate Change, 06, 328–359, doi: 10.4236/ajcc.2017.62017, 2017.

Jones, G., Curran, M., Deschaseaux, E., Omori, Y., Tanimoto, H., Swan, H., Eyre, B., Ivey, J., McParland, E., Gabric, A., and Cropp, R.: The flux and emission of dimethylsulfide from the Great Barrier Reef region and potential influence on the climate of NE Australia, Journal of Geophysical Research: Atmospheres, doi: 10.1029/2018JD029210, 2018.

Jones, G. B.: Coral animals combat stress with sulphur, Nature, 502, 634–635, doi: 10.1038/nature12698, 2013.

Jones, G. B. and Trevena, A. J.: The influence of coral reefs on atmospheric dimethylsulphide over the Great Barrier Reef, Coral Sea, Gulf of Papua and Solomon and Bismarck Seas, Marine and Freshwater Research, 56, 85–93, doi: 10.1071/MF04097, 2005.

Jones, G. B., Curran, M., Broadbent, A., King, S., Fischer, E., and Jones, R. J.: Factors affecting the cycling of dimethylsulfide and dimethylsulfoniopropionate in coral reef waters of the great barrier reef, Environmental Chemistry, 4, 310–322, doi: 10.1071/EN06065, 2007.

Jung, E. and Shao, Y.: An intercomparison of four wet deposition schemes used in dust transport modeling, Global and Planetary Change, 52, 248–260, doi: 10.1016/j.gloplacha.2006.02.008, 2006.

Kameyama, S., Tanimoto, H., Inomata, S., Tsunogai, U., Ooki, A., Yokouchi, Y., Takeda, S., Obata, H., and Uematsu, M.: Equilibrator inlet-proton transfer reaction-mass spectrometry (EI-PTR-MS) for sensitive, high-resolution measurement of dimethyl sulfide dissolved in seawater, Analytical Chemistry, 81, 9021–9026, doi: 10.1021/ac901630h, 2009.

Kanaya, Y., Taketani, F., Komazaki, Y., Liu, X., Kondo, Y., Sahu, L. K., Irie, H., and Takashima, H.: Comparison of black carbon mass concentrations observed by multi-angle absorption photometer (MAAP) and continuous soot-monitoring system (COSMOS) on fukue Island and in Tokyo, Japan, Aerosol Science and Technology, 47, 1–10, doi: 10.1080/02786826.2012.716551, 2013.

Kato, S., Loeb, N. G., Rose, F. G., Doelling, D. R., Rutan, D. A., Caldwell, T. E., Yu, L., and Weller, R. A.: Surface irradiances consistent with CERES-derived top-of-atmosphere shortwave and longwave irradiances, Journal of Climate, 26, 2719–2740, doi: 10.1175/JCLI-D-12-00436.1, 2013.

Kettle, A. J. and Andreae, M.: Flux of dimethylsulfide from the oceans : A comparison of updated data sets and flux models, Journal of Geophysical Research, 105, 793–26, doi: 10.1029/2000JD900252, 2000.

Kettle, A. J., Amouroux, D., Andreae, T. W., Bates, T. S., Berresheim, H., Bingemer, H., Boniforti, R., Helas, G., Leck, C., Maspero, M., Matrai, P., McTaggart, A. R., Mihalopoulos, N., Nguyen, B. C., Novo, A., Putaud, J. P., Rapsomanikis, S., Roberts, G., Schebeske, G., Sharma, S., Simó, R., Staubes, R., Turner, S., and Uher, G.: A global data base of sea surface dimethyl sulfide (DMS) measurements and a simple model to predict sea surface DMS as a function of latitude, longitude, and month, Global Biogeochem. Cycles, 13, 399–444, 1999.

Khan, M. A., Gillespie, S. M., Razis, B., Xiao, P., Davies-Coleman, M. T., Percival, C. J., Derwent, R. G., Dyke, J. M., Ghosh, M. V., Lee, E. P., and Shallcross, D. E.: A modelling study of the atmospheric chemistry of DMS using the global model, STOCHEM-CRI, Atmospheric Environment, 127, 69–79, doi: 10.1016/j.atmosenv.2015.12.028, 2016.

Kim, I., Hahm, D., Park, K., Lee, Y., Choi, J.-O., Zhang, M., Chen, L., Kim, H.-C., and Lee, S.: Characteristics of the horizontal and vertical distributions of dimethyl sulfide throughout the Amundsen Sea Polynya, Science of The Total Environment, 584, 154–163, doi: 10.1016/j.scitotenv.2017.01.165, 2017.

King, A. D., Karoly, D. J., and Henley, B. J.: Australian climate extremes at 1.5 °C and 2 °C of global warming, Nature Climate Change, 7, doi: 10.1038/nclimate3296, 2017.

Klein, S. A., Zhang, Y., Zelinka, M. D., Pincus, R., Boyle, J., and Gleckler, P. J.: Are climate model simulations of clouds improving? An evaluation using the ISCCP simulator, Journal of Geophysical Research Atmospheres, 118, 1329–1342, doi: 10.1002/jgrd.50141, 2013.

Kloster, S., Feichter, J., Maier-Reimer, E., Six, K. D., Stier, P., and Wetzel, P.: DMS cycle in the marine ocean-atmosphere system – a global model study, Biogeosciences, 3, 29–51, doi: 10.5194/bg-3-29-2006, 2006.

Kloster, S., Six, K. D., Feichter, J., Maier-Reimer, E., Roeckner, E., Wetzel, P., Stier, P., and Esch, M.: Response of dimethylsulfide (DMS) in the ocean and atmosphere to global warming, Journal of Geophysical Research: Biogeosciences, 112, 1–13, doi: 10.1029/2006JG000224, 2007.

Korhonen, H., Carslaw, K. S., Spracklen, D. V., Mann, G. W., and Woodhouse, M. T.: Influence of oceanic dimethyl sulfide emissions on cloud condensation nuclei concentrations and seasonality over the remote Southern Hemisphere oceans: A global model study, Journal of Geophysical Research: Atmospheres, 113, 1–16, doi: 10.1029/2007JD009718, 2008.

Kulmala, M., Laaksonen, A., and Pirjola, L.: Parameterizations for sulfuric acid/water nucleation rates, Journal of Geophysical Research, 103, 8301, doi: 10.1029/97JD03718, 1998.

Kushta, J., Kallos, G., Astitha, M., Solomos, S., Spyrou, C., Mitsakou, C., and Lelieveld, J.: Impact of natural aerosols on atmospheric radiation and consequent feedbacks with the meteorological and photochemical state of the atmosphere, Journal of Geophysical Research: Atmospheres, 119, 1463–1491, doi: 10.1002/2013JD020714, 2014.

Lamarque, J. F., Bond, T. C., Eyring, V., Granier, C., Heil, A., Klimont, Z., Lee,

D., Liousse, C., Mieville, A., Owen, B., Schultz, M. G., Shindell, D., Smith, S. J., Stehfest, E., Van Aardenne, J., Cooper, O. R., Kainuma, M., Mahowald, N., McConnell, J. R., Naik, V., Riahi, K., and Van Vuuren, D. P.: Historical (1850-2000) gridded anthropogenic and biomass burning emissions of reactive gases and aerosols: Methodology and application, Atmospheric Chemistry and Physics, 10, 7017–7039, doi: 10.5194/acp-10-7017-2010, 2010.

Lana, A., Bell, T. G., Simó, R., Vallina, S. M., Ballabrera-Poy, J., Kettle, A. J., Dachs, J., Bopp, L., Saltzman, E. S., Stefels, J., Johnson, J. E., and Liss, P. S.: An updated climatology of surface dimethlysulfide concentrations and emission fluxes in the global ocean, Global Biogeochemical Cycles, 25, 1–17, doi: 10.1029/2010GB003850, 2011.

Lana, A., Simó, R., Vallina, S. M., and Dachs, J.: Re-examination of global emerging patterns of ocean DMS concentration, Biogeochemistry, 110, 173–182, doi: 10.1007/s10533-011-9677-9, 2012.

Leahy, S. M., Kingsford, M. J., and Steinberg, C. R.: Do Clouds Save the Great Barrier Reef? Satellite Imagery Elucidates the Cloud-SST Relationship at the Local Scale, PLoS ONE, 8, e70 400, doi: 10.1371/journal.pone.0070400, 2013.

Leck, C. and Bigg, E. K.: Source and evolution of the marine aerosol - A new perspective, Geophysical Research Letters, 32, 1–4, doi: 10.1029/2005GL023651, 2005.

Leon, D. C., Wang, Z., and Liu, D.: Climatology of drizzle in marine boundary layer clouds based on 1 year of data from CloudSat and Cloud-Aerosol Lidar and Infrared Pathfinder Satellite Observations (CALIPSO), Journal of Geophysical Research Atmospheres, 114, doi: 10.1029/2008JD009835, 2009.

Liss, P. S. and Merlivat, L.: Air-Sea Gas Exchange Rates: Introduction and Synthesis, in: The Role of Air-Sea Exchange in Geochemical Cycling, edited by Buat-Ménard, P., pp. 113–127, Springer Netherlands, Dordrecht, doi: 10.1007/978-94-009-4738-2{_}5, 1986.

Liu, P. S. K., Deng, R., Smith, K. A., Williams, L. R., Jayne, J. T., Canagaratna, M. R., Moore, K., Onasch, T. B., Worsnop, D. R., and Deshler, T.: Transmission Efficiency of an Aerodynamic Focusing Lens System: Comparison of Model Calculations and Laboratory Measurements for the Aerodyne Aerosol Mass Spectrometer, Aerosol Science and Technology, 41, 721–733, doi: 10.1080/02786820701422278, 2007.

Lock, A. and Edwards, J.: Unified Model Documentation Paper 24: The Parametrization of Boundary Layer Processes, Tech. rep., UK Met Office, Exeter, UK, 2012.

Loeb, N. G., Wielicki, B. A., Doelling, D. R., Smith, G. L., Keyes, D. F., Kato, S., Manalo-Smith, N., and Wong, T.: Toward Optimal Closure of the Earth's Top-of-Atmosphere Radiation Budget, Journal of Climate, 22, 748–766, doi: 10.1175/2008JCLI2637.1, 2009.

Longo, K. M., Freitas, S. R., Andreae, M. O., Setzer, A., Prins, E., and Artaxo, P.: The coupled aerosol and tracer transport model to the brazilian developments on the regional atmospheric modeling system (catt-brams)-part 2: Model sensitivity to the biomass burning inventories, Atmospheric Chemistry and Physics, 10, 5785–5795, doi: 10.5194/acp-10-5785-2010, 2010.

Lovelock, J. and Whitfield, M.: Life span of the biosphere, doi: 10.1038/296561a0, 1982.

Lovelock, J. E. and Margulis, L.: Atmospheric homeostasis by and for the biosphere: the gaia hypothesis, Tellus A, 26, 1–2, doi: 10.3402/tellusa.v26i1-2.9731, 1974.

Lovelock, J. E., Maggs, R. J., and Rasmussen, R. A.: Atmospheric dimethyl sulfide and the natural sulfur cycle, Nature, 237, 452–453, doi: 10.1038/237452a0, 1972.

Magnan, A. K., Colombier, M., Billé, R., Joos, F., Hoegh-Guldberg, O., Pörtner, H.-O., Waisman, H., Spencer, T., and Gattuso, J.-P.: Implications of the Paris agreement for the ocean, Nature Climate Change, 6, 732–735, doi: 10.1038/nclimate3038, 2016.

Mahajan, A. S., Fadnavis, S., Thomas, M. a., Pozzoli, L., Gupta, S., Royer, S.-j., Saiz-Lopez, A., and Simó, R.: Quantifying the impacts of an updated global dimethyl sulfide climatology on cloud microphysics and aerosol radiative forcing, Journal of Geophysical Research: Atmospheres, 120, 2524–2536, doi: 10.1002/2014JD022687, 2015.

Mann, G. W., Carslaw, K. S., Spracklen, D. V., Ridley, D. A., Manktelow, P. T., Chipperfield, M. P., Pickering, S. J., and Johnson, C. E.: Description and evaluation of GLOMAP-mode: a modal global aerosol microphysics model for the UKCA composition-climate model, Geosci. Model Dev, 3, 519–551, doi: 10.5194/gmd-3-519-2010, 2010.

Mann, G. W., Carslaw, K. S., Ridley, D. A., Spracklen, D. V., Pringle, K. J., Merikanto, J., Korhonen, H., Schwarz, J. P., Lee, L. A., Manktelow, P. T., Woodhouse, M. T., Schmidt, A., Breider, T. J., Emmerson, K. M., Reddington, C. L., Chipperfield, M. P., and Pickering, S. J.: Intercomparison of modal and sectional aerosol microphysics representations within the same 3-D global chemical transport model, Atmospheric Chemistry and Physics, 12, 4449–4476, doi: 10.5194/acp-12-4449-2012, 2012.

Matus, A. V. and L'Ecuyer, T. S.: The role of cloud phase in Earth's radiation budget, Journal of Geophysical Research: Atmospheres, pp. 2559–2578, doi: 10.1002/2016JD025951, 2017.

McCormick, R. A. and Ludwig, J. H.: Climate Modification by Atmospheric Aerosols, Science, 156, 1358–1359, doi: 10.1126/science.156.3780.1358, 1967.

Metzger, A., Verheggen, B., Dommen, J., Duplissy, J., Prevot, A. S. H., Weingartner, E., Riipinen, I., Kulmala, M., Spracklen, D. V., Carslaw, K. S., and Baltensperger, U.: Evidence for the role of organics in aerosol particle formation under atmospheric conditions., Proceedings of the National Academy of Sciences of the United States of America, 107, 6646–51, doi: 10.1073/pnas.0911330107, 2010.

Millar, J. R., Nicholls, Z. R., Friedlingstein, P., and Allen, M. R.: A modified impulse-response representation of the global near-surface air temperature and atmospheric concentration response to carbon dioxide emissions, Atmospheric Chemistry and Physics, 17, 7213–7228, doi: 10.5194/acp-17-7213-2017, 2017.

Modini, R. L., Ristovski, Z. D., Johnson, G. R., He, C., Surawski, N., Morawska, L., Suni, T., and Kulmala, M.: New particle formation and growth at a remote, sub-tropical coastal location, Atmospheric Chemistry and Physics Discussions, 9, 12 101–12 139, doi: 10.5194/acpd-9-12101-2009, 2009.

Monin, A. S. and Obukhov, A. M.: Basic laws of turbulent mixing in the atmosphere near the ground, Tr. Akad. Nauk SSSR Geofiz. Inst, 24, 163–187, 1954.

Morrison, H., Thompson, G., and Tatarskii, V.: Impact of Cloud Microphysics on the Development of Trailing Stratiform Precipitation in a Simulated Squall Line: Comparison of One- and Two-Moment Schemes, Monthly Weather Review, 137, 991–1007, doi: 10.1175/2008mwr2556.1, 2008.

Mungall, E. L., Croft, B., Lizotte, M., Thomas, J. L., Murphy, J. G., Levasseur, M., Martin, R. V., Wentzell, J. J. B., Liggio, J., and Abbatt, J. P. D.: Dimethyl sulfide in the summertime Arctic atmosphere: measurements and source sensitivity simulations, Atmospheric Chemistry and Physics, 16, 6665–6680, doi: 10.5194/acp-16-6665-2016, 2016.

Muñiz-Unamunzaga, M., Borge, R., Sarwar, G., Gantt, B., de la Paz, D., Cuevas, C. A., and Saiz-Lopez, A.: The influence of ocean halogen and sulfur emissions in the air quality of a coastal megacity: The case of Los Angeles, Science of the Total Environment, 610-611, 1536–1545, doi: 10.1016/j.scitotenv.2017.06.098, 2018.

Murphy, D.: Influence of sea-salt on aerosol radiative properties in the Southern Ocean marine boundary layer, Nature, 392, 62–66, 1998.

Myhre, G., Samset, B. H., Schulz, M., Balkanski, Y., Bauer, S., Berntsen, T. K., Bian, H., Bellouin, N., Chin, M., Diehl, T., Easter, R. C., Feichter, J., Ghan, S. J., Hauglustaine, D., Iversen, T., Kinne, S., Kirkeväg, A., Lamarque, J. F.,

Lin, G., Liu, X., Lund, M. T., Luo, G., Ma, X., Van Noije, T., Penner, J. E., Rasch, P. J., Ruiz, A., Seland, Skeie, R. B., Stier, P., Takemura, T., Tsigaridis, K., Wang, P., Wang, Z., Xu, L., Yu, H., Yu, F., Yoon, J. H., Zhang, K., Zhang, H., and Zhou, C.: Radiative forcing of the direct aerosol effect from AeroCom Phase II simulations, Atmospheric Chemistry and Physics, 13, 1853–1877, doi: 10.5194/acp-13-1853-2013, 2013a.

Myhre, G., Shindell, D., Bréon, F.-M., Collins, W., Fuglestvedt, J., Huang, J., Koch, D., Lamarque, J.-F., Lee, D., Mendoza, B., Nakajima, T., Robock, A., Stephens, G., Takemura, T., and Zhang, H.: Anthropogenic and Natural Radiative Forcing, Climate Change 2013: The Physical Science Basis. Contribution of Working Group I to the Fifth Assessment Report of the Intergovernmental Panel on Climate Change, pp. 659–740, doi: 10.1017/CBO9781107415324.018, 2013b.

Nam, C., Bony, S., Dufresne, J. L., and Chepfer, H.: The too few, too bright tropical low-cloud problem in CMIP5 models, Geophysical Research Letters, 39, 1–7, doi: 10.1029/2012GL053421, 2012.

NERC: Dimethyl Sulphide (DMS), URL `https://www.bodc.ac.uk/solas_integration/implementation_products/group1/dms/`, 2014.

Nguyen, B. C., Gaudry, A., Bonsang, B., and Lambert, G.: Reevaluation of the role of dimethyl sulphide in the sulphur budget, Nature, 275, 637–639, 1978.

Nightingale, D., Malin, G., Law, C. S., Watson, J., Liss, S., and Liddicoat, I.: In situ evaluation of air-sea gas exchange parameterizations using novel conservative and volatile tracers, Global Biogeochemical Cycles, 14, 373–387, doi: 10.1029/1999GB900091, 2000.

Nishant, N., Sherwood, S. C., and Geoffroy, O.: Aerosol-induced modification of organised convection and top-of-atmosphere radiation, npj Climate and Atmospheric Science, 2, 33, doi: 10.1038/s41612-019-0089-1, 2019.

Nomura, D., Kasamatsu, N., Tateyama, K., Kudoh, S., and Fukuchi, M.: DMSP and DMS in coastal fast ice and under-ice water of Lützow-Holm Bay, eastern

Antarctica, Continental Shelf Research, 31, 1377–1383, doi: 10.1016/j.csr.2011.05.017, 2011.

O'Dowd, C. D., Smith, M. H., and Jennings, S. G.: Physico-chemical properties of aerosol over the Northeast Atlantic: Evidence for wind speed related submicron sea salt production, Journal of Geophysical Research-Atmospheres, 98, 1137–1149, 1993.

O'Dowd, C. D., Ceburnis, D., Young, J. Y., Facchini, M. C., Cavalli, F., Mircea, M., Decesari, S., Fuzzi, S., and Putaud, J.-P.: Biogenically driven organic contribution to marine aerosol, Nature, 431, 676–680, doi: 10.1038/nature02959, 2004.

Olivier, J., Peters, J., Granier, C., Petron, G., Muller, J., and Wallens, S.: Present and future surface emissions of atmospheric compounds, POET report #2, EU project EVK2-1999-00011, Tech. rep., Netherlands Environmental Assessment Agency,CNRS/IPSL, IASB, URL `http://accent.aero.jussieu.fr/POET_metadata.php`, 2003.

Omori, Y., Tanimoto, H., Inomata, S., Kameyama, S., Takao, S., and Suzuki, K.: Evaluation of using unfiltered seawater for underway measurement of dimethyl sulfide in the ocean by online mass spectrometry, Limnology and Oceanography: Methods, 11, 549–560, doi: 10.4319/lom.2013.11.549, 2013.

Omori, Y., Tanimoto, H., Inomata, S., Ikeda, K., Iwata, T., Kameyama, S., Uematsu, M., Gamo, T., Ogawa, H., and Furuya, K.: Sea-to-air flux of dimethyl sulfide in the South and North Pacific Ocean as measured by proton transfer reaction-mass spectrometry coupled with the gradient flux technique, Journal of Geophysical Research, 122, 7216–7231, doi: 10.1002/2017JD026527, 2017.

Parungo, F. P., Nagamoto, C. T., Rosinski, J., and Haagenson, P. L.: A study of marine aerosols over the Pacific Ocean, Journal of Atmospheric Chemistry, 4, 199–226, doi: 10.1007/BF00052001, 1986.

Pavolonis, M.: ABI Surface Albedo, NOAA NESDIS Center for Satellite Applications and Research Algorithm Theoretical Basis Document, 2, 1–60, 2010.

Pincus, R. and Baker, M. B.: Effect of precipitation on the albedo susceptibility of clouds in the marine boundary layer, Nature, 372, 250–252, doi: 10.1038/372250a0, 1994.

Plaisance, L., Caley, M. J., Brainard, R. E., and Knowlton, N.: The Diversity of Coral Reefs: What Are We Missing?, PLoS ONE, 6, e25 026, doi: 10.1371/journal.pone.0025026, URL http://dx.plos.org/10.1371/journal.pone.0025026, 2011.

Quinn, P. K. and Bates, T. S.: The case against climate regulation via oceanic phytoplankton sulphur emissions, Nature, 480, 51–56, doi: 10.1038/nature10580, 2011.

Quinn, P. K., Coffman, D. J., Johnson, J. E., Upchurch, L. M., and Bates, T. S.: Small fraction of marine cloud condensation nuclei made up of sea spray aerosol, Nature Geoscience, 10, 674–679, doi: 10.1038/ngeo3003, 2017.

Raes, F.: Entrainment of free tropospheric aerosols as a regulating mechanism for cloud condensation nuclei in the remote marine boundary layer, doi: 10.1029/94JD02832, 1995.

Rahn, D. A. and Garreaud, R.: Marine boundary layer over the subtropical southeast Pacific during VOCALS-REx-Part 1: Mean structure and diurnal cycle, Atmospheric Chemistry and Physics, 10, 4491–4506, doi: 10.5194/acp-10-4491-2010, 2010.

Raina, J.-B., Tapiolas, D. M., Forêt, S., Lutz, A., Abrego, D., Ceh, J., Seneca, F. O., Clode, P. L., Bourne, D. G., Willis, B. L., and Motti, C. A.: DMSP biosynthesis by an animal and its role in coral thermal stress response., Nature, 502, 677–80, doi: 10.1038/nature12677, 2013.

Revell, L. E., Kremser, S., Hartery, S., Harvey, M., Mulcahy, J. P., Williams, J., Morgenstern, O., Mcdonald, A. J., Varma, V., Bird, L., and Schuddeboom, A.: The sensitivity of Southern Ocean aerosols and cloud microphysics to sea spray and sulfate aerosol production in the HadGEM3-GA7.1 chemistry-

climate model, Atmospheric Chemistry and Physics, 19, 15 447–15 466, doi: 10.5194/acp-19-15447-2019, URL https://www.atmos-chem-phys.net/19/15447/2019/, 2019.

Ristovski, Z. D.: GBR as a significant source of climatically relevant aerosol particles, URL https://rms.arc.gov.au/RMS/Report/Download/Report/d6b15b2b-3a50-4021-8e6f-6c7ef1cba553/0, 2015.

Rosenfeld, D., Sherwood, S., Wood, R., and Donner, L.: Climate Effects of Aerosol-Cloud Interactions, Science, 343, 379–380, doi: 10.1126/science.1247490, 2014.

Rotstayn, L. D., Collier, M. A., and Luo, J.-J.: Effects of declining aerosols on projections of zonally averaged tropical precipitation, Environmental Research Letters, 10, 44 018, doi: 10.1088/1748-9326/10/4/044018, 2015.

Saide, P. E., Spak, S. N., Carmichael, G. R., Mena-Carrasco, M. A., Yang, Q., Howell, S., Leon, D. C., Snider, J. R., Bandy, A. R., Collett, J. L., Benedict, K. B., De Szoeke, S. P., Hawkins, L. N., Allen, G., Crawford, I., Crosier, J., and Springston, S. R.: Evaluating WRF-chem aerosol indirect effects in southeast pacific marine stratocumulus during VOCALS-REx, Atmospheric Chemistry and Physics, 12, 3045–3064, doi: 10.5194/acp-12-3045-2012, 2012.

Saltzman, E. S., King, D. B., Holmen, K., and Leck, C.: Experimental Determination of the Diffusion Coefficient of Dimethylsulfide in Water, Journal of Geophysical Research, 98, 16 481–16 486, doi: http://dx.doi.org/10.1029/93JC01858, 1993.

Schwinger, J., Tjiputra, J., Goris, N., Six, K., Kirkevåg, A., Seland, ., Heinze, C., and Ilyina, T.: Amplification of global warming through pH-dependence of DMS-production simulated with a fully coupled Earth system model, Biogeosciences Discussions, 20, 1–26, doi: 10.5194/bg-2017-33, 2017.

Seifert, A. and Beheng, K. D.: A two-moment cloud microphysics parameterization for mixed-phase clouds. Part 2: Maritime vs. continental deep convective storms, Meteorology and Atmospheric Physics, 92, 67–82, doi: 10.1007/

s00703-005-0113-3, 2006.

Seinfeld, J. H. and Pandis, S. N.: Atmospheric Chemistry and Physics: From Air Pollution to Climate Change, Wiley, New York, 1st edn., 1998.

Seinfeld, J. H., Bretherton, C., Carslaw, K. S., Coe, H., DeMott, P. J., Dunlea, E. J., Feingold, G., Ghan, S., Guenther, A. B., Kahn, R., Kraucunas, I., Kreidenweis, S. M., Molina, M. J., Nenes, A., Penner, J. E., Prather, K. A., Ramanathan, V., Ramaswamy, V., Rasch, P. J., Ravishankara, A. R., Rosenfeld, D., Stephens, G., and Wood, R.: Improving our fundamental understanding of the role of aerosol-cloud interactions in the climate system, Proceedings of the National Academy of Sciences, 113, 5781–5790, doi: 10.1073/pnas.1514043113, 2016.

Shao, Y., Ishizuka, M., Mikami, M., and Leys, J. F.: Parameterization of size-resolved dust emission and validation with measurements, Journal of Geophysical Research Atmospheres, 116, 1–19, doi: 10.1029/2010JD014527, 2011.

Shaw, G. E.: Bio-controlled thermostasis involving the sulphur cycle, Climate Change, 5, 297–303, 1983.

Sheng, J. X., Weisenstein, D. K., Luo, B. P., Rozanov, E., Stenke, A., Anet, J., Bingemer, H., and Peter, T.: Global atmospheric sulfur budget under volcanically quiescent conditions: Aerosol-chemistry-climate model predictions and validation, Journal of Geophysical Research Atmospheres, 120, 256–276, doi: 10.1002/2014JD021985, 2015.

Shin, H. H. and Hong, S. Y.: Intercomparison of Planetary Boundary-Layer Parametrizations in the WRF Model for a Single Day from CASES-99, Boundary-Layer Meteorology, 139, 261–281, doi: 10.1007/s10546-010-9583-z, 2011.

Simmel, M. and Wurzler, S.: Condensation and activation in sectional cloud microphysical models, Atmospheric Research, 80, 218–236, doi: 10.1016/j.atmosres.2005.08.002, 2006.

Simó, R.: From cells to globe: approaching the dynamics of DMS(P) in the ocean at

multiple scales, Canadian Journal of Fisheries and Aquatic Sciences, 61, 673–684, doi: 10.1139/f04-030, 2004.

Simó, R. and Dachs, J.: Global ocean emission of dimethylsulfide predicted from biogeophysical data, Global Biogeochemical Cycles, 16, 26–1, doi: 10.1029/2001GB001829, 2002.

Simpson, D., Guenther, A., Hewitt, C. N., and Steinbrecher, R.: Biogenic emissions in Europe: 1. Estimates and uncertainties, Journal of Geophysical Research, 100, 22 875, doi: 10.1029/95JD02368, 1995.

Sindelarova, K., Granier, C., Bouarar, I., Guenther, A., Tilmes, S., Stavrakou, T., Müller, J. F., Kuhn, U., Stefani, P., and Knorr, W.: Global data set of biogenic VOC emissions calculated by the MEGAN model over the last 30 years, Atmospheric Chemistry and Physics, 14, 9317–9341, doi: 10.5194/acp-14-9317-2014, 2014.

Six, K. D., Kloster, S., Ilyina, T., Archer, S. D., Zhang, K., and Maier-Reimer, E.: Global warming amplified by reduced sulphur fluxes as a result of ocean acidification, Nature Climate Change, 3, 975–978, doi: 10.1038/nclimate1981, 2013.

Slinn, W. G.: Predictions for particle deposition to vegetative canopies, Atmospheric Environment (1967), 16, 1785–1794, doi: 10.1016/0004-6981(82)90271-2, 1982.

Spalding, M., Burke, L., Wood, S. A., Ashpole, J., Hutchison, J., and zu Ermgassen, P.: Mapping the global value and distribution of coral reef tourism, Marine Policy, 82, 104–113, doi: 10.1016/j.marpol.2017.05.014, 2017.

Spracklen, D. V., Pringle, K. J., Carslaw, K. S., Chipperfield, M. P., and Mann, G. W.: A global off-line model of size-resolved aerosol microphysics: I. Model development and prediction of aerosol properties, Atmospheric Chemistry and Physics, 5, 2227–2252, doi: 10.5194/acpd-5-3437-2005, 2005.

Staniforth, A., White, A., Wood, N., Thuburn, J., Zerroukat, M., Cordero, E.,

Davies, T., and Diamantakis, M.: Unified Model Documentation Paper No. 15: New Dynamics, Tech. rep., UK Met Office, Exeter, UK, 2006.

Stefels, J., Steinke, M., Turner, S., Malin, G., and Belviso, S.: Environmental constraints on the production and removal of the climatically active gas dimethylsulphide (DMS) and implications for ecosystem modelling, Phaeocystis, Major Link in the Biogeochemical Cycling of Climate-Relevant Elements, pp. 245–275, doi: 10.1007/978-1-4020-6214-8{_}18, 2007.

Stephens, G. L., L'Ecuyer, T., Forbes, R., Gettelmen, A., Golaz, J.-C., Bodas-Salcedo, A., Suzuki, K., Gabriel, P., and Haynes, J.: Dreary state of precipitation in global models, Journal of Geophysical Research: Atmospheres, 115, doi: 10.1029/2010JD014532, 2010.

Stephens, G. L., Li, J., Wild, M., Clayson, C. A., Loeb, N. G., Kato, S., L'Ecuyer, T., Stackhouse, P. W., Lebsock, M., and Andrews, T.: An update on Earth's energy balance in light of the latest global observations, Nature Geoscience, 5, 691–696, doi: 10.1038/ngeo1580, 2012.

Stratton, R., Willett, M., Derbyshire, S., and Wong, R.: Unified Model Documentation Paper No. 27: Convection scheme, Tech. rep., UK Met Office, Exeter, UK, 2009.

Su, C.-H., Eizenberg, N., Steinle, P., Jakob, D., Fox-Hughes, P., White, C. J., Rennie, S., Franklin, C., Dharssi, I., and Zhu, H.: BARRA v1.0: The Bureau of Meteorology Atmospheric high-resolution Regional Reanalysis for Australia, Geoscientific Model Development Discussions, pp. 1–33, doi: 10.5194/gmd-2018-277, 2018.

Swan, H. B.: Atmospheric dimethylsulfide surface concentrations and supermicron particle number concentrations at Garners Beach (17.82°S, 146.10°E) October 2016., doi: http://doi.org/10.4226/47/59c47939e8324, 2017.

Swan, H. B., Jones, G. B., and Deschaseaux, E.: Dimethylsulfide, Climate and Coral Reef Ecosystems, in: Proceedings of the 12th International Coral Reef

Symposium, edited by Yellowlees, D. and Hughes, T. P., James Cook University, Cairns, QLD, Australia, 2012.

Swan, H. B., Ivey, J. P., Jones, G. B., and Eyre, B. D.: The validation and measurement uncertainty of an automated gas chromatograph for marine studies of atmospheric dimethylsulfide, Analytical Methods, 7, 3893–3902, doi: 10.1039/c5ay00269a, 2015.

Swan, H. B., Jones, G. B., Deschaseaux, E. S. M., and Eyre, B. D.: Coral reef origins of atmospheric dimethylsulfide at Heron Island, southern Great Barrier Reef, Australia, Biogeosciences Discussions, 14, 229–239, doi: 10.5194/bg-2016-387, 2017.

Tao, W. K., Chen, J.-P., Li, Z., Wang, C., and Zhang, C.: Impact of Aerosols on boundary layer clouds and precipitation, Reviews of Geophysics, 50, 2011RG000 369, doi: 10.1029/2011RG000369.1.INTRODUCTION, 2012.

Taylor, K. E., Williamson, D., and Zwiers, F. W.: AMIP Sea Surface Temperature and Sea Ice Concentration Boundary Conditions, 2015.

Tesdal, J. E., Christian, J. R., Monahan, A. H., and Von Salzen, K.: Sensitivity of modelled sulfate aerosol and its radiative effect on climate to ocean DMS concentration and air-sea flux, Atmospheric Chemistry and Physics, 16, 10 847–10 864, doi: 10.5194/acp-16-10847-2016, 2016a.

Tesdal, J. E., Christian, J. R., Monahan, A. H., and Von Salzen, K.: Evaluation of diverse approaches for estimating sea-surface DMS concentration and air-sea exchange at global scale, Environmental Chemistry, 13, 390–412, doi: 10.1071/EN14255, 2016b.

Thomas, M. A., Suntharalingam, P., Pozzoli, L., Rast, S., Devasthale, A., Kloster, S., Feichter, J., and Lenton, T. M.: Quantification of DMS aerosol-cloud-climate interactions using the ECHAM5-HAMMOZ model in a current climate scenario, Atmospheric Chemistry and Physics, 10, 7425–7438, doi: 10.5194/acp-10-7425-2010, 2010.

Thomas, M. A., Suntharalingam, P., Pozzoli, L., Devasthale, A., Kloster, S., Rast,

S., Feichter, J., and Lenton, T. M.: Rate of non-linearity in DMS aerosol-cloud-climate interactions, Atmospheric Chemistry and Physics, 11, 11 175–11 183, doi: 10.5194/acp-11-11175-2011, 2011.

Tie, X.: Effect of clouds on photolysis and oxidants in the troposphere, Journal of Geophysical Research, 108, doi: 10.1029/2003jd003659, 2003.

Tiedtke, M.: Representation of clouds in large-scale models, doi: 10.1175/1520-0493(1993)121⟨3040:ROCILS⟩2.0.CO;2, 1993.

Twohy, C. H. and Anderson, J. R.: Droplet nuclei in non-precipitating clouds: composition and size matter, Environmental Research Letters, 3, 045 002, doi: 10.1088/1748-9326/3/4/045002, 2008.

Twomey, S.: Pollution and the Planetary Albedo, Atmospheric Environment, 8, 1251–1256, 1974.

UNEP-WCMC, WorldFish Centre, WRI, and TNC: Global distribution of coral reefs, compiled from multiple sources including the Millennium Coral Reef Mapping Project. Version 1.3. Includes contributions from IMaRS-USF and IRD (2005), IMaRS- USF (2005) and Spalding et al. (2001)., Tech. rep., UNEP World Conservation Monitoring Centre, Cambridge (UK), 2010.

Vairavamurthy, A., Andreae, M. O., and Iverson, R. L.: Biosynthesis of dimethlysulfide and dimethylpropiothetin by Hymenomonas carterae in relation to sulfur source and salinity variations, Limnology and Oceanography, 30, 59–70, doi: 10.4319/lo.1985.30.1.0059, 1985.

Vallina, S. M., Simó, R., and Gassó, S.: What controls CCN seasonality in the Southern Ocean? A statistical analysis based on satellite-derived chlorophyll and CCN and model-estimated OH radical and rainfall, Global Biogeochemical Cycles, 20, 1–13, doi: 10.1029/2005GB002597, 2006.

van der Werf, G. R., Randerson, J. T., Giglio, L., van Leeuwen, T. T., Chen, Y., Rogers, B. M., Mu, M., van Marle, M. J. E., Morton, D. C., Collatz, G. J., Yokelson, R. J., and Kasibhatla, P. S.: Global fire emissions estimates during

1997–2015, Earth System Science Data Discussions, Online, 1–43, doi: 10.5194/essd-2016-62, 2017.

van Vuuren, D. P., Edmonds, J., Kainuma, M., Riahi, K., Thomson, A., Hibbard, K., Hurtt, G. C., Kram, T., Krey, V., Lamarque, J. F., Masui, T., Meinshausen, M., Nakicenovic, N., Smith, S. J., and Rose, S. K.: The representative concentration pathways: An overview, Climatic Change, 109, 5–31, doi: 10.1007/s10584-011-0148-z, 2011.

Vincent, C. L., Protat, A., Alexander, S. P., Harvey, M., Fiddes, S. L., Lane, T. P., Gray, S., and Ryan, R. G.: The observed and simulated tropical sea breeze over the Great Barrier Reef, Quarterly Journal of the Royal Meteorological Society, Submitted, 1–11, 2019.

Vincent, E. M., Lengaigne, M., Menkes, C. E., Jourdain, N. C., Marchesiello, P., and Madec, G.: Interannual variability of the South Pacific Convergence Zone and implications for tropical cyclone genesis, Climate Dynamics, 36, 1881–1896, doi: 10.1007/s00382-009-0716-3, 2011.

Vlahos, P. and Monahan, E. C.: A generalized model for the air-sea transfer of dimethyl sulfide at high wind speeds, Geophysical Research Letters, 36, L21 605, doi: 10.1029/2009GL040695, 2009.

Vogt, M., Vallina, S. M., Buitenhuis, E. T., Bopp, L., and Le Quéré, C.: Simulating dimethylsulphide seasonality with the Dynamic Green Ocean Model PlankTOM5, Journal of Geophysical Research: Oceans, 115, 1–21, doi: 10.1029/2009JC005529, 2010.

von Glasow, R. and Crutzen, P. J.: Model study of multiphase DMS oxidation with a focus on halogens, Atmospheric Chemistry and Physics Discussions, 3, 6733–6777, doi: 10.5194/acpd-3-6733-2003, 2010.

Wallace, J. M. and Hobbs, P. V.: Atmospheric Science, Elsevier, doi: 10.1016/C2009-0-00034-8, 2006.

Wang, H. and Su, W.: Evaluating and understanding top of the atmosphere cloud

radiative effects in Intergovernmental Panel on Climate Change (IPCC) Fifth Assessment Report (AR5) Coupled Model Intercomparison Project Phase 5 (CMIP5) models using satellite observations, Journal of Geophysical Research: Atmospheres, 118, 683–699, doi: 10.1029/2012JD018619, 2013.

Wanninkhof, R.: Relationship Between Wind Speed and Gas Exchange, Journal of Geophysical Research, 97, 7373–7382, doi: 10.1029/92JC00188, 1992.

Warner, J.: A Reduction in Rainfall Associated with Smoke from Sugar-Cane FiresAn Inadvertent Weather Modification?, Journal of Applied Meteorology, 7, 247–251, doi: 10.1175/1520-0450(1968)007⟨0247:ARIRAW⟩2.0.CO;2, 1968.

Wexler, A. S., Lurmann, F. W., and Seinfeld, J. H.: Modelling urban and regional aerosols-I. model development, Atmospheric Environment, 28, 531–546, doi: 10.1016/1352-2310(94)90129-5, 1994.

Wilkinson, J.: Unified Model Documentation Paper No. 26: The Large-Scale Precipitation Parametrization Scheme, Tech. Rep. 10.2, UK Met Office, Exeter, UK, 2012.

Wilks, D. S.: Statistical Methods in the Atmospheric Sciences, Elsevier, 3rd edn., doi: 10.1016/B978-0-12-385022-5.00026-9, 2011.

Wilson, D., Bushell, A., Morcrette, C., and Wilson, D.: The PC2 Cloud Scheme. Annexe to Unified Model Documentation Paper No. 29, Tech. Rep. 29, UK Met Office, Exeter, UK, 2011.

Wilson, D. R. and Ballard, S. P.: A microphysically based precipitation scheme for the UK meteorological office unified model, Quarterly Journal of the Royal Meteorological Society, 125, 1607–1636, doi: 10.1002/qj.49712555707, 1999.

WMO: Scientific assessment of ozone depletion : 2010, Global Ozone Research and Monitoring Project, Report 52, 2010.

Wood, R., Mechoso, C. R., Bretherton, C. S., Weller, R. A., Huebert, B., Straneo, F., Albrecht, B. A., Coe, H., Allen, G., Vaughan, G., Daum, P., Fairall, C., Chand, D., Gallardo Klenner, L., Garreaud, R., Grados, C., Covert, D. S., Bates, T. S.,

Krejci, R., Russell, L. M., De Szoeke, S., Brewer, A., Yuter, S. E., Springston, S. R., Chaigneau, A., Toniazzo, T., Minnis, P., Palikonda, R., Abel, S. J., Brown, W. O., Williams, S., Fochesatto, J., Brioude, J., and Bower, K. N.: The VAMOS ocean-cloud-atmosphere-land study regional experiment (VOCALS-REx): Goals, platforms, and field operations, Atmospheric Chemistry and Physics, 11, 627–654, doi: 10.5194/acp-11-627-2011, 2011.

Woodhouse, M. T., Carslaw, K. S., Mann, G. W., Vallina, S. M., Vogt, M., Halloran, P. R., and Boucher, O.: Low sensitivity of cloud condensation nuclei to changes in the sea-air flux of dimethyl-sulphide, Atmospheric Chemistry and Physics, 10, 7545–7559, doi: 10.5194/acp-10-7545-2010, 2010.

Woodhouse, M. T., Mann, G. W., Carslaw, K. S., and Boucher, O.: Sensitivity of cloud condensation nuclei to regional changes in dimethyl-sulphide emissions, Atmospheric Chemistry and Physics, 13, 2723–2733, doi: 10.5194/acp-13-2723-2013, 2013.

Woodhouse, M. T., Luhar, A. K., Stevens, L., Galbally, I., Thatcher, M., Uhe, P., Noonan, J., and Molloy, S.: Australian reactive-gas emissions in a global chemistry-climate model and initial results, Air Quality and Climate Change, 49, 31–38, 2015.

Woodhouse, M. T., Cravigan, L. T., Harvey, M. J., Lawson, S. J., Bell, T. G., Ristovski, Z., Fiddes, S. L., Arnold, S. R., and Walker, H.: Simulating the marine organic contribution to aerosol during the Surface Ocean Aerosol Production ( SOAP ) experiment, Unsubmitted, 2019.

Woodward, S.: Modeling the atmospheric life cycle and radiative impact of mineral dust in the Hadley Centre climate model, Journal of Geophysical Research: Atmospheres, 106, 18 155–18 166, doi: 10.1029/2000JD900795, 2001.

Xiang, Y., Zhang, T., Liu, J., Lv, L., Dong, Y., and Chen, Z.: Atmosphere boundary layer height and its effect on air pollutants in Beijing during winter heavy pollution, Atmospheric Research, 215, 305–316, doi: 10.1016/j.atmosres.2018.09.014,

2019.

Xu, K.-M. and Randall, D. A.: A Semiempirical Cloudiness Parameterization for Use in Climate Models, Journal of the Atmospheric Sciences, 53, 3084–3102, doi: 10.1175/1520-0469(1996)053⟨3084:ASCPFU⟩2.0.CO;2, 1996.

Yang, Q., Fast, J. D., Wang, H., Easter, R. C., Morrison, H., Lee, Y.-N., Chapman, E. G., Spak, S. N., and Mena-Carrasco, M. A.: Assessing regional scale predictions of aerosols, marine stratocumulus, and their interactions during VOCALS-REx using WRF-Chem, Atmospheric Chemistry and Physics, 11, 11 951–11 975, doi: 10.5194/acp-11-11951-2011, URL https://www.atmos-chem-phys.net/11/11951/2011/, 2011.

Yang, Q., Gustafson, W. I., Fast, J. D., Wang, H., Easter, R. C., Wang, M., Ghan, S. J., Berg, L. K., Leung, L. R., and Morrison, H.: Impact of natural and anthropogenic aerosols on stratocumulus and precipitation in the Southeast Pacific: a regional modelling study using WRF-Chem, Atmospheric Chemistry and Physics, 12, 8777–8796, doi: 10.5194/acp-12-8777-2012, 2012.

Yu, S., Eder, B., Dennis, R., Chu, S.-H., and Schwartz, S. E.: New unbiased symmetric metrics for evaluation of air quality models, Atmospheric Science Letters, 7, 26–34, doi: 10.1002/asl.125, 2006.

Zaveri, R. A.: Development and Evaluation of a Comprehensive Tropospheric Chemistry Model for Regional and Global Applications Development and Evaluation of a Comprehensive Tropospheric Chemistry Model for Regional and Global Applications, Ph.D. thesis, Virginia Polytechnic Institute and State University, URL http://scholar.lib.vt.edu/theses/available/etd-7197-18361/, 1997.

Zaveri, R. A.: A new lumped structure photochemical mechanism for large-scale applications, Journal of Geophysical Research Atmospheres, 104, 30 387–30 415, doi: 10.1029/1999JD900876, 1999.

Zaveri, R. A., Easter, R. C., Fast, J. D., and Peters, L. K.: Model for Simulating Aerosol Interactions and Chemistry (MOSAIC), Journal of Geophysical Research

Atmospheres, 113, 1–29, doi: 10.1029/2007JD008782, 2008.

Zelinka, M. D., Myers, T. A., McCoy, D. T., Po-Chedley, S., Caldwell, P. M., Ceppi, P., Klein, S. A., and Taylor, K. E.: Causes of Higher Climate Sensitivity in CMIP6 Models, Geophysical Research Letters, 47, 1–12, doi: 10.1029/2019GL085782, 2020.

Zhang, L.: A size-segregated particle dry deposition scheme for an atmospheric aerosol module, Atmospheric Environment, 35, 549–560, doi: 10.1016/S1352-2310(00)00326-5, 2001.

Zilitinkevich, S.: Non-local Turbulent Transport: Pollution Dispersion Aspects Of Coherent Structure Of Connective Flows, Transactions on Ecology and the Environment, 6, 53–60, doi: 10.2495/AIR950071, 1995.